ANALYSIS AND OPTIMUM DESIGN OF
STRUCTURES UNDER STATIC AND DYNAMIC LOADS
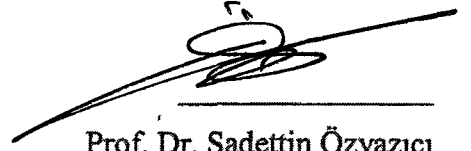
Ph. D. Thesis

in

Civil Engineering
University of Gaziantep

By
Nildem TAYŞİ
January 2005

Approval of the Graduate School of Natural and Applied Sciences

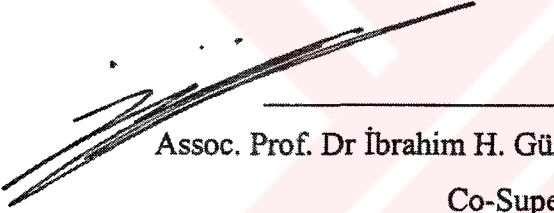Prof. Dr. Sadettin Özyazıcı

Director

I certify that this thesis satisfies all the requirements as a thesis for the degree of Doctor of Philosophy.

Assist. Prof. Dr. Hanifi Çanakçı

Head of Department

This is to certify that we have read this thesis and that in our opinion it is fully adequate, in scope and quality, as a thesis for the degree of Doctor of Philosophy.

Assoc. Prof. Dr İbrahim H. Güzelbey

Co-Supervisor

Prof. Dr. Mustafa Özakça

Supervisor

Examining Committee Members
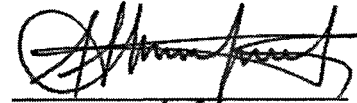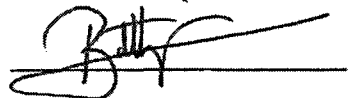
Prof. Dr. Orhan Aksoğan (Chairman)

Prof. Dr. Ragıp Erdöl

Prof. Dr. Mustafa Özakça

Assist. Prof. Dr. Hanifi Çanakçı

Assist. Prof. Dr. Bahattin Kanber

ii

ABSTRACT

ANALYSIS AND OPTIMUM DESIGN OF STRUCTURES UNDER STATIC AND DYNAMIC LOADS

Tayşi Nildem

Ph.D. in Civil Engineering

Supervisor: Prof. Dr. Mustafa Özakça

Co-supervisor: Assoc. Prof. Dr. İbrahim H. Güzelbey

January 2005, 260 pages

This thesis deals with the development of reliable, and efficient computational tools for the linearly elastic analysis and optimum design of 2D and 3D discrete structures under static, free vibration and dynamic loads. Structural optimization procedures considered in this thesis involve the efficient integration of computer aided geometry modeling, automatic mesh generation, structural analysis and genetic algorithm.

The procedures for structural shapes and thickness definition using parametric cubic splines for complex discrete structures are developed. A versatile, efficient and inexpensive algorithm for mesh generation, which is integrated with the shape definition is implemented. Finite element formulations for the static and free vibration analysis of 2D and 3D trusses, beams, arches and frame structures are developed and implemented. The use of a reliable and competitive procedure for finding the optimum solutions for problems involving discrete and continuous design variables based on genetic algorithms is demonstrated. A reliable finite element formulation for the transient analysis of 2D and 3D beams, arches and frame structures is implemented and the dynamic characteristics of various optimized beam and frame structure are considered. The validity of the formulations and programs is verified by comparing with literature, commercial software and analytical solution whenever possible.

Key words: Finite element, geometric modeling, mesh generation, static analysis, free vibration analysis, transient dynamic analysis, structural shape optimization, genetic algorithm.

ÖZ

STATİC VE DİNAMİK YÜKLER ALTINDAKİ YAPILARIN ANALİZ VE OPTİMUM TASARIMI

Tayşi Nildem

Doktora Tezi, İnşaat Mühendisliği Bölümü

Tez Yöneticisi: Prof. Dr. Mustafa Özakça

Yardımcı Tez Yöneticisi: Doç. Dr. İbrahim H. Güzelbey

Ocak 2005, 260 sayfa

Bu tez, statik, serbest titreşim ve dinamik yükler altındaki iki ve üç boyutlu yapıların analizi ve optimum tasarımı için güvenli ve verimli bir sonlu elemanlar bilgisayar programı geliştirilmesiyle ilgilidir. Bu tezde kullanılan yapı optimizasyon prosedürü, verimli bir bilgisayar destekli geometri modeli oluşturulmasını, otomatik ağ üretimini, yapı analizini ve genetik algoritmayı içermektedir.

Kompleks yapıların şekillerinin ve kalınlıklarının parametrik kübik eğriler kullanılarak tanımlanması için bir prosedür geliştirilmiştir. Ağ üretim için şekil tanımlanmasının da entegre edildiği, esnek, verimli ve hızlı bir algoritma uygulanmıştır. İki ve üç boyutlu kafes, kiriş, kemer ve çerçeve sistemlerin statik ve serbest titreşim analizi için sonlu elemanlar formülü geliştirilmiş ve uygulanmıştır. Sürekli ve süreksiz tasarım değişkenlerini içeren problemlerin optimum çözümlerini bulmak için genetik algoritmasına bağlı etkili ve uyumlu bir prosedür sunulmuştur. İki ve üç boyutlu kiriş, kemer ve çerçevelerin zamana bağlı dinamik analizi için etkili bir sonlu elemanlar formülü uygulanmıştır ve optimize edilmiş olan çeşitli kiriş ve çerçeve örneklerinin dinamik karakteristikleri yorumlanmıştır. Kullanılan model ve programların geçerliliği, mümkün olduğu kadar literatürdeki yayınlarla, çeşitli paket programlarla ve analitik çözümlerle karşılaştırılarak ispatlanmıştır.

Anahtar kelimeler: Sonlu elemanlar, geometrik modelleme, ağ üretimi, statik analiz, serbest titreşim analizi, zaman bağlı dinamik analiz, yapı şekil optimizasyonu, genetik algoritma.

ACKNOWLEDGMENTS

TABLE OF CONTENTS

Chapter 5   STATIC ANALYSIS OF TWO AND THREE DIMENSIONAL STRUCTURES

Chapter 8 STATIC OPTIMIZATION OF TWO AND THREE DIMENSIONAL STRUCTURES

Chapter 9 FREE VIBRATION OPTIMIZATION OF TWO AND THREE DIMENSIONAL STRUCTURES

Chapter 10 TRANSIENT DYNAMIC ANALYSIS

Chapter 11 CONCLUSION

REFERENCES

APPENDIX A TRANSFORMATION MATRICES

CURRICULUM VITAE

LIST OF TABLES

xiv

LIST OF FIGURES

LIST OF SYMBOLS

Abbreviations

FE	Finite Element
FEM	Finite Element Method
DOF	Degrees Of Freedom
DV	Design Variable
GA	Genetic Algorithm
MR	Mindlin-Reissner
SE	Strain Energy
SO	Shape Optimization
SSO	Structural Shape Optimization
1D	One Dimensional
2D	Two Dimensional
3D	Three Dimensional

Scalars

a_0, a_1	Rayleigh damping proportionality constants
A	Cross-sectional area
c	damping coefficient
c	cosine alpha
c_i^e	normalized constraint of element e
$C(0)$, $C(1)$, $C(2)$	order of continuity
b_i	binary number
b^e	inertia body forces
d	displacement
D_m, D_b, D_s	membrane, bending and shear rigidities
E	Young's modulus
EI	flexural rigidity

Scalars (continued)

F_b	body force
$f(s)$	objective function
$\hat{f}(s)$	fitness function
f_n	natural cyclic frequency for nth mode
g_j	'pure' (non penalized) objective
$\hat{g}_j$	modified objective
G	modulus of rigidity
h	the parametric coordinate
$\overline{h}_{i,j}$	the normalized constraint
$h_{i,j}$	the current equality constraint,
$h_{i,max}$	the allowable value of constraint
$\hat{h}_j$	sum of all absolute, normalized constraints
i_{pos}	current integer position number
I	moment of inertia
I_z, I_y	moment of inertia with respect to z and y axies
I^e	total work from element e
J	Jacobian, polar moment of inertia
ℓ	length
L	span length
m	binary string length
M	bending moment
n_D	number of total values in the discrete value
n	number of design variables
n_c	length of chromosome
N	axial force
N_i	shape function associated with node i
P_0, P_1	curve end points
$p(h)$	position vector of any point on the curve

Scalars (continued)

p_c	the fixed penalty coefficient
P_i	force acting at point i
$p(t)$	applied loading varying with time t
Q	shear force
Q_y, Q_z	shear forces in y and z directions
q	traction force
q_x, q_y, q_z	distributed pressure loading along x, y, and z axes
r	resolution
R	radius of curvature
s	sine alpha
$s(\ell)_i$	mesh density function
s	design variables
s_k	k th design variable
s_k^l	lower bounds on a typical design variable
s_k^u	upper bounds on a typical design variable
t	thickness, time
t_i	thickness at node i
t_r	impulse duration
T	period of vibration, torque
T_{min}	minimum period of vibration
T_n	period of nth normal mode
$U^{(e)}$	element strain energy
u, v, w	global displacement parameters
u_ℓ, v_ℓ, w_ℓ	displacement components in ℓ, y and n-directions
$\bar{u}_\ell, \bar{w}_\ell$ and $\bar{\theta}$	the corresponding displacement and rotation values at $\ell = \bar{\ell}$.
$u_1^{(e)}, u_2^{(e)}$	nodal displacements of element
u_{max}	maximum allowable displacement
$\ddot{u}$	axial acceleration

Scalars (continued)

V_y, V_z	lateral forces along y and z axes
$W_I^{(e)}$	potential energy of the inertia body forces for element e
W_T	target weight
$\|\mathbf{W}\|^2$	total strain energy
$\|\mathbf{W}\|_b^2$	strain energy due to bending
$\|\mathbf{W}\|_m^2$	strain energy due to membrane
$\|\mathbf{W}\|_s^2$	strain energy due to shear
x, y	global cartesian coordinates
x_i, y_i	cartesian coordinates of node i
$x_1^{(e)}, x_2^{(e)}$	x coordinates of element
z	size of population

Vectors

$\mathbf{b}_0, \mathbf{b}_1, \mathbf{b}_2, \mathbf{b}_3$	position vectors
$\mathbf{c}_0, \mathbf{c}_1, \mathbf{c}_2$ and $\mathbf{c}_3$	position vectors of the control vertices
$\mathbf{d}$	vector of unknown displacements
$\ddot{\mathbf{d}}$	accelerations of the displacement components vector
$\mathbf{d}'$	displacement vectors in local coordinate systems
$\overline{\mathbf{d}}$	displacement vector in local direction
$\overline{\mathbf{d}}_p$	p^{th} mode shape
$\mathbf{d}^0$	global displacement vector
$\mathbf{d}_i^e$	displacement vector (eigenvector) associated with element e and node i
$\hat{\mathbf{d}}_p$	pth vibration mode (eigenvector)
$\overline{\mathbf{d}}_i$	displacement vector (eigenvector) at node i

Vectors (continued)

$f(t)$	applied force vector
$\mathbf{f}^0$	global force vector
$\mathbf{f}_i^e$	nodal force vector associated with node i
$\mathbf{f}^e$	element body force vector
$\mathbf{F}(t)_I$	inertia force acting on the node masses vector
$\mathbf{F}(t)_D$	viscous damping or energy forces vector
$\mathbf{F}(t)_S$	internal forces vector
$\mathbf{F}(t)$	externally applied loads vector
$\mathbf{p}_i$	position vectors
$\mathbf{p}(t)$	load vector in the time domain
$\mathbf{p}(0)$, $\mathbf{p}(1)$	position vectors
$\mathbf{q}^e$	element distributed load vector
$\mathbf{s}$	design variables vector
$\mathbf{u}(t)$	displacement field vector in the time domain
$\dot{\mathbf{u}}(t)$	velocity field vector in the time domain
$\ddot{\mathbf{u}}(t)$	acceleration field vector in the time domain
$\mathbf{u}(t + \Delta t)$	displacement field vector at time $t + \Delta t$
$\dot{\mathbf{u}}(t + \Delta t)$	velocity field vector at time $t + \Delta t$
$\ddot{\mathbf{u}}(t + \Delta t)$	acceleration field vector at time $t + \Delta t$

Matrices

$\mathbf{B}$	strain-displacement matrix
$\mathbf{B}_{mi}^e$	membrane strain-displacement matrix for element e and node i
$\mathbf{B}_{bi}^e$	bending strain-displacement matrix for element e and node i
$\mathbf{B}_{si}^e$	shear strain-displacement matrix for element e and node i

Matrices (continued)

$\mathbf{B}_{mi}$	membrane strain-displacement matrix for node i
$\mathbf{B}_{bi}$	bending strain-displacement matrix for node i
$\mathbf{B}_{si}$	shear strain-displacement matrix for node i
$\overline{\mathbf{B}}_{mi}, \overline{\mathbf{B}}_{bi}, \overline{\mathbf{B}}_{si}$	transformed strain-displacement matrices
$\mathbf{B}_{pi}$	in-plane strain displacement matrix
$\mathbf{C}_{ij}^{e}$	damping matrix associated with element e and node i and j
$\mathbf{C}_{n}$	generalized damping matrix for nth mode
$\mathbf{C}$	symmetric, banded damping matrix
$\mathbf{D}$	matrix of rigidities
$\mathbf{D}_m, \mathbf{D}_b, \mathbf{D}_s$	matrices of membrane, bending and shear rigidities
$\mathbf{D}_p, \mathbf{D}_s$	in-plane and transverse elasticity matrix
$\mathbf{I}_3$	the 3×3 identity matrix
$\mathbf{J}$	Jacobian matrix
$\mathbf{K}^{e}$	element stiffness matrices
$\mathbf{K}_{ij}^{e}$	stiffness matrix associated with element e and nodes i and j
$\mathbf{K}$	symmetric, banded stiffness matrix
$\mathbf{K}_{mij}^{e}$	membrane stiffness matrix for element e and nodes i and j
$\mathbf{K}_{bij}^{e}$	bending stiffness matrix for element e and nodes i and j
$\mathbf{K}_{sij}^{e}$	shear stiffness matrix for element e and nodes i and j
$\mathbf{M}$	global mass matrix
$\mathbf{M}_{ij}^{e}$	mass matrix associated with element e and nodes i and j
$\mathbf{M}_{fer}, \mathbf{M}_{bez}, \mathbf{M}_B$	Ferguson, Bezier and B-spline M matrices
$\mathbf{N}$	shape function matrix
$\mathbf{R}_{fer}, \mathbf{R}_{bez}, \mathbf{R}_B$	Ferguson, Bezier and B-spline R matrices
$\mathbf{T}$	transformation matrix

Greek Symbols:

α	angle between local and global axes, Newmark's Method modification factor
β	arch opening angle, non-dimensional time parameter
ε	axial strains
$\varepsilon_m, \varepsilon_b, \varepsilon_s$	membrane, bending and transverse shear strains
$\boldsymbol{\varepsilon}_m, \boldsymbol{\varepsilon}_b, \boldsymbol{\varepsilon}_s$	membrane, bending and transverse shear strain vectors
$\boldsymbol{\varepsilon}_\ell, \boldsymbol{\varepsilon}_y$	strain in ℓ direction and longitudinal strain
$\varepsilon_y, \varepsilon_z$	bending strain in y and z axes
ε_j	tolerance factor
δ	stiffness proportional damping coefficient
γ	non-dimensional time parameter
$\gamma_{\ell y}, \gamma_{yn}$	shear strain
$\gamma_{xx}, \gamma_{xy}, \gamma_{xz}$	shear strain in x, y and z axes
Δt	time increment
κ	shear modification factor
κ_ℓ	curvature in the ℓ-direction
κ_y	longitudinal curvature
$\kappa_{\ell y}$	twisting curvature
μ	coefficient of friction
$\phi(\ell)$	piecewise linear spacing function
$\theta_x, \theta_y, \theta_z$	rotational degrees of freedom about x, y and z axes
ν	Poisson's ratio
ξ, ξ_n	damping ratios
ζ_i	damping ratio for ith mode
ω_p	natural frequency for pth mode
ω_i	circular frequency for ith mode

Greek Symbols: (continued)

ω_n	fundamental frequency
ξ	isoparametric element natural (curvilinear) coordinates
σ	stress component
$\sigma_{c\,max}$, $\sigma_{t\,max}$	maximum allowable compression and tension stresses
Π	total potential energy
τ	arbitrary time between time t and time $t+\Delta t$
Λ	the level of penalty occurring
σ_m, σ_b, σ_s	membrane, bending and shear stress resultant vectors
ρ	mass density
λ	frequency parameter
$\partial\ell$	partial differential of ℓ

CHAPTER 1

INTRODUCTION

1.1 Introduction

In structural design, it is necessary to obtain an appropriate form for a structure so that it can carry the imposed loads safely and economically. Traditional approaches towards the task of finding such forms for structures have been by the use of experimental models or by intuition and experience. However, in many cases the optimum shapes for structures are not evident from experiments and experience. There is therefore a need for better approaches which offer a more general and reliable way for determining optimum shapes under static and free vibration cases.

Structural Shape Optimization (SSO) of linear elastic structures has advanced steadily by the deepening of its theoretical foundations from different disciplines and the widening of its field of applicability. The significant progress in this field, in the last three decades, is a result of parallel progress in structural analysis, optimization algorithms (such as nonlinear programming, Genetic Algorithm (GA), neural network) geometric modeling and computer hardware. Structural optimization combines mathematics and mechanics with engineering and has become a multidisciplinary field with applications in areas such as civil, mechanical, aeronautical, nuclear and marine engineering. In its present state of maturity, it is regarded as a practical, automated and integrated numerical tool for research and design.

In order to establish the functional requirements of a SSO scheme it is desirable to examine the objectives. The objectives of the design process are twofold:

1

- to achieve a safe design which simultaneously satisfies manufacturing (or constructional) and functional requirements, and

- to reduce the cost of the manufacture (or construction) and maintenance of a structural component (or structure).

In other words, structural optimization is concerned with achieving the best design for a given objective while satisfying certain restrictions.

1.2 Thesis Objectives

The main objective of the thesis is to develop reliable, creative and efficient computational tools for the linearly elastic analysis and optimum design of 2D and 3D discrete structures under static, free vibration and dynamic loads. Structural optimization procedure of the type considered in this work involve the efficient integration of computer aided geometry modeling, automatic mesh generation, structural analysis and GA. The specific objectives of this thesis can be summarized as follows:

- To develop procedures for structural shapes and thickness definition using parametric cubic splines for complex discrete structures.

- To implement a versatile, efficient and inexpensive algorithm for mesh generation which is integrated with the shape definition and has a facility for automatically updating the loading and boundary conditions.

- To present and implement a Finite Element (FE) formulation for the static and free vibration analysis of 2D and 3D trusses.

- To develop and implement a reliable FE formulation for the static and free vibration analysis of 2D and 3D beam, arch and frame structures. The curved, variable thickness, isoparametric Mindlin-Reissner (MR) FE method employed is tested for accuracy by comparing with previous solutions and measuring the discrepancy between linear, quadratic and cubic FE sub-element divisions.

- To develop and demonstrate the use of a reliable and competitive procedure for finding the optimum solutions for problems involving discrete and continuous design variables based on GAs.

- To develop and implement a reliable FE formulation for the transient analysis of 2D and 3D beam, arch and frame structures.
- To determine the dynamic characteristics of various optimized beam and frame structures.

During the course of this research work, a series of studies is undertaken to provide evidence of the effectiveness of the proposed models, comparing numerical predictions with analytical or experimental results whenever possible.

Principally, it is hoped that this thesis will provide firm foundations for further investigation, leading to a more intensive use of structural optimization algorithms to solve practical problems.

1.3 Structure Types Considered in This Thesis

Because of the wide variety of structures encountered in practice, it becomes clear that a thesis dealing with analysis and structural optimization should focus on selected topics. For this reason, structures considered in this thesis are composed of members whose lengths are significantly larger than their cross-sectional dimensions. Truss, beam, arch and frame structures will be examined in depth in this thesis.

Trusses: Initially, we consider the analysis and optimization of 2D and 3D trusses under static and free vibration conditions. This enables us to develop some introductory tools and gain some useful experience in optimization prior to considering beam, arch and frame structures.

Beams, arches and frames: Later, we turn our attention to the analysis and optimization of beam, arch and frame structures under static, free vibration and transient dynamic conditions. Types of the structures dealt with in this thesis include variable thickness beam and arch, and single and multistory frame structures. The examples in this thesis include well known test examples often treated in the literature.

1.4 Structural Shape Definition and Automatic Mesh Generation

In SSO, the manual preparation of FE analysis data for each optimization trial is discouragingly tedious, time consuming, error-prone and requires user intervention at each iteration. For these reasons, the geometric shape definition and automatic mesh generator are of prime importance in the automated structural optimization process. We present the mesh generation schemes used in this thesis for various types of structures considered in Chapter 3.

In the present work, a mesh generator for discrete structures has been developed which has the capability of the controlling mesh density distribution on the natural axis of the structure which is defined using parametric cubic splines. The mesh generator can generate meshes of two, three and four noded elements. Moreover, the thickness and distributed loading are interpolated from the key points to the nodal points using cubic splines. A bandwidth minimization is carried out before the boundary and loading conditions are transferred to the FE model. The mesh generator is also updating boundary condition and loading at each optimization iteration.

1.5 Structural Analysis

Structural analysis is a vital part of the overall design optimization task because one has to be able to predict structural behavior for various designs in order to guide the design improvement process.

Trusses: Matrix and FE methods for the analysis of truss problems are well developed and details of their formulation can be found in standard textbooks. These methods are reviewed in Chapter 4 for static and free vibration analysis and used for optimization of trusses in Chapters 8 and 9.

Beams, arches and frames: The FE method has proven to be an inexpensive and useful tool in the static and dynamic analysis of beam, arch and frame structures in 2D and 3D. Two basic theories are used for analysis. Thin beam theories neglect

4

transverse shear deformation and rotatory inertia effects and consequently may yield incorrect results, especially for higher values of the ratio of the thickness to length. For example, in beam and arch analyses, the frequencies are overestimated for all modes in shear weak situations and for the higher modes in shear stiff cases. In such circumstances, the effects of shear deformation and rotatory inertia should be taken into account. MR beam theory allows for transverse shear deformation effects and thus offers an attractive alternative to classical Kirchhoff-Love thin beam theory. The accuracy and relative performance of the elements are verified.

A formulation is developed to produce a family of MR, curved, isoparametric and variable thickness FEs which include shear deformation and rotatory inertia effects for static and free vibration analyses of beam, arch and frame structures in 2D and 3D.

1.6 Optimization Method Considered in This Thesis

In this thesis, GA is adopted for the optimization process. Here, it is important to note that GA requires no sensitivity analysis in the search method. The search method depends solely on the objective function information and mimics the 'survival of the fittest' process found in nature.

Most mathematical programming algorithms assume that the design variables are continuous, but in many practical problems in engineering like truss and frame structures, the design variables are discrete. This is what makes GAs so useful as they accept both discrete and continuous design variables.

1.6.1 Classification of structural optimization problems

Because of the wide variety of SSO problems encountered in practice, it is convenient to consider classifications based on several criteria.

5

Classification based on mode of behavior: In the first classification, problems are identified by the mode of behavior under consideration. Thus we have:

- *Static optimization* in which the structure is subjected to static external loads. Here, the aim of structural optimization is generally to obtain the best geometric shape for the structure so that it can carry the imposed loads safely and economically.

- *Dynamic optimization* in which the structure is subjected to dynamic forces or excitations of its supports. The aim of the structural optimization is generally to avoid resonance by maximizing the difference between the forcing frequency (or frequencies) and the natural frequencies of the structure, subjected to certain geometric restrictions.

Classification according to type of design variable: Alternatively, the form of structural optimization problem can usually be described by two types of design variables:

- In *sizing optimization*, sizing variables may be used to define the thickness and widths of rectangular or diameter of circular members or cross sectional areas of the structural components.

- In *shape optimization*, geometrical or shape variables may be used to define the structural geometry.

1.7 Software Developed in This Thesis

In this thesis, reliable, efficient and robust computer programs are developed to assist structural engineers in designing structurally efficient forms and provide considerable insight into the structural behavior. Five main computer programs have been developed and verified using benchmark examples for analysis and optimization:

- STATT deals with the static analysis and shape optimization of 2D and 3D trusses.

- FREET deals with the free vibration analysis and shape optimization of 2D and 3D trusses.

- BAFS-GA deals with static analysis and GA optimization of 2D and 3D beam, arch and frame structures.

- BAFF-GA deals with free vibration analysis and GA optimization of 2D and 3D beam, arch and frame structures.

- DYNABAF deals with the transient dynamic analysis of 2D and 3D beam, arch and frame structures.

All programs are written in FORTRAN 90 using double precision and run on LINUX mainframe and personal computers.

1.8 Layout of Thesis

This thesis consists of eleven chapters. The contents of each chapter are now briefly described:

- A literature survey for static, free vibration, transient analysis of truss, beam, arch and frame structures and some optimization algorithms are summarized in Chapter 2

- Chapter 3 covers various terms typically used for structural shape definition, the automatic mesh generation process occurring before FE analysis, and allocation of size/shape design information for structures.

- Chapter 4 describes the basic formulation for 2D and 3D static and free vibration trusses. The matrix displacement methods adopted are described.

- Chapter 5 presents the basic formulation for the static analysis of beam, arch and frame structures. The analyses are carried out using curved, variable thickness, isoparametric MR FEs.

- Chapter 6 describes the formulation for the free vibrations of beam, arch and frame structures. FEs based on curved, variable thickness, isoparametric MR theory are adopted.

- Chapter 7 gives a detailed review of important aspects of the GA. The flow chart of the GA optimization is explained.

7

- Chapter 8 includes static optimization examples for 2D and 3D truss, beam, arch and frame structures. Both shape and size optimizations are tested with continuous and discrete design variables or a combination of them.

- Chapter 9 includes free vibration optimization examples for 2D and 3D truss, beam, arch and frame structures. Comparisons are made with previous works.

- Chapter 10 describes the transient dynamic analysis and gives some time dependent analysis examples. The transient dynamic characteristics of optimized structures are dealt.

- Chapter 11 provides the conclusions of the present work and discusses the scope for further work.

CHAPTER 2

LITERATURE SURVEY

2.1 Introduction

Computer based structural analysis and optimization technologies have now passed their thirtieth birthday. Over these last three decades, Structural Optimization (SO) and FE analysis have been continually developed and improved so that these techniques have matured to become useful design tools. We now provide a brief and selective review of the literature on structural analysis and shape optimization which are limited to the type of structures and conditions considered in this thesis.

2.2 Static Analysis of Structures

The development of computing techniques has made it possible to study structural analysis problems with numerical methods, which are far more powerful than analytical approaches. During the last four decades considerable advances have been made in the applications of numerical techniques to analyze basic structural elements as well as highly sophisticated structures in various fields of engineering. Among these numerical procedures, the FE method is the most frequently used today for the solution of structural problems. With the versatility of the FE method and the availability of high-performance computers, extremely complicated and multi degree of freedom problems can now be solved with high accuracy [1-3].

FE method basically consists of point-wise discretization for the satisfaction of boundary conditions in terms of nodal values and interpolation of shape function, and piecewise discretization to simplify the assumed trial solution. There are a few different formulations for FE. The FE can be formulated based on the assumed displacement

field and the principle of the minimization of potential energy and it is called the displacement element, which is the most common one used. If the FE formulation is based on an assumed stress field and the principle of complementary potential energy, it is called an equilibrium element. There is a third kind of elements, which is called a mixed element. In mixed elements, force and displacement are the primary unknowns and treated as field variables [1].

Trusses: Detailed treatment of the matrix formulation for the analysis of linearly elastic trusses can be found in any text book [2-5]. Standard FE matrix displacement methods are used in this thesis for 2D and 3D static analysis, such as those mentioned in Chandrupatla and Belegundu [5].

Beams, Arches and Frames: The analysis of beam and arch structures is perhaps the most widely studied class of problems in engineering literature. The analysis of curved beams is quite complex due to the presence of bending stretching coupling and, including the effects of shear deformation and rotatory inertia add to the complexity. Many methods of analysis have been used to study the analysis of curved beams. Closed form solutions for classical arch geometries under various boundary conditions have been obtained to establish rough guidelines for the analysis of complex arch structures [6]. Various structural analysis procedures based on Rayleigh-Ritz, FE and differential quadrature element methods have also been used.

The FE approach has proved to be a powerful and widely applicable method for complex problems encountered by designers and considerable research work has been subsequently directed towards the improvement of solution accuracy and versatility of application as well as computational efficiency. The question of the choice of the proper FEs for the analysis of curved structures have been the subject of numerous papers and many authors have devoted their efforts to it [7-10]. A variety of new elements have been proposed based on different structural theories (e.g. Kirchhoff-Love, MR theories), interpolation functions and formulation procedures (e.g. assumed strain methods and hybrid/mixed methods) in order to achieve a more accurate prediction of the structural response. The elaboration of the

10

simple FE, which would give the correct results for the wide range of elements, still remains the main goal of their work.

The development of FE for a curved beam has received considerable attention in recent years. Before proceeding, we will briefly review more recent achievements with particular attention to element derivations.

- Analytical solution of MR straight and curved beam is certainly valuable for basic understanding of analysis of frame (beam) and arch structures. There has been much achievement in computational methodology for arch analysis in the past two decades. Shape functions are formed from the product of two-dimensional polynomials and appropriate basic functions, which ensure the satisfaction of piecewise boundary geometric conditions [14].

- Lee and Sin [15] presented a formulation of a curved beam element with 3 nodes of curvature to eliminate the shear/membrane locking phenomenon. The element is based on curvature so that it may represent the bending energy fully, and the shear/membrane Strain Energy (SE) is incorporated into the formulation by the equilibrium equations.

- Litewka and Rakowski [8] derived the exact stiffness matrix for a thick, curved beam element with constant curvature. The plane two-node six degree of freedom element was considered in which effects of flexural, axial and shear deformations was taken into account. The analytical shape functions describing radial and tangential displacements as well as cross-section rotations were found in the algebraic trigonometric form.

- Two node (three degree of freedom per node) FE for curved shear deformable beams was developed by Friedman and Kosmatka [16]. The element formulation is based on shape functions that satisfy the homogeneous form of the partial differential equations of motion which renders it free of shear and membrane locking.

- FE methods for Timoshenko beam, circular arch and MR plate problems were discussed by Cheng et al. [17]. In this study, to avoid locking phenomenon, the reduced integration technique was used and a bubble function space was added to increase the solution accuracy.

11

- The behaviors of MR arch element are usually very good and it is only in shear stiff thin beams that real problem arise. In thin, displacement based elements, full integration of stiffness matrices leads to locking or over-stiff behavior and reduced integration process is required to overcome these difficulties [11].

- Zhang and Di [18] presented accurate two-noded FEs which were derived from the potential energy principle and the Hellinger–Reissner functional principle respectively. They introduced the internal displacement parameters in developing a high-order related displacement-rotation interpolation field.

- Chapelle [19] defined an approximation procedure based on a discretization by linear Timoshenko beam elements for arbitrary three dimensional rods and established optimal error estimates independent of the thickness, thereby proving that shear and membrane locking was avoided.

- A shear-flexible three-noded curved beam element based on coupled displacement field interpolation is proposed by Raveendranath et al. [20]. The shear flexibility was based on Timoshenko beam theory and the element has three degrees of freedom.

- The plane two-node curved beam FE with six degrees of freedom was considered by Litewka and Rakowski [8]. Knowing the set of 18 exact shape functions their approximation was derived using the expansion of the trigonometric functions in the power series.

- Kim and Kim [21] showed the use of nodeless degrees of freedom in developing a highly accurate, locking free hybrid-mixed $C(0)$ curved beam element. In the performance evaluation process of the field-consistent higher-order element, the effect of field consistency and the role of higher-order interpolation on both displacement-type and hybrid-mixed-type elements were carefully examined.

- The effect of shear deformation on deflection and shear deformation together with rotatory inertia on natural and cross over frequencies of curved beams were obtained using a cubic linear beam element having 4 degrees of freedom per node by Krishnan and Suresh [22].

All the above-mentioned studies have been successfully applied to achieve locking free elements with different levels of accuracy. Most of the formulations dealt with

two or three noded curved beam element. It has been noticed that higher accuracy of some of these elements is at the cost of more complex mathematical formulations. The literature review indicates the need to develop simpler and more accurate curved beam elements which can handle both straight and curved situations as well as *thick*, *thin* and *variable thickness* cases.

Initially, when FE based models were first introduced, Kirchhoff-Love (or Euler-Bernoulli) formulation were favored and strictly required $C(1)$ inter-element continuity although this condition was relaxed with non-conforming elements which had to pass the patch test to ensure convergence. Subsequently, MR (or Timoshenko) formulations came into vogue. Unfortunately, MR elements tended to lock or exhibit over stiff behavior in shear-weak (e.g. thin) situations. Reduced integration [11] of the element stiffness matrices helped to overcome such difficulties in many cases but introduced the accompanying problem of mechanisms or zero (or low) energy modes which in turn led to unreliable results. Over the years many researches have been carried out to improve our understanding of such elements and indeed many new elements have been developed. For example, assumed strain elements [12,13] avoid locking, contain no mechanisms, are convergent and provide general good behavior.

The elaboration of the simple FE, which would give the correct results for the wide range of elements, still remains the main goal of their work. In this thesis the variable thickness curved beam element is considered. The structures are modeled using linear, quadratic or cubic, curved, variable thickness, $C(0)$ continuity MR FEs. These belong to a family of elements introduced by Potts and Day [23] and subsequently extended by Hinton and co-workers [14]. This element has over performance than Kirchhoff-Love based FE. In this present study the shell element extended by Hinton and his coworkers will be adapted to curved beam element.

2.3 Free Vibration Analysis

Truss, beam, arch and frame structures are quite common. Examples of these structures abound in contemporary society and in engineering practice: multistory

buildings, bridges, roofs, transmission towers and automobile chassis --- the list almost endless. Our knowledge of the dynamic behavior of these structures and components is vital for sound design.

The literature contains results of many FE studies of truss, beam, arch and frame structures in free vibration situations. However, the author could find few references in the literature to the FE based on MR beam theory for free vibration analysis of variable thickness structures which may be curved in cross-section.

Studies which have been carried out on free vibration analysis of curved and straight Timoshenko beams can be summarized as follows:

- Mou et al. [24] derived the exact dynamic stiffness matrix for the transverse vibration beams whose cross-sectional areas and moment of inertia vary in accordance to any two arbitrary real-number powers. This approach enabled most beams to be modeled by just one element, and for beams having abrupt profile changes or with very complex profiles.

- Rossi et al. [25] reported numerical experiments performed on vibrating orthogonal beam grillages rigidly clamped at two adjacent edges. The first five natural frequencies of transverse vibrations were determined by using a FE code based on Timoshenko's mathematical model. Dynamic stiffening was successfully achieved in orthogonal grillages by judiciously introducing discontinuities in the thicknesses of beam element.

- Corn et al. [26] proposed a new method for simply and systematically constructing finite beam elements. The continuous model considered both rotary inertia and transverse shear deformation.

- Howson and Jemah [27] presented a method for finding exact out-of-plane natural frequencies of plane structures composed of curved Timoshenko beams. The required natural frequencies correspond to the roots of a transcendental eigenvalue problem and any natural frequency could be obtained with certainty to any desired accuracy, by using a modification to a well-established algorithm, which ensures that no natural frequencies could be missed.

14

The following studies mentioned about stepped beams, discontinuities in the thickness and tapered beams.

- Lee and Lee [28] presented a FE method based on the basis of a first-order shear deformation beam theory for the analysis of free vibration of arbitrarily stepped beams and investigated effects of shear deformation, step geometry, step eccentricity and multiple stepped sections and also analyzed phenomenon of dynamic stiffening.

- Gupta [29] derived stiffness and consistent mass matrices for linearly tapered beam element of any cross-sectional shape in explicit form. The variation of the area and moment of inertia of cross-section along the axis of the element exactly represented by simple functions involving shape factors.

- Stanley and Ganesan [30] analyzed cantilever beams with discontinuity in the thickness subjected to harmonic point load. A beam element with two degrees of freedom per node was used for the analysis. Three beam models were analyzed for possible reduction of maximum displacement and maximum stress by choosing discontinuity at different locations.

- Free vibrations of Bernoulli beams of bilinearly varying thickness were studied by Laura et al. [31] by using the optimized Rayleigh-Ritz method, the differential quadrature technique and the FE approach. The fundamental frequencies of vibration of the structural elements as determined by the optimized Rayleigh-Ritz method and the FE approach which showed good agreement while rather considerable discrepancies were found when using the differential quadrature technique was determined.

- Houmat [32] presented variable order Timoshenko beam FE and formulated in terms of a cubic polynomial and a variable number of trigonometric sine terms for both the transverse displacement and the rotation of the beam cross-sections. Advantage of this element is that highly accurate frequencies for Timoshenko beams can be obtained with small number of system degrees of freedom.

Cross section variations of curved beams were studied by the following researchers:

- Krishnan and Suresh [33] presented a two-node FE model with four degrees of freedom per node that gives satisfactory results for static and free vibration

15

behavior of arches of varied curvatures and thicknesses. The element developed in Cartesian coordinates and Margurre's shell theory was adapted to obtain bending-stretching coupling.

- Auciello and Rosa [34] presented a critical brief review of the free dynamics of circular arches. A simple and efficient method was proposed, which allows one to take into account quite naturally the cross-section variations and the presence of flexible supports. Uniform arches with rotationally flexible and axially flexible supports have been extensively examined, together with three different kinds of stepped arches and two different arches of linearly varying cross-section.

- Morales [35] applied Rayleigh-Ritz based substructure synthesis method to the dynamic analysis of multi-story framed structures. Because these structures were multiply supported, it was necessary to combine a suitable kinematical procedure with a constraining process.

- Lee et al. [36,37] proposed an efficient numerical method calculating vibration mode shape derivatives of the proportionally and non-proportionally damped systems with multiple eigenvalues. The method was found to be efficient in the case of the multiple eigenvalue problems since the computer storage and analysis time required were smaller than those of Dailey's method.

- Baychev [38] presented formulas and algorithms for more efficient application of FE method in the static and dynamic analysis of frames with variable characteristics. Numerical formulation of the stiffness matrix, load vector and mass matrix were presented for frame elements with smoothly varying geometrical and physical characteristics according to the arbitrary law. The greater amount of input data for a single element with variable characteristics was compensated by the less number of elements necessary for the structure modeling.

2.4 Transient Dynamic Analysis

This thesis is also concerned with the transient dynamic behavior of the optimum structures subjected to dynamic loads. Dynamic means time varying and the application and/or removal of the loads necessarily varies with time [39]. Moreover,

the response such as resulting deflections, internal stresses, etc. of a structure resisting such loads is also time dependent or dynamic in nature.

There are many different mathematical models to solve dynamic equilibrium equations [3]. These methods are mode superposition and direct integration.

Mode Superposition Methods: Mode superposition analysis is ideally suited for situations where the dynamic disturbance is confined to the lowest modes of vibration system, and the duration of the disturbance is relatively long [40].

Direct Integration Methods: A direct integration analysis should be conducted in situations when a large number of vibration modes must be included in response calculations. This is generally the scenario for structures subjected to high-intensity, short duration impulse type loading, such as shock or blast load. Finally, for nonclasically damped systems or systems exhibiting any nonlinear characteristics a direct integration analysis is required [3,40,41]. Numerical techniques can fundamentally be classified as either explicit or implicit integration methods;
a) Explicit Methods
- Central Difference Method
b) Implicit Methods
- Newmark Family Methods
- Houbolt Method
- Wilson θ Method
- Hilber, Hughes and Taylor α Method

Explicit Methods: The discrete multi degree of freedom system equilibrium equations are a set of simultaneous ordinary differential equations with constant coefficients. Therefore, any convenient finite difference expressions that approximate the acceleration and velocities in terms of the displacements may be used. However, only a small number of finite difference expressions would render an effective solution scheme. One particular finite difference algorithm that has proved

to be quite effective in these types of applications is the central difference method [3].

Implicit Methods: Focusing attention on the inertial class of dynamical elasticity problems, implicit methods are attractive (although some analysts prefer explicit methods). The implicit *Houbolt* method [42] was developed in 1950 and is one of the earliest employed for the calculation of the structural response of an airplane subjected to dynamic loads. It uses the concept of displacement difference equivalents to approximate the velocity and acceleration components, and thereby establishes a recurrence relation that can be used to solve for the step-by-step response of the structure. In the Houbolt method, the generality and physical aspects of the basic equilibrium are preserved. From a stability and accuracy point of view, it is unconditionally stable, second-order accurate, and is not suitable for higher frequency dynamic problems. A disadvantage is the need to use a large historical data pool.

In 1959, *Newmark* [43] introduced an implicit method of computation for the solution of problems in structural dynamics. The algorithm assumes that the average acceleration is constant over an integration time step. Belytschko and Hughes [44] document the Newmark- β family of approaches which are either implicit or explicit depending upon the choices of the two free parameters which control the stability and accuracy of the algorithms. As an implicit scheme, the Newmark method is unconditionally stable and second-order accurate. As an explicit scheme, the Newmark method is only conditionally stable and second-order accurate.

The *Wilson*-θ method [41] is essentially an extension of the average acceleration approximation in which the variation between time levels n and n+1 is assumed to be linear. In particular, the Wilson-θ method assumes that the acceleration is linear between t and t+θ, with $\theta \geq 1.0$. It is indicated that when θ= 1.4 the obtained solution is most accurate and stable [44,45].

Park [46] developed a stable algorithm applicable for both linear and nonlinear structural dynamic problems which retains good accuracy in the low frequencies and strong dissipative characteristics in the high frequency regime. The Park method is unconditionally stable and second-order accurate. However, the method requires a large historical data pool.

Zienkiewicz and co-workers [47,48] described a different class of recurrence formulae for the equations of motion using a weighted residual approach. Several previously described algorithms were identified as special cases of these formulations. The collocation methods generalize and combine aspects of the Newmark and Wilson methods. The collocation methods can be adjusted to reduce to either the Newmark or the Wilson methods and an analysis of these is contained in *Hilber and Hughes* [49].

It has been long recognized that many basic problems of mechanics, including those of vibration, are nonlinear. Although the linear treatments commonly adopted are quite satisfactory for most purposes [3,40,41]. Contribution to the linear dynamic analysis of structures have been made by Velestos and Ventura [50] Clough and Penzien [51], Wilson and Itoh [52], Wilson et al. [53], Caughey [54], İbrahimbegoviç and Wilson [55], Choi and Park [56].

Hence, a solution for dynamic response is commonly sought through the modal transformation that employs a set of real mode shapes. Some possibilities for generating a set of vectors for modal transformation are the Rayleigh-Ritz approximations [51], exact undamped eigenvectors [52] or load-dependent Ritz vectors [53]. Two other possibilities for the solution of the set of coupled modal equations are a step-by-step procedure [57] and further modal transformation to the uncoupled form by solution of the quadratic eigenvalue problem for the set of modal equations [58].

İbrahimbegoviç and Wilson [55] proposed an integration algorithm, which produce an exact solution for proportional damping and for loading that varies linearly within

an arbitrary time interval. Choi and Park [56] developed a method, was based on transformation of dynamic loads into equivalent static loads. This method seems feasible for SO of dynamic systems.

In *nonlinear dynamic analysis* of structures the incremental equation of motions are often solved using the Newmark method in conjunction with the pseudo force method, which is reviewed in detail in Subbaraj et al. [59]. Kasımali [60] and Saka and Hayalioğlu [61] employed a method for the nonlinear response of an in-plane frame with prismatic members, subjected to external loads applied at the joints. The displacement restrictions are kept large enough to allow the frame to have comparatively large deflections.

2.5 Optimization Algorithms

Analytical methods for solving SO problems have been used for a long time. During the last 30 years, optimal structural design has received considerable attention. The development of powerful computers and the implementation of efficient general algorithms have stimulated renewed interest in this field, which is as old as structural engineering [62-65]. One of the first treatments of the problem of selecting an optimum shape of a structure is done by Zienkiewicz and Campbell [65]. They used the FE method with node coordinates as design variables to find an optimum shape. In the field of optimal design of structures, the main emphasis and most significant progress have been SO in static and dynamic situations [63].

Many methods and algorithms have been developed for optimum design of structural systems in the last three decades. Most of the methods deal with continuous design variables and use mathematical programming techniques. In most practical design problems, the design variables are discrete. This is due to the availability of standard sizes and their limitations for construction and manufacturing reasons. A number of methods have been reported for optimum deign of discrete structural systems [66,67] In general optimization techniques used in structural engineering design can be categorized into four distinct approaches: (1) mathematical programming; (2) optimality criteria methods; (3) heuristic search methods (GA); and (4) evolution

strategies. Several textbooks discuss these methods, among them Reklaitis et al. [68], Vanderplaats [69], Arora [70], Brandt [71], Haftka and Gurdal [72], and Adeli [73]. Review papers Vanderplaats and Thanedar [74], Schittkowski et al. [75], Arora et al. [76], and Huang and Arora [77] also illustrate methods applied for mixed discrete-integer, continuous variable nonlinear optimization for structural design applications with the focus on problems having linked discrete variables. These methods as well as the literature review are presented in the following sections.

2.5.1 Mathematical programming

The mathematical programming optimization algorithms make use of the information supplied by the FE analysis and sensitivity analysis. However, there is no single efficient method available for solving all optimization problems. Hence a number of mathematical programming optimization algorithms have been developed for solving different types of optimization problems. The most common mathematical programming optimization methods used in SSO are: sequential linear programming Zienkiewicz [65], Vanderplaats [69], sequential quadratic programming Vanderplaats [69] and the method of moving asymptotes Svanberg [78].

Mathematical programming can be subdivided into linear and nonlinear programming. The major characteristics of linear programming are that the objective functions and the associated constraints are expressed as a linear combination of the design variables. To apply linear programming techniques to structural optimization, the relationship between the objective function and the constraints to the design variables have to be linearized [79-81]. However, when a linear relationship is used to model a nonlinear structural response, errors are inevitable.

Nonlinear mathematical model is developed for nonlinear unconstrained optimization problems. The well-known Kuhn-Tucker conditions [82] provide the necessary conditions for optimal solutions. Direct application of the Kuhn-Tucker conditions is extremely difficult for most problems. The calculation of gradients and the solution of the correlated nonlinear equations prohibit the direct application of the Kuhn-Tucker conditions for most engineering situations.

21

2.5.2 Optimality criteria

Optimality criteria methods are developed from indirectly applying the Kuhn-Tucker conditions of nonlinear mathematical programming combined with Lagrangian multipliers [70]. Optimality criteria methods are based on continuous design variables. For the case where discrete variables are desired using optimality criteria methods a two-step procedure is typically used. First, the optimization problem is solved using continuous variables. Second, a set of discrete values is estimated by matching the values obtained from the continuous solution. Optimality criteria methods use a single cross-sectional property of a structural member as the design variable. All other cross-sectional properties are expressed as a function of the selected design variable. Optimization using optimality criteria methods have been widely applied in engineering design [61,83,84].

Ding [62] reviewed numerical and analytical methods for SSO. Tadjbakhsh [64] developed an algorithm which determines the optimum profile of an arch considering the stability constraints. Zhou and Rozvany [85] used optimality criterion to optimize structures.

Uzman and Daloğlu [9] used optimality criteria method to develop an optimum design of arch structures with uniform and/or varying cross section subjected to displacement, stresses and minimum depth constraints. The optimality criteria method was employed to obtain its solution which was reported to be quite effective in solving nonlinear optimum design problems by Saka and Hayalioğlu [61] and Saka and Ülker [86].

Optimum design of frame structures including stability constraint along with stress and displacement constraints has been reported by Barsan [87], Lin and Liu [83] and Pezeshk and Hjelmstad [88] using optimality criteria methods and Karihaloo and Kanagasundaram [89] using a non-linear mathematical programming method.

22

2.5.3 Genetic Algorithms

GAs are an evolutionary optimization approach which are an alternative to traditional optimization methods. GA are most appropriate for complex non-linear models where location of the global optimum is a difficult task. It may be possible to use GA techniques to consider problems which may not be modelled as accurately using other approaches. Therefore, GA appears to be a potentially useful approach.

GA is a fairly new optimization technique based on the Darwinian survival of the fittest theory. The method has been proposed first by John Holland in 1975 [90] at the University of Michigan, but has not become popular until one of his graduate students Goldberg in 1989 [91] applied it to solve a difficult problem.

John Holland was one of the first developers of artificial reproduction schemes. A good introduction to the topic is found in his book *Adaptation in Natural and Artificial Systems* [90]. Goldberg [91] has written an excellent survey text on GAs which is highly recommended. A good survey article is found in Forrest [92].

Philosophically, GAs are based on Darwin's theory of survival of the fittest. Since then GA have been used in many science and engineering fields to successfully solve optimization problems. A detailed information for GAs is given in references [90-95]. GA represents a step forward in the optimization field because they are a "weak" method.

The core characteristics of a GA are based on the principles of survival of the fittest and adaptation and the ability to deal with discrete optimum design problems and do not require derivatives of functions, unlike classical optimization. The advantages of applying a GA to optimized design of structures include discrete design variables, open format for constraint statements and multiple load cases [96]. A GA does not require an explicit relationship between the objective function and the constraints. Instead, the value of the objective function for a set of design variables is adjusted to reflect any violation of the constraints.

23

Many research works have been recently reported for the solution of SO problem via GAs. Optimization using GAs have been successfully applied to structural design by Goldberg and Samtani [97], Lin and Hajela [98] and Rajeev and Krishnamoorthy [94]. Hayalioğlu [93] presented a GA which is applied to the optimum design of geometrically non-linear frames made of an elastic-plastic material.

Adeli and Cheng [95] presented optimization of space structures by integrating GA with the penalty function method. Subsequently, Adeli and Cheng [95] presented an improved augmented Lagrangian GA for the optimization of space structures, where the problem of the trial-and-error selection of the initial value for the penalty function coefficient is avoided.

2.5.4 Evolution strategies

Generally, evolutionary algorithms require more function evaluations than gradient-based methods. The investigation of different techniques is important to speed up these algorithms. The advantages of applying these optimization techniques are discussed in many textbooks such as Arora [70], Brandt [71], Haftka and Gurdal [72], Adeli [73], and Xie and Steven [99]. These advantages can be summarized as follows:

- Some optimization techniques do not need any prior information about the objective function or constraint functions.
- The possibility and flexibility of dealing with complex structures under different loading conditions and constraints.
- The ability of dealing with sections from standard catalogues classified as discrete design variables.
- The capability of achieving more than one design solution.
- The flexibility of formulating the engineer experiences and skills into the design optimization problem. For examples, the number of design variables, the linking of the design variables to the structural members, the acceptance of the design obtained according to the practical experiences of the designer.

During the last fifteen years there has been a growing interest in problem solving systems based on algorithms, which rely on analogies to natural processes. The best-known algorithms in this class include evolutionary programming, GAs, and evolution strategies. Evolution-based [100] algorithms maintain a population of potential solutions. Evolution strategies [101] are the application of combinatorial optimization methods based on probabilistic searching. These algorithms have some selection process based on fitness of individuals and some recombination operators. Both evolution strategies and GAs imitate biological evolution in nature and combine the concept of artificial survival of the fittest with evolutionary operators to form a robust search mechanism.

When a gradient-based optimizer is used the most time-consuming part of the optimization process is devoted to the sensitivity analysis phase, which is an important ingredient of all mathematical programming optimization methods [102]. On the other hand evolution strategies, do not need gradient information and therefore avoid performing the computationally expensive sensitivity analysis step [103]. Furthermore, it is widely recognized that combinatorial optimization techniques are in general more robust and present a better global behavior than mathematical programming methods. They may suffer, however, from a slow rate of convergence towards the global optimum.

Xie and Steven [99] has proposed evolution strategies optimization and some examples of this method for problems with stress or frequency or stiffness constraints can be found in [99,104].

2.5.5 Multi-objective optimization problem

In the practical optimization problems, usually more than one objective are required to be optimized, such as, minimum mass or cost, maximum stiffness, minimum displacement at specific structural points, maximum natural frequency of free vibration, minimum structural SE while all the constraints are satisfied. The constraints provide bounds on member stress, deflection, frequency, local buckling, dynamic response, etc.

This makes it necessary to formulate a multi-objective optimization problem, and look for the set of compromise solution in the objective space. More and more design problems can now be optimized using a variety of algorithms. Despite the advancements in SO, a solution to an optimization problem involving a large number of design variables and constraints is still less tractable from a computational view in that the computational cost is a highly nonlinear function of the problem size. The multilevel decomposition technique is probably a good solution to the difficulty [105]. This technique decomposes the original optimization problem into a set of sub-problems, and each of them can be optimized independently.

2.5.6 Other optimization aspects

Salajegheh [106] presented an efficient method for optimum design of frame structures, using approximation concepts. A dual strategy in which the design variables can be considered as discrete variables was used. A two level approximation concept was used. In the first level, all the structural response quantities such as forces and displacements are approximated as functions of some intermediate variables. Then the second level approximation is employed to convert the first-level approximation problem into a series of separable forms, which can be solved easily by dual methods with discrete variables. In the second level approximation, the objective function and the approximate constraints are linearized. The objective of the first level approximation is to reduce the number of structural analyses required in the optimization problem and the second level approximation reduces the computational cost of the optimization technique.

Saka and Kameshki [107] presented an algorithm for the optimum design of unbraced rigid frames, which takes into account the non-linear response of the frame due to the effect of axial loads. It considers the sway constraints and combined stress limitations in the design problem.

In the traditional optimization algorithms, constraints are satisfied within a tolerance defined by a crisp number. In actual engineering practice, constraint evaluation involves many sources of imprecision and approximation. When an optimization

algorithm is forced to satisfy the design constraints exactly, it can miss the global optimum solution within the confine of commonly acceptable approximations. Sarma et al. [108] presented extending the augmented Lagrangian GA of Adeli and Cheng [95] a fuzzy augmented Lagrangian GA for optimization of steel structures subjected to the constraints of the AISC allowable stress design specifications taking into account the fuzziness in the constraints.

To address the problem of non-convex solution spaces, which arise due to dynamic response constraints, researchers [109] have investigated the application of stochastic search techniques. The uses of stochastic optimization algorithms pose challenges for the incorporation of approximation concepts in design space search. This is primarily due to the fact that stochastic search techniques do not make use of line search procedures, and hence conventional approximation concepts, which are valid only for small changes, become useless for predicting the modified design characteristics. Recent research [110] at the Computational Engineering and Design Center has focused on the development of algorithmic frameworks for integrating approximation concepts with genetic search procedures. However, to fully exploit the potential of such frameworks, there exists the requirement for approximation concepts which are valid for large changes in the design variables.

Nair et al. [110] proposed a reduced basis approximation method for approximation of eigenvalues and eigenvectors. The terms of a local approximation based on Taylor or matrix power series were used as basis vectors for approximating the perturbed eigen parameters. For each eigenmode, a reduced eigensystem was generated by using the baseline eigenvector and the first-order approximation term as Ritz vectors. The solution of the reduced eigensystem laid to two possible estimates of each perturbed eigenvalue and eigenvector.

CHAPTER 3

STRUCTURAL SHAPE DEFINITION AND AUTOMATIC MESH GENERATION FOR FRAME AND ARCH STRUCTURES

3.1 Introduction

The spline and mesh generation techniques discussed herein, are used for the subsequent FE analysis. The spline and mesh generation process is coupled together as an automatic pre-processing routine, incorporated within the FE analysis code. It serves to alleviate the laborious, monotonous task of data preparation and subsequent mesh generation, and also helps to reduce the risk of errors in initial input data.

The mesh generator is capable of generating two, three or four noded elements of specified size, along a cubic spline. The merits of using parametric representations such as cubic splines become obvious when considering an arch built up of multiple elements. Typically under a Cartesian approach, numerous coordinates need to be specified for each element. Parametric spline representation simplifies the curved member definition by implementing a coordinate system independent of the shape of the curved structures [111].

Another advantage of using cubic splines is the ability to interpolate pressure loading and thickness information from spline key points to mesh nodal points. Cubic splines are the typical and most favorable choice for representing curved shapes due to their simplicity and numerical stability. The three main types of cubic spline curves are: Ferguson, Bezier, and cubic-B spline curves. The difference between them are shown in Figure 3.1 and described in further detail in the chapter.

28
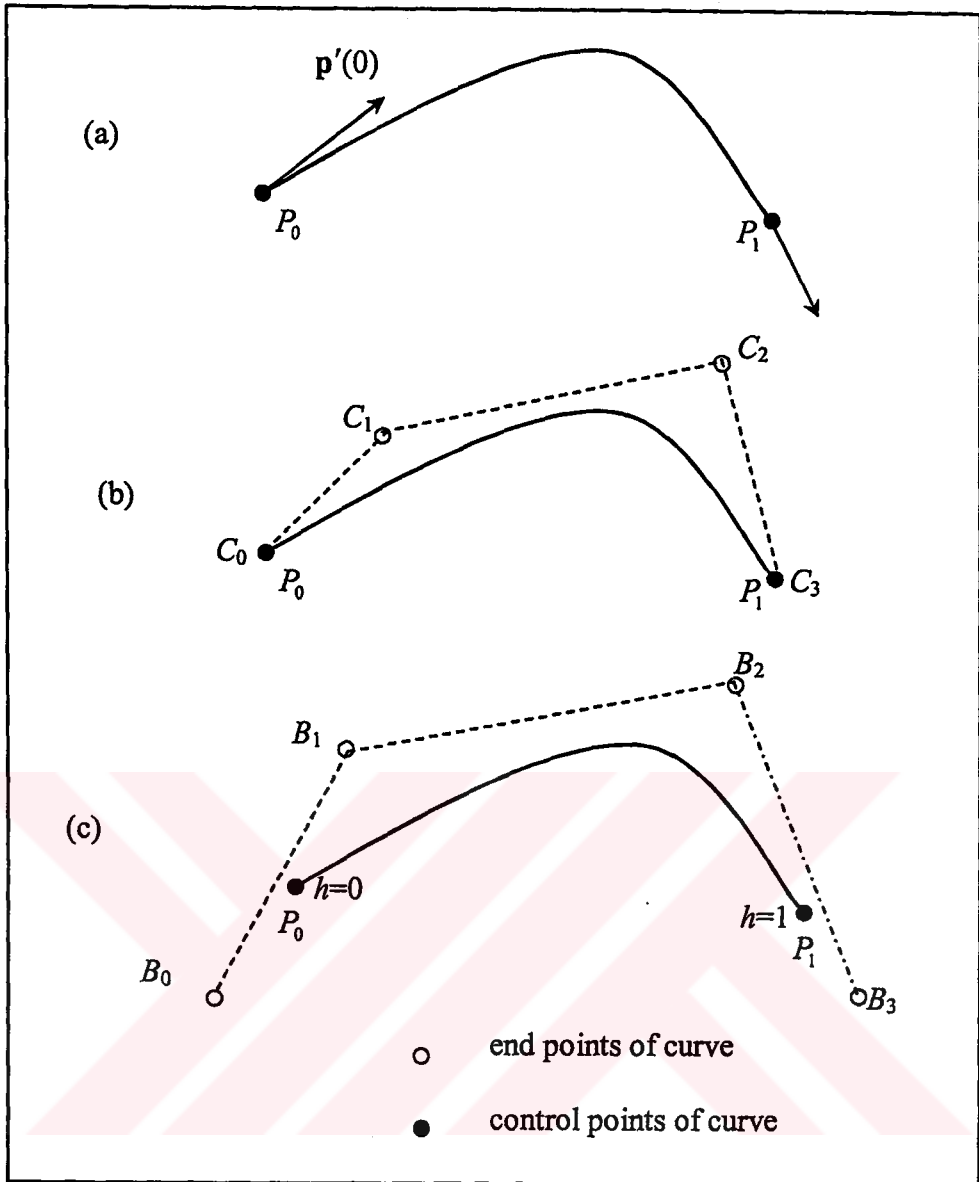
Figure 3.1 Three equivalent representations of a cubic spline curve:
(a) Ferguson representation, (b) cubic Bezier representation and
(c) cubic B-spline representation

Among the various types of curves used for representing a shape, cubic splines are the most popular. The cubic spline is the spline of lowest degree with $C(2)$ continuity which meets the needs of most problems arising in practical applications [112]. Further, it is numerically simple to handle and stable. Cubic spline curves (Ferguson curves), cubic B-spline curves and cubic Bezier curves may be regarded as certain varieties of the cubic spline functions. The basic difference is that in the Ferguson representation, the cubic spline curve is expressed in terms of the position

coordinates of a set of points and their corresponding tangents, whereas in the Bezier and B-spline representations the curve is represented in terms of control points of a polygon. This scheme is particularly advantageous when fitting of the curve is to be done interactively. The iterative process of spline fitting involves a first, initial curve approximation via a control polygon. Adjustment of the curve shape is then done in subsequent iterations by updating the positions of the polygon vertices, and sometimes the addition of new polygon control points. After a small number of iterations, an accurate curve representation is made. It should be noted that all three methods produce the same curve when fitted through a given set of data points.

To avoid the time consuming iterative procedure mentioned above, a modified cubic-B spline curve representation was implemented within the FE code.

In this chapter a flexible system of representation is used which offers facilities for both interpolation and interactive manipulation. This can be achieved by the process of inverse design i.e. for a given set of points on the curve, the corresponding vertices of the control polygon are found. Using this procedure the exact location and number of vertices of the polygon can be determined and, furthermore, the cubic spline curve passes through the given set of points. In the next section a brief mathematical description of the three equivalent representations of parametric cubic curve segments will initially be given to avoid any confusion arising from the terminology. Later, the method adopted in the present work will be described with details regarding the computer implementation. In the following section, the integration of automatic mesh generation and the shape definition procedures will be described.

3.2 Structural Shape Definition

This section defines the differences between the Bezier, Ferguson and interactive cubic-B spline representations for a simple example. For the curve of end points P_0 to P_1 (see Figure 3.1), with the parametric coordinate h, which varies along the curve segment from 0 to 1 respectively, and for a curve of 4 points, h is evenly distributed

as 0, 0.333, 0.666, 1. The position vector of any point on the curve is $p(h)$, and can be represented for cubic splines as:

$$[p(h)]^T = HRM \tag{3.1}$$

$$H = [h^3 \quad h^2 \quad h \quad 1] \qquad 0 \leq h \leq 1 \tag{3.2}$$

The **R** and **M** matrices vary for each of the three cubic splines, and are now classified.

For the Ferguson cubic spline segment shown in Figure 3.1(a)

$$R = R_{fer} = \begin{bmatrix} 2 & -2 & 1 & 1 \\ -3 & 3 & -2 & -1 \\ 0 & 0 & 1 & 0 \\ 1 & 0 & 0 & 0 \end{bmatrix} \quad \text{and} \quad M = M_{fer} = \begin{bmatrix} p(0)^T \\ p(1)^T \\ p'(0)^T \\ p'(1)^T \end{bmatrix} \quad 0 \leq h \leq 1 \tag{3.3}$$

where the position vectors $p(0)$ and $p(1)$ have associated tangents $p'(0)$ and $p'(1)$ at $h = 0$ and $h = 1$ of the curve at the starting and end points of the curve segment respectively. This representation is simple and suitable for numerical computation.

For the cubic Bezier spline curve shown in Figure 3.1(b)

$$R = R_{bez} = \begin{bmatrix} -1 & 3 & -3 & 1 \\ 3 & -6 & 3 & 0 \\ -3 & 3 & 0 & 0 \\ 1 & 0 & 0 & 0 \end{bmatrix} \quad \text{and} \quad M = M_{bez} = \begin{bmatrix} c_0^T \\ c_1^T \\ c_2^T \\ c_3^T \end{bmatrix} \quad 0 \leq h \leq 1 \tag{3.4}$$

where c_0, c_1, c_2 and c_3 are the position vectors of the control vertices C_0, C_1, C_2 and C_3 of the polygon representing the curve. It can be readily observed from Figure 3.1(b) that for the cubic Bezier curve, vertices C_0 and C_3 coincide with the parametric positions $h = 0$ and $h = 1$ (start and end points) respectively.

The cubic B-splines **R** and **M** matrices follow the same logic as for the Bezier curve, with control vertices B_0, B_1, B_2, B_3, having respective position vectors b_0, b_1, b_2, b_3. In this case however, vertices B_0 and B_3 do not coincide with the curve end points.

$$R = R_B = \frac{1}{6}\begin{bmatrix} -1 & 3 & -3 & 1 \\ 3 & -6 & 3 & 0 \\ -3 & 0 & 3 & 0 \\ 1 & 4 & 1 & 0 \end{bmatrix} \quad \text{and} \quad M = M_B = \begin{bmatrix} b_0^T \\ b_1^T \\ b_2^T \\ b_3^T \end{bmatrix} \quad 0 \le h \le 1 \qquad (3.5)$$

3.2.1 The cubic B-spline representation

For the shape definition of structures we have adopted the B-spline representation of the cubic spline curve, which is represented by Eq (3.5). Joining the end points of vectors $b_0,...,b_3$ forms the B-characteristic polygon. All the points on the B-spline curve lie within the convex hull of the corresponding B-characteristic polygon.

The tangent at any point on a cubic B-spline curve can be computed using the expression

$$p'(h) = [3h^2 \quad 2h \quad 1 \quad 0]R_B M_B \qquad 0 \le h \le 1 \qquad (3.6)$$

and the curvature at any point on a cubic B-spline curve can be computed using

$$p''(h) = [6h \quad 2 \quad 0 \quad 0]R_B M_B \qquad 0 \le h \le 1 \qquad (3.7)$$

The following relations can be easily derived from the above equations for a cubic B-spline curve segment and are very useful for manipulation and computer implementation of shape definition [113].

$$p(0) = 1/6(b_0 + 4b_1 + b_2) \qquad \text{and} \qquad p(1) = 1/6(b_1 + 4b_2 + b_3)$$

$$p'(0) = 1/2(b_2 - b_0) \qquad \text{and} \qquad p'(1) = 1/2(b_3 - b_1)$$

$$p''(0) = (b_2 - b_1) + (b_0 - b_1) \qquad \text{and} \qquad p''(1) = (b_3 - b_2) + (b_1 - b_2) \qquad (3.8)$$

All these relations have a geometrical interpretation. For example, consider Figure 3.2, which shows some of the geometrical features of the cubic B-spline curve segment mentioned above. The starting point P_0 is on the median $B_1 B_1^*$ of the triangle $B_0 B_1 B_2$ and the tangent vector $p'(0)$ at this point is parallel to the side $B_0 B_2$ of the triangle and the magnitude of $B_0 B_2$ is twice that of $p'(0)$. A similar geometrical characteristic can also be described for the end point P_1.
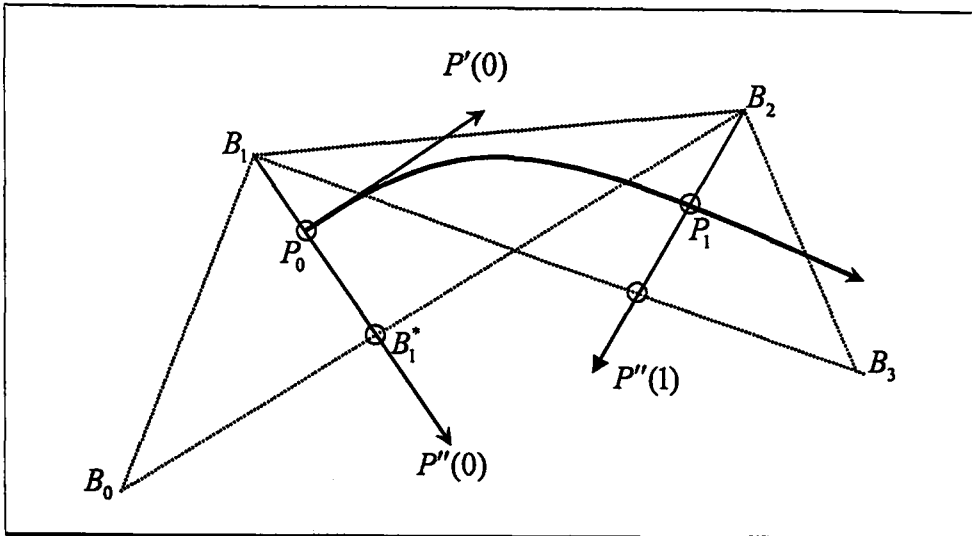
Figure 3.2 Geometrical properties of the cubic B-spline representation

3.2.2 Terminology

At this stage it is convenient to define certain terms, which will be used frequently in this thesis. The profile of typical structures is shown in Figure 3.3 and is formed by an assembly of segments. Further each segment is formed by an assembly of sub-segments passing through certain key points all of which lie on the midsurface of the structure. Each subsegment is a cubic spline curve and spans between two adjacent key points within a segment. Some key points are common to different segments at their points of intersection.
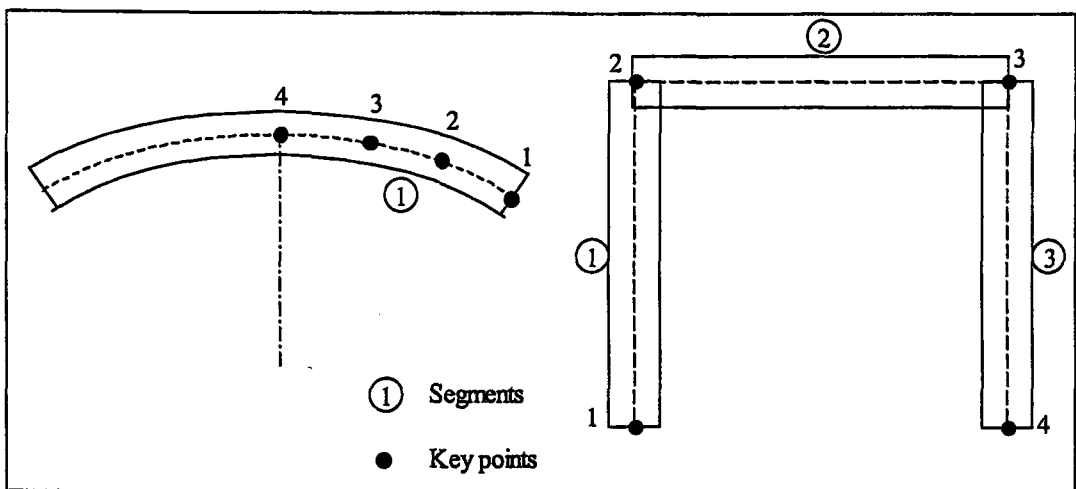
Figure 3.3 Representation of structural geometry of arch and frame structures

33

3.2.3 Computer implementation

Consider a cubic spline segment passing through a set of representative key points P_i which lie on the midsurface of the curved structure and whose position vectors are $\mathbf{p}_i$ where $i = 1,2,...,k$; see Figure 3.4. To represent this structure midsurface using B-splines we can make use of the relations in Eq (3.8). Thus we have a system of linear algebraic equations of the form

$$\mathbf{b}_{i-1} + 4\mathbf{b}_i + \mathbf{b}_{i+1} = 6\mathbf{p}_i \qquad (i = 1,2,...,k) \tag{3.9}$$

in which $\mathbf{b}_i$ is the position vectors of the control vertices B_i of the polygon and $\mathbf{p}_i$ is the position vectors of the points on the curve segment.
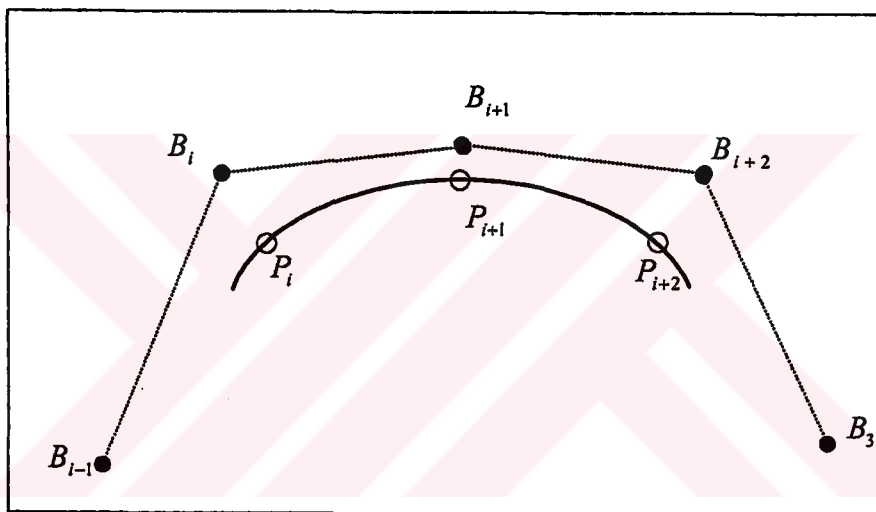
Figure 3.4 A cubic spline segment passing through a set of key points and the associated control points

The cubic spline segment is formed by an assembly of several subsegments. The first subsegment is determined by the polygon which has vertices B_0, B_1, B_2, and B_3. If one more vertex B_4 is added then B_1, B_2, B_3 and B_4 determines the second subsegment. Such an arrangement always ensures $C(2)$ continuity between the junction of two subsegments the proof of which can be found in [113]. Thus adding one more vertex adds another subsegment and so on. Therefore, the number of vertices defining

the curve is $B_0, B_1, \ldots, B_k, B_{k+1}$. The relation Eq (3.9) for the curve can be written in matrix form as

$$\begin{bmatrix} a & b & & & & & \\ 1 & 4 & 1 & & & & \\ & & \ddots & & & & \\ & & 1 & 4 & 1 & & \\ & & & & \ddots & & \\ & & & & 1 & 4 & 1 \\ & & & & & c & d \end{bmatrix} \begin{bmatrix} \mathbf{b}_1^T \\ \mathbf{b}_2^T \\ \vdots \\ \mathbf{b}_i^T \\ \vdots \\ \mathbf{b}_{k-1}^T \\ \mathbf{b}_k^T \end{bmatrix} = \begin{bmatrix} \mathbf{e}^T \\ 6\mathbf{p}_2^T \\ \vdots \\ 6\mathbf{p}_i^T \\ \vdots \\ 6\mathbf{p}_{k-1}^T \\ \mathbf{f}^T \end{bmatrix} \qquad (3.10)$$

where the values of a, b, c and d and $\mathbf{e}$ and $\mathbf{f}$ can be determined from the end condition specified for the segment and explained in Table 3.1. The unknowns for the curve are the position vectors of the control vertices $\mathbf{b}_0$ to $\mathbf{b}_{k+1}$ and can be determined by solving Eq (3.10) which are tridiagonal equations and hence inexpensive to solve. To solve Eq (3.10) we require two additional pieces of information, so that the system of equations may have a unique solution. This additional information can be obtained by specifying the end conditions of the spline. Once the position vectors $\mathbf{b}_0, \ldots, \mathbf{b}_{k+1}$ of the vertices are known the whole curve can be defined, manipulated and all points on the curve can be evaluated using Eq (3.5).

Table 3.1 Values of a, b, c, d and the vectors $\mathbf{e}$ and $\mathbf{f}$ for different boundary conditions

Variable name	Type of boundary condition	
	Specified tangents at end points	Natural spline condition
$\mathbf{e}$	$3\{\mathbf{p}(1) + (1/3)\mathbf{p}'(1)\}$	$\mathbf{p}(1)$
$\mathbf{f}$	$3\{\mathbf{p}(k) + (1/3)\mathbf{p}'(k)\}$	$\mathbf{p}(k)$
a,d	2	1
b,c	1	0
$\mathbf{b}_0$	$\mathbf{b}_2 - 2\mathbf{p}'(0)$	$2\mathbf{b}_1 - \mathbf{b}_2$
$\mathbf{b}_{k+1}$	$\mathbf{b}_{k-1} - 2\mathbf{p}'(k)$	$2\mathbf{b}_k - \mathbf{b}_{k-1}$

3.2.4 Spline end conditions

To distinguish between "smooth" (i.e. continuous) and kinks between connecting splines, two end conditions are considered. The end conditions have an important influence in the matrix system of equation 3.10. End conditions can either be "natural" or have some specified tangent and weight.

Natural Spline End Condition: If no influence of curvature is desired between successive splines, the natural spline end condition is defined. This condition is also known as $C(0)$ continuity, and is imposed by specifying zero curvature at the relevant end points, therefore relieving the need to specify tangent values. Examples of structures with $C(0)$ continuity include the edges of frame, between column and beams.

End Tangent Condition: The majority of arch structures are smooth in profile. To allow for this smooth transition in curvature between cubic splines (also known as $C(2)$ continuity) the end tangents are specified. The magnitude of these end tangents at the spline ends can have a profound effect on the overall shape of spline. Faux and Pratt [114] summarized this with an interesting example: for a parametric cubic spline of R key points, the end tangents $\mathbf{p}'(0)$ and $\mathbf{p}'(1)$ can be represented by the product of weighting factors β_0 and β_1 with unit tangents $\mathbf{t}(0)$ and $\mathbf{t}(1)$:

$$\mathbf{p}'(0) = \beta_0 \mathbf{t}(0) \quad \text{and} \quad \mathbf{p}'(1) = \beta_1 \mathbf{t}(1) \tag{3.11}$$

The significance of the tangent vector magnitudes is as follows. A simultaneous increase of both β_0 and β_1 simply gives more "fullness" to the curve, whereas increasing only β_0 causes the curve to remain close to the direction of $\mathbf{t}(0)$ for a greater part of its length before turning into the direction of $\mathbf{t}(1)$. See Figure 3.5. For large values of β_0 and β_1 kinks and loops occur. For cubic curves, a safe rule is to ensure that the tangent magnitudes β_0 and β_1 do not exceed three times the chord length $|\mathbf{p}(1) - \mathbf{p}(0)|$.
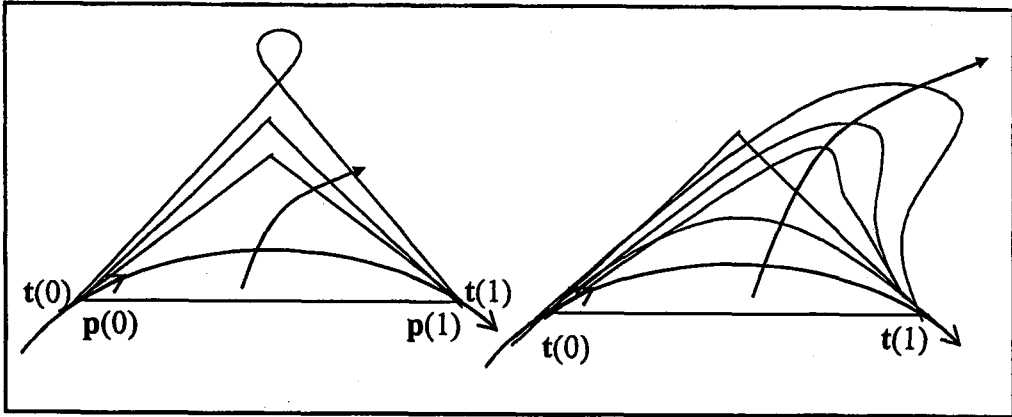
Figure 3.5 Significance of the specification of end tangents for a cubic spline curve

3.3 Structural Thickness Definition

The thickness of the structure is specified at some or all of the *key points* of the structure and then interpolated using cubic splines with *natural spline end condition*. This results in smooth structure shapes. The implementation of the thickness definition in the present work is entirely independent of the shape definition to allow flexibility in having different types of thickness variation. Thus it is left to the user's discretion to use some or all of the key points for thickness interpolation. Moreover, since the thickness values at different nodal positions are obtained by interpolation, there is no need to use a cubic B-spline representation; in fact, the classical cubic spline representation is used here only because of its simplicity.

Consider a segment of a curve, which is defined using k key points. The location of the key points on the segments can be expressed in terms of the parameter l which is the arc length of the curve from the starting point of a segment as shown in Figure 3.6. Assume that the key points are located at a distance $\ell_i, (i=1,...,k)$ from the starting position. Since $f(\ell)$ is a cubic spline function it is cubic in each subinterval $\ell_i \rightarrow \ell_{i-1}$, $(i=1,...,k)$. Further, if an associated set of thickness values f_k (or any other parameter such as pressure, temperature, etc.) is prescribed at the key points then the values of the thickness at any distance ℓ from the starting point can be evaluated using the expression [113]

37
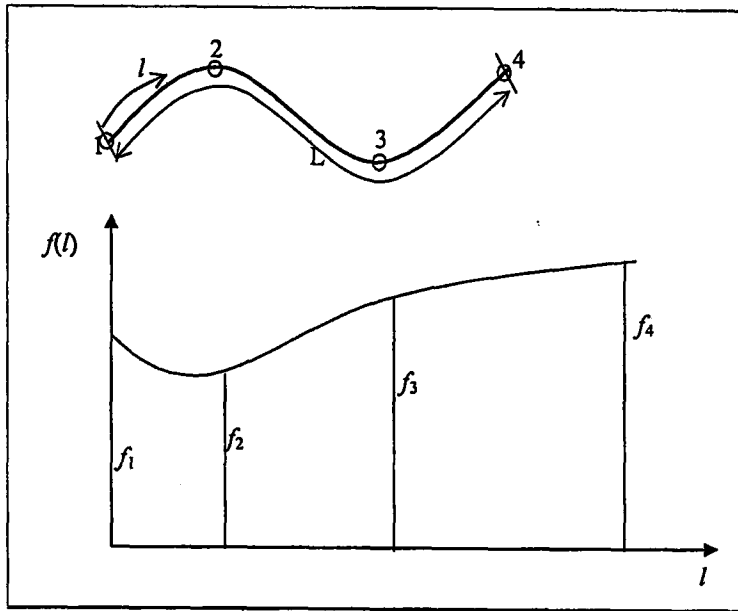
Figure 3.6 Cubic spline interpolation of thickness values along the curve segment

$$f(\ell) = \begin{bmatrix} 1 & (\ell - \ell_{k-1}) & (\ell - \ell_{k-1})^2 & (\ell - \ell_{k-1})^3 \end{bmatrix} \begin{bmatrix} \alpha_1 \\ \alpha_2 \\ \alpha_3 \\ \alpha_4 \end{bmatrix}_i \qquad \ell_i \le \ell \le \ell_{i+1} \qquad (3.12)$$

for $i = 1,...,k-1$ where $\alpha_1, \alpha_2, \alpha_3$ and α_4 can be determined by solving a set of tridiagonal equations [113].

3.4 Automatic Mesh Generation

3.4.1 General requirements

Many frame and arch structures have complex cross-sections, which must be discretized before any FE analysis can be carried out. Manual or semi-automatic procedures are often inefficient, tedious and prone to errors. To make the process of mesh generation automatic, efficient and reliable the following requirements should be met:

- The mesh generation algorithm should be efficient and fully automatic.

- It should incorporate a convenient geometric representation of boundaries and be able to represent complex shapes easily.

- It should be able to automatically generate meshes of different sizes over the cross-section of the structure as specified by the user.

- It should possess a convenient means of prescribing the element size variation over the domain.

- The input data to the mesh generator should be minimized.

- The mesh generator should be portable, so that it can be attached as a part of the analysis module.

- It should be flexible; so that its potential can be exploited in other applications (e.g. shape optimization or generation of boundary elements).

Here, the mesh generator is based on an approach similar to that of Peraire et al. [115] and Peiro [116], which incorporates a *remeshing* facility to allow for the possibility of refinement (or derefinement). It also allows a significant variation of mesh spacing throughout the region of interest.

3.4.2 Algorithm for mesh generation

Assume that the cross-section of a structure surface is represented by a segment, which passes through a set of k key points.

Mesh Density Definition: To control the mesh density or spatial distribution of element size throughout the region of interest, it is convenient to specify the mesh density δ_i at a sequence of k key points in the structure. At the initial stages of the analysis mesh density values given at the two end points of each segment will be sufficient if only a uniform or a linearly varying mesh density is required.

Discretization of Segments: Based on the prescribed mesh density, the profile of the structure is discretized into a series of straight elements (linear) or curved (quadratic or cubic) elements. A brief description of the algorithmic steps involved in the mesh generation procedure is now presented.

Step 1 Find the arc length coordinate ℓ_k of the key points at which the mesh density δ_i is specified by making use of the values of the h coordinate at those key points (which is either 0 or 1) and relation Eq (3.5).

Step 2 Evaluate the inverse mesh density function $s(\ell)_i$

$$s(\ell)_i = 1/\delta_i \qquad i = 1,...,k \qquad (3.13)$$

at the key points which represents the concentration of elements along the length of the curve.

Step 3 Construct a piecewise linear spacing function $\phi(\ell)$ along the length of the segment using

$$\phi(\ell)_i = \phi(\ell_{i-1}) + 0.5\phi(s(\ell_i) + s(\ell_{i-1}))\Delta\ell_i, \qquad i = 2,...,k \qquad (3.14)$$

in which the value at $\phi(\ell_1) = 0$ and $\Delta\ell_i = (\ell_i - \ell_{i-1})$.

Step 4 The number of elements n_e into which the structure midsurface is divided is taken as an integer value of the spacing function at the last key point i.e. $\phi(\ell_k)$.

Step 5 The position and arc length coordinate of the nodes $\ell_i, (i = 1,...,n_e + 1)$ to be generated along the curve is then determined from the number of points and the spacing function by solving iteratively

$$\phi(\ell) = i \qquad (i = 1,...,n_e) \qquad (3.15)$$

The first node lies at $\ell = 0$ and the last node at $\ell = L$.

Step 6 The number of nodes n_n for the linear elements generated is equal to $n_n = n_e + 1$. However, if higher order elements are to be generated then additional internal nodes are equally spaced and the number of nodes is equal to $n_n = (2n_e + 1)$ for the quadratic element and $n_n = (3n_e + 1)$ for the cubic element.

Step 7 From the known values of ℓ_i of the nodes, the h coordinate of the nodes is evaluated using an iterative procedure.

Step 8 Once the h coordinates are known, the x_1, x_2, x_3 coordinates (Note that x_1, x_2, x_3 correspond to coordinates x, y and z in the analysis) of the nodes, the tangent values and the curvature values at the nodes can be evaluated using the relations Eq (3.5) to (3.7).

Steps 1 to 8 are repeated for every segment. The mesh generation procedure is illustrated graphically in Figure 3.7.
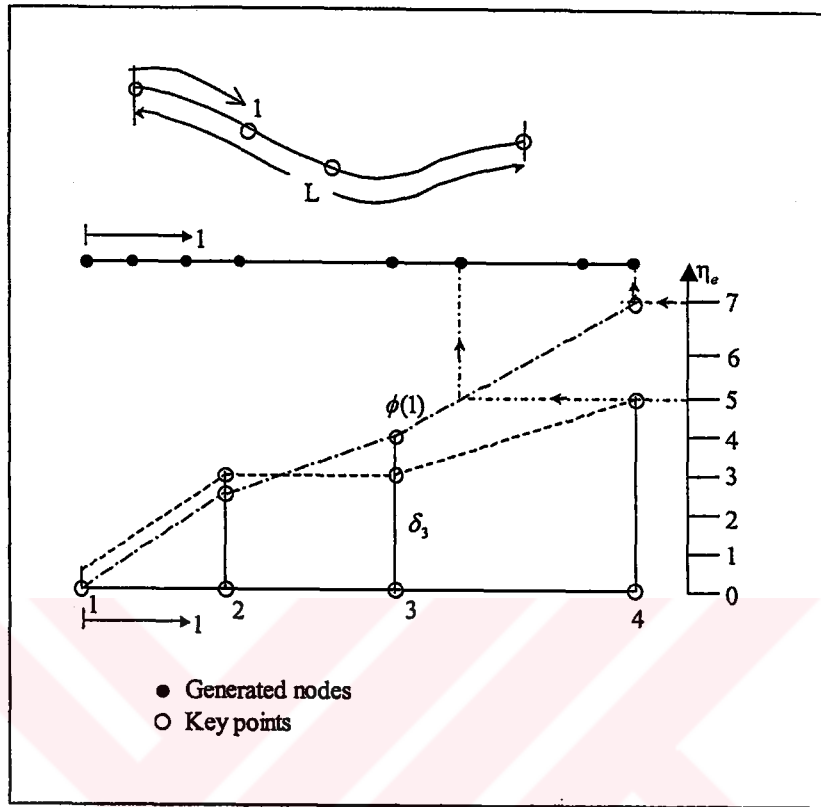
Figure 3.7 Generation of nodes along the length of the segment

In the mesh generator the following additional features have been incorporated:

- The loading and boundary conditions are automatically updated after every remeshing.

- If desired the mesh generator gives the values of ℓ and h coordinates at every node. This information is especially useful in sensitivity analysis for shape optimization of structures. In addition this information is useful where graphic visualization of geometry, mesh etc. are necessary.

3.5 Shape Definitions and Mesh Generation in Structural Analysis

The above tools have been implemented into the program and have been extensively used in subsequent chapters for the structural analysis of variable thickness of arches

41

and frame structures with varying loading and boundary conditions. The real advantage of using the present tool lies in the generation of meshes (either uniform or graded) even for complicated cross-sections by just specifying the location of only a few key points and the desired mesh size. The whole process of shape definition and mesh generation is computationally inexpensive and provides the user with greater flexibility when deciding on the type of element, mesh density etc.

However, it should be noted that the cubic spline represents the real geometry only in an approximated form. Therefore, in some special cases, for example, the evaluation of the convergence properties of the FE solutions, it is essential to carry out a geometric correction of the evaluated nodal coordinates to ensure that all the nodes generated lie exactly on the midsurface of the arch structure to be analyzed. Another important aspect in the definition of the structural shape is the number of key points used to define the shape of the structure. For curved structures, the more key points used the better the representation of the middle surface of the structure.

3.6 Shape Definition and Mesh Generation in Structural Optimization

In SSO procedures the shape or the thickness of the structure is varied to improve the structural performance. Since such procedures are iterative they should involve automatic updating of shape and/or thickness variation as well as the mesh during the optimization process. The shape or the thickness variation of a structure is modified by the shape or thickness design variables. In the following section the various approaches available for the selection of shape and thickness variables are discussed as well as how the present tools developed for shape definition are exploited for the purpose of optimization.

3.6.1 Shape design variables

The choice of design variables is a key factor in obtaining the optimum shape, since it changes the character of the problem by changing the degree of nonlinearity of the objective or constraint functions or by imposing additional implicit side constraints. It is desirable to have a direct connection between the values of the design variables

and the actual geometry. The following general approaches for design variables have been used:

Nodal Coordinates: In early work on shape optimization the positions of the nodes on the boundary were used as design variables; see Zienkiewicz and Campbell [65]. This approach is simple but leads to a large number of design variables. Compatibility and slope continuity between adjacent nodes cannot be achieved easily, often leading to unrealistic shapes and designs.

Polynomials: Polynomials have been used in shape design problems to represent the shape of the structure; see Bhavikatti and Ramakrishnan [117]. The coefficients of these polynomials are taken as design variables. Use of polynomials for shape representation can obviously reduce the total number of shape variables, but may result in an oscillatory shape due to numerical instability associated with higher order polynomial curves.

Control Points of Splines: Braibant and Fleury [118] use Bezier and B-spline curves for shape representation in a method they call the design element technique. The region of the structure to be modified during the optimization process is defined by one or more design elements, which contain a part of the mesh. Blending functions are employed to determine the coordinates of any points inside the design element or on the boundary. The shape variables are the position vectors of the points, which control the curves, which define the design element. Ramm et al. [119] also use this approach which leads to a considerable decrease in the number of design variables and has been found to give more realistic shapes. This approach is general, but the number of design elements used to represent the structure and the degree of the curve affects the performance considerably [118].

Present Approach: In the present approach the position vectors of the key points used to define the structure midsurface are taken as design variables. The midsurface of the structure to be optimized is represented by cubic spline curves passing through key points on the structure. This procedure has been extensively discussed earlier.

43

The position vectors of the key points chosen to be the design variables can be selected at the discretion of the user. Therefore the design variables are no longer the position vectors of the control points as in reference [118] but the position vectors of the key points, which are used to define the structure midsurface.

Figure 3.8 shows a general curve which passes through position vectors $\mathbf{p}_i$ where

$$\mathbf{p}_i = [p_{xi} \quad p_{yi}]^T \tag{3.16}$$
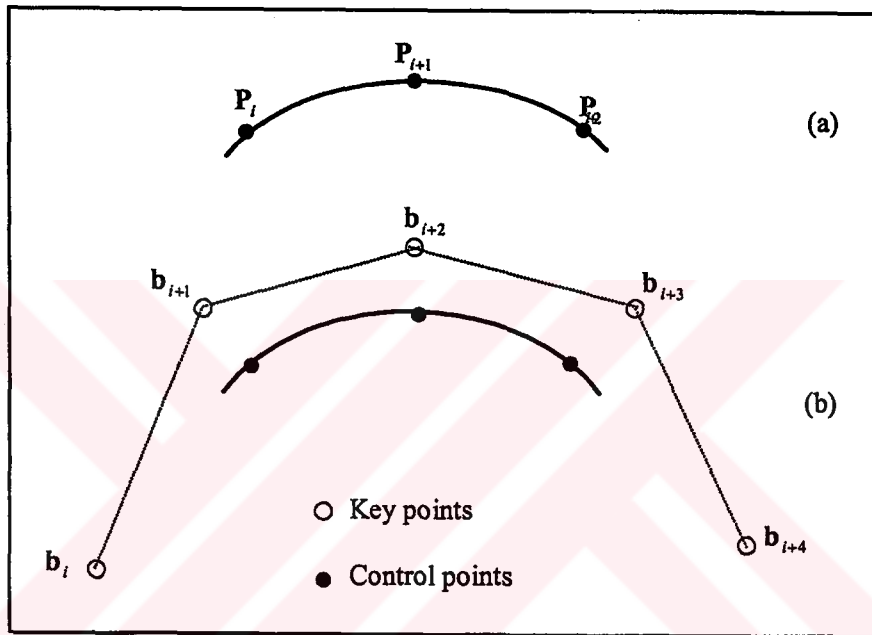
Figure 3.8 Alternative approaches for selection of design variables: (a) position vectors of the key points as design variables and (b) position vectors of the control points as design variables.

The position vector of the vertices or control points of the polygon defining this curve are designated $\mathbf{b}_i$. Therefore in the present approach the position vectors $\mathbf{p}_i$ are taken as design variables instead of the position vectors of the control vertices $\mathbf{b}_i$. We can now define the shape variables $\mathbf{s}$ as

$$\mathbf{s} = [p_{x1} \quad p_{y1} \quad p_{x2} \quad p_{y2} \quad \cdots\cdots \quad p_{xn} \quad p_{yn}]^T \tag{3.17}$$

where the position vectors of the point P_i are defined with respect to the Cartesian coordinate system. Choosing the position vectors of the key points as design variables has the following advantages:

- the number of design variables is considerably reduced; and

- the positions of the design variables can be selected with convenience even for complex shapes.

The shape design variables can be expressed either in a Cartesian or a polar coordinate system. Figure 3.9 shows an example of shape variables adopted in the present work.
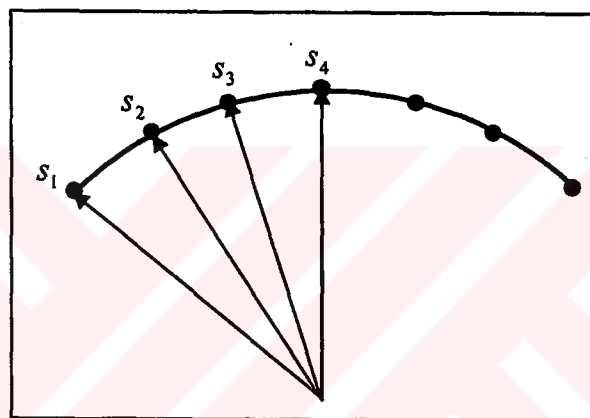
Figure 3.9 Typical shape design variables used in the present work

3.6.2 Selection of thickness design variables

In previous research work on structures only uniform or piecewise uniform thickness variation has been allowed (see Mota Soares et al. [120]). This over constrains the optimization process and does not give the greatest opportunity for weight reduction. In this work, the use of cubic splines for thickness distribution along the structures gives greater flexibility and a smooth variation of thickness. A similar approach to that adopted for the shape design variables is used in which the thickness values at some key points are specified as design variables.

45

To demonstrate the different variations of thickness that can be achieved consider the case of a beam shown in Figure 3.10(a), which is modeled using one segment and four key points.
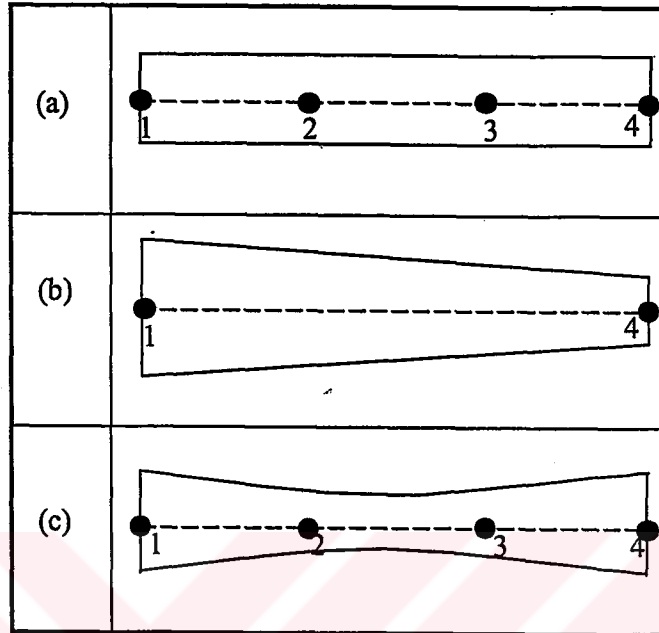
Figure 3.10 Thickness design variables: (a) geometric definition (b) linear thickness variation obtained by using 1 and 4 as master variables and 2 and 3 as slave variables and (c) cubic thickness variation obtained by using 1 to 4 as master variables

For example, to obtain a linear thickness variation, the interpolation is performed using the thickness values at key points 1 and 4 and the thicknesses t_1 and t_4 are taken as design variables. Figure 3.10(b) shows the linear thickness variation that can be obtained. The design variables in this case can be defined as

$$\mathbf{s} = [t_1 \quad t_4]^T \qquad (3.18)$$

Similarly, to obtain a cubic variation of thickness, the thicknesses at three or more key points are considered for interpolation. Figure 3.10(c) shows the cubic variation of thickness obtained by considering all the key points for interpolation. The number of design variables in this case can be defined as

$$\mathbf{s} = [t_1 \quad t_2 \quad t_3 \quad t_4]^T \qquad (3.19)$$

46

3.6.3 Linking of design variables

Sometimes for practical reasons and computational efficiency it is necessary to link the design variables at two or more key points to satisfy certain requirements. Linking of design variables also has the following main advantages:

- the number of design variables is reduced considerably;
- the movement of a whole segment (as a rigid body) can be treated with a single design variable; and
- symmetry of shape can be easily achieved.

Linking of Shape Design Variables: Figure 3.11 shows the cross-section of an arch. The shape design variables are linked by the relations $s_1 = s_7$, $s_2 = s_6$ and $s_3 = s_5$ by which symmetry of shape is obtained. Further the number of design variables is reduced from seven to four. However, if no symmetry is required then linking is not necessary.
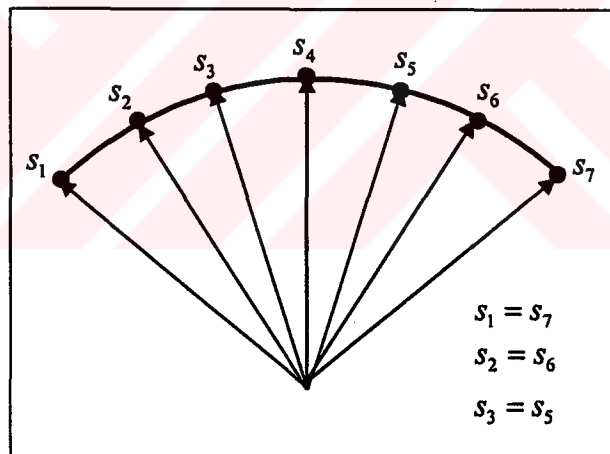
Figure 3.11 Linking of shape design variables of an arch

Linking of Thickness Design Variables: To demonstrate the linking of thickness variables consider the case of a beam modeled using two segments and three key points. In this particular case each segment has two key points. It is convenient to use the notation $t_i^{(j)}$ for each thickness variable in which the subscript i refers to the key point and the superscript (j) refers to the segment. Thus, for example, for the plate in

47

Figure 3.12(b) we have $t_1^{(1)}$, $t_2^{(1)}$, $t_2^{(2)}$ and $t_3^{(2)}$ where $t_2^{(1)}$ implies the thickness at key point 2 associated with segment 1 and $t_2^{(2)}$ means thickness at key point 2 but associated with segment 2. In practice, these two quantities can be identical or totally different.
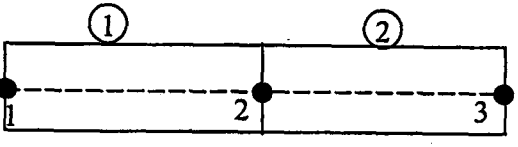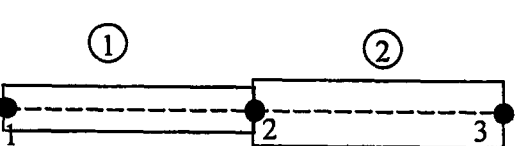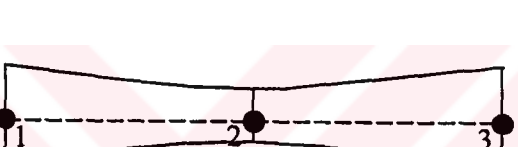
Figure 3.12 Linking of thickness design variables: (a) geometric definition, (b) piecewise constant thickness variation and (c) piecewise linear variation

i. *Piecewise constant variation:* To obtain piecewise constant thickness variation across each segment the thickness variables have to be linked where linking here implies equating different thickness variables. Equating $t_1^{(1)} = t_2^{(1)}$, $t_2^{(2)} = t_3^{(2)}$ gives a piecewise constant thickness variation as shown in Figure 3.12(b). The number of design variables is equal to two so that

$$s = [t_1^{(1)} \quad t_2^{(2)}]^T \tag{3.20}$$

ii. *Piecewise linear variation:* Similarly, by imposing the condition $t_2^{(1)} = t_2^{(2)}$ a piecewise linear thickness variation is obtained across each segment. See Figure 3.12(c). In this case the number of design variables is equal to three so that

$$s = [t_1^{(1)} \quad t_2^{(1)} \quad t_3^{(2)}]^T. \tag{3.21}$$

Figure 3.13 shows the design variables for a box girder bridge that has been adopted in the present work. Such design variables can be used after linking as described above.
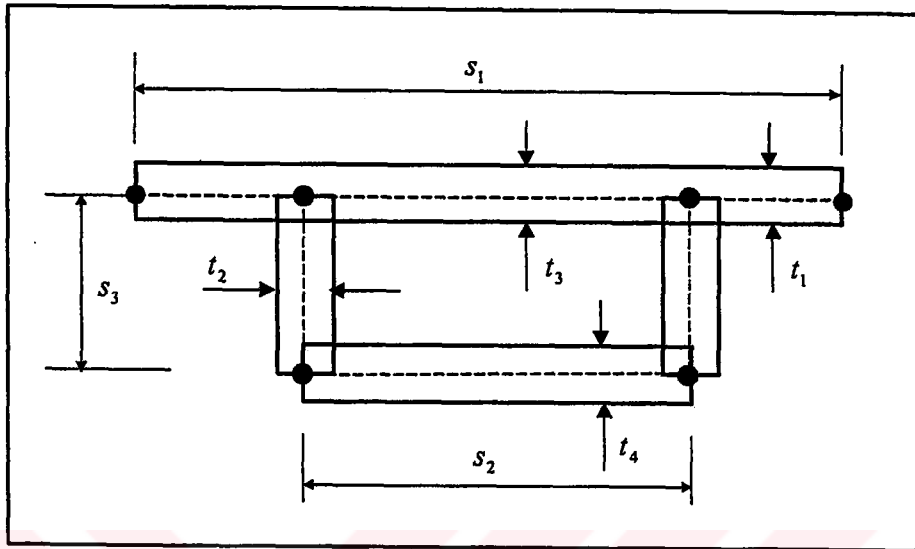
Figure 3.13 Typical design variables for a box-girder frame

CHAPTER 4

STATIC AND FREE VIBRATION
ANALYSES OF TRUSSES

4.1 Introduction

Although the topic of truss analysis and optimization had been discussed frequently over recent years, this chapter was included to illustrate the validity of analysis program, which is used in GA optimization program. In this chapter, static and free vibration matrix displacement methods are introduced and before any optimization was carried out, each analysis program was tested against known benchmark solutions, to confirm integrity of the analyses.

4.2 Static Analysis of One Dimensional Rod Elements

Given the 1D rod element shown in Figure 4.1 which has element local node numbers 1 and 2 with coordinates $x_1^{(e)}$ and $x_2^{(e)}$ and nodal displacements $u_1^{(e)}$ and $u_2^{(e)}$ we will demonstrate how to derive the stiffness matrix of the member.

The total potential energy for the general elastic body is

$$\Pi = \frac{1}{2}\int \sigma^T \varepsilon A dx - \int u^T F_b A dx - \int u^T q dx - \sum_i u_i P_i \tag{4.1}$$

The quantities σ and ε are the axial stresses and strains in the element respectively, and A is the cross-sectional area. The length ℓ, body force F_b and traction force q terms are used. In the last term P_i represents a force acting at point i, and u_i is the x displacement at that point. The summation on i gives the potential energy due to all point loads.

Since the continuum has been discretized into FEs; the Eq (4.1) becomes

$$\Pi = \sum_e U^{(e)} - \sum_e \int_{l^{(e)}} u^T F_b A\,dx - \sum_e \int u^T q\,dx - \sum_i u_i P_i \qquad (4.2)$$

where

$$U^{(e)} = \frac{1}{2}\int \sigma^T \varepsilon A\,dx \qquad (4.3)$$

is the element SE
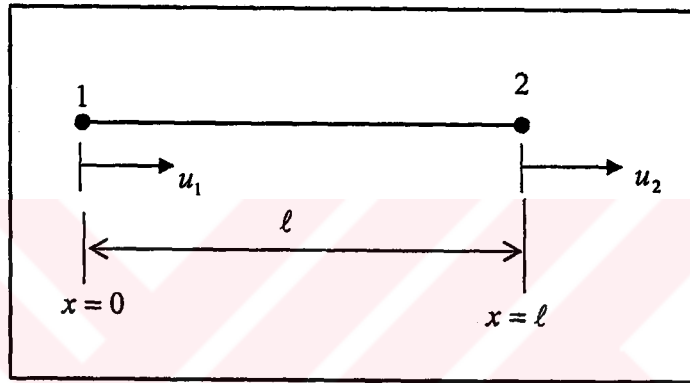
Figure 4.1 Two-noded 1D rod element (showing local node numbers)

4.2.1 Element stiffness matrix

The SE $U^{(e)}$ of each element may be written as

$$U^{(e)} = \int_{l^{(e)}} \frac{[\sigma^{(e)}]^2}{2E^{(e)}} A^{(e)}\,d\ell \qquad (4.4)$$

or

$$U^{(e)} = \int_{l^{(e)}} \frac{1}{2}[\varepsilon^{(e)}]^2 E^{(e)} A^{(e)}\,d\ell \qquad (4.5)$$

Note that the total SE for the whole assemblage may be written as the sum of the contribution from each element.

$$U = \sum_{e=1}^{ne} U^{(e)} = \sum_{e=1}^{ne} \int_{l^{(e)}} \frac{1}{2}[\varepsilon^{(e)}]^2 E^{(e)} A^{(e)}\,d\ell \qquad (4.6)$$

51

Now let us assume that the axial displacement u has a linear variation over each individual element, so that

$$u(x) = N_1^{(e)} u_1^{(e)} + N_2^{(e)} u_2^{(e)} \tag{4.7}$$

where

$$N_1 = \left(\ell^{(e)} - x \right) / \ell^{(e)} \qquad \text{and} \qquad N_2 = x / \ell^{(e)} \tag{4.8}$$

or

$$N_1^{(e)} = (1 - \xi) \qquad \text{and} \qquad N_2^{(e)} = \xi \tag{4.9}$$

where $\xi = x / \ell^{(e)}$ is a non-dimensional coordinate and where $N_1^{(e)}$ and $N_2^{(e)}$ are known as shape functions and are illustrated in Figure 4.2.
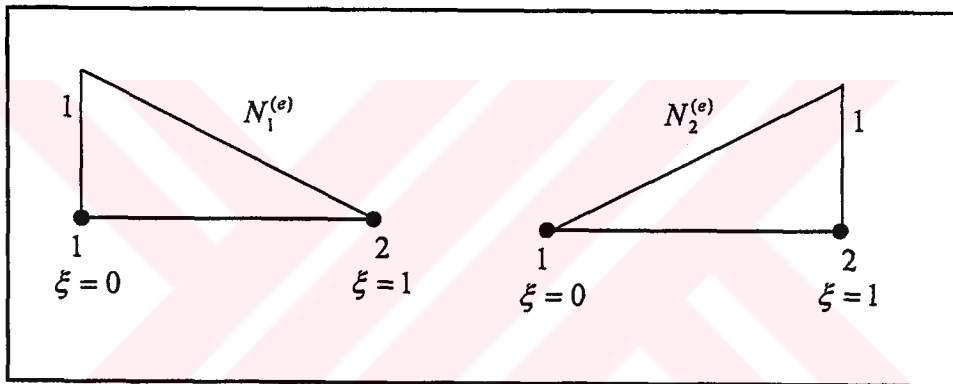
Figure 4.2 Linear shape function for 1D rod element

Equation (4.7) may be written in matrix shorthand form as

$$u_1^{(e)} = \mathbf{N}^{(e)} \mathbf{d}^{(e)} \tag{4.10}$$

where

$$\mathbf{N}^{(e)} = [N_1^{(e)} \quad N_2^{(e)}] \tag{4.11}$$

and

$$\mathbf{d}^{(e)} = [u_1^{(e)} \quad u_2^{(e)}]^T \tag{4.12}$$

The axial strain in element e may then expressed as

$$\varepsilon^{(e)} = \left(\frac{du}{dx} \right)^{(e)} = \frac{1}{\ell^{(e)}} \frac{du}{d\xi} \tag{4.13}$$

so that from Eq (4.7) and Eq (4.13)

$$\varepsilon^{(e)} = [-1/\ell^{(e)} \quad 1/\ell^{(e)}] \begin{Bmatrix} u_1^{(e)} \\ u_2^{(e)} \end{Bmatrix} \tag{4.14}$$

or

$$\varepsilon^{(e)} = \mathbf{B}^{(e)} \mathbf{d}^{(e)} \tag{4.15}$$

where

$$\mathbf{B}^{(e)} = [B_1^{(e)} \quad B_2^{(e)}] \quad \text{or} \quad [-1/\ell^{(e)} \quad 1/\ell^{(e)}]. \tag{4.16}$$

Thus the SE of element e may be expressed as

$$U^{(e)} = \frac{1}{2} [\mathbf{d}^{(e)}]^T \mathbf{K}^{(e)} \mathbf{d}^{(e)} \tag{4.17}$$

where the element stiffness matrix

$$\begin{aligned}
\mathbf{K}^{(e)} &= \int_{\ell^{(e)}} \mathbf{B}^{(e)^T} E^{(e)} \mathbf{B}^{(e)} A^{(e)} d\ell \\
&= \int_0^1 \begin{bmatrix} -1/\ell^{(e)} \\ 1/\ell^{(e)} \end{bmatrix} E^{(e)} [-1/\ell^{(e)} \quad 1/\ell^{(e)}] \ell^{(e)} A^{(e)} d\xi \\
&= \left(\frac{EA}{\ell} \right)^{(e)} \begin{bmatrix} 1 & -1 \\ -1 & 1 \end{bmatrix}.
\end{aligned} \tag{4.18}$$

4.2.2 Force vector

Body Force: The element body force term $\int u^T F_b A dx$ appearing in the total potential energy is considered. Substituting $u(x) = N_1^{(e)} u_1^{(e)} + N_2^{(e)} u_2^{(e)}$ we have

$$\int u^T F_b A dx = A F_b \int (N_1^{(e)} u_1^{(e)} + N_2^{(e)} u_2^{(e)}) dx \tag{4.19}$$

Recall that the body force F_b has units of force per unit volume. In Eq (4.19), A and F_b are constant within the element and are consequently brought outside the integral. This equation can be written as

$$\int u^T F_b A dx = \mathbf{d}^T \begin{Bmatrix} A F_b \int N_1^{(e)} dx \\ A F_b \int N_2^{(e)} dx \end{Bmatrix} \tag{4.20}$$

53

The integrals of shape functions evaluated by making the substitution $dx = (\ell_e / 2)d\xi$ and Eq (4.9) into Eq (4.20). Thus the body force term in Eq (4.20) reduces to

$$\int u^T F_b A\, dx = \mathbf{d}^T \frac{A_e}{2}\ell_e F_b \begin{Bmatrix} 1 \\ 1 \end{Bmatrix} \tag{4.21}$$

which is of the form

$$\int u^T F_b A\, dx = \mathbf{d}^T \mathbf{f}^e \tag{4.22}$$

Thus, the element body force vector, $\mathbf{f}^e$, is identified as

$$\mathbf{f}^e = \frac{A\ell_e F_b}{2} \begin{Bmatrix} 1 \\ 1 \end{Bmatrix} \tag{4.23}$$

The element body force above has a simple physical explanation. Since $A\ell_e$ is the volume of the element and F_b is the body force per unit volume, we see that $A\ell_e F_b$ gives the total body force acting on the element. The factor $\dfrac{1}{2}$ in Eq (4.23) tells us that this total body force is equally distributed to the two nodes of the element.

Distributed Load: The element distributed load term $\int u^T q\, dx$ appearing in the total potential energy is now considered. We have

$$\int u^T q\, dx = \int (N_1^{(e)} u_1^{(e)} + N_2^{(e)} u_2^{(e)}) q\, dx \tag{4.24}$$

Since the distributed load q is constant within the element, we have

$$\int u^T q\, dx = \mathbf{d}^T \begin{Bmatrix} q \int N_1^{(e)} dx \\ q \int N_2^{(e)} dx \end{Bmatrix} \tag{4.25}$$

Thus, the element distributed load vector is given by

$$\mathbf{q}^e = \frac{q\ell_e}{2} \begin{Bmatrix} 1 \\ 1 \end{Bmatrix} \tag{4.26}$$

54

4.2.3 Assemble of equations

Element matrices $\mathbf{K}^e, \mathbf{f}_b^e$ and $\mathbf{q}^e$ have been obtained. After we account for the element connectivity, the total potential energy defined by Eq (4.2) can be written as

$$\Pi = \frac{1}{2}\sum_{e=1}^{ne}[\mathbf{d}^{(e)}]^T \mathbf{K}^{(e)}\mathbf{d}^{(e)} - \mathbf{d}^T\mathbf{q}. \qquad (4.27)$$

For equilibrium, Π must be a minimum for which the conditions are

$$\frac{\partial \Pi}{\partial d_i} = 0 \quad i = 1, np \qquad (4.28)$$

This leads to the well known stiffness equation

$$\mathbf{K}\,\mathbf{d} = \mathbf{f} \qquad (4.29)$$

where

$$\mathbf{f} = \mathbf{f}_b + \mathbf{q} \qquad (4.30)$$

4.3 Static Analysis of Two Dimensional Trusses

The derivation of stiffness along with the ultimate stress terms for a constant cross-section truss element is now discussed. Standard FE matrix displacement methods were used in this calculation, such as those mentioned in [5].

Equation (4.18) represent the stiffness matrix for a 1D rod element expressed in terms of the end axial degrees of freedom $u_1^{(e)}$ and $u_2^{(e)}$. In this section we derive similar expression for truss members expressed in terms of degrees of freedom $u_1^{o(e)}$, $u_2^{o(e)}$, $v_1^{o(e)}$ and $v_2^{o(e)}$. Whereas $u_1^{o(e)}$ and $u_2^{o(e)}$ represent displacements in the x^o direction, $v_1^{o(e)}$ and $v_2^{o(e)}$ represent displacements in the y^o direction.

Now let us consider the rod element of Figure 4.3 which is lying at an angle $\alpha^{(e)}$ to the x^o axis, where the $x^o - y^o$ are global reference axes and the $x - y$ axes are the local axes of the rod [25].
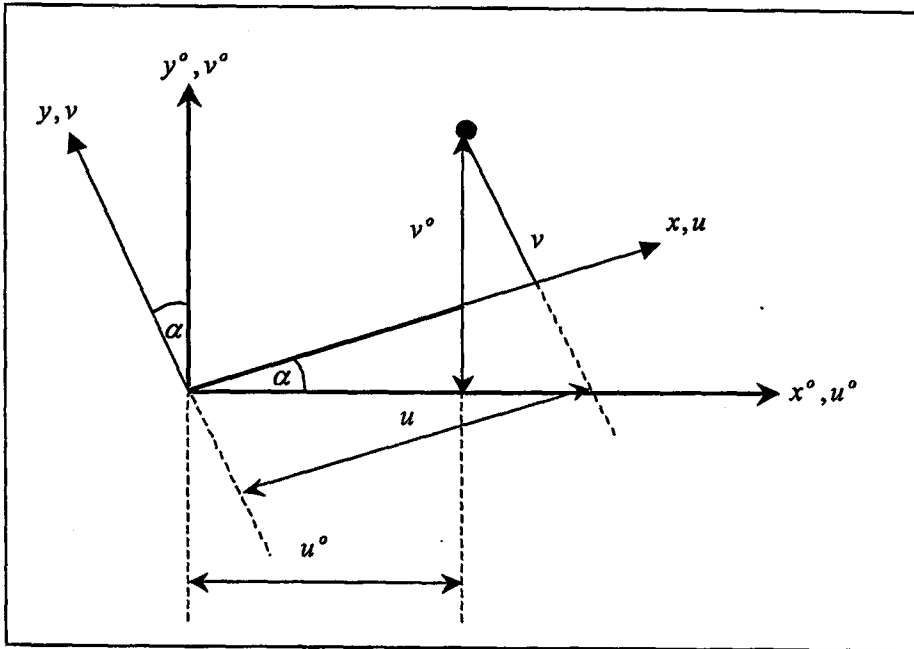
Figure 4.3 Global and local coordinates systems for a 2D truss element

For the point shown in Figure 4.3, it can be seen that,

$$u = u^0 \cos\alpha^{(e)} + v^0 \sin\alpha^{(e)}$$

$$v = -u^0 \sin\alpha^{(e)} + v^0 \cos\alpha^{(e)} \tag{4.31}$$

or in matrix form

$$\begin{Bmatrix} u \\ v \end{Bmatrix} = \begin{bmatrix} c & s \\ -s & c \end{bmatrix} \begin{Bmatrix} u^0 \\ v^0 \end{Bmatrix} \tag{4.32}$$

or

$$\begin{Bmatrix} u \\ v \end{Bmatrix} = \lambda^{(e)} \begin{Bmatrix} u^0 \\ v^0 \end{Bmatrix} \tag{4.33}$$

where

$$\lambda^{(e)} = \begin{bmatrix} \cos\alpha^{(e)} & \sin\alpha^{(e)} \\ -\sin\alpha^{(e)} & \cos\alpha^{(e)} \end{bmatrix}. \tag{4.34}$$

For the two-node 2D truss element, the relationship between local and global displacement is given by

$$\begin{Bmatrix} u_1^{(e)} \\ v_1^{(e)} \\ u_2^{(e)} \\ v_2^{(e)} \end{Bmatrix} = \begin{bmatrix} \lambda^{(e)} & 0 \\ 0 & \lambda^{(e)} \end{bmatrix} \begin{Bmatrix} u_1^{o(e)} \\ v_1^{o(e)} \\ u_2^{o(e)} \\ v_2^{o(e)} \end{Bmatrix}$$

(4.35)

or

$$\mathbf{d}^{(e)} = \mathbf{T}^{(e)} \mathbf{d}^{o(e)}$$

(4.36)

where $\mathbf{T}^{(e)}$ is the matrix of direction cosine and $\mathbf{0}$ is a 2×2 null matrix. Note that it can be shown that

$$\mathbf{T}^{(e)-1} = \mathbf{T}^{(e)^T} .$$

(4.37)

For the 2D truss element shown in Figure 4.4 the total potential energy Π may be expressed in the following form for static problems

$$\Pi = \frac{1}{2} \sum_{e=1}^{ne} \left\{ [\mathbf{d}^{o(e)}]^T \mathbf{T}^{(e)^T} \mathbf{K}^{(e)} \mathbf{T}^{(e)^T} \mathbf{d}^{o(e)} - [\mathbf{d}^{o(e)}]^T \mathbf{f}^{o(e)} \right\}$$

$$= \sum_{e=1}^{n_e} \left\{ [\mathbf{d}^{o(e)}]^T \mathbf{K}^{o(e)} \mathbf{d}^{o(e)} - [\mathbf{d}^{o(e)}]^T \mathbf{f}^{o(e)} \right\}$$

(4.38)

where

$$\mathbf{K}^{(e)} = \left(\frac{EA}{\ell} \right)^{(e)} \begin{bmatrix} 1 & 0 & -1 & 0 \\ 0 & 0 & 0 & 0 \\ -1 & 0 & 1 & 0 \\ 0 & 0 & 0 & 0 \end{bmatrix}$$

(4.39)

and where the vectors of nodal displacements and forces expressed in terms of the global x^o and y^o axis may be listed as

$$\mathbf{d}^o = [u_1^o \quad v_1^o \quad u_2^o \quad v_2^o \quad \cdots\cdots \quad u_{np}^o \quad v_{np}^o]^T, \text{ and}$$

$$\mathbf{f}^o = [f_{x1}^o \quad f_{y1}^o \quad f_{x2}^o \quad f_{y2}^o \quad \cdots\cdots \quad f_{xnp}^o \quad f_{ynp}^o]^T$$

(4.40)

in which f_{xi}^o and f_{yi}^o are the applied nodal forces in the x^o and y^o directions respectively.

From Eq (4.38) the truss element stiffness matrix may be written as

$$\mathbf{K}^{o(e)} = \left(\frac{EA}{\ell}\right)^{(e)} \begin{bmatrix} c^2 & cs & -c^2 & -cs \\ cs & s^2 & -cs & -s^2 \\ -c^2 & -cs & c^2 & cs \\ -cs & -s^2 & cs & s^2 \end{bmatrix} \qquad (4.41)$$
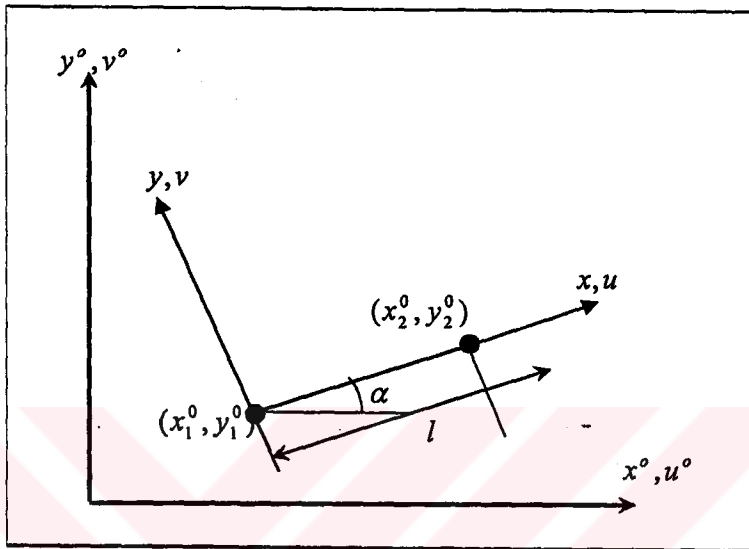
Figure 4.4 Two-noded 2D truss element

4.4 Static Analysis of Three Dimensional Trusses

Figure 4.5 shows a 3D truss element. Using the same concepts as those described in Section 4.3 it can be easily shown that the element stiffness and mass matrices for a 3D truss element may be expressed as

$$\mathbf{K}^{o(e)} = \begin{bmatrix} \mathbf{a} & -\mathbf{a} \\ -\mathbf{a} & \mathbf{a} \end{bmatrix}^{(e)} \qquad (4.42)$$

in which

$$\mathbf{a} = \left(\frac{EA}{\ell}\right) \begin{bmatrix} C_x^2 & C_x C_y & C_x C_z \\ C_x C_y & C_y^2 & C_y C_z \\ C_x C_z & C_y C_z & C_z^2 \end{bmatrix} \qquad (4.43)$$

where

58

$$C_x = (x_2^0 - x_1^0)/\ell$$

$$C_y = (y_2^0 - y_1^0)/\ell$$

$$C_z = (z_2^0 - z_1^0)/\ell$$

$$\ell = [(x_2^o - x_1^o)^2 + (y_2^o - y_1^o)^2 + (z_2^o - z_1^o)^2]^{1/2} \qquad (4.44)$$

The global displacement vector for the 3D truss element can be written in the form

$$\mathbf{d}^o = [u_1^o \quad v_1^o \quad w_1^o \quad u_2^o \quad v_2^o \quad w_2^o \quad \cdots \quad u_{np}^o \quad v_{np}^o \quad w_{np}^o]^T \qquad (4.45)$$
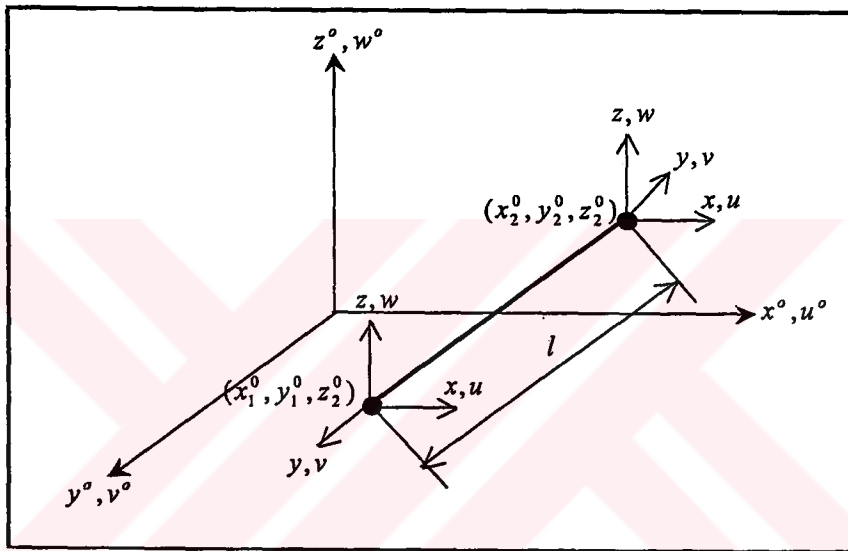
Figure 4.5 Global and local coordinate systems for a 3D truss element

4.5 Free Vibration Analysis of One Dimensional Rod Elements

For a rod element undergoing dynamic excitation, each element e experiences inertia body forces $b^{(e)}$ which has the form

$$b^{(e)} = -\int_{\ell^{(e)}} \rho^{(e)} A^{(e)} \ddot{u} d\ell \qquad (4.46)$$

where $\rho^{(e)}$ is the density of the element. A superposed $(\ddot{u})$ implies differentiation with respect to time so that the axial acceleration in the element may be written as

$$\ddot{u} = N_1^{(e)} \ddot{d}_1^{(e)} + N_2^{(e)} \ddot{d}_2^{(e)} \qquad (4.47)$$

59

If simple harmonic motion is taking place

$$\mathbf{d}^{(e)} = \overline{\mathbf{d}}^{(e)} e^{i\omega t} \tag{4.48}$$

and

$$\ddot{\mathbf{d}}^{(e)} = -\omega^2 \overline{\mathbf{d}}^{(e)} e^{i\omega t} \tag{4.49}$$

where ω is the frequency (in radians), $i = \sqrt{-1}$ and t is time.

The potential energy of the inertia body forces for element e may then be expressed in the form

$$W_I^{(e)} = \int_{\ell^{(e)}} u^{(e)} b^{(e)} d\ell$$

$$= -\omega^2 [\overline{\mathbf{d}}^{(e)}]^T \mathbf{M}^{(e)} \overline{\mathbf{d}}^{(e)} e^{i\omega t} \tag{4.50}$$

where the mass matrix $\mathbf{M}^{(e)}$ for element e can be written as

$$\mathbf{M}^{(e)} = \int_{\ell^{(e)}} [\mathbf{N}^{(e)}]^T (\rho A)^{(e)} \mathbf{N}^{(e)} d\ell$$

$$= \int_{\ell^{(e)}} \begin{bmatrix} (1-\xi) \\ \xi \end{bmatrix} (\rho A)^{(e)} [(1-\xi) \quad \xi] \ell d\xi$$

$$= \frac{(\rho A \ell)^{(e)}}{6} \begin{bmatrix} 2 & 1 \\ 1 & 2 \end{bmatrix} . \tag{4.51}$$

For simple harmonic motion the total potential of the assemblage may then be expressed as

$$\Pi = \sum_{e=1}^{ne} \frac{1}{2} \left[[\overline{\mathbf{d}}^{(e)}]^T \mathbf{K}^{(e)} \overline{\mathbf{d}}^{(e)} - \omega^2 [\overline{\mathbf{d}}^{(e)}]^T \mathbf{M}^{(e)} \overline{\mathbf{d}}^{(e)} \right] e^{2i\omega t} \tag{4.52}$$

As before, for equilibrium, Π must be a minimum which, using condition Eq (4.28), leads to the well known eigenvalue matrix equation for free vibration

$$[\mathbf{K} - \omega_p^2 \mathbf{M}] \overline{\mathbf{d}}_p = 0 \qquad\qquad p = 1, \dots np \tag{4.53}$$

where $\mathbf{M}$ is the assembled mass matrix, $\overline{\mathbf{d}}_p$ is the pth mode shape and ω_p is the associated frequency. For a representation with np nodes there will be np frequencies and mode shapes. In the present studies the eigenvalues are evaluated using the subspace iteration algorithm [3].

60

4.6 Free Vibration Analysis of Two Dimensional Trusses

Equations (4.51) represent the mass matrices for a 1D rod element expressed in terms of the end axial degrees of freedom $u_1^{(e)}$ and $u_2^{(e)}$. In this section we derive similar expression for truss members expressed in terms of degrees of freedom $u_1^{o(e)}$, $u_2^{o(e)}$, $v_1^{o(e)}$ and $v_2^{o(e)}$. Whereas $u_1^{o(e)}$ and $u_2^{o(e)}$ represent displacements in the x^o direction, $v_1^{o(e)}$ and $v_2^{o(e)}$ represent displacements in the y^o direction. Figure 4.3 shows a 2D truss element.

The total potential energy Π for trusses under inertia forces may be written as

$$\Pi = \frac{1}{2} \sum_{e=1}^{ne} [\overline{\mathbf{d}}^{o(e)}]^T \mathbf{K}^{o(e)} \, \overline{\mathbf{d}}^{o(e)} \, e^{2iwt} - \omega^2 \sum_{e=1}^{ne} [\overline{\mathbf{d}}^{o(e)}]^T \mathbf{M}^{o(e)} \, \overline{\mathbf{d}}^{o(e)} \, e^{2iwt} \qquad (4.54)$$

The derivation of stiffness matrices and the vectors of nodal displacements expressed in terms of the global x^o and y^o axis. Using the same concepts as those described in Section 4.3 it can be easily shown that the element mass matrices for a 2D truss element may be expressed as

$$\mathbf{M}^{o(e)} = [\mathbf{T}^{o(e)}]^T \mathbf{M}^{(e)} \mathbf{T}^{o(e)} \qquad (4.55)$$

where

$$\mathbf{M}^{(e)} = \left(\frac{\rho A \ell}{6}\right)^{(e)} \begin{bmatrix} 2 & 0 & 1 & 0 \\ 0 & 2 & 0 & 1 \\ 1 & 0 & 2 & 0 \\ 0 & 1 & 0 & 2 \end{bmatrix}$$

$$\mathbf{M}^{o(e)} = \mathbf{M}^{(e)} \qquad (4.56)$$

4.7 Free Vibration Analysis of Three Dimensional Trusses

Figure 4.5 shows a 3D truss element. Using the same concepts as those described in Section 4.6 it can be easily shown that the element mass matrices for a 3D truss element may be expressed as

61

$$\mathbf{M}^{o(e)} = \left(\frac{\rho A \ell}{6}\right)^{(e)} \begin{bmatrix} 2 & 0 & 0 & 1 & 0 & 0 \\ 0 & 2 & 0 & 0 & 1 & 0 \\ 0 & 0 & 2 & 0 & 0 & 1 \\ 1 & 0 & 0 & 2 & 0 & 0 \\ 0 & 1 & 0 & 0 & 2 & 0 \\ 0 & 0 & 1 & 0 & 0 & 2 \end{bmatrix} \tag{4.57}$$

The global displacement vector for the 3D trusses element can be written in the form

$$\mathbf{d}^{o} = [u_1^{o} \quad v_1^{o} \quad w_1^{o} \quad u_2^{o} \quad v_2^{o} \quad w_2^{o} \quad \cdots \cdots \quad u_{np}^{o} \quad v_{np}^{o} \quad w_{np}^{o}]^{T}$$

4.8 Example

The assemblage and solution processes and some simple benchmark examples are illustrated in references. The topic of truss analysis had been discussed frequently over recent years and there are a lot of known simple analysis techniques. Some analysis examples are given in this chapter, and each analysis program was tested against known benchmark solutions, commercial package programs, and controlled the validity and accuracy of programs. Static and free vibration analysis programs of 2D and 3D truss structures gives accurate results when compared with commercial package programs, books and exact solutions.

4.8.1 Static analysis of two and three dimensional trusses

4.8.1.1 Three-bar two dimensional truss

Problem definition: The three-bar truss of Figure 4.6 is to be analyzed. A load of 20 kip acts at $45°$ to the horizontal at node 4. Nodes 1, 2 and 3 are the locations of pin-jointed static supports. Material properties for the truss are: Young's modulus, $E = 2.07 \times 10^8$ Kip/in^2, material density, $\rho = 1.01$ b/in^3. Cross-sectional areas of members 1, and 3 are 3.0 in^2, and member 2 is 6.0 in^2.
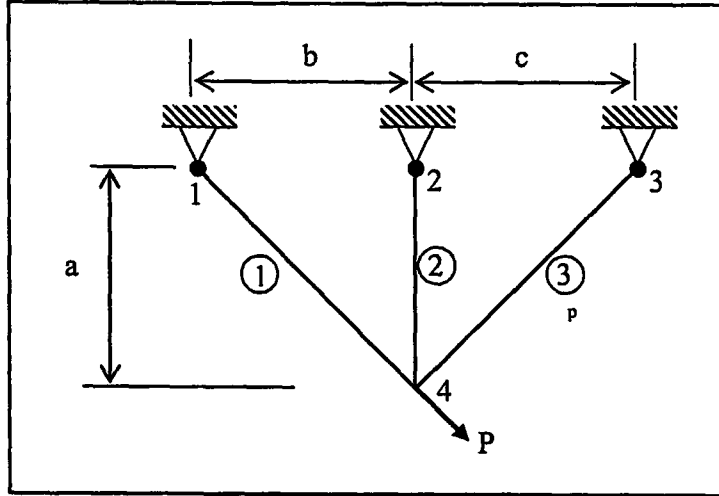
Figure 4.6 Nodal and element numbering for three bar truss (a = b = c = 100 in,
P = 20 kip)

Discussion of the results: Table 4.1 illustrates the displacements of point 4 in x and y
directions and it was compared with CME-Truss program. Close agreement between
results can be observed.

Table 4.1 Comparison of displacements at point 4 for three bar 2D truss

Displacements	Present	CME-Truss
u (in)	3.22×10^{-6}	3.22×10^{-6}
v (in)	-0.841×10^{-6}	-0.841×10^{-6}

4.8.1.2 Four-bar two dimensional truss

Problem definition: The four-bar truss of Figure 4.7 is to be analyzed. Vertical download
point loads of 10 kip and 20 kip act on nodes 2 and 3 respectively. Material properties
for the truss are: Young's modulus, $E = 1.0 \times 10^4$ kip/in^2, material density, $\rho = 1.0$
lb/in^3. Cross-sectional areas of members 1, 2, and 3 are 0.006 in^2, and member 4 is 0.008
in^2.
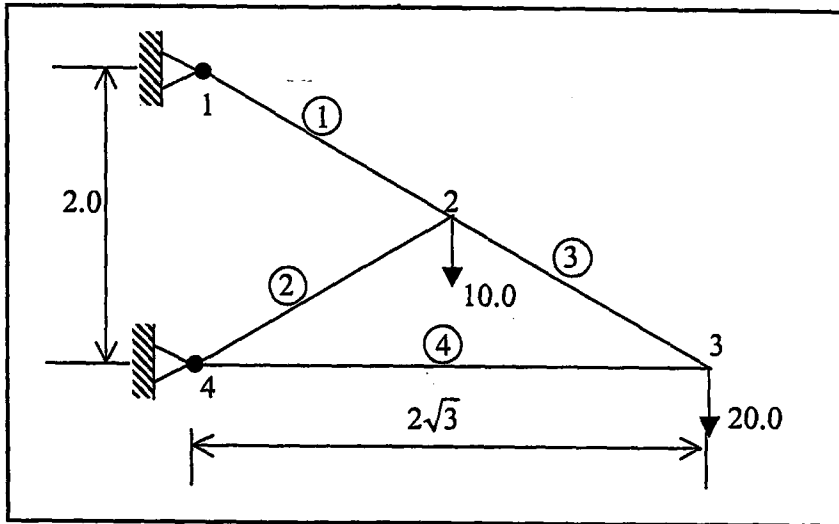
Figure 4.7 Nodal and element numbering for four bar truss

Discussion of the results: Table 4.2 illustrates the displacements of point 2 and 3 in x and y directions and it was compared with CME-Truss program. Close agreement between results can be observed.

Table 4.2 Comparison of displacements of four bar 2D truss

Point	Displacements	Present	CME-Truss
2	u (in)	0.0741	0.077
	v (in)	-0.2040	-0.200
3	u (in)	-0.1441	-0.150
	v (in)	-0.8412	-0.860

4.8.1.3 Ten-bar two dimensional truss

Problem definition: The ten-bar truss of Figure 4.8 is to be analyzed. Material properties for the truss are: Young's modulus, $E = 1.0 \times 10^7$ kip/in^2, and material density $\rho = 0.1$ lb/in^3. Cross-sectional areas of members are 5.0 in^2.

64
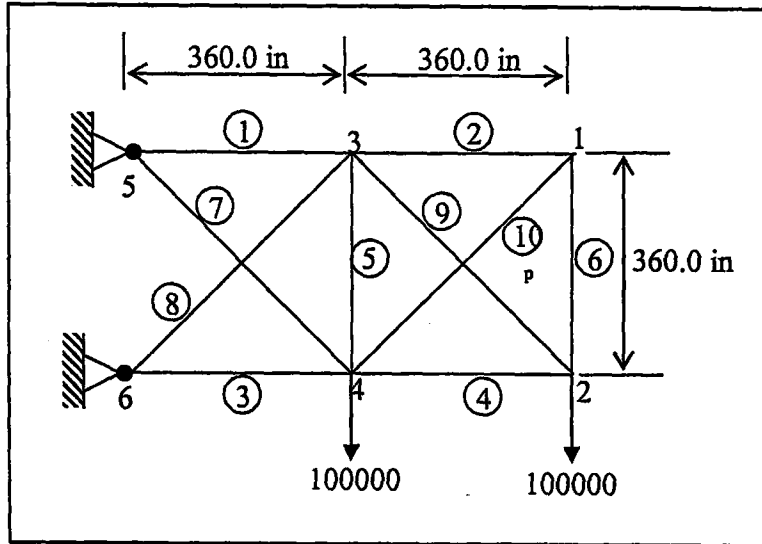
Figure 4.8 Nodal and element numbering for ten-bar truss

Discussion of the results: Table 4.3 illustrates the displacements of points in x and y directions and it was compared with CME-Truss program. Close agreement between results can be observed.

Table 4.3 Comparison of displacements of ten bar 2D truss

Point	Displacement	Present	CME-Truss
1	u (in)	0.4317	0.424
	v (in)	-1.7566	-1,900
2	u (in)	-0.4681	-0.476
	v (in)	-1.8325	-1,970
3	u (in)	0.3558	0.352
	v (in)	-0.7853	-0.837
4	u (in)	-0.3641	-0.368
	v (in)	-0.8336	-0.901

4.8.1.4 Four-bar three dimensional truss

Problem definition: The four bar truss of Figure 4.9 is to be analyzed. Material properties for the truss are: Young's modulus, $E = 0.2 \times 10^9 \, \text{kN/m}^2$ and material density $\rho = 1.0 \, \text{kg/m}^3$. Two horizontal loads of 2.0 kN and -4.0 kN are imposed in the x and y-directions at node 5, along with a 3.0 kN downward vertical load. Cross-sectional areas of members are 0.001 m².
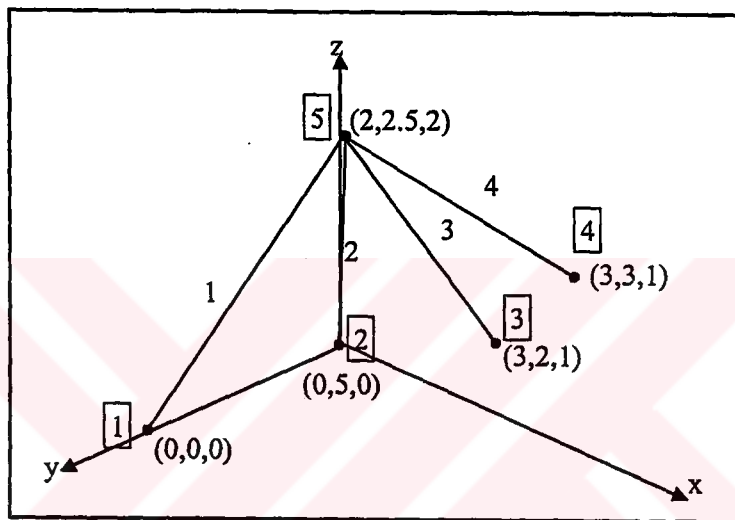
Figure 4.9 Nodal and element numbering for four-bar 3D truss

Discussion of results: Table 4.4 illustrates the displacements of point 5 in x, y and z directions and it was compared with SAP 2000. Close agreement between results can be observed.

Table 4.4 Comparison of displacements at point 5 for four bar 3D truss

Displacements	Present	SAP 2000
u (m)	0.39916×10^{-4}	0.399160×10^{-4}
v (m)	-0.525593×10^{-4}	-0.525595×10^{-4}
w (m)	0.441348×10^{-4}	0.441346×10^{-4}

4.8.1.5 Twenty five-bar three dimensional truss

The 25-bar 3D truss of Figure 4.10 is to be analyzed. Material properties for the truss are: Young's modulus, $E = 1.0 \times 10^4$ ksi, material density, $\rho = 0.1$ lb/in^3, Nodes 7, 8, 9 and 10 are fully constrained, and nodes 1, 2, 3 and 6 are loaded with different loads values see Table 4.5. Cross-sectional areas of members are 3.0 in^2.

Table 4.5 Loading details for 25-bar truss

Joint	P_x (lb)	P_y (lb)	P_z (lb)
1	1000	-10000	-10000
2	0	-10000	-10000
3	500	0	0
6	600	0	0
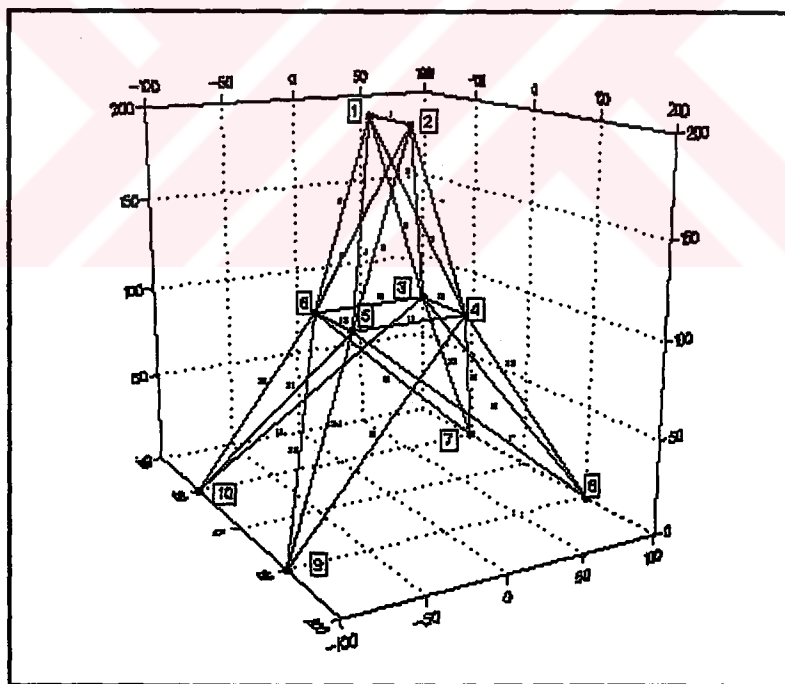
Figure 4.10 Nodal and element numbering for 25-Bar 3D truss

67

Discussion of results: Table 4.6 illustrates the displacements of points in x, y and z directions.

Table 4.6 Displacements of 25 bar 3D truss

Point	u (in)	v (in)	w (in)
1	0.01313	0.25929	-0.01411
2	0.01495	0.25865	-0.02161
3	0.86335×10^{-3}	0.01726	-0.06395
4	0.45629×10^{-2}	0.01784	-0.06846
5	0.34359×10^{-3}	0.01633	0.04188
6	0.42620×10^{-2}	0.01675	0.04683

4.8.2 Free vibration analysis of two and three dimensional trusses

4.8.2.1 Three-bar two dimensional truss

Problem definition: The three-bar truss of Figure 4.11 is to be analyzed. Material properties for the truss are: Young's modulus, $E = 2.0 \times 10^{11} \text{N/m}^2$, material density, $\rho = 7860.0 \text{ kg/m}^3$, Nodes 1, 2 and 3 are the locations of pin-jointed static supports. Cross-sectional areas of members are 0.001 m^2.
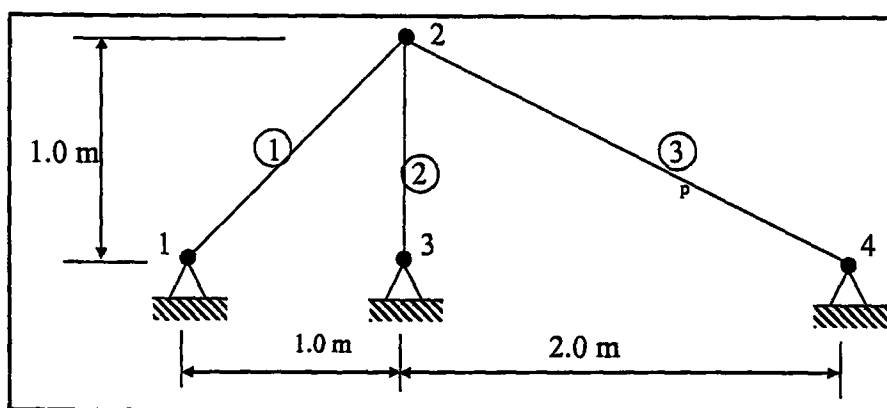
Figure 4.11 Nodal and element numbering for three bar truss

68

Discussion of results: Table 4.7 shows the three lowest natural frequencies of three bar truss. It can be seen that solutions compare very favorably with the solution obtained using GS-USA [128].

Table 4.7 Natural frequencies of three bar 2D truss

Mode	Frequencies (Hz)		
	Present	GS-USA[128]	Ref. [112]
1	528.529	515.436	542.61
2	785.117	761.558	-

4.8.2.2 Nine-bar two dimensional truss

Problem definition: The nine bar truss of Figure 4.12 is to be analyzed. Material properties for the truss are: Young's modulus, $E = 2.0 \times 10^{11} \text{N/m}^2$, material density, $\rho = 7860.0 \text{ kg/m}^3$. Node 1 acts as a pin-jointed static support, while node 6 is free to move in the x-direction. Cross-sectional areas of members are 0.2 m^2.
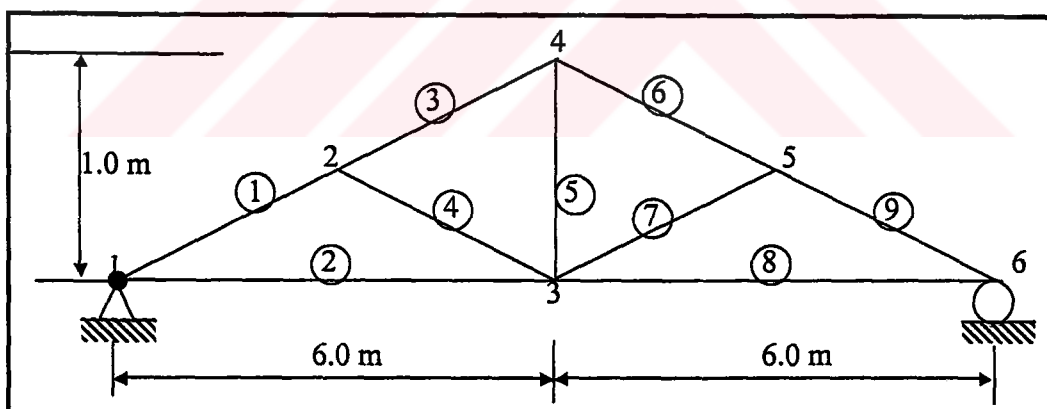
Figure 4.12 Nodal and element numbering for nine-bar truss

Discussion of results: The five lowest natural frequencies of nine bar are listed in Table 4.8. The results of the analyses compare very well with those obtained using GS-USA [128] program.

Table 4.8 Natural frequencies of nine bar 2D truss

Mode	Frequencies (Hz)	
	Present	GS-USA [128]
1	30.788	30.332
2	81.222	80.367
3	112.166	107.095
4	225.089	209.049
5	251.368	246.256

4.8.2.3 Three-bar three dimensional truss

Problem definition: The 3D three-bar truss of Figure 4.13 is to be analyzed. Material properties for the truss are: Young's modulus, $E = 6.7 \times 10^{10}\,\text{N/m}^2$, material density, $\rho = 2700.0\,\text{kg/m}^3$. Nodes 1, 2 and 3 are the locations of pin-jointed static supports. Cross-sectional areas of members are $0.0004\,\text{m}^2$.
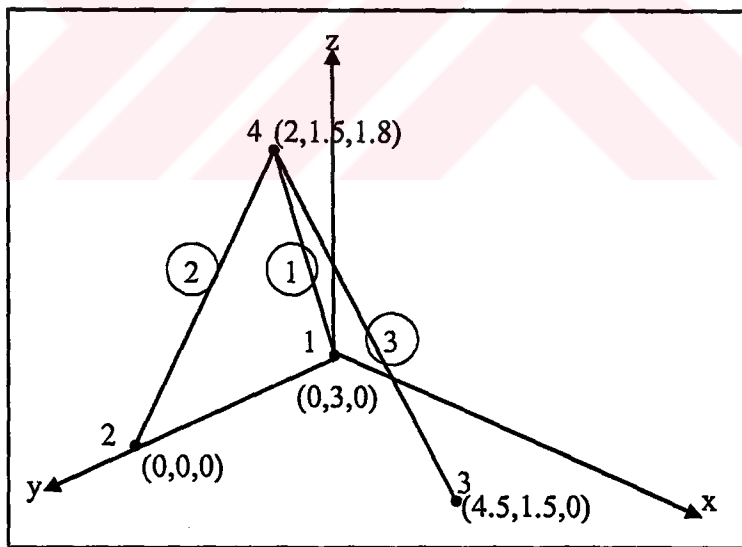
Figure 4.13 Nodal and element numbering for three bar 3D truss

Discussion of results: Table 4.9 shows the first three modes of frequencies of three bar 3D truss. There is remarkably good agreement between the present results and those obtained using SAP 2000 commercial program. Once again, this comparison clearly indicates the accuracy of the present formulation.

Table 4.9 Natural frequencies of three bar 3D truss

Mode	Frequencies (Hz)	
	Present	SAP 2000
1	177.083	178.752
2	242.912	245.376
3	328.620	332.078

CHAPTER 5

STATIC ANALYSIS OF TWO AND THREE DIMENSIONAL STRUCTURES

5.1 Introduction

Considerable research effort has been directed towards the development of accurate and inexpensive analysis procedures for structures in static situations. Most structural analysis problems can be treated as *linear static* problems, which can provide most of the information about the behavior of a structure, and can be a good approximation for many analyses.

In the analysis of beams, arches and frames, structural engineers use mathematical models which may or may not take into account the effect of transverse shear deformation; two types of beam theory are widely used: Thin beam theory and thick beam theory. The kinematic assumptions of these theories are:

1) Kirchhoff-Love (or Euler-Bernoulli) theory: the planes normal to the midline are assumed to remain plane and normal; this is also called engineering beam theory or thin beam theory. See Figure 5.1.

2) MR (or Timoshenko-Hencky) theory: the planes normal to the midsurface remain straight, but not necessarily normal to the midsurface after deformation. In other words, the normals undergo an extra rotation due to transverse shear deformation. This theory is also called shear beam theory or thick beam theory. See Figure 5.2.

MR arch theory is similar to Timoshenko beam theory. Only difference is that MR theory can be applicable to the arch structures. Several benefits have accrued from the

use of MR theory such as automatic inclusion of transverse shear deformation effects and thus offer an attractive alternative to classical Kirchhoff-Love beam theory. It is well known that displacement based MR FEs requires only $C(0)$ continuity of the displacements and independent normal rotations between adjacent elements. This provides an important advantage over FEs based on classical Kirchhoff-Love theory where $C(1)$ continuity is strictly required.
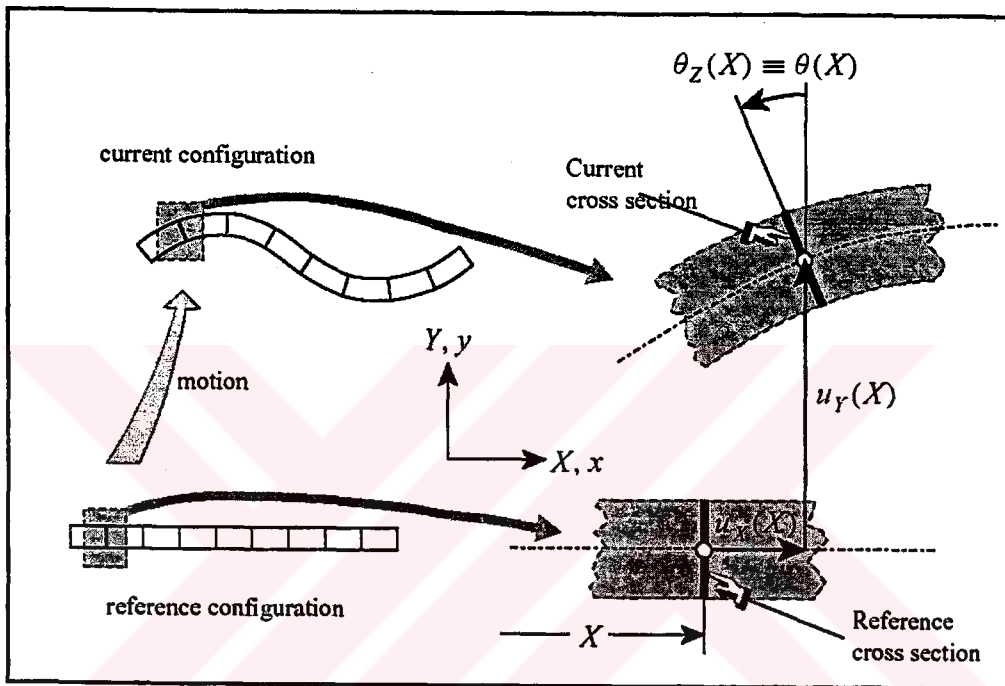
Figure 5.1 Euler-Bernoulli beam theory [11]

The behaviors of MR straight and curved (arch) beam element are usually very good and it is only in shear stiff thin beams that real problems arise. In thin, displacement based elements, full integration of stiffness matrices leads to locking or over stiff behavior and reduced integration process is required to overcome these difficulties [11].

In the present study, the structures are modeled using linear, quadratic or cubic, curved, variable thickness, $C(0)$ continuity MR FEs. These belong to a family of elements introduced by Day and Potts [23] and subsequently extended by Hinton and co-workers [14]. This element has over performance than Kirchhoff-Love based FE. In this present study the shell element extended by Hinton and his coworkers will be

73

adopted to curved beam element. In the following sections, the fundamental theory of FE formulation is presented.
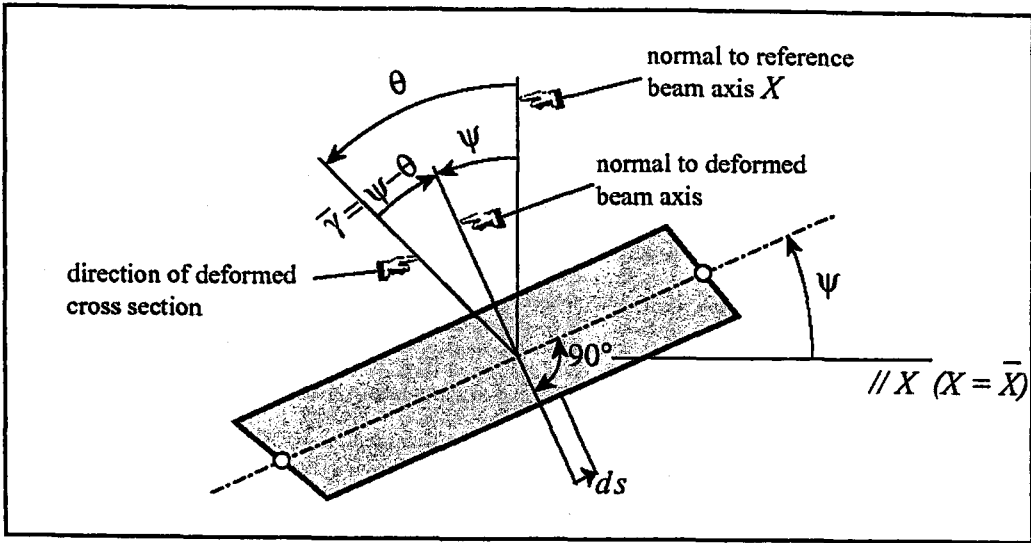
Figure 5.2 Timoshenko beam theory [11]

5.2 Planar Structures

In this section, we consider the basic formulation and associated FE idealization based on the MR type models for linearly elastic analysis of variable thickness beam, arch and frame structures.

5.2.1 Theory of structural matrix

Consider the MR curved beam element shown in Figure 5.3. The displacement components u_ℓ and w_ℓ, are associated with movements in ℓ and n directions respectively, expressed in terms of axes which are tangential and normal to the arch, may be written in terms of global displacements u and w in the x and y directions as

$$u_\ell = u\cos\alpha + w\sin\alpha$$

$$w_\ell = -u\sin\alpha + w\cos\alpha \qquad (5.1)$$

where α is shown in Figure 5.3. The radius of curvature R may be obtained from the expression

$$\frac{d\alpha}{d\ell} = -\frac{1}{R} \qquad (5.2)$$

74
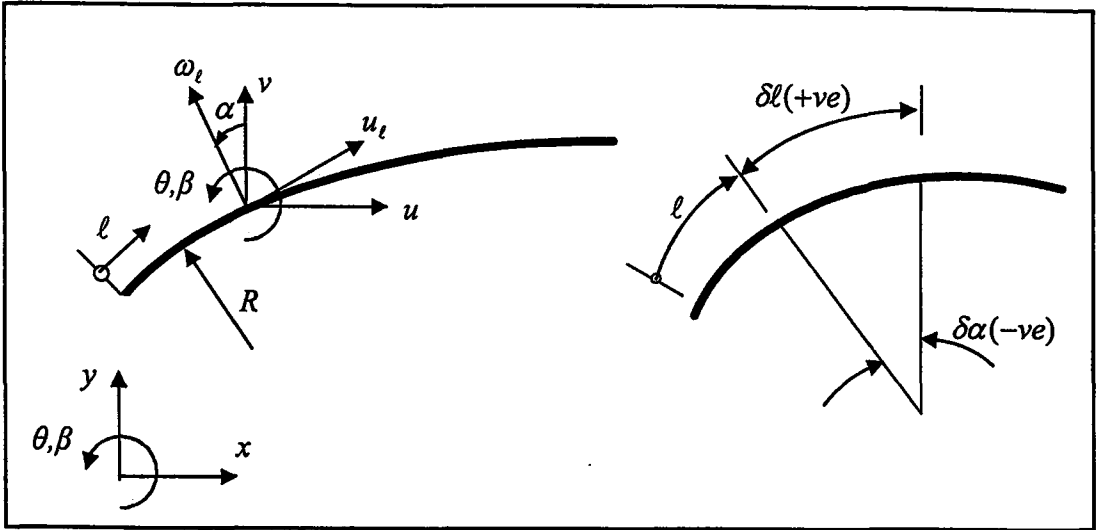
Figure 5.3 Definition of curved Mindlin-Reissner arch FEs

The total potential energy for a typical MR curved beam element resting on elastic Winkler type foundation of modulus k shown in Figure 5.3 is given in terms of the global displacements u and w and rotation θ of the midsurface normal in the ℓn plane by expression.

$$\Pi(u_\ell, w_\ell, \theta) = 1/2 \int \left([\varepsilon_m]^T D_m \varepsilon_m + [\varepsilon_b]^T D_b \varepsilon_b + [\varepsilon_s]^T D_s \varepsilon_s + k w_\ell^2 \right) d\ell$$
$$- \int u_\ell q_u d\ell - \int w_\ell q_w d\ell - \int \theta_\ell q_\theta d\ell - (M \bar{\theta} + N \bar{u}_\ell + \bar{w}_\ell) \tag{5.3}$$

where the membrane (axial) strain is given by the expression

$$\varepsilon_m = \frac{du_\ell}{d\ell} + \frac{w_\ell}{R} \tag{5.4}$$

or re-writing in terms of the global displacements

$$\varepsilon_m = \frac{du}{d\ell} \cos\alpha + \frac{dw}{d\ell} \sin\alpha \tag{5.5}$$

The bending (flexural) strain or curvature may be written as

$$\varepsilon_b = -\frac{d\theta}{d\ell} \tag{5.6}$$

and the shear strain is given as

$$\varepsilon_s = \frac{dw_\ell}{d\ell} - \theta - \frac{u_\ell}{R} \tag{5.7}$$

or

75

$$\varepsilon_s = -\theta - \frac{du}{d\ell}\sin\alpha + \frac{dw}{d\ell}\cos\alpha \qquad (5.8)$$

Also, note that the membrane, bending and shear rigidities have the form

$$D_m = EA; \qquad D_b = EI; \qquad D_s = \kappa GA \qquad (5.9)$$

where E is the elastic modulus, A is the cross-sectional area, I is the moment of inertia, G is the shear modulus and κ is the shear modification factor and is taken as $5/6$ for an arch of rectangular cross-section.

Note that the displacement field vector $\mathbf{u}$ has the form

$$\mathbf{u} = [u_\ell, w_\ell, \theta] \qquad (5.10)$$

and the corresponding distributed loading $\mathbf{q}$ may be written as

$$\mathbf{q} = [q_u, q_w, q_\theta]^T \qquad (5.11)$$

in which the distributed forces are q_u and q_w and the distributed couples q_θ.

The loading in Eq (5.3) consists of a distributed pressure loading $\mathbf{q}$, as well as couples M, axial forces N or lateral forces Q applied at $\ell = \overline{\ell}$. Note that $\overline{u}_\ell$, $\overline{w}_\ell$ and $\overline{\theta}$ are the corresponding displacement and rotation values at $\ell = \overline{\ell}$.

5.2.2 Finite element idealization

Using n-noded, $C(0)$ line elements, the global displacement parameters u, w and θ may be interpolated, within each beam element by the expressions

$$u = \sum_{i=1}^{n} N_i u_i; \qquad w = \sum_{i=1}^{n} N_i w_i; \qquad \theta = \sum_{i=1}^{n} N_i \theta_i \qquad (5.12)$$

where u_i, w_i and θ_i are typical nodal displacement degrees of freedom and $N_i(\xi)$ is the shape function expressed in terms of the natural coordinates ξ and associated with node i which, for 2-noded linear elements, have the form

$$N_1 = 1/2(1-\xi); \qquad N_2 = 1/2(1+\xi) \qquad (5.13)$$

for 3-noded, quadratic elements

$$N_1 = \xi/2(\xi-1); \qquad N_2 = (1-\xi^2); \qquad N_3 = \xi/2(\xi+1) \qquad (5.14)$$

and for 4-noded, cubic elements

$$N_1 = -9/16(\xi^2 - 1/9)(\xi - 1); \qquad N_2 = 27/16(\xi^2 - 1)(\xi - 1/3);$$

$$N_3 = -27/16(\xi^2 - 1)(\xi + 1/3); \qquad N_4 = -9/16(\xi^2 - 1/9)(\xi + 1) \qquad (5.15)$$

These elements are essentially isoparametric and variable thickness so that

$$x = \sum_{i=1}^{n} N_i x_i; \qquad y = \sum_{i=1}^{n} N_i y_i; \qquad t = \sum_{i=1}^{n} N_i t_i; \qquad b = \sum_{i=1}^{n} N_i b_i \qquad (5.16)$$

where x_i, y_i, t_i and b_i are typical coordinates, thickness and width of node i respectively. Note also that the Jacobian may be written as

$$J = \frac{d\ell}{d\xi} = \left[\left(\frac{\partial x}{\partial \xi} \right)^2 + \left(\frac{\partial y}{\partial \xi} \right)^2 \right]^{1/2}; \qquad d\ell = J d\xi \qquad (5.17)$$

where

$$\frac{\partial x}{\partial \xi} = \sum_{i=1}^{n} \frac{\partial N_i}{\partial \xi} x_i; \qquad \frac{\partial y}{\partial \xi} = \sum_{i=1}^{n} \frac{\partial N_i}{\partial \xi} y_i \qquad (5.18)$$

Also

$$\sin\alpha = \frac{dy}{d\xi}\frac{1}{J}; \qquad \cos\alpha = \frac{dx}{d\xi}\frac{1}{J} \qquad (5.19)$$

and

$$\frac{dN_i}{d\ell} = \frac{dN_i}{d\xi}\frac{1}{J} \qquad (5.20)$$

The axial strains ε_m may then be expressed as

$$\varepsilon_m = \sum_{i=1}^{n} \mathbf{B}_{mi}^{e} \mathbf{d}_{i}^{e} \qquad (5.21)$$

where

$$\mathbf{B}_{mi}^{e} = \left[(\partial N_i / \partial \ell)\cos\alpha \quad (\partial N_i / \partial \ell)\sin\alpha \quad 0 \right] \qquad (5.22)$$

and

$$\mathbf{d}_{i}^{e} = [u_i, w_i, \theta_i]^T \qquad (5.23)$$

The flexural strain or curvatures ε_b can be written as

$$\varepsilon_b = \sum_{i=1}^{n} \mathbf{B}_{bi}^{e} \mathbf{d}_{i}^{e} \qquad (5.24)$$

where

$$\mathbf{B}_{bi}^{e} = \left[0 \quad 0 \quad -dN_i / d\ell \right] \qquad (5.25)$$

and the shear strain ε_s is approximated as

$$\varepsilon_s = \sum_{i=1}^{n} \mathbf{B}_{si}^e \mathbf{d}_i^e \tag{5.26}$$

where

$$\mathbf{B}_{si}^e = \left[-(dN_i/d\ell)\sin\alpha \quad (dN_i/d\ell)\cos\alpha \quad -N_i \right] \tag{5.27}$$

Thus, neglecting point loads and couples, the contribution to the total potential from element e may be expressed as

$$\Pi^e = \sum_{i=1}^{n} \sum_{j=1}^{n} \frac{1}{2} [\mathbf{d}_i^e]^T \mathbf{K}_{ij}^e \mathbf{d}_j^e - \sum_{i=1}^{n} [\mathbf{d}_i^e]^T \mathbf{f}_i^e \tag{5.28}$$

where the submatrix of the stiffness matrix $\mathbf{K}_{ij}^e$ linking nodes i and j has the form

$$\mathbf{K}_{ij}^e = \int_{-1}^{+1} \{ \mathbf{B}_{mi}^T D_m \mathbf{B}_{mj} + \mathbf{B}_{bi}^T D_b \mathbf{B}_{bj} + \mathbf{B}_{si}^T D_s \mathbf{B}_{sj} \} J d\xi + \left[\overline{K}_{ij}^e \right] \tag{5.29}$$

where

$$\left[\overline{K}_{ij}^e \right] = \begin{bmatrix} k_{uu} & k_{uw} & 0 \\ k_{wu} & k_{ww} & 0 \\ 0 & 0 & 0 \end{bmatrix} \tag{5.30}$$

in which

$$k_{uu} = \int_{-1}^{+1} k N_i N_j \sin^2\alpha \, J d\xi$$

$$k_{wu} \text{ and } k_{uw} = -\int_{-1}^{+1} k N_i N_j \sin\alpha\cos\alpha \, J d\xi$$

$$k_{ww} = \int_{-1}^{+1} k N_i N_j \cos^2\alpha \, J d\xi \tag{5.31}$$

and the consistent nodal force vector associated with node i is written as

$$\mathbf{f}_i^e = \begin{bmatrix} \int_{-1}^{+1} N_i q_u \cos\alpha \, J d\xi \\ \int_{-1}^{+1} N_i q_u \sin\alpha \, J d\xi \\ 0 \end{bmatrix} + \begin{bmatrix} \int_{-1}^{+1} N_i q_w \sin\alpha \, J d\xi \\ \int_{-1}^{+1} N_i q_w \cos\alpha \, J d\xi \\ 0 \end{bmatrix} + \begin{bmatrix} 0 \\ 0 \\ \int_{-1}^{+1} N_i q_\theta \, J d\xi \end{bmatrix} + \begin{bmatrix} N \\ Q \\ M \end{bmatrix} \tag{5.32}$$

To avoid locking behavior, reduced integration is adopted, i.e. 1-, 2- and 3- point Gauss-Legendre quadrature is used for 2-, 3- and 4- noded elements respectively [14]. Note also that since the rigidities D_m, D_b and D_s all depend on t and since t is

interpolated within each element e from the nodal values t_i, elements of variable thickness can be easily accommodated in the present formulation.

5.3 Three Dimensional Frame Analysis

3D frames also called as space frames, are frequently encountered in the analysis of multistory buildings. They can also be found in the modeling of the car body and the bicycle frames. In this section, we consider the basic formulation and associated FE idealization based on the MR type models for linearly elastic analysis of variable thickness grid and frame structures. The elements used are based on Day and Potts [23].

5.3.1 Theory of structural matrix

Consider the MR 3D frame element shown in Figure 5.4. Each node has six degrees of freedom (as opposed to only three degrees of freedom in a planar structure). The degrees of freedom numbering is shown in Figure5.4. For node i, u, v and w represent translational degrees of freedom, while θ_x, θ_y and θ_z represent rotational degrees of freedom in x, y and z axes. The element displacement vectors in local and global coordinate systems are denoted as $\mathbf{d'}$ and $\mathbf{d}$ respectively. These vectors are

$$\mathbf{d'} = [u' \quad v' \quad w' \quad \theta_x' \quad \theta_y' \quad \theta_z'] \qquad \mathbf{d} = [u \quad v \quad w \quad \theta_x \quad \theta_y \quad \theta_z] \qquad (5.33)$$

The global displacements may be written in terms of local displacement as

$$\mathbf{d} = \mathbf{d'T} \qquad (5.34)$$

where $\mathbf{T}$ is the transformation matrix which is given in Appendix A,

The total potential energy for a typical MR space frame element is given as

$$\Pi(u',v',w',\theta_x',\theta_y',\theta_z') = 1/2 \int \left([\varepsilon_m]^T \mathbf{D}_m \varepsilon_m + [\varepsilon_b]^T \mathbf{D}_b \varepsilon_b + [\varepsilon_s]^T \mathbf{D}_s \varepsilon_s \right) d\ell$$
$$- \int (u'q_x + v'q_y + w'q_z) d\ell - (Nu + Q_y v + Q_z w + T\theta_x + M_y \theta_y + M_z \theta_z) \qquad (5.35)$$

where the membrane (axial) strain is given by the expression

$$\varepsilon_m = \left[\frac{du'}{dx'} \right] \qquad (5.36)$$
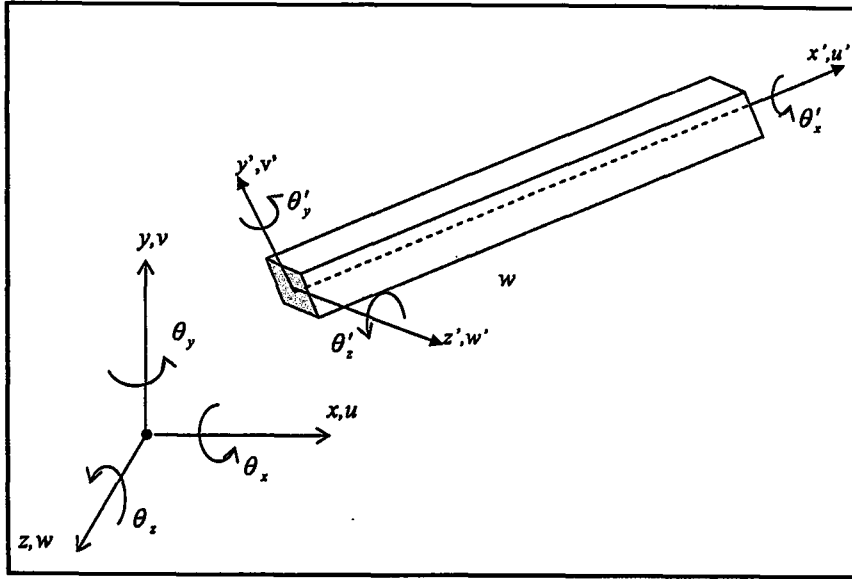
Figure 5.4 Local and global coordinates of Mindlin-Reissner 3D frame element

The bending (flexural) strain may be written as

$$\varepsilon_b = [\varepsilon_y \quad \varepsilon_z] \tag{5.37}$$

the flexural strain in y and z axes are given as

$$\varepsilon_y = -\frac{d\theta'_z}{dz'}; \qquad \varepsilon_z = -\frac{d\theta'_y}{dy'} \tag{5.38}$$

The shear strain is given as

$$\varepsilon_s = [\gamma_{xx} \quad \gamma_{xy} \quad \gamma_{xz}] \tag{5.39}$$

the shear strain in x, y and z axes are given as

$$\gamma_{xx} = \frac{d\theta'_x}{dx'} \qquad \gamma_{xy} = \frac{dw'_x}{dx'} + \theta'_y \qquad \gamma_{xz} = \frac{dv'_x}{dx'} - \theta'_z \tag{5.40}$$

The axial, flexural and shear rigidities have the form

$$\mathbf{D}_m = [EA]; \qquad \mathbf{D}_b = \begin{bmatrix} EI_z & 0 \\ 0 & EI_y \end{bmatrix}; \qquad \mathbf{D}_s = \begin{bmatrix} GA/\alpha & 0 & 0 \\ 0 & GA/\alpha & 0 \\ 0 & 0 & GJ \end{bmatrix} \tag{5.41}$$

where E is the elastic modulus, A is the cross-sectional area, I_z, I_y are the moment of inertia with respect to z and y axes, J is the polar moment of inertia, G is the shear modulus and κ is the shear modification factor and is taken as $5/6$ for rectangular cross-section.

80

The loading in Eq (5.31) consists of a distributed pressure loading q_x, q_y, q_z as well as couples M_y, M_z, torque T, axial forces N or lateral forces V_y, V_z applied along the member.

5.3.2 Finite element idealization

Using n-noded, $C(0)$ line elements, the global displacement parameters u, and θ may be interpolated, within each beam element by the expressions

$$u = \sum_{i=1}^{n} N_i u_i \ ; \qquad v = \sum_{i=1}^{n} N_i v_i \ ; \qquad w = \sum_{i=1}^{n} N_i w_i \ ;$$

$$\theta_x = \sum_{i=1}^{n} N_i \theta_{xi} \ ; \qquad \theta_y = \sum_{i=1}^{n} N_i \theta_{yi} \ ; \qquad \theta_z = \sum_{i=1}^{n} N_i \theta_{zi} \qquad (5.42)$$

where u_i, v_i, w_i, θ_{xi}, θ_{yi} and θ_{zi} are typical nodal displacement degrees of freedom and $N_i(\xi)$ is the shape function associated with node i which, for 2-noded linear elements, have the form

$$N_1 = 1/2(1-\xi); \qquad\qquad N_2 = 1/2(1+\xi) \qquad (5.43)$$

for 3-noded, quadratic elements

$$N_1 = \xi/2(\xi-1); \qquad N_2 = (1-\xi^2); \qquad N_3 = \xi/2(\xi+1) \qquad (5.44)$$

and for 4-noded, cubic elements

$$N_1 = -9/16(\xi^2 - 1/9)(\xi - 1); \qquad\qquad N_2 = 27/16(\xi^2 - 1)(\xi - 1/3);$$

$$N_3 = -27/16(\xi^2 - 1)(\xi + 1/3); \qquad\qquad N_4 = -9/16(\xi^2 - 1/9)(\xi + 1) \qquad (5.45)$$

These elements are essentially isoparametric so that

$$x = \sum_{i=1}^{n} N_i x_i \ ; \quad y = \sum_{i=1}^{n} N_i y_i \ ; \quad z = \sum_{i=1}^{n} N_i z_i \ ; \quad h = \sum_{i=1}^{n} N_i h_i \ ; \quad b = \sum_{i=1}^{n} N_i b_i \quad (5.46)$$

where x_i, y_i, z_i, h_i and b_i are typical coordinates, thickness and width of node i respectively. Note also that the Jacobian

$$J = \frac{d\ell}{d\xi} = \left[\left(\frac{\partial x}{\partial \xi} \right)^2 + \left(\frac{\partial y}{\partial \xi} \right)^2 + \left(\frac{\partial z}{\partial \xi} \right)^2 \right]^{1/2} ; \qquad d\ell = J d\xi \qquad (5.47)$$

where

$$\frac{\partial x}{\partial \xi} = \sum_{i=1}^{n} \frac{\partial N_i}{\partial \xi} x_i ; \qquad \frac{\partial y}{\partial \xi} = \sum_{i=1}^{n} \frac{\partial N_i}{\partial \xi} y_i \qquad \frac{\partial z}{\partial \xi} = \sum_{i=1}^{n} \frac{\partial N_i}{\partial \xi} z_i \qquad (5.48)$$

81

and

$$\frac{dN_i}{d\ell} = \frac{dN_i}{d\xi} \frac{1}{J} \tag{5.49}$$

The axial strains ε_m may then be expressed as

$$\varepsilon_m = \sum_{i=1}^{n} \mathbf{B}_{mi}^e \mathbf{d}_i^e \tag{5.50}$$

where

$$\mathbf{B}_{mi}^e = [dN/dx' \quad 0 \quad 0 \quad 0 \quad 0 \quad 0] \tag{5.51}$$

and

$$\mathbf{d}_i^e = [u_i, v_i, w_i, \theta_{xi}, \theta_{yi}, \theta_{zi}]^T \tag{5.52}$$

The flexural strain or curvatures ε_b can be written as

$$\varepsilon_b = \sum_{i=1}^{n} \mathbf{B}_{bi}^e \mathbf{d}_i^e \tag{5.53}$$

where

$$\mathbf{B}_{bi}^e = \begin{bmatrix} 0 & 0 & 0 & 0 & 0 & dN/dx' \\ 0 & 0 & 0 & 0 & dN/dx' & 0 \end{bmatrix} \tag{5.54}$$

and the shear strain ε_s is approximated as

$$\varepsilon_s = \sum_{i=1}^{n} \mathbf{B}_{si}^e \mathbf{d}_i^e \tag{5.55}$$

where

$$\mathbf{B}_{si}^e = \begin{bmatrix} 0 & dN/dx' & 0 & 0 & 0 & -N \\ 0 & 0 & dN/dx' & 0 & N & 0 \\ 0 & 0 & 0 & dN/dx' & 0 & 0 \end{bmatrix} \tag{5.56}$$

Thus, neglecting point loads and couples, the contribution to the total potential from element e may be expressed as

$$\Pi^e = \sum_{i=1}^{n} \sum_{j=1}^{n} \frac{1}{2} [\mathbf{d}_i^e]^T \mathbf{K}_{ij}^e \mathbf{d}_j^e - \sum_{i=1}^{n} [\mathbf{d}_i^e]^T \mathbf{f}_i^e \tag{5.57}$$

as we wish to set up the governing matrix in terms of strain expressed in global rather than local directions, it is worth noting the membrane strain displacement matrix is then modified to

82

$$\overline{\mathbf{B}}_{mi} = \mathbf{B}_{mi}\,\mathbf{T} \tag{5.58}$$

with similar expression for $\overline{\mathbf{B}}_{bi}$ and $\overline{\mathbf{B}}_{si}$. T is the transformation matrix and given in appendix A.

The submatrix of the stiffness matrix linking nodes i and j can then be written as

$$\mathbf{K}_{ij}^e = \int_{-1}^{+1}\{\overline{\mathbf{B}}_{mi}^T\mathbf{D}_m\overline{\mathbf{B}}_{mj} + \overline{\mathbf{B}}_{bi}^T\mathbf{D}_b\overline{\mathbf{B}}_{bj} + \overline{\mathbf{B}}_{si}^T\mathbf{D}_s\overline{\mathbf{B}}_{sj}\}J\,d\xi \tag{5.59}$$

and the consistent nodal force vector associated with node i is written as

$$\mathbf{f}_i^e = \begin{bmatrix} \int_{-1}^{+1}N_iq_{ux}J\,d\xi \\ \int_{-1}^{+1}N_iq_{uy}J\,d\xi \\ \int_{-1}^{+1}N_iq_{uz}J\,d\xi \\ 0 \\ 0 \\ 0 \end{bmatrix} + \begin{bmatrix} \int_{-1}^{+1}N_iq_{wx}J\,d\xi \\ \int_{-1}^{+1}N_iq_{wy}J\,d\xi \\ \int_{-1}^{+1}N_iq_{wz}J\,d\xi \\ 0 \\ 0 \\ 0 \end{bmatrix} + \begin{bmatrix} 0 \\ 0 \\ 0 \\ \int_{-1}^{+1}N_iq_{\theta x}J\,d\xi \\ \int_{-1}^{+1}N_iq_{\theta y}J\,d\xi \\ \int_{-1}^{+1}N_iq_{\theta z}J\,d\xi \end{bmatrix} + \begin{bmatrix} N \\ Q_y \\ Q_z \\ M_x \\ M_y \\ M_z \end{bmatrix} \tag{5.60}$$

5.4 Stress Resultant and Strain Energy Evaluation

The stress resultant vector can be expressed as

$$\sigma = \begin{bmatrix} \sigma_m \\ \sigma_b \\ \sigma_s \end{bmatrix} \tag{5.61}$$

where σ_m, σ_b and σ_s are the stress resultant vectors due to membrane, bending and shear effects, so that

$$\sigma_m = [N]; \qquad \sigma_b = [M_y \quad M_z]; \qquad \sigma_s = [M_x \quad Q_y \quad Q_z] \tag{5.62}$$

the stress resultants can be obtained by the expressions

$$\sigma_m = \mathbf{D}_m\sum_{i=1}^n\mathbf{B}_{mi}\mathbf{d}_i\,, \qquad \sigma_b = \mathbf{D}_b\sum_{i=1}^n\mathbf{B}_{bi}\mathbf{d}_i\,, \qquad \sigma_s = \mathbf{D}_s\sum_{i=1}^n\mathbf{B}_{si}\mathbf{d}_i \tag{5.63}$$

The SE of the FE solution $\|\hat{\mathbf{W}}\|^2$ for the beam is computed as the sum of the bending, membrane and shear SEs

$$\|\hat{\mathbf{W}}\|^2 = \|\hat{\mathbf{W}}\|_b^2 + \|\hat{\mathbf{W}}\|_m^2 + \|\hat{\mathbf{W}}\|_s^2$$

$$\left\| \hat{W} \right\|_{b}^{2} \approx \int_{\Omega} [\hat{\sigma}_{b}]^{T} D_{b}^{-1} \hat{\sigma}_{b} d\Omega$$

$$\left\| \hat{W} \right\|_{m}^{2} \approx \int_{\Omega} [\hat{\sigma}_{m}]^{T} D_{m}^{-1} \hat{\sigma}_{m} d\Omega$$

$$\left\| \hat{W} \right\|_{s}^{2} \approx \int_{\Omega} [\hat{\sigma}_{s}]^{T} D_{s}^{-1} \hat{\sigma}_{s} d\Omega \qquad (5.64)$$

5.5 Static Analysis Examples

To verify that the formulation of the FE model can be successfully used for the static analysis of the structures, several examples for which solutions are available have been considered. Note that in all cases the nodes of the structures have six degrees of freedom, because of 3D analyses. These degrees of freedom are translations in x, y and z directions and rotations about x, y and z-axes, respectively.

5.5.1 Thick beams

Problem definition: The thick beams with various combinations of loading and boundary conditions have been analyzed by Chen [136] using the differential quadrature element method based on the Timoshenko beam model. The beams are 3 m long and the cross-sectional dimension of 5×5 m as shown in Figure 5.5. The following material properties are used: modulus of elasticity $E = 2.6 \, \text{Pa}$, Poisson's ratio $v = 0.3$ and rigidity modulus $G = 1.0 \, \text{Pa}$. The thick beam is analyzed for two separate loading and boundary conditions:

1. A fixed- free beam subject to point load at the free end. See Figure 5.5(a)
2. A fixed- fixed beam subject to a uniformly distributed load. See Figure 5.5(b)
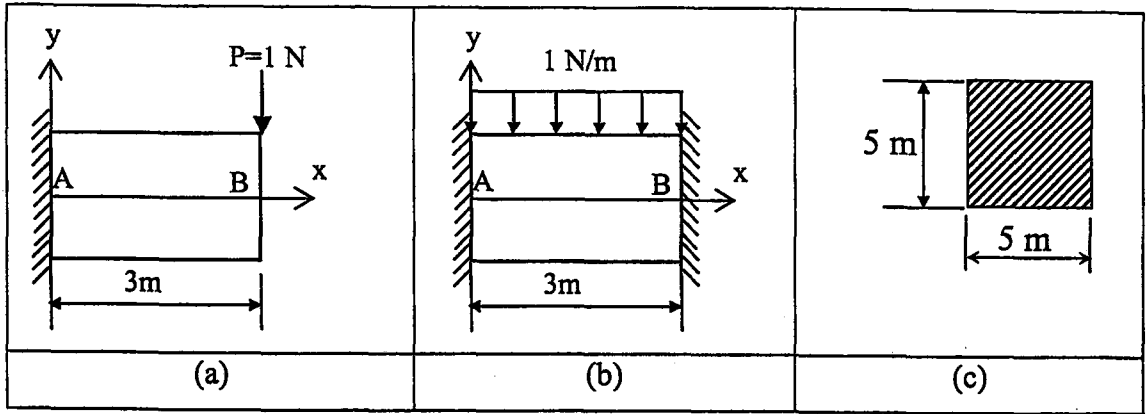
Figure 5.5 Thick beams (a) fixed-free subject to a point load, (b) fixed-fixed subject to a uniformly distributed load, (c) cross sectional dimension of the beams

Table 5.1 Results of a fixed-free Timoshenko beam subjected to transverse force at the free end

Element type	DOF	Displacement at B (m)	Moment at A (Nm)	Shear force at A (N)
Linear	18	-0.207176	2.75000	1.10788
	36	-0.207540	2.88462	1.05223
	54	-0.207581	2.91176	1.04032
	183	-0.207634	2.97541	1.01148
Quadratic	18	-0.207638	3.00000	1.01308
	36	-0.207638	3.00000	1.00327
	54	-0.207638	3.00000	1.00145
Cubic	18	-0.207638	3.00000	1.00000
	36	-0.207638	3.00000	1.00000
	54	-0.207638	3.00000	1.00000
Chen [136]		-0.207638	3.00000	1.00000
Exact solution		-0.207638	3.00000	1.00000

Discussion of results: In this example, the convergence and general performance of the linear, quadratic and cubic FEs are examined. The beam is discretized using three sets of meshes of 18, 36 and 54 degrees of freedom. The deflections and stress resultants are listed in Tables 5.1 and 5.2 for fixed-free and fixed-fixed beams

85

respectively. The results of the analyses are found to be in excellent agreement with exact solution and the results presented by Chen [136]. As we can see from Tables 5.1 and 5.2, the quadratic and cubic elements give better performance and convergence than the linear elements.

Table 5.2 Results of a fixed-fixed Timoshenko beam subjected to uniformly distributed load

Element type	DOF	Displacement at middle (m)	Moment at A (Nm)	Moment at middle (Nm)	Shear force at A (N)
Linear	18	-0.0543258	-0.416667	0.333333	1.26635
	36	-0.0544556	-0.572917	0.364583	1.38624
	54	-0.0544796	-0.629630	0.370370	1.42490
	183	-0.0544972	-0.714100	0.374610	1.47852
Quadratic	18	-0.0544796	-0.666667	0.333333	1.51308
	36	-0.0544989	-0.729167	0.395833	1.50409
	54	-0.0544989	-0.740741	0.370370	150194
Cubic	18	-0.0544989	-0.750000	0.375000	1.50441
	36	-0.0544989	-0.750000	0.375000	1.50055
	54	-0.0544989	-0.750000	0.375000	1.50016
Chen [136]		-0.0544988	-0.750000	0.375000	1.50000
Exact solution		-0.0544988	-0.750000	0.375000	1.50000

5.5.2 Beam on elastic foundation

Problem definition: Consideration is given to beams with span length ℓ and with rectangular cross-section resting on elastic Winkler foundations as shown in Figure 5.6. The analysis of bending of beams on elastic foundation is developed on the assumption that the reaction forces of the foundation are proportional at every point to the deflection of the beam at that point. In the study of beams on elastic foundation, use is made of the non-dimensional quantity λ known as the foundation modulus which is defined as

$$\lambda = \left(\frac{bk}{4EI} \right)^{1/4} \tag{5.65}$$

where b is the constant width of the beam in contact with the foundation; and EI is the flexural rigidity of the beam. A value of $\lambda = 0$ indicates no elastic foundation whereas a value of $\lambda = 5$ corresponds to a stiff elastic foundation [121].

Three types of beams are considered: thick beams with $t / \ell = 0.1$, moderately thick beam $t / \ell = 0.05$ and thin beam with $t / \ell = 0.01$. Both ends of the beam are fixed. The following material properties are assumed in the analysis so that the results can be expressed in a non-dimensional form: the elastic rigidity $EI = 1$ and Poisson's ratio $v = 0.3$. The beam has a span length $\ell = 10$ and a width $b = 1$. Two load cases are considered. These are; a concentrated vertical load $P = 1$ and uniformly distributed load with an intensity of 0.1.
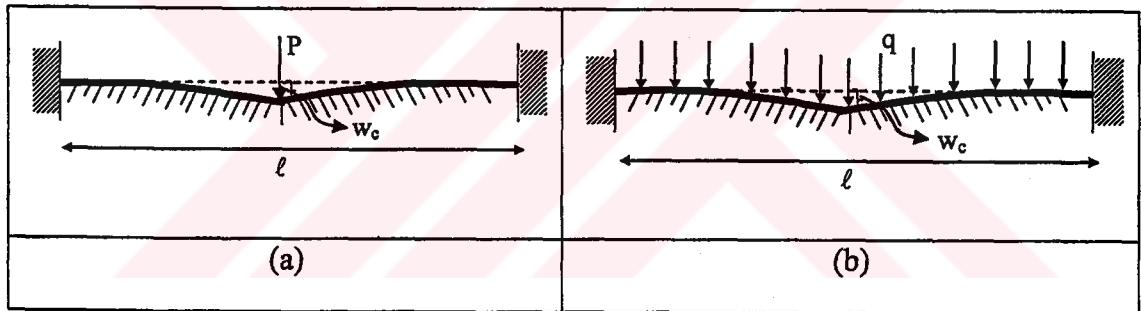
Figure 5.6 Clamped beam on elastic foundation a) concentrated force in the middle
b) uniformly distributed loading over the whole span

Discussion of results: Tables 5.3 and 5.4 present the values of the maximum deflections and strain energies and its composition for the different span to thickness ratios and foundation moduli for point load and uniformly distributed load respectively. The results are compared with closed form solution given by Heteny [121] based on thin beam (Euler beam) model. The closed form solutions for maximum deflections presented by Hetény [121] are:

$$w_c = \frac{P\lambda}{2k} \frac{Cosh\lambda\ell + \cos\lambda\ell - 2}{Sinh\lambda\ell + \sin\lambda\ell} \qquad \text{for point load and,} \tag{5.66}$$

$$w_c = \frac{q}{k}\left[1 - \frac{2\left(Sinh\frac{\lambda\ell}{2}\cos\frac{\lambda\ell}{2} + Cosh\frac{\lambda\ell}{2}\sin\frac{\lambda\ell}{2}\right)}{Sinh\lambda\ell + \sin\lambda}\right] \quad \text{for uniformly distributed load (5.67)}$$

The present results compare very well with Hetény [121] closed form solution for both point load and uniformly distributed load conditions.

Table 5.3 Deflections and strain energies of beams on elastic foundation subject to point load

Foundation modulus λ	Thick ratio t/ℓ	Point load					
		Maximum deflection		SE and its percent composition			
		Present	Ref. [121]	Membrane	Bending	Shear	Total
0.5	0.01	0.99073		0.00	99.64	0.36	0.272578
	0.05	1.01408	0.98975	0.00	91.64	8.36	0.289218
	0.1	1.08518		0.00	77.58	27.42	0.339217
1.0	0.01	0.12546		0.00	98.46	1.54	0.031710
	0.05	0.13685	0.12497	0.00	71.11	28.89	0.040071
	0.1	0.16926		0.00	35.34	64.66	0.062562

Table 5.4 Deflections and strain energies of beams on elastic foundation subject to uniformly distributed load

Foundation modulus λ	Thick. ratio t/ℓ	Distributed load					
		Maximum deflection		SE and its percent composition			
		Present	Ref. [121]	Membrane	Bending	Shear	Total
0.5	0.01	0.41285		0.00	99.65	0.35	0.045698
	0.05	0.41266	0.40000	0.00	91.87	8.13	0.046142
	0.1	0.41206		0.00	73.13	26.87	0.046924
1.0	0.01	0.02523		0.00	98.46	1.54	0.001256
	0.05	0.02520	0.02500	0.00	71.08	28.92	0.001335
	0.1	0.02514		0.00	35.32	64.68	0.001364

5.5.3 Arches with uniform cross-section

Problem definition: This example involves a series of arches with rectanglar cross-sections, which have been studied by Litewka and Rakowski [8]. The arches have a radius of curvature of $R = 4\,\text{m}$, the opening angle $\omega = 2\pi/3$ (length $l = 8\pi/3$), thickness $t = 0.6\,\text{m}$ and width $b = 0.4\,\text{m}$ as shown in Figure 5.7. The following material properties are used: elastic modulus $E = 30\,\text{GPa}$ and Poisson's ratio $v = 0.17$. The analysis is repeated for, two different boundary conditions: fixed-fixed and hinged-hinged and three different loading cases; a) vertical point load at the crown, b) horizontal point load at the crown and c) moment at the crown.
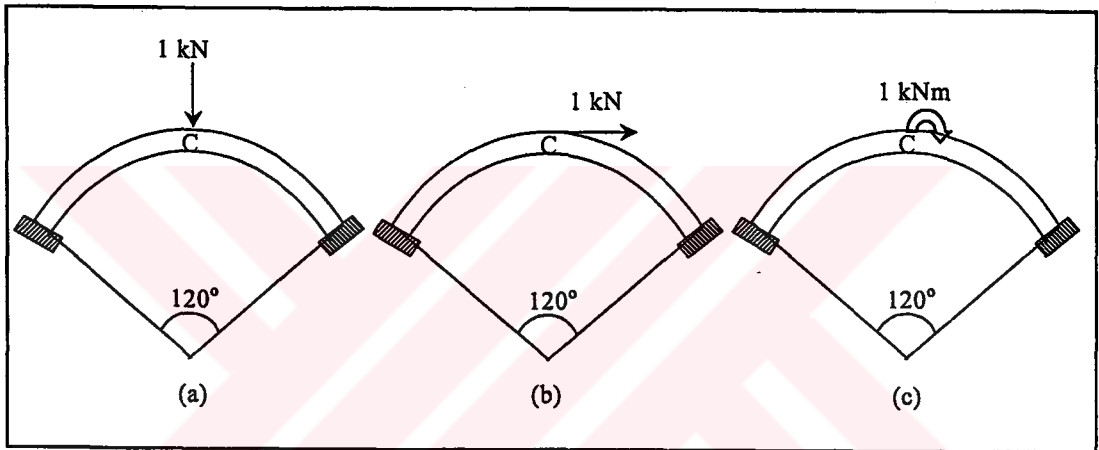
Figure 5.7 Loading conditions of uniform cross-section arch

Discussion of results: To avoid the possibility of significant discretization error, the arches are analyzed using 12 cubic elements. The results for maximum deflections are summarized in Tables 5.5 and 5.6 for fixed-fixed and hinged-hinged arches respectively. Table 5.7 contains the magnitude of the SE and its composition. The results of the analyses compare very well with those obtained by Litewka and Rakowski [8] based on thick beam model.

Table 5.5 Displacements of uniform cross-section arches for fixed-fixed boundary condition

Load	u_c/l (Disp. in x-direct.)		v_c/l (Disp. in y-direct.)		θ_c/ω (Rotation)	
	Present	Ref. [8]	Present	Ref. [8]	Present	Ref. [8]
a	6.19×10^{-10}	0.000	$-2.51 \times \times 10^{-7}$	-2.48×10^{-7}	2.16×10^{-8}	0.000
b	1.23×10^{-7}	1.25×10^{-7}	-6.19×10^{-10}	0.000	3.62×10^{-7}	3.78×10^{-7}
c	9.09×10^{-8}	-9.49×10^{-8}	-5.43×10^{-9}	0.000	1.07×10^{-6}	1.08×10^{-6}

Table 5.6 Displacements of uniform cross-section arches for hinged-hinged boundary condition

Load	u_c/l (Disp. in x-direct.)		v_c/l (Disp. in y-direct.)		θ_c/ω (Rotation)	
	Present	Ref. [8]	Present	Ref. [8]	Present	Ref. [8]
a	9.243×10^{-9}	0.000	-2.799×10^{-7}	3.047×10^{-7}	3.741×10^{-8}	0.000
b	2.765×10^{-7}	2.880×10^{-7}	-9.243×10^{-9}	0.000	7.770×10^{-7}	-8.064×10^{-7}
c	1.952×10^{-7}	-2.016×10^{-7}	-9.396×10^{-9}	0.000	1.362×10^{-6}	1.361×10^{-7}

Table 5.7 SE values and their composition for uniform cross section arch

Boundary condition	Load type	Total SE $(\times 10^{-8})$	% Energy distributions		
			Membrane	Bending	Shear
Fixed-fixed	a	0.2084	40.40	48.28	11.32
	b	0.1049	28.98	61.75	9.27
	c	0.2266	0.61	95.29	4.10
Hinged-hinged	a	0.2416	14.67	81.43	3.90
	b	0.2353	28.17	62.47	9.36
	c	0.2855	0.25	98.06	1.69

5.5.4 Arches with non-uniform cross-section

Problem definition: To check that the present formulation is applicable to curved beams of non-uniform cross section two examples are investigated. The arches were originally analyzed to compute natural frequencies by Gutierrez and Laura [125]. Two types of cross sectional variation $A(\overline{\alpha}) = A_o f(\overline{\alpha})$ are studied:

(a) symmetric stepwise cross sectional variations as shown in Figure 5.8(a),

$$f(\overline{\alpha}) = \frac{t_o}{\eta}, \qquad -\beta \le \overline{\alpha} \le \frac{-\beta}{3}$$

$$f(\overline{\alpha}) = t_o, \qquad \frac{-\beta}{3} \le \overline{\alpha} \le \frac{\beta}{3}$$

$$f(\overline{\alpha}) = \frac{t_o}{\eta}, \qquad \frac{\beta}{3} \le \overline{\alpha} \le \beta \qquad (5.68)$$

where $\eta = t_0/t_1$ 0.4 and $\beta = 30°$.

(b) nonsymmetric linear continuous cross sectional variations as shown in Figure 5.8(b)

$$f(\overline{\alpha}) = 1 - \frac{\eta\overline{\alpha}}{\beta}, \qquad -\beta \le \overline{\alpha} \le \beta \qquad (5.69)$$

where $\eta = t_0/t_1$ 0.4 and $\beta = 30°$.
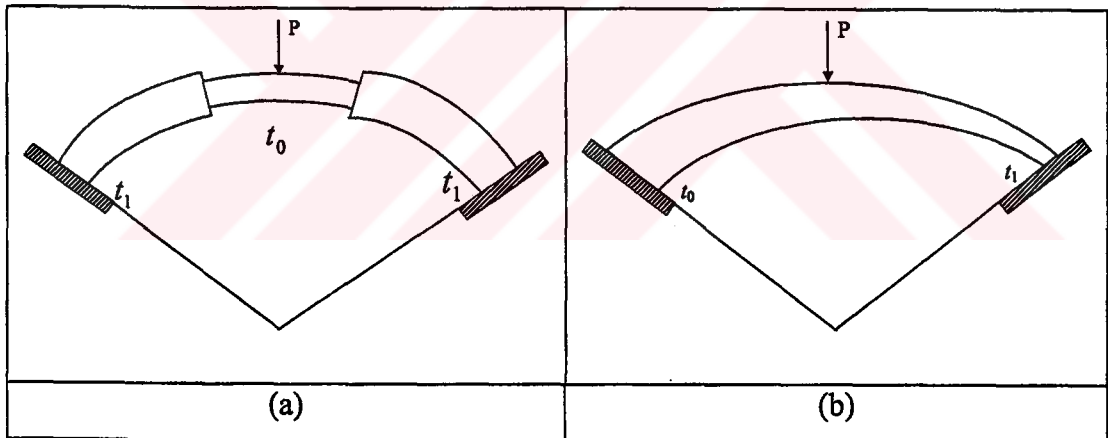
Figure 5.8 (a) Clamped arch of symmetric discontinuously varying cross section
(b) clamped arch of nonsymmetric linear continuously varying cross section

The dimensions adopted for variable thickness arch are identical to those given in reference [125]. The arches are clamped at their ends. The arch has a radius of curvature of $R = 20$ m and the width b is equal to 1 m and area of section is equal to $A_o = 0.5 \, \text{m}^2$. The following material properties are used: elastic modulus

$E = 200\,\text{GPa}$, Poisson's ratio $v = 0.3$. The arches are subject to a concentrated vertical downward load of $P = 1\,\text{kN}$ at the crown.

Discussion of results: The FE analysis of an arch with symmetric stepwise cross-section variations are carried out using quadratic elements. The arch is discretized using five set of meshes of 21, 45, 93, 165 and 333 degrees of freedom. The displacements in the direction of the force obtained using the present formulation are listed in Table 5.8 and compared with SAP 2000 program results which are obtained using linear elements and same degrees of freedom. Note that SAP 2000 has only linear beam element. A close agreement between the results can be observed. However, present formulation gives better rate of convergence and requires less degrees of freedom.

Table 5.8 The vertical deflection w_c of arches with non-uniform
(symmetric stepwise) cross-section

DOF	Deflection $w_c \times 10^{-3}$	
	Present	SAP2000
21	-0.945984	-0.938026
45	-0.962389	-0.957064
93	-0.963417	-0.961886
165	-0.963479	-0.962963
333	-0.963486	-0.963357

Arch with non-symmetric continuously varying cross-section is analyzed using 4 cubic elements with 33 degrees of freedom. The resulting maximum vertical deflection of -0.2599×10^{-2} compares well with the value of -0.2568×10^{-2} obtained using SAP 2000. The SAP 2000 results are obtained using plane stress elements and 252 degrees of freedom.

5.5.5 A Circular cantilever arch

Problem definition: A tip-loaded circular cantilever ring shown in Figure 5.9 is a standard example to test curved beam FEs [16-21]. The quarter ring is subjected to a

radial point load $P = 1$ at the free end. The ring has a radius of curvature $R = 10$ and the width of section is $b = 1$.
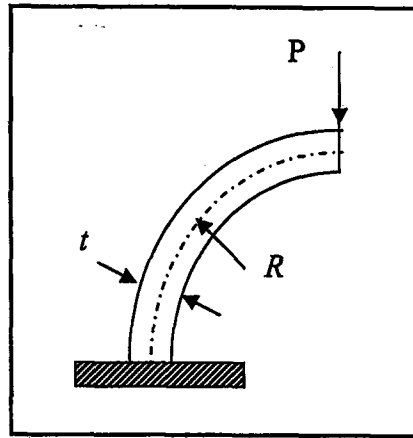
Figure 5.9 A tip-loaded circular cantilever ring

The numerical values of geometrical dimensions and the material properties given for the test problem are in consistent units. The following material properties are used: elastic modulus $E = 10.5 \times 10^6$, Poisson's ratio $v = 0.3125$. The tip deflections in the direction of the applied load are derived in closed-form based on Castigliano's energy theorem [16-21].

$$u_c = \frac{PR}{2}\left(\frac{R^2}{EI} - \frac{1}{GA\kappa} - \frac{R}{EA}\right)$$

$$w_c = \frac{\pi PR}{4}\left(\frac{R^2}{EI} + \frac{1}{GA\kappa} + \frac{1}{EA}\right)$$

$$\theta_c = \frac{PR^2}{EI} \tag{5.70}$$

Using the FEs, a range of ratios of R/t from 5 to 1000 is used.

Discussion of results: The circular cantilever arch is analyzed using one and two cubic elements with 9 and 18 degrees of freedom, respectively. Table 5.9 shows that the results of the present analysis compare very well with the Castigliano's solutions for different radius-thickness R/t ratios, without exhibiting any locking in the thin

situations. The results indicate that even one-element idealization yields very accurate tip displacements.

Table 5.9 Comparison of present FE solutions (u_f, w_f, θ_f) for tip displacement of the circular cantilever arch with Castigliano's energy solutions (u_c, w_c, θ_c)

R/t	One element			Two elements		
	u_f/u_c	w_f/w_c	θ_f/θ_c	u_f/u_c	w_f/w_c	θ_f/θ_c
5	1,0054	1,0016	-1,0013	1,0054	1,0003	-1,0002
10	1,0016	1,0016	-1,0013	1,0013	1,0003	-1,0002
100	1,0008	1.0016	1.0013	1.0002	1.0003	1.0002
1000	1.0007	1.0016	1.0013	1.0001	1.0003	1.0002

5.5.6 A pinched ring

Problem definition: The final example investigated is the pinched ring which was considered by many authors [16-21]. The ring is subject to two pinching concentrated loads as shown in Figure 5.10(a). A pinched ring serves as the best illustration to evaluate the element behavior in a deep arch problem. The exact radial displacement w_A at the loaded point can be easily derived using Castigliano's theorem [16-21].

$$w_A = -\left(\frac{PR^3}{8\pi EI}\left(\pi^2 - 8\right) + \frac{PR}{8GAk} + \frac{PR}{8EA} \right) \tag{5.71}$$

The tangential axial force, radial shear force and bending moment at certain point B on the ring,

$$N = -\frac{P}{2}\sin\varphi_B$$

$$M = -\frac{PR}{2}\left(\frac{2}{\pi} - \sin\varphi_B\right)$$

$$Q = \frac{P}{2}\cos\varphi_B \tag{5.72}$$

The following material properties are used: modulus of elasticity $E = 10.5 \times 10^6$, Poisson's ratio $\nu = 0.3125$. For the present model, we use $R = 4.953$, $t = 0.5554$ with

94

the $b = 1$. The units are consistent. Using symmetry only quarter of the ring is analyzed with appropriate boundary conditions, as shown in Figure 5.10(b).
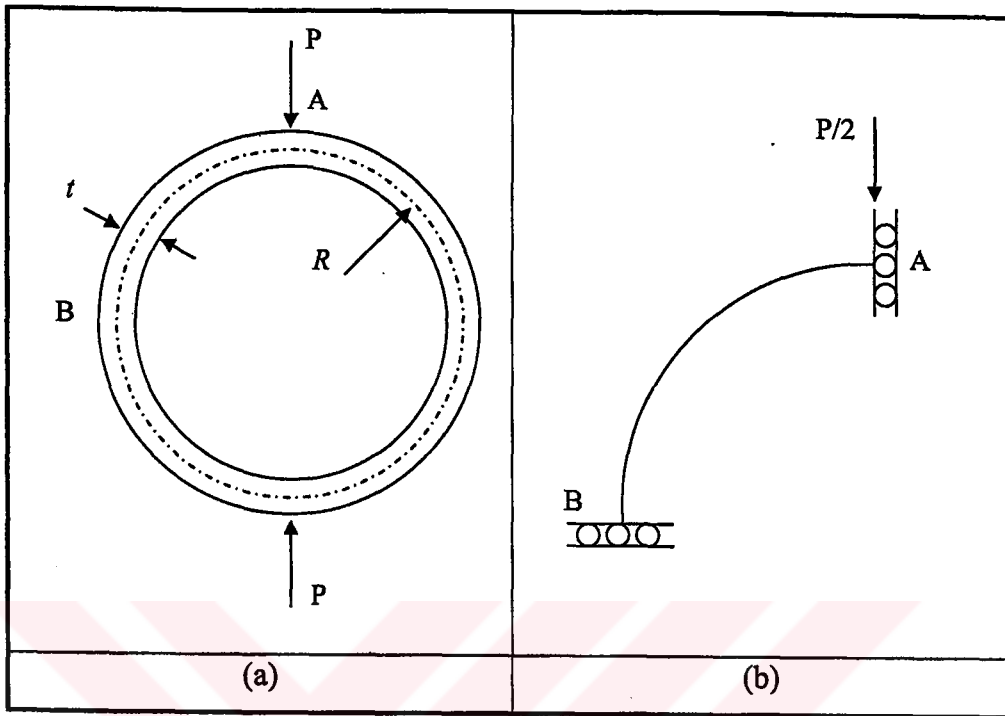
Figure 5.10 (a) a pinched ring model, (b) ring is modeled with appropriate boundary conditions

Discussion of results: The pinched ring is analyzed using linear, quadratic and cubic elements. Figure 5.11 shows the convergence trend for the vertical deflection w_A of the present linear, quadratic and cubic FEs solutions compared with Castigliano's solutions. The results are normalized with respect to the exact solution given by equation (5.71) which is based on Castigliano's energy theorem. Note the superior performance of the quadratic and cubic elements compared to the linear element. This reflects the superior convergence characteristic of the higher order elements and the fact that the linear element models the curved shapes less accurately. The minimum two elements are used in the case of the linear element solutions. The results agree very well with the exact solution. Figures 5.12-15.14 show distribution of bending moment, shear force and axial force over the quadrant AB of the pinched ring which is analyzed using 30 degree of freedom of linear, quadratic and cubic elements.

95
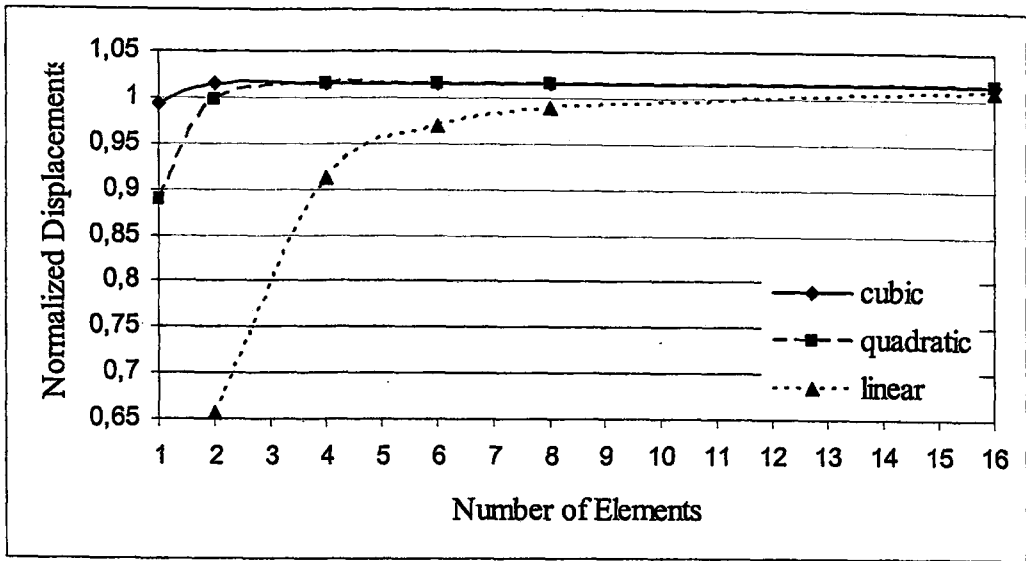
Figure 5.11 Convergence of normalized radial deflection under the point load of the pinched ring
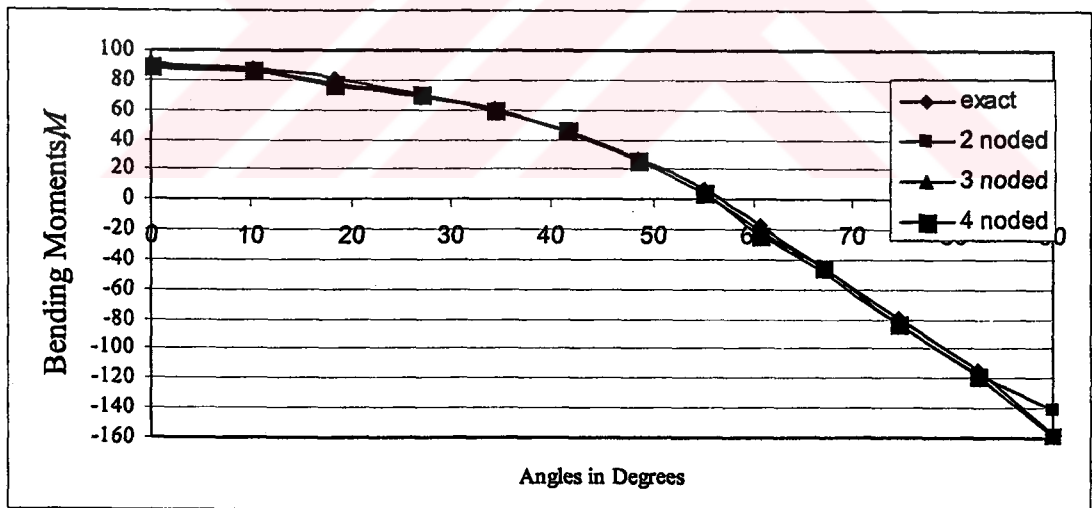
Figure 5.12 Bending moment distribution in a quadrant of the pinched ring
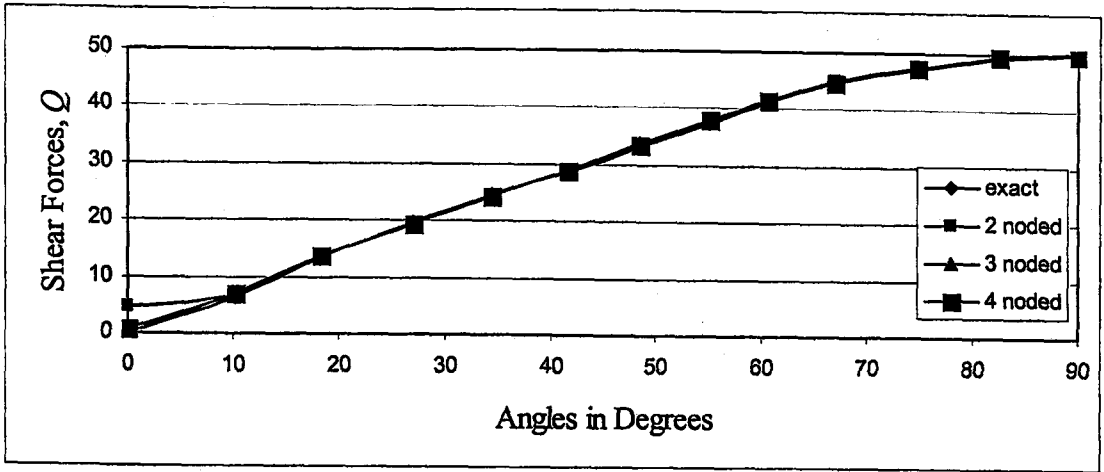
Figure 5.13 Shear force distribution in a quadrant of the pinched ring
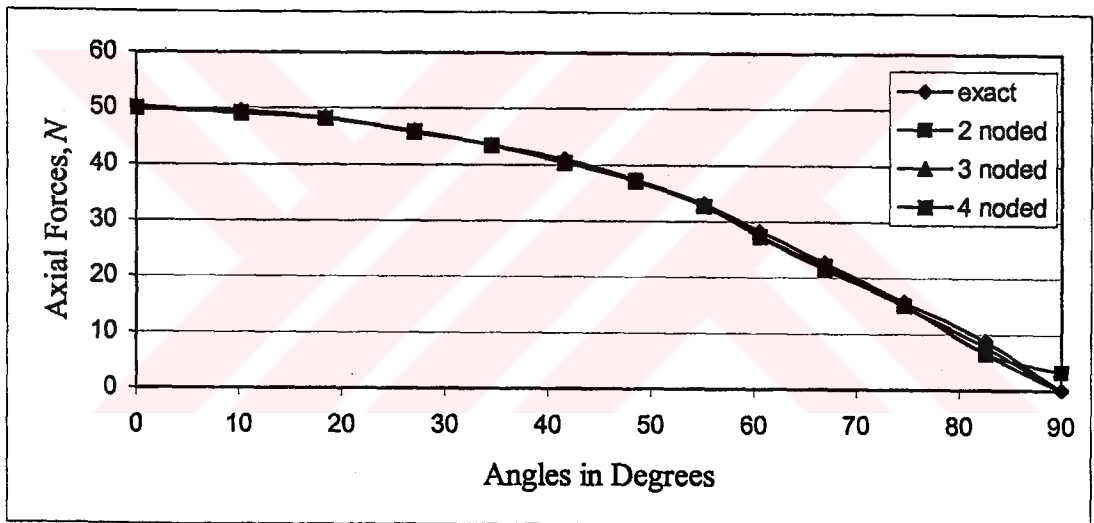
Figure 5.14 Axial force distribution in a quadrant of the pinched ring

5.5.7 Frame structure with curved members

Problem definition: In this example, a frame structure is analyzed and then results are compared with SAP2000 structural analysis package. The geometry of the structure and the cross sections of the members are shown in Figure 5.15. The structure has the following material properties: elastic modulus $E = 200\,\text{GPa}$ and Poisson's

ratio $\nu = 0.3$. The curved part of the frame, which is shown in Figure 5.15, has a uniform cross-section with opening angle 60° and radius of curvature is $R = 6\,\text{m}$.

The analysis is repeated for three different loading cases;

  a) At point C, a concentrated vertical 5 kN load,

  b) At point C, a concentrated horizontal 5 kN load,

  c) On curved member, distributed load with an intensity of 3 kN/m, which is normal to the member.
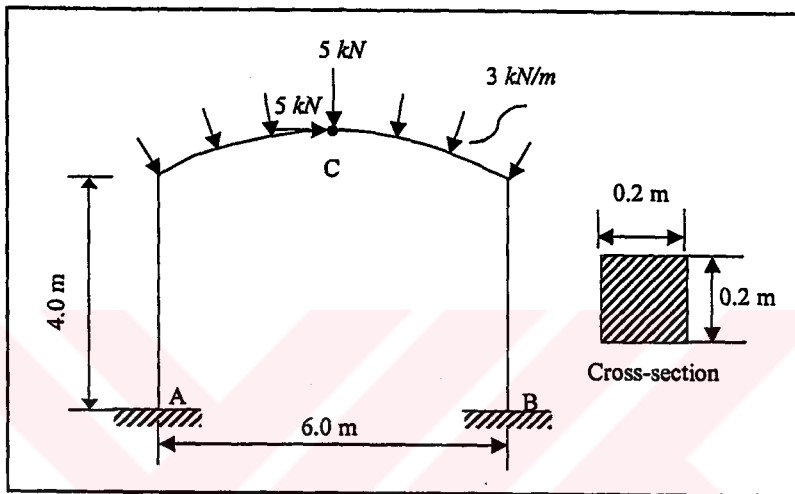
Figure 5.15 Geometry and cross section of frame structure

Table 5.10 Horizontal displacement and rotations at point C for frame structure

Load	Disp.&rot.	Present	SAP2000
(a)	w (m)	0.295×10^{-5}	0.295×10^{-5}
	θ (rad)	0.401×10^{-13}	0.000
(b)	w (m)	0.371×10^{-12}	0.000
	θ (rad)	0.937×10^{-5}	0.937×10^{-5}
(c)	w (m)	0.540×10^{-4}	0.540×10^{-4}
	θ (rad)	0.145×10^{-12}	0.000

Discussion of results: The frame structure is analyzed by using four noded 50 elements with 447 degrees of freedom. The analysis results are tabulated in Tables 5.10 and 5.11, and compared with SAP2000 results. A close agreement between the

results can be observed. In Table 5.12 total strain energies and % distributions of membrane, bending and shear energies for three different loading conditions are given.

Table 5.11 Comparison of reaction forces for frame structure

Load	Reactions	A		B	
		Present	SAP2000	Present	SAP2000
(a)	N	2.500	2.500	2.500	2.500
	Q	1.063	1.063	-1.063	-1.063
	M	-1.699	-1.699	1.699	1.699
(b)	N	1.942	1.942	-1.942	-1.942
	Q	-2.500	-2.500	-2.500	-2.500
	M	6.185	6.185	6.185	6.185
(c)	N	9.000	9.000	9.000	9.000
	Q	2.367	2.367	-2.367	-2.367
	M	-3.714	-3.714	3.714	3.714

Table 5.12 Total SE and % distribution of frame structure

Load	Total SE $(\times 10^{-3})$	% SE distributions		
		Membrane	Bending	Shear
(a)	0.147	0.57	98.43	1.00
(b)	0.449	0.23	99.24	0.53
(c)	0.548	1.89	97.11	1.00

5.6 Two Dimensional Frame Examples

5.6.1 T-shape frame

Problem definition: This example involves the static analysis of the frame, which is shown in Figure 5.16. The system has uniform rectangular cross sections 0.2×0.1, density $\rho = 800$, Poisson's ratio $v = 0.3$ and modulus of elasticity 2×10^8 and is

analyzed under three point loads and gravitational force due to self-weight. (All units are consistent).
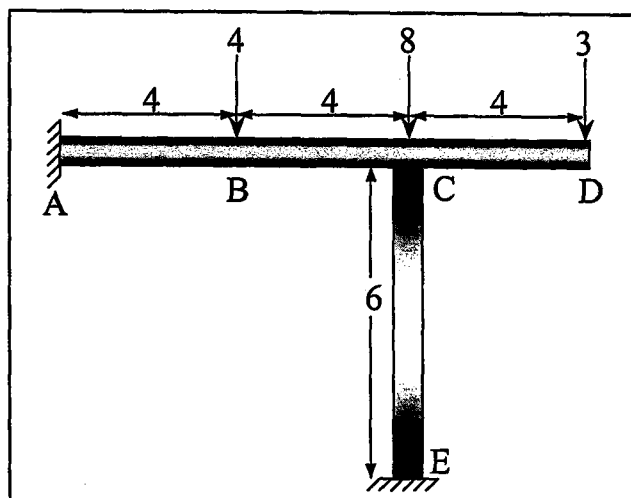
Figure 5.16 Loads and dimensions of frame example

Discussion of results: The resulting displacements at key points are found and compared with SAP 2000 v. 7.40. Remarkably good agreement is obtained and tabulated in Table 5.13.

Table 5.13 Comparison of displacements

Point	Horizontal displacement		Vertical displacement	
	Present	SAP 2000	Present	SAP 2000
B	0.6128×10^{-4}	0.6128×10^{-4}	-0.10097	-0.1010
C	$0,1226 \times 10^{-3}$	$0,1226 \times 10^{-3}$	-0.266×10^{-2}	-0.266×10^{-2}
D	$0,1226 \times 10^{-3}$	$0,1226 \times 10^{-3}$	-0.4960	-0.4960

5.7 Three Dimensional Frame Examples

5.7.1 Grid under distributed load

Problem definition: A frame example analyzed with matrix stiffness method [4] is considered first. The geometry of the frame is shown in Figure 5.17. The frame has

100

the following material properties: elastic modulus $E = 29000$ ksi and rigidity modulus $G = 11500$ ksi. Typical properties of members are; moment of inertia $I = 5310$ in^4 and polar moment of inertia $J = 41.3$ in^4. The frame is analyzed for distributed load with an intensity of 2 k/ft, which is shown in Figure 5.17.
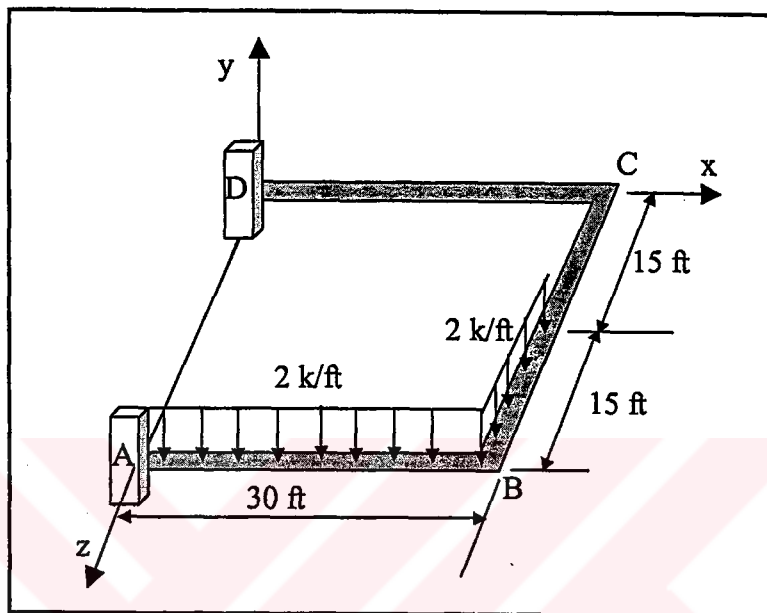
Figure 5.17 Geometry of distributed loaded frame

Discussion of results: The frame is analyzed by using three noded two elements with 12 degrees of freedom. The results are tabulated with the matrix stiffness method [4] solutions of the example. Table 5.14 shows that the results of the present solution are in good agreement with the reference solution.

Table 5.14 Deflection and rotations of frame

Point	Deflection in y direction (in)		Rotation about x axis (rad)		Rotation about z axis (rad)	
	Present	Ref. [4]	Present	Ref. [4]	Present	Ref. [4]
C	-0.7792	-0.71317	0.01144	0.011346	-0.003233	-0.003233
B	-4.57	-4.529	0.009343	0.0092457	-0.01781	-0.017808

5.7.2 Frame under concentrated moment

Problem definition: A frame example analyzed with the matrix stiffness method [4] is considered again. The geometry of the frame is shown in Figure 5.18. The frame has the following material properties: elastic modulus $E = 10000$ ksi and rigidity modulus $G = 4000$ ks$i$. All members have circular cross-sections with; $A = 4.52$ in^2; moment of inertia $I_x = I_y = 18.7$ in^4 and polar moment of inertia $J = 37.4$ in^4. The frame is analyzed under two concentrated moments with 150 k-ft.
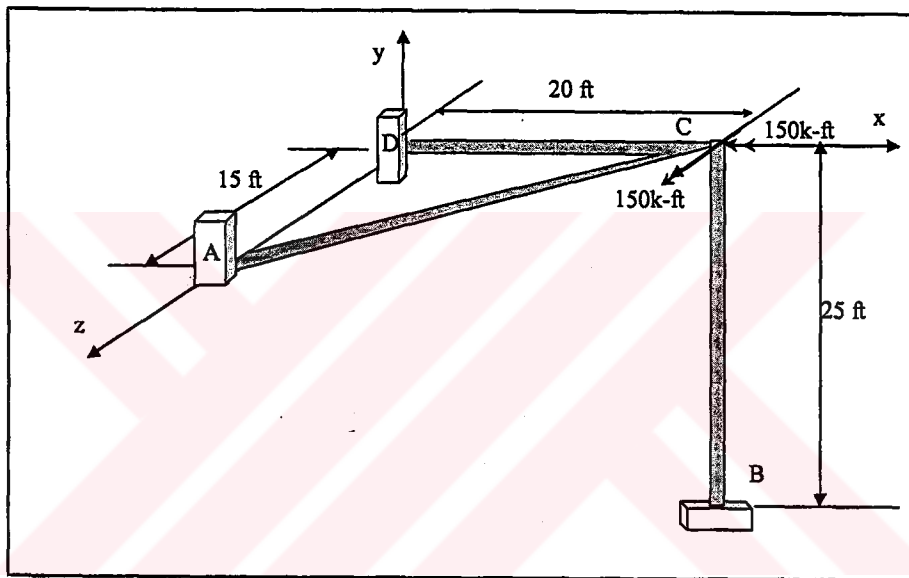
Figure 5.18 Frame subject to concentrated moment

Discussion of results: The frame is analyzed by using three noded two elements. The results are tabulated with the matrix stiffness method [4] solutions of the example. Table 5.15 shows that the results of the present solution are in good agreement with the reference solution.

Table 5.15 Deflections and rotations of point C in x, y and z directions

Displacement		Present study	Ref. [4]
Translation (in)	in x direction	-0.0626945	-0.06273
	in y direction	0.0358446	0.03588
	in z direction	-0.194109	-0.1942
Rotation (rad)	about x axis	-0.484089	-0.4836
	about y axis	0.00101191	0.001013
	about z axis	0.307100	0.3067

CHAPTER 6

FREE VIBRATION ANALYSES OF TWO AND THREE
DIMENSIONAL STRUCTURES

6.1 Introduction

For decades, the vibration analyses of beams and frames have been important
research topics due to their wide applications in structural, civil, aerospace and
mechanical engineering. One of the most successful theories for beams is based on
the Kirchhoff-Love model, which assumes that the thickness of the beam is very
small comparing to its shortest dimension. However, as the beam thickness increases,
the classical Kirchhoff-Love model loses its validity because of the transverse shear
strain. To accommodate this effect the MR beam theory, commonly used in thick
beam analysis, has been extended to arch studies [14], which yields linearly varying
transverse shear strain in contrast to the constant distribution. A shear correction
factor is therefore introduced to compensate for the errors resulting from the
approximation of non-linear transverse shear strain distribution by the linear
distribution. Since then, extensive research work has been conducted in the field.

All real physical structures, when subjected to loads or displacements, behave
dynamically. The additional inertia forces from *Newton's second law* are equal to the
mass times the acceleration. If the loads or displacements are applied very slowly
then the inertia forces can be neglected and a static load analysis can be justified.
Hence, dynamic analysis is a simple extension of static analysis.

When free vibration is under consideration, the structure is not subjected to any
external excitation (force or support motion) and its motion is governed only by the

initial conditions. There are occasional circumstances for which it is necessary to determine the motion of the structure under conditions of free vibration, but this is seldom the case. Nevertheless, the analysis of the structure in free motion provides the most important dynamic properties of the structure which are the natural frequencies and the corresponding modal shapes.

In addition, all real structures potentially have an infinite number of displacements. Therefore, the most critical phase of a structural analysis is to create a computer model, with a finite number of massless members and a finite number of node (joint) displacements that will simulate the behavior of the real structure. The mass of a structural system can be accurately estimated by two basic formulations. To construct mass matrix, these formulations employed:

- the lumped mass formulation resulting in a lumped mass matrix and
- the consistent mass formulation resulting in a consistent mass matrix.

The lumped mass matrix is the simpler to construct and is more frequently employed. In the construction of a lumped mass matrix, the distributed mass properties are lumped or localized at the predefined node points, or joints, defining the degree of freedom in the structure.

The consistent mass matrix is constructed by a procedure similar to that used for the stiffness coefficients for a structure. The consistent mass formulation is generally used for continuous or distributed parameter systems, rather than for discrete systems.

The dynamic analysis of a consistent mass system generally requires considerably more computational effort than a lumped mass system does, for two reasons:

(1) the lumped mass matrix is diagonal, while the consistent mass matrix has many off diagonal terms;

(2) the rotational DOF can be eliminated from a lumped mass analysis, whereas all rotational and translational DOF must be included in a consistent mass analysis [41-51].

105

6.2 Theory of Free Vibration Analysis of 2D Arch and Frame Structures

Consider the free vibrations of the MR curved arch element shown in Figure 6.1. The displacement components u_ℓ and w_ℓ, expressed in terms of axes which are tangential and normal, may be written in terms of global displacements u and w as

$$u_\ell = u\cos\alpha + w\sin\alpha$$

$$w_\ell = -u\sin\alpha + w\cos\alpha \tag{6.1}$$
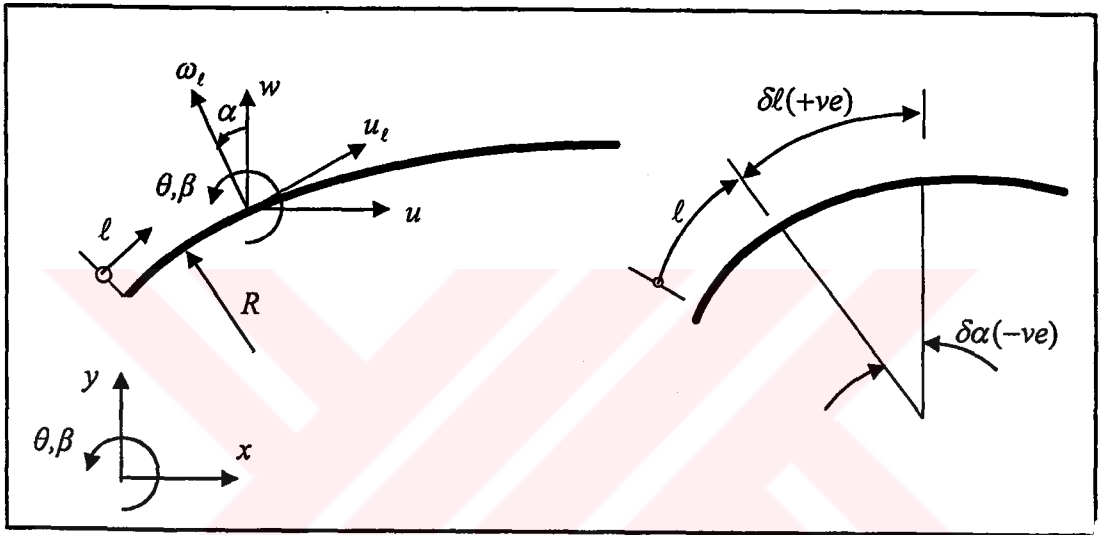
Figure 6.1 Definition of curved Mindlin-Reissner arch FEs

where α is shown in Figure 6.1. The radius of curvature R may be obtained from the expression

$$\frac{d\alpha}{d\ell} = -\frac{1}{R} \tag{6.2}$$

In the absence of external loads and damping effects, the virtual work (or more precisely the virtual power) expression for 2D dynamic analysis can be written as

$$I_e = \int (\delta\varepsilon_m^T D_m \varepsilon_m + \delta\varepsilon_b^T D_b \varepsilon_b + \delta\varepsilon_s^T D_s \varepsilon_s + \delta\mathbf{d}^T \mathbf{P}\ddot{\mathbf{d}})\,d\ell = 0 \tag{6.3}$$

where the membrane (axial) strain is given by the expression

$$\varepsilon_m = \frac{du_\ell}{d\ell} + \frac{w_\ell}{R} \tag{6.4}$$

106

or re-writing in terms of the global displacements

$$\varepsilon_m = \frac{du}{d\ell}\cos\alpha + \frac{dw}{d\ell}\sin\alpha \qquad (6.5)$$

The bending (flexural) strain or curvature may be written as

$$\varepsilon_b = -\frac{d\theta}{d\ell} \qquad (6.6)$$

and the shear strain is given as

$$\varepsilon_s = \frac{dw_\ell}{d\ell} - \theta - \frac{u_\ell}{R} \qquad (6.7)$$

or

$$\varepsilon_s = -\theta - \frac{du}{d\ell}\sin\alpha + \frac{dw}{d\ell}\cos\alpha \qquad (6.8)$$

Also, note that the membrane, bending and shear rigidities have the form

$$D_m = EA; \qquad D_b = EI; \qquad D_s = \kappa GA \qquad (6.9)$$

where E is the elastic modulus, A is the cross-sectional area, I is the moment of inertia, G is the shear modulus and κ is the shear modification factor and is taken as $5/6$ for rectangular cross-section. Note that $\delta\mathbf{d}, \delta\varepsilon_m, \delta\varepsilon_b$ and $\delta\varepsilon_s$ are the virtual displacements, membrane strain, bending strain and shear strain respectively. Note also that the displacement field vector $\mathbf{d}$ has the form

$$\mathbf{d} = [u_\ell, w_\ell, \theta]^T \qquad (6.10)$$

and that

$$\mathbf{P} = \begin{bmatrix} \rho A & 0 & 0 \\ 0 & \rho A & 0 \\ 0 & 0 & \rho I \end{bmatrix} \qquad (6.11)$$

where ρ is the density of the material and I is the moment of inertia of the cross-section, thus rotatory inertia effects are included. The vector $\ddot{\mathbf{d}}$ contains the accelerations of the displacement components u_ℓ and w_ℓ as well as the normal rotations θ, a superposed dot implies differentiation with respect to time.

As we wish to set up the governing equation in terms of displacements expressed in global rather than local directions, it is worth noting the following relationship

$$\mathbf{d} = \mathbf{T}\overline{\mathbf{d}} \qquad (6.12)$$

107

where

$$\overline{\mathbf{d}} = [u, w, \theta]^T \tag{6.13}$$

and the transformation matrix

$$\mathbf{T} = \begin{bmatrix} \cos\alpha & \sin\alpha & 0 \\ -\sin\alpha & \cos\alpha & 0 \\ 0 & 0 & 1 \end{bmatrix} \tag{6.14}$$

the detailed derivation of transformation matrix is given in appendix A.

Thus the last term in the virtual power expression of Eq (6.3) has the form

$$\int \delta \mathbf{d}^T \mathbf{P} \ddot{\mathbf{d}} d\ell \equiv \int \delta \overline{\mathbf{d}}^T \mathbf{P} \ddot{\overline{\mathbf{d}}} d\ell \tag{6.15}$$

since

$$\mathbf{T}^T \mathbf{P} \mathbf{T} = \mathbf{P} \tag{6.16}$$

6.2.1 Finite element idealization

Using n-noded, $C(0)$ line elements, the global displacement parameters u, w and θ may be interpolated, within each beam element by the expressions

$$u = \sum_{i=1}^{n} N_i u_i \ ; \qquad w = \sum_{i=1}^{n} N_i w_i \ ; \qquad \theta = \sum_{i=1}^{n} N_i \theta_i \tag{6.17}$$

where u_i, w_i and θ_i are typical nodal displacement degrees of freedom and $N_i(\xi)$ is the shape function associated with node i which, for 2-noded linear elements, have the form

$$N_1 = 1/2(1-\xi); \qquad N_2 = 1/2(1+\xi) \tag{6.18}$$

for 3-noded, quadratic elements

$$N_1 = \xi/2(\xi-1); \qquad N_2 = (1-\xi^2); \qquad N_3 = \xi/2(\xi+1) \tag{6.19}$$

and for 4-noded, cubic elements

$$N_1 = -9/16(\xi^2 - 1/9)(\xi-1); \qquad N_2 = 27/16(\xi^2-1)(\xi-1/3);$$

$$N_3 = -27/16(\xi^2-1)(\xi+1/3); \qquad N_4 = -9/16(\xi^2-1/9)(\xi+1) \tag{6.20}$$

These elements are essentially isoparametric so that

$$x = \sum_{i=1}^{n} N_i x_i \ ; \qquad y = \sum_{i=1}^{n} N_i y_i \ ; \qquad t = \sum_{i=1}^{n} N_i t_i \ ; \tag{6.21}$$

108

where x_i, y_i and t_i are typical coordinates and thickness of node i respectively. Note also that the Jacobian

$$J = \frac{d\ell}{d\xi} = \left[\left(\frac{\partial x}{\partial \xi}\right)^2 + \left(\frac{\partial y}{\partial \xi}\right)^2 \right]^{1/2}; \quad d\ell = J\,d\xi \tag{6.22}$$

where

$$\frac{\partial x}{\partial \xi} = \sum_{i=1}^{n} \frac{\partial N_i}{\partial \xi} x_i; \quad \frac{\partial y}{\partial \xi} = \sum_{i=1}^{n} \frac{\partial N_i}{\partial \xi} y_i \tag{6.23}$$

Also note that

$$\sin\alpha = \frac{dy}{d\xi}\frac{1}{J}; \quad \cos\alpha = \frac{dx}{d\xi}\frac{1}{J} \tag{6.24}$$

and

$$\frac{dN_i}{d\ell} = \frac{dN_i}{d\xi}\frac{1}{J} \tag{6.25}$$

The membrane strain ε_m may then be expressed as

$$\varepsilon_m = \sum_{i=1}^{n} \mathbf{B}_{mi}^e \mathbf{d}_i^e \tag{6.26}$$

where

$$\mathbf{B}_{mi}^e = \left[(\partial N_i/\partial \ell)\cos\alpha \quad (\partial N_i/\partial \ell)\sin\alpha \quad 0 \right] \tag{6.27}$$

and

$$\mathbf{d}_i^e = [u_i, w_i, \theta_i]^T \tag{6.28}$$

The bending strain or curvatures ε_b can be written as

$$\varepsilon_b = \sum_{i=1}^{n} \mathbf{B}_{bi}^e \mathbf{d}_i^e \tag{6.29}$$

where

$$\mathbf{B}_{bi}^e = \left[0 \quad 0 \quad -dN_i/d\ell \right] \tag{6.30}$$

and the shear strain ε_s is approximated as

$$\varepsilon_s = \sum_{i=1}^{n} \mathbf{B}_{si}^e \mathbf{d}_i^e \tag{6.31}$$

where

$$\mathbf{B}_{si}^e = \left[-(\partial N_i/\partial \ell)\sin\alpha \quad (\partial N_i/\partial \ell)\cos\alpha \quad -N_i \right]$$

109

If we list the nodal displacements and accelerations in a vector $\mathbf{d}$ and $\ddot{\mathbf{d}}$ respectively, then upon substitution of Eq (6.17)-(6.31) into Eq (6.3) we obtain the expression

$$\delta \, \mathbf{d}[\mathbf{Kd} + \mathbf{M}\ddot{\mathbf{d}}] = 0 \qquad (6.32)$$

where $\mathbf{K}$ and $\mathbf{M}$ are the stiffness and mass matrices respectively and contributed from each element e linking nodes i and j which has the form

$$\mathbf{K}_{ij} = \mathbf{K}_{mij} + \mathbf{K}_{bij} + \mathbf{K}_{sij} \qquad (6.33)$$

where

$$\mathbf{K}_{mij} = \int_{-1}^{+1}\mathbf{B}_{mi}^{T}\mathbf{D}_{m}\mathbf{B}_{mj}^{T}Jd\xi \qquad (6.34)$$

$$\mathbf{K}_{bij} = \int_{-1}^{+1}\mathbf{B}_{bi}^{T}\mathbf{D}_{b}\mathbf{B}_{bj}^{T}Jd\xi \qquad (6.35)$$

$$\mathbf{K}_{sij} = \int_{-1}^{+1}\mathbf{B}_{si}^{T}\mathbf{D}_{s}\mathbf{B}_{sj}^{T}Jd\xi \qquad (6.36)$$

and

$$\mathbf{M}_{ij}^{e} = \int_{-1}^{+1}\mathbf{N}_{i}^{T}\mathbf{P}\mathbf{N}_{j}Jd\xi \qquad (6.37)$$

where $\mathbf{N}_{i} = \mathbf{N}_{i}\mathbf{I}_{3}$ in which $\mathbf{I}_{3}$ is the 3×3 identity matrix. To avoid locking behavior, reduced integration is adopted i.e. 1-, 2- and 3-point Gauss-Legendre quadrature is used for the 2-, 3- and 4-noded elements respectively. Note also that since the rigidities $\mathbf{D}_{m}$, $\mathbf{D}_{b}$ and $\mathbf{D}_{s}$ depend on the thickness t and since t is interpolated with each element e from the nodal values t_{i}, elements of variable thickness in the ξ-direction may be easily accommodated in the present formulation.

Since the discretized virtual power expression Eq (6.32) must be true for any set of virtual displacements $\delta \mathbf{d}$, then by taking advantage of the orthogonality conditions Eq (6.32) may be re-written n uncoupled form for each harmonic p as

$$\mathbf{Kd} + \mathbf{M}\ddot{\mathbf{d}} = 0 \qquad (6.38)$$

The general solution of (6.38) is written as

$$\mathbf{d}_{p} = \hat{\mathbf{d}}_{p}e^{i\omega_{p}t} \qquad (6.39)$$

where $e^{i\omega_{p}t} = cos(\omega_{p}t) + isin(\omega_{p}t)$ and ω_{p} and $\hat{\mathbf{d}}_{p}$ are pth natural frequency and vibration mode (eigenvector). Thus Eq (6.38) may be rewritten in the standard eigenvalue form

$$(\mathbf{K} - \omega_p^2 \mathbf{M})\hat{\mathbf{d}}_p = 0 \qquad (6.40)$$

In the present study the eigenvalues are evaluated using the subspace iteration algorithm [3].

6.3 Theory of Free Vibration Analysis of 3D Frame Structures

Consider the MR 3D frame element shown in Figure 6.2. Each node has six degrees of freedom (as opposed to only three degrees of freedom in a planar structure). The numbering of the degrees of freedom is shown in Figure 6.2. For node i, u, v and w represent translational degrees of freedom, while θ_x, θ_y and θ_z represent rotational degrees of freedom about x, y and z axes.
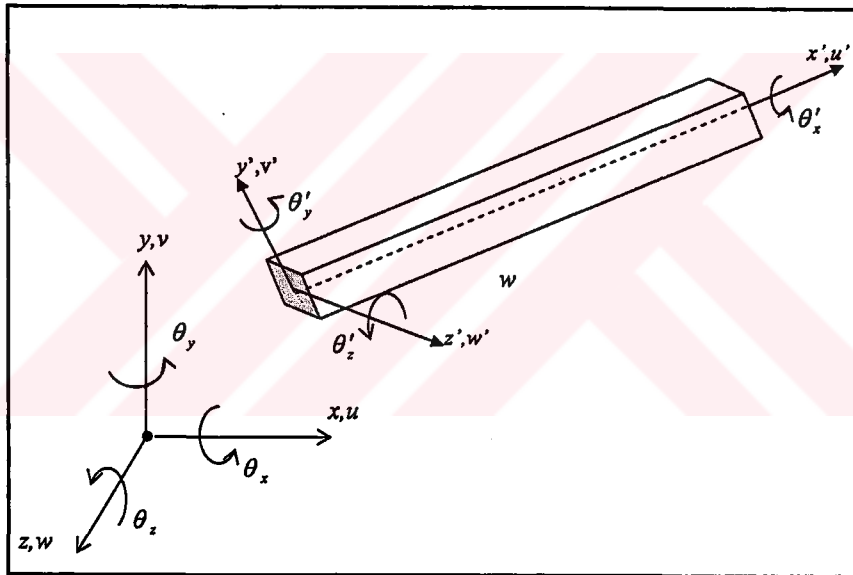
Figure 6.2 Local and global coordinates of Mindlin-Reissner 3D frame element

In the absence of external loads and damping effects, the virtual work (or more precisely the virtual power) expression for 3D dynamic analysis can be written as

$$I_e = \int (\delta\varepsilon_m^T \mathbf{D}_m \varepsilon_m + \delta\varepsilon_b^T \mathbf{D}_b \varepsilon_b + \delta\varepsilon_s^T \mathbf{D}_s \varepsilon_s + \delta\mathbf{d}^T \mathbf{P}\ddot{\mathbf{d}}) d\ell = 0 \qquad (6.41)$$

where the membrane (axial) strain is given by the expression

$$\varepsilon_m = \left[\frac{du'}{dx'}\right] \qquad (6.42)$$

111

The bending (flexural) strain may be written as

$$\boldsymbol{\varepsilon}_b = [\varepsilon_y \quad \varepsilon_z] \tag{6.43}$$

the bending strain in y and z axes are given as

$$\varepsilon_y = -\frac{d\theta_z'}{dz'}; \quad \varepsilon_z = -\frac{d\theta_y'}{dy'} \tag{6.44}$$

The shear strain is given as

$$\boldsymbol{\varepsilon}_s = [\gamma_{xx} \quad \gamma_{xy} \quad \gamma_{xz}] \tag{6.45}$$

the shear strain in x, y and z axes are given as

$$\gamma_{xx} = \frac{d\theta_x'}{dx'} \qquad \gamma_{xy} = \frac{dw_x'}{dx'} + \theta_y' \qquad \gamma_{xz} = \frac{dv_x'}{dx'} - \theta_z' \tag{6.46}$$

The membrane, bending and shear rigidities have the form

$$\mathbf{D}_m = [EA]; \qquad \mathbf{D}_b = \begin{bmatrix} EI_z & 0 \\ 0 & EI_y \end{bmatrix}; \qquad \mathbf{D}_s = \begin{bmatrix} GA/\alpha & 0 & 0 \\ 0 & GA/\alpha & 0 \\ 0 & 0 & GJ \end{bmatrix} \tag{6.47}$$

where E is the elastic modulus, A is the cross-sectional area, I_z, I_y are the moments of inertia with respect to z and y axes, J is the polar moment of inertia, G is the shear modulus and κ is the shear modification factor and is taken as $5/6$ for a rectangular cross-section. Note that $\delta \mathbf{d}, \delta \boldsymbol{\varepsilon}_m, \delta \boldsymbol{\varepsilon}_b$ and $\delta \boldsymbol{\varepsilon}_s$ are the virtual displacements, membrane strain, bending strain and shear strain respectively. Note also that the displacement field vector $\mathbf{d}$ has the form

$$\mathbf{d} = [u_\ell, v_\ell, w_\ell, \theta_x, \theta_y, \theta_z]^T \tag{6.48}$$

and that

$$\mathbf{P} = \begin{bmatrix} \rho A & 0 & 0 & 0 & 0 & 0 \\ 0 & \rho A & 0 & 0 & 0 & 0 \\ 0 & 0 & \rho A & 0 & 0 & 0 \\ 0 & 0 & 0 & \rho J & 0 & 0 \\ 0 & 0 & 0 & 0 & \rho I_z & 0 \\ 0 & 0 & 0 & 0 & 0 & \rho I_y \end{bmatrix} \tag{6.49}$$

where ρ is the density of the material and , I_z, I_y are the moments of inertia of the cross-section with respect to z and y axes, J is the polar moment of inertia, thus rotatory inertia effects are included. The vector $\ddot{\mathbf{d}}$ contains the accelerations of the

displacement components u_ℓ, v_ℓ and w_ℓ as well as the rotations $\theta_x, \theta_y, \theta_z$, a superposed dot implies differentiation with respect to time.

As we wish to set up the governing equation in terms of displacements expressed in global rather than local directions, it is worth noting the following relationship

$$\mathbf{d} = \mathbf{T\overline{d}} \qquad (6.50)$$

where

$$\mathbf{\overline{d}} = [u, v, w, \theta_x, \theta_y, \theta_z]^T \qquad (6.51)$$

$\mathbf{T}$ is the transformation matrix and the detailed derivation of transformation matrix is given in appendix A.

Thus the last term in the virtual power expression of Eq (6.41) has the form

$$\int \delta\mathbf{d}^T \mathbf{P\ddot{d}} d\ell \equiv \int \delta\mathbf{\overline{d}}^T \mathbf{P\ddot{\overline{d}}} d\ell \qquad (6.52)$$

since

$$\mathbf{T}^T \mathbf{PT} = \mathbf{P} \qquad (6.53)$$

6.3.1 Finite element idealization

Using n-noded, $C(0)$ line elements, the global displacement parameters u, and θ may be interpolated, within each beam element by the expressions

$$u = \sum_{i=1}^{n} N_i u_i ; \qquad v = \sum_{i=1}^{n} N_i v_i ; \qquad w = \sum_{i=1}^{n} N_i w_i ;$$

$$\theta_x = \sum_{i=1}^{n} N_i \theta_{xi} ; \qquad \theta_y = \sum_{i=1}^{n} N_i \theta_{yi} ; \qquad \theta_z = \sum_{i=1}^{n} N_i \theta_{zi} \qquad (6.54)$$

where u_i, v_i, w_i, θ_{xi}, θ_{yi} and θ_{zi} are typical nodal displacement degrees of freedom and $N_i(\xi)$ is the shape function associated with node i which, for 2-noded linear elements, have the form

$$N_1 = 1/2(1-\xi); \qquad N_2 = 1/2(1+\xi) \qquad (6.55)$$

for 3-noded, quadratic elements

$$N_1 = \xi/2(\xi-1); \qquad N_2 = (1-\xi^2); \qquad N_3 = \xi/2(\xi+1) \qquad (6.56)$$

and for 4-noded, cubic elements

113

$$N_1 = -9/16(\xi^2 - 1/9)(\xi - 1); \qquad N_2 = 27/16(\xi^2 - 1)(\xi - 1/3);$$

$$N_3 = -27/16(\xi^2 - 1)(\xi + 1/3); \qquad N_4 = -9/16(\xi^2 - 1/9)(\xi + 1) \qquad (6.57)$$

These elements are essentially isoparametric so that

$$x = \sum_{i=1}^{n} N_i x_i; \quad y = \sum_{i=1}^{n} N_i y_i; \quad z = \sum_{i=1}^{n} N_i z_i; \quad h = \sum_{i=1}^{n} N_i h_i; \quad b = \sum_{i=1}^{n} N_i b_i \quad (6.58)$$

where x_i, y_i, z_i, h_i and b_i are typical coordinates, thickness and width of node i respectively. Note also that the Jacobian

$$J = \frac{d\ell}{d\xi} = \left[\left(\frac{\partial x}{\partial \xi} \right)^2 + \left(\frac{\partial y}{\partial \xi} \right)^2 + \left(\frac{\partial z}{\partial \xi} \right)^2 \right]^{1/2}; \qquad d\ell = J d\xi \qquad (6.59)$$

where

$$\frac{\partial x}{\partial \xi} = \sum_{i=1}^{n} \frac{\partial N_i}{\partial \xi} x_i; \qquad \frac{\partial y}{\partial \xi} = \sum_{i=1}^{n} \frac{\partial N_i}{\partial \xi} y_i \qquad \frac{\partial z}{\partial \xi} = \sum_{i=1}^{n} \frac{\partial N_i}{\partial \xi} z_i \qquad (6.60)$$

and

$$\frac{dN_i}{d\ell} = \frac{dN_i}{d\xi} \frac{1}{J} \qquad (6.61)$$

The membrane strains ε_m may then be expressed as

$$\varepsilon_m = \sum_{i=1}^{n} \mathbf{B}_{mi}^e \mathbf{d}_i^e \qquad (6.62)$$

where

$$\mathbf{B}_{mi}^e = \begin{bmatrix} dN/dx' & 0 & 0 & 0 & 0 & 0 \end{bmatrix} \qquad (6.63)$$

and

$$\mathbf{d}_i^e = [u_i, v_i, w_i, \theta_{xi}, \theta_{yi}, \theta_{zi}]^T \qquad (6.64)$$

The bending strain or curvatures ε_b can be written as

$$\varepsilon_b = \sum_{i=1}^{n} \mathbf{B}_{bi}^e \mathbf{d}_i^e \qquad (6.65)$$

where

$$\mathbf{B}_{bi}^e = \begin{bmatrix} 0 & 0 & 0 & 0 & 0 & dN/dx' \\ 0 & 0 & 0 & 0 & dN/dx' & 0 \end{bmatrix} \qquad (6.66)$$

and the shear strain ε_s is approximated as

$$\boldsymbol{\varepsilon}_s = \sum_{i=1}^{n} \mathbf{B}_{si}^e \mathbf{d}_i^e \qquad (6.67)$$

where

$$\mathbf{B}_{si}^e = \begin{bmatrix} 0 & dN/dx' & 0 & 0 & 0 & -N \\ 0 & 0 & dN/dx' & 0 & N & 0 \\ 0 & 0 & 0 & dN/dx' & 0 & 0 \end{bmatrix} \qquad (6.68)$$

If we list the nodal displacements and accelerations in a vector $\mathbf{d}$ and $\ddot{\mathbf{d}}$ respectively, then upon substitution of Eq (6.54)-(6.68) into Eq (6.41) we obtain the expression

$$\delta\,\mathbf{d}\big[\mathbf{Kd} + \mathbf{M\ddot{d}}\big] = 0 \qquad (6.69)$$

where $\mathbf{K}$ and $\mathbf{M}$ are the stiffness and mass matrices respectively and contributed from each element e linking nodes i and j which has the form

$$\mathbf{K}_{ij} = \mathbf{K}_{mij} + \mathbf{K}_{bij} + \mathbf{K}_{sij} \qquad (6.70)$$

where

$$\mathbf{K}_{mij} = \int_{-1}^{+1} \mathbf{B}_{mi}^T \mathbf{D}_m \mathbf{B}_{mj}^T J d\xi \qquad (6.71)$$

$$\mathbf{K}_{bij} = \int_{-1}^{+1} \mathbf{B}_{bi}^T \mathbf{D}_b \mathbf{B}_{bj}^T J d\xi \qquad (6.72)$$

$$\mathbf{K}_{sij} = \int_{-1}^{+1} \mathbf{B}_{si}^T \mathbf{D}_s \mathbf{B}_{sj}^T J d\xi \qquad (6.73)$$

and

$$\mathbf{M}_{ij}^e = \int_{-1}^{+1} \mathbf{N}_i^T \mathbf{P} \mathbf{N}_j J d\xi \qquad (6.74)$$

where $\mathbf{N}_i = N_i \mathbf{I}_3$ in which $\mathbf{I}_3$ is the 3×3 identity matrix. To avoid locking behavior, reduced integration is adopted i.e. 1-, 2- and 3-point Gauss-Legendre quadrature is used for the 2-, 3- and 4-noded elements respectively. Note also that since the rigidities $\mathbf{D}_m$, $\mathbf{D}_b$ and $\mathbf{D}_s$ depend on the thickness t and since t is interpolated with each element e from the nodal values t_i, elements of variable thickness in the ξ-direction may be easily accommodated in the present formulation.

Since Eq (6.69) must be true for any set of virtual displacements $\delta\,\mathbf{d}$, Eq (6.69) may be written as

$$\mathbf{Kd} + \mathbf{M\ddot{d}} = 0 \qquad (6.75)$$

115

The general solution of Eq (6.75) is written as

$$\mathbf{d}_p = \hat{\mathbf{d}}_p e^{i\omega_p t} \tag{6.76}$$

where $e^{i\omega_p t} = cos(\omega_p t) + isin(\omega_p t)$ and ω_p and $\hat{\mathbf{d}}_p$ are pth natural frequency and vibration mode (eigenvector). Thus Eq (6.75) may be rewritten in the standard eigenvalue form

$$(\mathbf{K} - \omega_p^2 \mathbf{M})\hat{\mathbf{d}}_p = 0 \tag{6.77}$$

In the present study the eigenvalues are evaluated using the subspace iteration algorithm [3].

6.4 Beam and Arch Examples

To verify that the free vibration formulation of the FE model can be successfully used for the analysis of the beam and frame structures, several examples for which solutions are available have been considered

Note that in 2D examples, the nodes of the structures have three degrees of freedom and these degrees of freedom are translations in x and y directions and rotation about x-axis, respectively. In 3D examples the nodes of the structures have six degrees of freedom and these degrees of freedom are translations in x, y and z directions and rotations about x, y and z-axes, respectively.

6.4.1 A two dimensional deep beam example

Problem definition: This example is a 2D deep beam with a square cross-section, which is simply supported at each end, as shown in Figure 6.3. The example is taken from the free vibration benchmarks of NAFEMS [123]. The beam, which is of length 10 m, has the following material properties: elastic modulus $E = 200\,\text{GPa}$, Poisson's ratio $v = 0.3$ and mass density $\rho = 8000\,\text{kg/m}^3$. Boundary conditions are $u = v = 0$ at A and $v = 0$ at B.
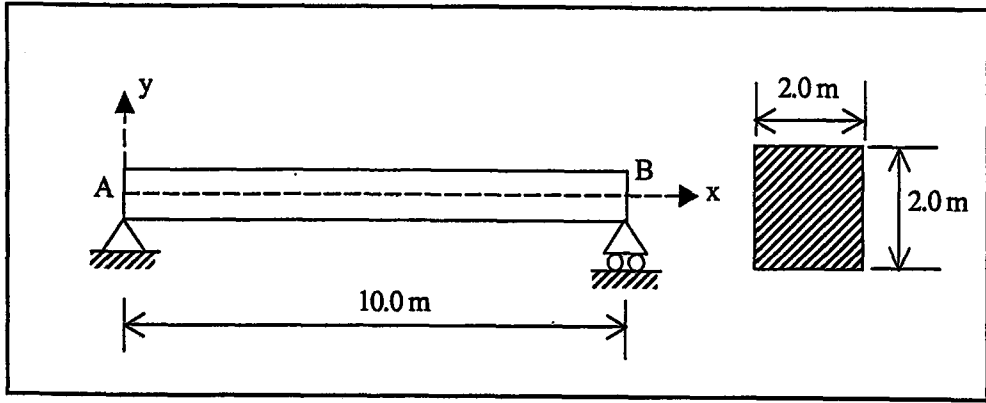
Figure 6.3 Cross-section of 2D deep beam

Discussion of results: The relative performance of the various types of elements is examined. Table 6.1 presents a comparison of frequencies for linear, quadratic and cubic elements for 3 different degrees of freedom. The convergence rate of the cubic and quadratic elements are considerably higher than that of the linear elements. The results are compared with a FE solution obtained by Abbassian et al. [123] and Jantan et al. [124] in Table 6.1. Close agreement between the results can be observed. The accuracy of the developed program is excellently proved by using world-wide accepted benchmark examples of NAFEMS.

Table 6.1 Natural frequencies (Hz) for 2D deep beam

Mode	DOF	Linear	Quadratic	Cubic	Ref. [124]	Ref. [123]
1	12	51.178	43.212	43.138	42.608	42.649
	21	43.994	42.735	42.619		
	66	42.759	42.609	42.608		
2	12	127.936	125.064	125.016	125.000	125.000
	21	125.527	125.013	125.000		
	66	125.058	125.000	125.000		
3	12	326.614	173.826	208.216	148.786	148.310
	21	166.202	153.330	149.423		
	66	149.658	147.822	147.789		

117

6.4.2 Two dimensional pin-ended double cross frame

Problem definition: This example is another NAFEMS benchmark frame with a square cross-section which is pin-ended at each end, as shown in Figure 6.4. The frame is $0.125 \, \text{m} \times 0.125 \, \text{m}$ in cross-section and has the following material properties: elastic modulus E=200 GPa, Poisson's ratio $v = 0.0$ and mass density $\rho = 8000 \, \text{kg/m}^3$.
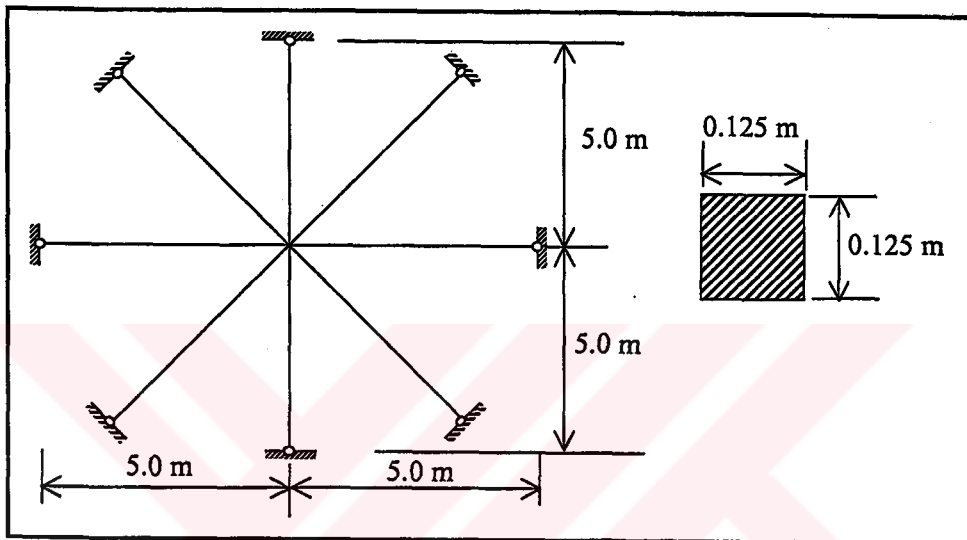
Figure 6.4 Dimensions of pin-ended double cross frame

Discussion of results: The natural frequencies, obtained using a fine mesh of 3-noded elements are listed in Table 6.2. The results are compared with the analytical solution and those obtained by Abbassian et al. [123] where isoparametric beam elements were used. Close agreement between the results can be observed.

Table 6.2 Natural frequencies for double cross frame

Mode	Frequencies (Hz)		
	Present	Exact [123]	Ref. [123]
1	11.3380	11.336	11.332
2&3	17.6885	17.687	17.670
4,5,6,7&8	17.7172	17.715	17.698
9	45.8658	45.477	45.667
10&11	58.0656	57.364	57.716
12,13,14,15&16	58.4093	57.683	58.052

6.4.3 Arches of non-uniform cross-section

Problem definition: To check that the present formulation is applicable to arches of non-uniform cross-section some examples presented by Gutierrez et al. [125] are investigated. Two types of cross-sectional variations are studied:

(a) symmetric discontinuous cross-sectional variations as shown in Figure 6.5 where $t_o / t_1 = 1.25$ and $\beta = 40°$ and

(b) non-symmetric linear continuous variation of cross-section as shown in Figure 6.6 where $t_o / t_1 = 0.43$ and $\beta = 60°$.
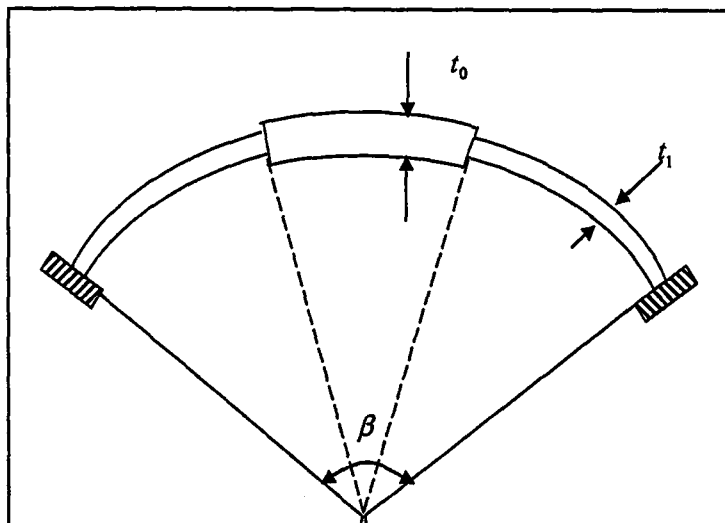
Figure 6.5 Clamped arches of discontinuously varying cross-section

119
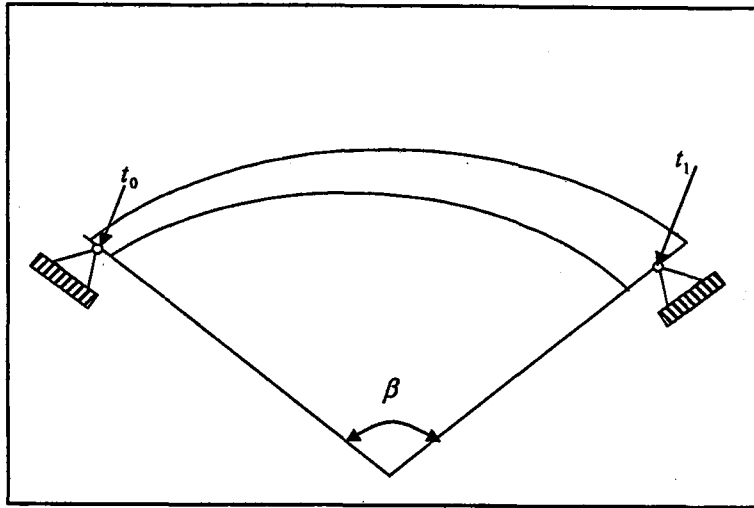
Figure 6.6 Pinned-pinned arches of continuously varying cross-section

The frequencies are given in terms of a frequency parameter λ defined as

$$\lambda^2 = \frac{\rho A_0}{EI_0}(R\beta_0)^4 \omega^2$$

(6.78)

where R is the radius of arch.

Discussion of results: The first three frequency parameters obtained using a fine mesh of 4-noded elements in each case are also tabulated in Table 6.3 with results obtained by Jantan et al. [124] and Gutierrez et al. [125]. Again, remarkably good agreement in the results is obtained.

Table 6.3 Frequency parameters for arches of non-uniform cross-section

Cross-section	Mode	Frequency parameters λ		
		Present	Ref. [124]	Ref. [125]
Sym. discont.	1	49.65	49.80	49.91
	2	76.14	86.60	-
	3	133.78	161.11	-
Non-sym. cont	1	35.44	35.39	35.32
	2	76.41	78.88	-
	3	137.57	148.89	-

6.4.4 A 3D deep beam example

This example is a 3-D deep beam with a square cross-section, which is analyzed as a 2-D problem in section 6.4.1. The example is taken from the free vibration benchmarks of NAFEMS [123]. Boundary conditions of the beam are $u = v = w = R_x = 0$ at A and $v = w = 0$ at B

Discussion of results: The results obtained using a fine mesh of 4-noded elements are compared with a FE solution obtained by Abbassian et al. [123] in Table 6.4. Close agreement between the results can be observed.

Table 6.4 Natural frequencies for 3D deep beam

Mode shapes	Frequencies (Hz)	
	Present	Ref. [123]
Bending (modes1&2)	42.619	42.649
Torsional (mode 3)	77.522	77.542
Extensional (mode 4)	125.000	125.000
Bending (modes 5&6)	148.177	148.310
Torsional (mode 7)	232.684	233.100
Bending (modes 8&9)	285.564	285.140

6.5 Three Dimensional Portal Frame Examples

6.5.1 Single story portal frame

Problem definition: The following example deals with a single story portal frame which is originally presented by Yu and Wang [126] and shown in Figure 6.7. The following material properties are assumed: the modulus of elasticity 1×10^7 psi, Poisson's ratio 0.25 and the mass density 0.1/386.4 lb/in^3. The frame is modeled using three segments and four key points.

121
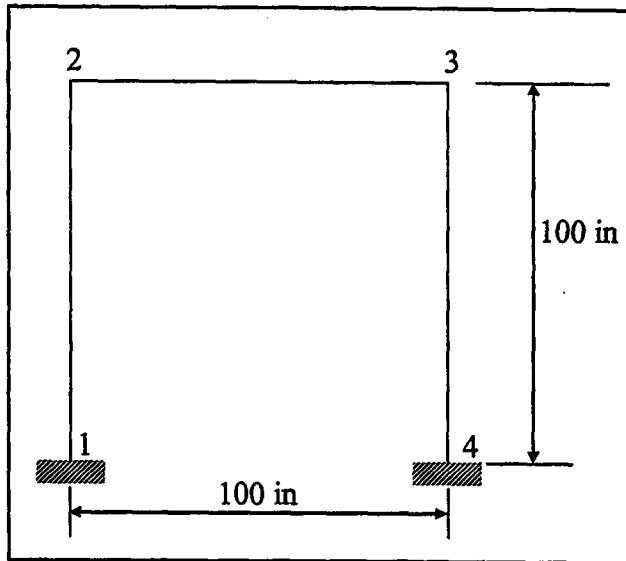
Figure 6.7 Three dimensional portal frame

Discussion of results: The analysis result is tested against the reference solution [126]. The result is obtained using a fine mesh of 3-noded elements. The fundamental frequency is equal to 3.6092 Hz both in the present study and the reference solution.

6.5.2 Two story portal frame

Problem definition: This example, which involves the optimization of the two story portal frame is shown in Figure 6.8, was also originally presented by Yu and Wang [126]. The following material properties are assumed: the modulus of elasticity $1x10^7$ psi, Poisson's ratio 0.25 and the mass density $0.1/386.4$ lb/in^3. The frame structure is completely fixed at nodes 1 and 4.

Discussion of results: The analysis result is tested against the reference solution [126]. The result is obtained using a fine mesh of 3-noded elements. The fundamental frequency is equal to 1.0885 Hz both in the present study and the reference solution [126].
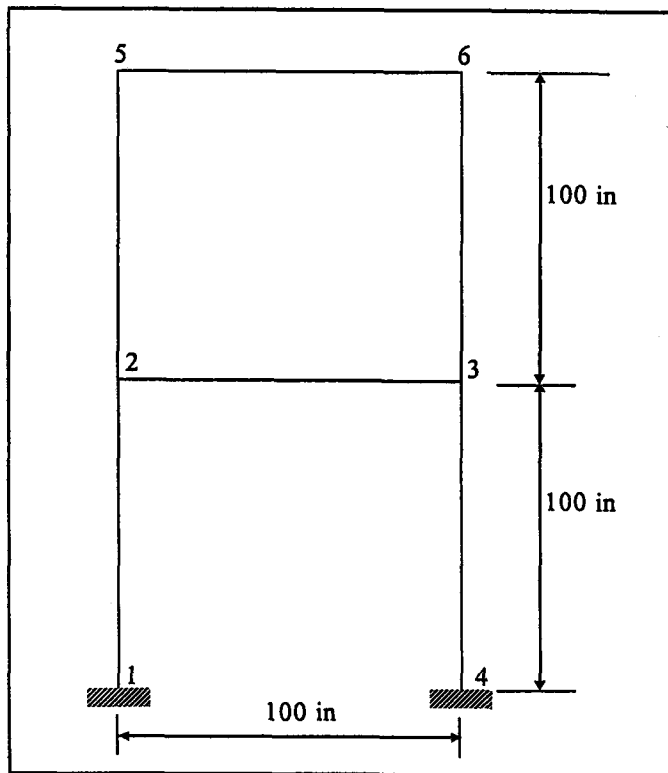
Figure 6.8 Two level portal frame

6.5.3 Three story space frame

Problem definition: This example, which involves the optimization of the three-story space frame structure is shown in Figure 6.9, was also originally presented by Yu and Wang [126]. The frame structure is completely fixed at nodes 1, 2, 3 and 4. The following material properties are assumed: the modulus of elasticity 1×10^{7} psi, Poisson's ratio 0.25 and the mass density 0.1/386.4 lb/in^3.

Discussion of results: The analysis result is tested against the reference solution [126]. The result is obtained using a fine mesh of 3-noded elements. The fundamental frequencies are equal to 1.4397 Hz and 1.4399 Hz in the present study and the reference solution [126] respectively.
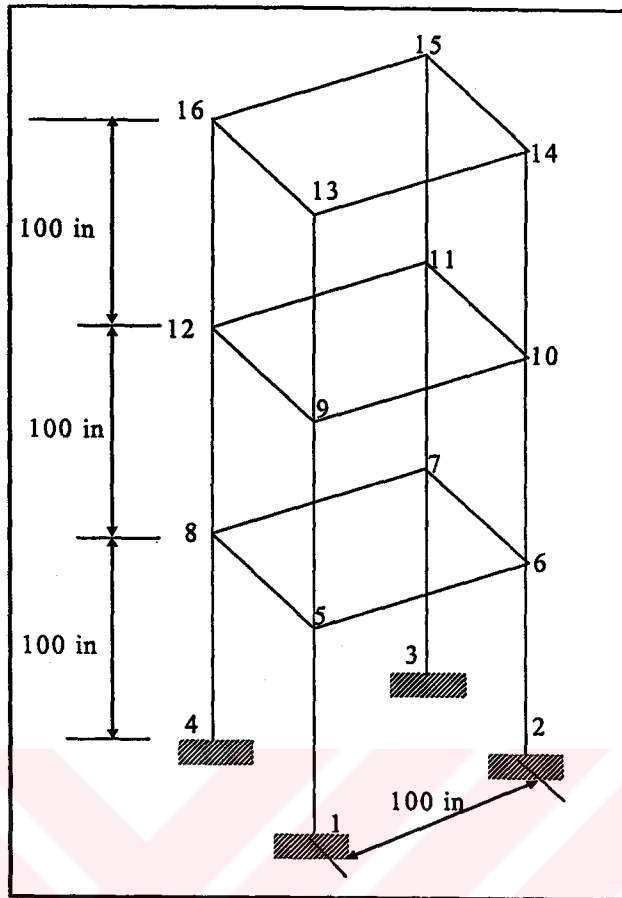
Figure 6.9 Three-story space structure

CHAPTER 7

GENETIC ALGORITHMS

7.1 Introduction

The search for a better, or rather than 'optimal' solution to a number of tasks that man has to face throughout his life is perhaps as old as mankind itself. The pursuit of an optimum design has long been the quest of designers, philosophers, economists, engineers, environmentalists and many others.

The introduction of the large-scale digital computers allowed the adaptation of classic optimization algorithms to realistic engineering problems, as well as the advancement of new and more powerful techniques. The investment of time and resources required to develop an optimization capability can be considerable and the projected results must justify the costs. Finally, a FE method allows the design of a class of problems with the investment of a little more than an analysis.

In many cases, mechanical and civil engineering structures are assembled of rolled profiles available on the market, and listed in commercial catalogues. Minimum weight design of these structures has been commonly known as discrete SO. Recently, there has been an increasing interest in discrete SO, due to its importance in the modern technology. However, there are considerable difficulties in finding exact solutions of discrete SO for practical cases. This is because of a very large number of combinations arising from the number of structural members and catalogue elements. This is the reason for intensive research, which has been carried out, and directed on simpler, but not necessarily exact solutions. Among them, one of the best known, and applied in different branches of science and technology, is the GA. All advantages and

125

disadvantages of GA are rather well known. One of the latter is that once the coded chromosomes are introduced, the GA mutation doesn't carry any information about the physical properties of the considered problem. It is then the aim of the thesis to investigate a problem oriented GA for minimum weight and/or SE (or maximum fundamental frequency) design. Among others it consists in introducing mutation carrying information about stress levels in particular structural members.

GAs are categorized under the umbrella term evolutionary algorithms, which is used to describe computer-based problem solving systems which use computational models of evolutionary processes as key elements in their design and implementation. A variety of evolutionary algorithms have been proposed, of which the major ones are: GAs, evolutionary programming, evolution strategies, classifier systems, and genetic programming. They all share a common conceptual base of simulating the 'evolution' of individual structures via processes of selection, mutation and reproduction [112]. But these terms shoul not be confused with their respective meaning in molecular biology! There is some resemblance, as you will see below on this page, but the researchers in informatics allowed themselves quite some liberties in modelling certain ideas of evolution. This does not mean it isn't possible from a theoretical point of view to adjust the algorithm to work with DNA as input data, but at the moment this is certainly not the situation.

In the GA application, the number of strings with design variables (chromosomes) obtained from crossover carried over the previous populations is constant. In the initial population, the first string of design variables is given. The cross sectional areas A_i or thicknesses in the remaining strings are randomly generated. A constant number (defined by the user) of chromosomes, giving the highest values of the fitness function is carried over to the next population.

Many practical optimum design problems are characterized by mixed continuous-discrete variables, and discontinuous and nonconvex design spaces. If standard nonlinear programming techniques are used for discrete or discontinuous problems they will be inefficient, computationally expensive, and in most cases, find a relative

optimum that is closest to the starting point. GAs are well suited for solving such problems, and in most cases they can find the global optimum solution with a high probability.

The GA is a search strategy based on the rules of natural genetic evolution. Even before the traits of genetic systems were used in solving optimization problems biologists had used digital computers to perform simulations of genetic system by the early 1950s. The application of GA for adaptive systems was first proposed by John Holland (University of Michigan) in 1962, and the term "genetic algorithms" was first used in his student's dissertation [91].

Unlike many mathematical programming algorithms, GAs do not require the evaluation of the gradients of the objective function and constraints. GAs are computationally simple, but powerful in their search for improvement, and they are not limited by restrictive assumptions about the search space, such as continuity or existence of derivatives. GAs are search procedures based on the mechanics of natural genetics and natural selection. They combine the concept of the artificial survival of the fittest with genetic operators abstracted from nature to form a robust search mechanism [127].

7.2 Comparison of the Genetic Algorithm with the Gradient Based Optimization Techniques

GAs are based on the principles of natural genetics and natural selection. The basic elements of natural genetics-reproduction, crossover, and mutation are used in the genetic search procedure [127]. GAs differ from the traditional methods of optimization in the following respects:

1. A population of points (trial design vectors) is used for starting the procedure instead of a single design point. If the number of design variables is n, usually the size of the population is taken as $2n$ to $4n$. Since several points are used as candidate solutions, GAs are less likely to get trapped at a local optimum.

2. GAs use only the values of the objective function. The derivatives are not used in the search procedure.

3. In GAs the design variables are represented as strings of binary (or gray) variables that correspond to the chromosomes in natural genetics. Thus the search method is naturally applicable for solving discrete and integer programming problems. For continuous design variables, the string length can be varied to achieve any desired resolution.

4. The objective function value corresponding to a design vector plays the role of fitness in natural genetics.

5. In every new generation, a new set of strings is produced by using randomized parents selection and crossover from the old generation (old set of strings). Although randomized, GAs are not simple random search techniques. They efficiently explore the new combinations with the available knowledge to find a new generation with better fitness or objective function value.

7.3 Natural Selection —Survival of the Fittest

GAs make use of chromosomes which contain all of the necessary information about the individual they represent which in the present context is a structural design. The GA randomly creates an initial population of individuals (here structural designs) and subsequently breeds new generation using natural selection, which is based on the 'fittest' of the population. These fitnesses in the present context might be weight, SE (stiffness) or the fundamental frequency. Better designs have lower weight, lower SE (greater stiffness) or higher fundamental frequency. This process of natural selection was originally observed in nature by Darwin and is called 'survival of the fittest'.

Evolution takes place during reproduction and is driven by mechanism known as 'crossover' and 'mutation' of the parent chromosomes leading to new and hopefully fitter children. Here, the children will be new structural designs.

7.4 Problem Definition in Genetic Algorithm

The GA is used to solve the following problem.

$$\text{To minimize} \qquad \hat{f}(s)$$

$$\text{Subject to} \qquad s_k^L < s_k < s_k^U, \qquad k = 1, 2, ..., n$$

in which, s is the vector of design variables, and $\hat{f}(s)$ is the fitness function to be minimized (or maximized). s_k^l and s_k^u are the lower and upper bounds on a typical design variable s_k.

Note that the problem is primarily an unconstrained minimization problem with lower and upper bounds on the design variables. To solve a constrained minimization problem it needs to make transformation. We first present the necessary background and GA before describing constraint handling. In the language of the GA, we are computing $\hat{f}(s)$, the fitness function, not $f(s)$, the objective function. The two functions are related and the distinction between the two will be made later.

7.4.1 Binary encoding and decoding of design variables

A major task is the encoding of the variables into chromosomes so that the GA can use them. Later the chromosomes can be evaluated or decoded and the fitness function evaluated. Usually each variable is represented using a bitstring. Each bitstring is then merged to form a chromosome, which represents a design.

Binary encoding is the most popular way of encoding the design variables. A binary number is represented as $(b_m ... b_1 b_0)_2$ where b_i is either 0 or 1. The relationship between binary and decimal numbers is defined as

$$(b_m ... b_1 b_0)_2 = (2^0 b_0 + 2^1 b_1 + ... + 2^m b_m)_{10}$$

Hence, as an example, $(101)_2$ is a three digit or three-bit binary number

$$(101)_2 (2^0 \cdot 1 + 2^1 \cdot 0 + 2^2 \cdot 1)_{10} = (5)_{10}$$

In other words, the binary number $(101)_2$ is equal to decimal 5.

The process of taking a decimal number and constructing its binary representation (not value) is called encoding. Decoding is the inverse process of taking the binary encoded value and constructing its decimal equivalent.

7.4.2 Pseudo-continuous design variables

Since GAs can only approximate continuous real (coded as double precision) variables, the minimum range of possible DVs needs to be broken down to a list of catalogue values. The difference or step between each catalogue real value, the resolution r, is defined as:

$$r = \frac{s_i^u - s_i^l}{2^m - 1.0}$$ (7.1)

where m is the binary string length specified in the GA data file, and 2^m is the number of possible binary numbers in the catalogue table of possible design variables.

From this resolution, the real design variable s_i list can be generated. The binary catalogue number, used to reference the real design variables, is stored in a separate array as the binary form of each integer catalogue number. An example of this cross referencing is given in Table 7.1 for a required binary string length m of 4, a minimum design variable s^l value of 4.2, and a maximum design variable s^u value of 28.0. Hence, the resolution with 4 bits is $r = (28.0 - 4.2)/(2^4 - 1) = 1.5867$.

The decoding (real design variable value) is achieved using

$$s_{real} = s^l + Cat \times r$$ (7.2)

where, Cat is catalogue table real value and calculated during optimization process using

$$Cat = \mathrm{int}\,eger(rnd \times 2^m)$$ (7.3)

where, rnd is a random generated number between 0 and 1. The binary design variable is binary equivalence of Cat value. For example, rhe catalog value, binary and real design variables for $m = 4$ $s^l = 4.2$, $s^u = 28.0$ and $r = 1.5867$ is given in Table 7.1.

Table 7.1 Binary equivalent relations between real and catalogue values

Catalogue Value (*Cat*)	Binary Representation $s_{binary} = (b_3 b_2 b_1 b_0)_2$	Real value $s_{real} = s^l + r \times Cat$
0	0000	4.2000
1	0001	5.7867
2	0010	7.3734
3	0011	8.9601
4	0100	10.5468
5	0101	12.1335
6	0110	13.7202
7	0111	15.3069
8	1000	16.8936
9	1001	18.4803
10	1010	20.0670
11	1011	21.6537
12	1100	23.2404
13	1101	24.8271
14	1110	26.4138
16	1111	28.0000

7.4.3 Discrete design variables

Another option for input of the size and shape information in the developed GA is by lists of discrete design variables. Once read in, the chromosome bit strings are used as pointers to refer to the appropriate discrete value. It should be noted that the number of total values in the discrete list (n_D) input from file must be less than or equal to the number of possible binary values (2^m) to encompass all the discrete design variables. For example, if $n_D < 2^m$ several binary strings will point to each discrete value, but if $n_D > 2^m$ all discrete values (of course not their actual real value) above 2^m will never be chosen, as there are not enough binary strings in the catalogue list to encompass them. The evaluation of the binary and real design variable values follows the same method as

for the continuous design variables, with the only difference being the *Cat* value definition:

$$Cat = \frac{n_D \times i_{pos}}{2^m}$$ (7.4)

where i_{pos} is the current integer position number (ranging from 1 to the number of binary values 2^m).

7.5 Parameters Used in Genetic Algorithm

Many parameters play a major rule in the optimization process using GAs. Such parameters are chromosome, string length, population size and fitness evaluation.

7.5.1 Chromosome

To represent all the design variables in a problem, we need to create the chromosome for the problem. A chromosome is a concatenated binary string of all the binary representations of the design variables. If there are n design variables with $m = 3$ to represent each design variable, then the chromosome looks as shown in Figure 7.1, where X is 0 or 1. The number of bits need not be equal for all the design variables, nor need the design variables be ordered from 1 to n in the chromosome.
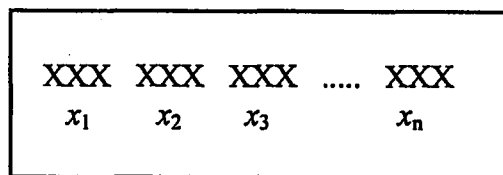
Figure 7.1 Possible chromosome or gene

It is found that, during the evolutionary process, the same chromosomes at times are repeatedly generated. Since the fitness evaluation in structural design involves FE analysis, a computationally expensive step, all generated chromosome and the associated fitness information are saved in memory. In this way, if a chromosome is repeated, a FE analysis is not necessary. Saved chromosomes may also be helpful for further processing of the design history.

132

7.5.2 String length

The string length represents each design variable and determines the size of the space search, the longer the string length the bigger the search space.

7.5.3 Initial population

The first step is to create the initial population. Unlike gradient-based methods, where the search for the optimal solution takes place by moving from one point to the next, in a GA the traits of a population (of members) are used to move from one generation to the next. Figure 7.2 shows the initial population consisting of members. The initial population is usually created randomly.

```
Member 1      XXX  XXX  XXX  .....  XXX
               x_1   x_2   x_3         x_n


Member 2      XXX  XXX  XXX  .....  XXX
               x_1   x_2   x_3         x_n


Member z      XXX  XXX  XXX  .....  XXX
               x_1   x_2   x_3         x_n
```
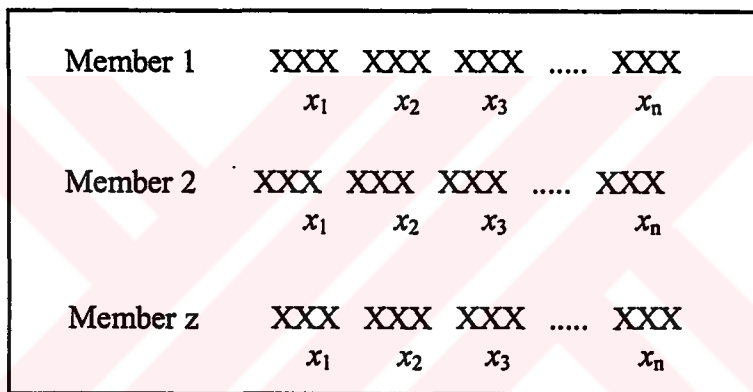
Figure 7.2 Initial Population

With the example in Figure 7.2, the size of the chromosome is $3n$ bits. A random number generator can be used to generate a random number between 0.0 and 1.0. *Invoking the random number generator 3n times, we can generate each member of the population as follows if the random number is less than 0.5 then a 0 is assigned to that bit, otherwise if the number is less than 0.5 a 1 is assigned to that bit.*

Population size is an important parameter in the GA process. The use of a large size of population leads to better chance for selection, but a greater amount of computational time will be required.

133

7.5.4 Fitness evaluation

Once the initial population is generated, the actual search process starts. The chromosome is decoded to obtain the values of the design variables s and the fitness function value is computed for each member of the population. In other words, fitness values $\hat{f}(s)$ are calculated for all population z.

7.6 Structure of Genetic Algorithm

The existing GAs are founded upon the following main principles:

- Reproduction
- Fitness
- Crossover
- Mutation

Figure 7.3 shows a simplified flow chart of GA and they will be discussed in more detail in following sections.

There are various flavours of GAs in circulation, varying in implementation of these three parameters, but in essence the algorithms all follow a standard procedure:

1. Start with a randomly generated population of n bit strings (candidate solutions to a problem). (These "solutions" are not to be confused with "answers" to the problem, think of them as possible characteristics that the system would employ in order to reach the answer)

2. Calculate the fitness $\hat{f}(s)$ of each string in the population.

3. Repeat the following steps until n new strings have been created:
   - Select a pair of parent strings from the current population, the probability of selection being an increasing function of fitness. Selection is done "with replacement" meaning that the same string can be selected more than once to become a parent.

- With the crossover probability, cross over the pair at a randomly chosen point to form two new strings. If no crossover takes place, form two new strings that are exact copies of their respective parents.

- Mutate the two new strings at each locus with the mutation probability, and place the resulting strings in the new population.

4. Replace the current population with the new population.

5. Go to step 2.
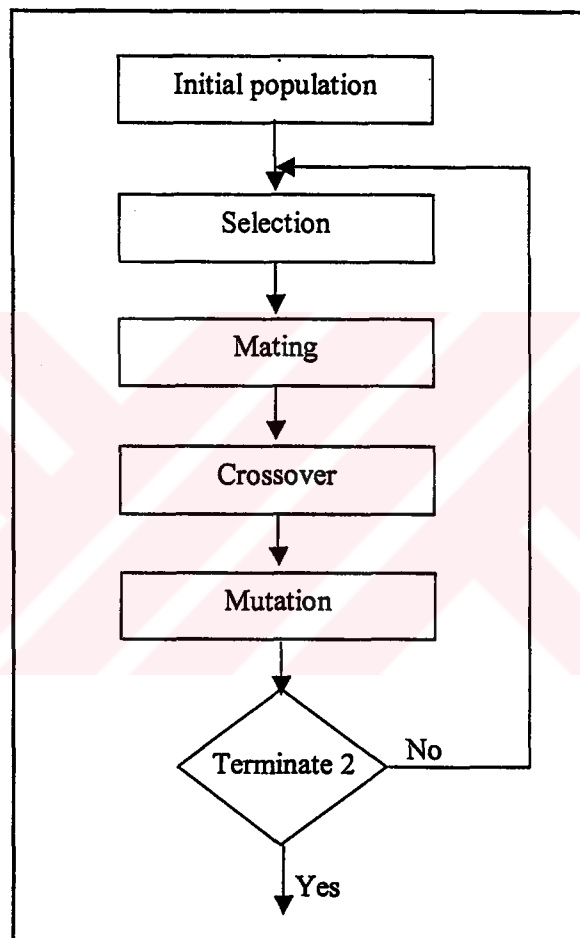
Figure 7.3 Simplified flow chart of a Genetic Algorithm

To generate the members of the next generation, the operation has at least three distinct steps. First the mating pool is created in reproduction step. Typically, the weaker members (higher fitness values) are replaced by stronger members (lower fitness values). To produce offspring, two members from the mating pool are selected and a crossover operation is carried out to create the chromosome of the offspring. Finally, to

135

bring diversity into the population, the mutation operation is carried out. The basic operations of natural genetics, reproduction, crossover, and mutation implemented are as follows.

7.6.1 Reproduction

Reproduction is a process in which the individuals are selected based on their fitness values relative to that of the population. In this process, each individual string (design vector) is assigned a probability of being selected for copying as

$$\frac{f_i}{\sum_{i=1}^{z} f_i} \tag{7.5}$$

where f_i is the fitness or objective function value of the ith individual (design vector, x_i) and z is the size of population. Thus designs (individuals) with higher fitness values have a greater chance of being selected for mating and subsequent genetic action. Consequently, highly fit individuals live and reproduce, and less fit individuals die (survival of the fittest).

The mating pool is constructed by selecting members from the population. In a simple GA, once the mating pool is constructed, two parents are selected and the reproduction process is carried out using the crossover and mutation operators [128]. There commonly used methods are described.

Roulette-Wheel Selection: In roulette-wheel selection, the chance of being selected is based on the fitness value. The individual members of the population are mapped to segments of a line such that the length of the segment is related to its fitness value.

Tournament Selection: In tournament selection, using a random number generator, two members of the population are selected. Their fitness values are compared head-to-head and the one with the lower fitness value is put into the mating pool. This is done z times to create the mating pool of size z. In a "double elimination" tournament selection method, all the individuals in the population are placed in a bag. Two individuals are chosen at random. Their fitness values are compared head-to-head and the one with the

136

lower fitness value is put into the mating pool. These two individuals are then eliminated from the bag and the process is repeated until the bag is empty. This will occur when the mating pool is half full. To complete the mating pool, the process is repeated once again.

Elitist Selection: Third selection scheme used in the GA is elitist selection, in which, for each iteration the best q % of individuals in the population (specified in the GA data files) is saved just before the genetic operators are applied. One the new parent population has been formed the q % of saved individuals are written over the worst q % of the new population. This selection process therefore provides a 'safety net', in case the genetic operations do not produce particularly desirable individuals, and ensures the survival of the fittest designs from the previous generation to the next.

7.6.2 Crossover

After reproduction, the crossover operation is implemented in two steps. First, two individual strings (designs) are selected at random from the mating pool generated by the reproduction operator. Next, a crossover site is selected at random along the string length, and the binary digits (alleles) are swapped between the two strings following the crossover site. Three methods of crossover can be adopted, one point, two point and uniform crossover.

One-point crossover: Two chromosomes selected randomly from the mating pool. They are labeled chromosome of parent individual 1 and 2 in Figure 7.4. Based on a predetermined probability, a single crossover point in chosen. If the length of chromosome is n_c bits, then a random number is generated between 1 and n_c and used as crossover point. The binary values of the chromosomes are then swapped from the right hand side of the new gene strings to binary crossover position. The resulting individual chromosomes are then passed onto the next generation.

Figure 7.4 One-point crossover process

Two-point crossover: This method is like *one-point crossover*, except that two cut points rather than one are selected at random, and chromosomal material is exchanged between the two cut points. Figure 7.5 illustrates the method.

Figure 7.5 Two-point crossover process

Uniform crossover: In this method, every location is potential crossover point. First, a crossover mask is created randomly. This mask has the same length as the chromosome and the bit value (parity) is used to select which parent will supply the offspring with the bit. If the mask value is 0 then the bit is taken from the first parent; otherwise the bit is taken from parent 2. If two offspring are needed, the mask is used with the parents to create the offspring and the inverse of the mask is used to create the second offspring. Figure 7.6 illustrates the method.

```
                        Chromosome

Parent individual 1     1  0  0  0  1  0  0  1

Parent individual 2     0  0  1  1  0  1  1  1

Mask                    0  0  1  0  1  0  1  1

Inverse mask            1  1  0  1  0  1  0  0

                   New chromosome

Parent individual 1     1  0  1  0  0  0  1  1

Parent individual 1     0  0  0  1  1  1  0  1
```

Figure 7.6 Uniform crossover process

7.6.3 Mutation

The new strings obtained from crossover (offsprings) are placed in the new population and the process is continued. The third operator of the simple GA is the mutation which plays a secondary role in the operation of the GA. Mutation is needed because, even though reproduction and crossover effectively search and recombine existing strings, to allow new genetic parents to be formed improving the search method. In artificial genetic systems, the mutation operator occasionally protects some useful genetic material against loss. In GAs, mutation is the occasional random alternation of the value of a string position.

The mutation operator is applied to the new string with a specified mutation probability. A mutation is the occasional random alteration of a binary digit (allele's value). Thus in mutation a 0 is changed to 1, and vice versa, at a random location. When used sparingly with the reproduction and crossover operators, mutation serves as a safeguard against a premature loss of important genetic material at a particular position.

7.6.4 Next generation and maximum number of generations

The new generation is formed when sufficient offspring are generated in the reproduction phase. The whole process of fitness evaluation and reproduction starts all over again with this new population. Obviously, somewhere in the evolutionary procedure the iterative process is stopped. Typically this is done if a predetermined number of iterations have been completed or if the fitness function does not change appreciably. Unlike most gradient-based techniques, there is no convergence criterion for the iterative process associated with the GA. Maximum number of generations is given by the user to control the convergence criteria (stop the optimization process) in the GA codes.

7.7 Constraint Handling for Genetic Algorithms

Since the GA scales individual's fitness values via the objective functions alone, constrained optimization problems require the incorporation of a penalty transformation method (first envisioned by Courrant [129] in the 1940s). This converts the constrained problem into an unconstrained one, which can then be utilized by the GA. The types of penalty functions used by researchers vary greatly [130], but the better algorithms are not problem specific, and therefore a certain degree of choice is available here.

The transformation method implemented in the current GA closely resembles the approaches of Rajeev et al [94], Goldberg [97] and Langley [111]. The method involves the normalization, squaring and summation of the violated constraints. The sum is multiplied by a prescribed penalty value and added to the original objective function, thus converting the optimization problem into its required unconstrained form. All the optimization problems tested in this thesis had both upper and lower design variable bounds, therefore an equality constraint transformation, which is mentioned above, was applied to the GA optimizer. One important aspect of equality constrain treatment is the need to penalize violations of the constraint boundaries equally. An uneven penalization of either side of the bounds is easily recognized, as the population of individuals would collectively drift away from the boundary of greater penalty.

140

7.7.1 Equality constraints

The ideal position for each of the individuals within the design space is of course at the intersection between upper and lower equality constraint bounds (the zero position). It is close to this position that the majority of individuals exist, and therefore care must be taken when allocating the severity of the penalty coefficient p_c. The penalty controls the 'steepness' of the constraint boundaries and too high a value can quite easily kill off individuals with small violations. This situations is highly undesirable, as the reduce genetic information in the gene pool can severely inhibit the evolutionary process. In the current implementation a linear penalty is applied for all levels of violation (Figure 7.7), so that individuals with small violations are allowed to continue to the next GA step, while individuals with large violations are eliminated. Constraints are normalized for all design problems. By doing this, a common set of GA optimization parameters can be used for most problems, and still give a satisfactory optimal solution.
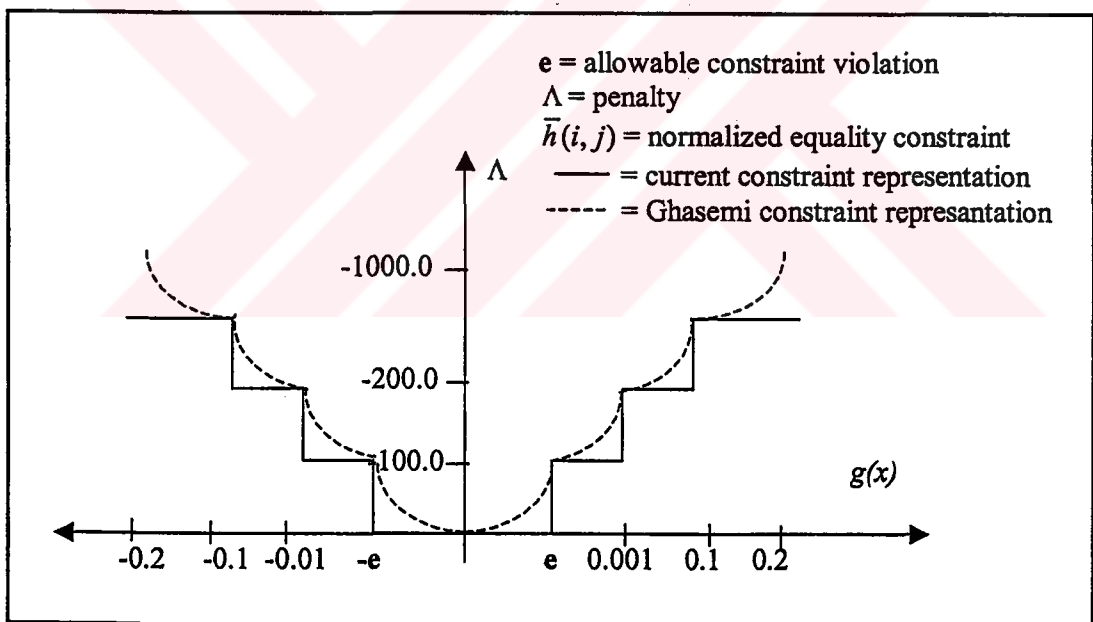
Figure 7.7 Comparison between normalized constraint $\bar{h}_{i,j}$ and penalty Λ when minimizing the objective function

Unless otherwise stated, the normalized constraint $\bar{h}_{i,j}$ takes the form:

$$\bar{h}_{i,j} = \frac{h_{i,j}}{h_{i,max}} - 1.0 \tag{7.6}$$

where, i is the constraint number, j is the design number, $h_{i,j}$ is the current equality constraint, $h_{i,\max}$ is the allowable value of constraint i before penalization occurs. Figure 7.7 illustrates the variation of $\overline{h}_{i,j}$ with the level of penalty occurring Λ. In relation to the Figure 7.7 for maximization problems $\Lambda = (1 - p_c \cdot \hat{h}_j)$, and minimization $\Lambda = (1 + p_c \cdot \hat{h}_j)$ (see equations 7.6(a) and 7.6(b) below). Two other constraint representations are also shown and although not exactly of the same scaling, are presented purely to compare the nature of application of the constraint. Note that a constraint tolerance factor e was implemented, which in doing so allows the 'optimal' objective to violate constraint limits. The technique of Ghasemi [131] follows a similar logic by introducing a constraint tolerance factor ε_j, which allows the objective to violate constraints to the maximum specified level of ε_j instead of 0.

For a non-penalized design, there are no constraint violations $(\overline{h}_{i,j} = 0.0)$. During the evolutionary process this is typically not the case, and so the objective function is modified to reflect this:

for objective minimization: $\hat{g}_j = g_j.(1 + p_c \hat{h}_j)$ (7.7a)

for objective maximization: $\hat{g}_j = g_j.(1 - p_c \hat{h}_j)$ (7.7b)

where, g_j is the 'pure' (non penalized) objective, $\hat{g}_j$ is the modified objective, p_c is the fixed penalty coefficient (from the input file), $\hat{h}_j$ is the sum of all absolute, normalized constraints $(\overline{h}_{i,j})$ for each individual j of the design space (n_c). In other words:

$$\hat{h}_j = \sum_{i=1}^{n_c} \overline{h}_{i,j}$$ (7.8)

Calculation of the fitness function $\hat{f}_j(s)$ then follows the straightforward technique of adding a large constant as suggested by [111]:

for objective minimization: $\hat{f}_j(s) = \left[Max\ \hat{g}_j + Min\ \hat{g}_j\right] - \hat{g}_j$ (7.9a)

for objective maximization: $\hat{f}_j(s) = \left[Max\ \hat{g}_j + Min\ \hat{g}_j\right] + \hat{g}_j$ (7.9b)

where, $Max\ \hat{g}_j$, $Max\ \hat{g}_j$ are respectively the maximum and minimum values of the modified objective $\hat{g}_j$.

7.7.2 Inequality constraints

The case for inequality constraints has also been used in this work, in which the tensile and compressive stresses and the nodal displacements are restricted to some values beyond which they are not allowed or else the constraints are said to be violated. Thus, the concept of penalizing the violated constraints used for the equality constraints is applied for the inequality constraints.

7.8 The Structure of Optimization Using Genetic Algorithm

The three examined operators; reproduction, crossover and mutation, have proved to be both computationally simple and effective in tackling a number of important optimization problems.

Figure 7.8 illustrates the structure chart for the GA. All the necessary data will be read in and the process of the GA will start for the first generation. The initial population will be generated randomly. The constraint violation may be computed so that the objective functions can be modified. By applying some statistics procedures, the average, the maximum and the fittest design will be found, and the convergence criteria will be checked. If the convergence is achieved the GA process will be terminated otherwise the GA process will resume by storing the best individual which will be used in the next generation. By producing the mating pool, the creation of the next population is started by applying the crossover operator, and the GA process will proceed continuously until convergence, or the maximum generation is achieved.

143
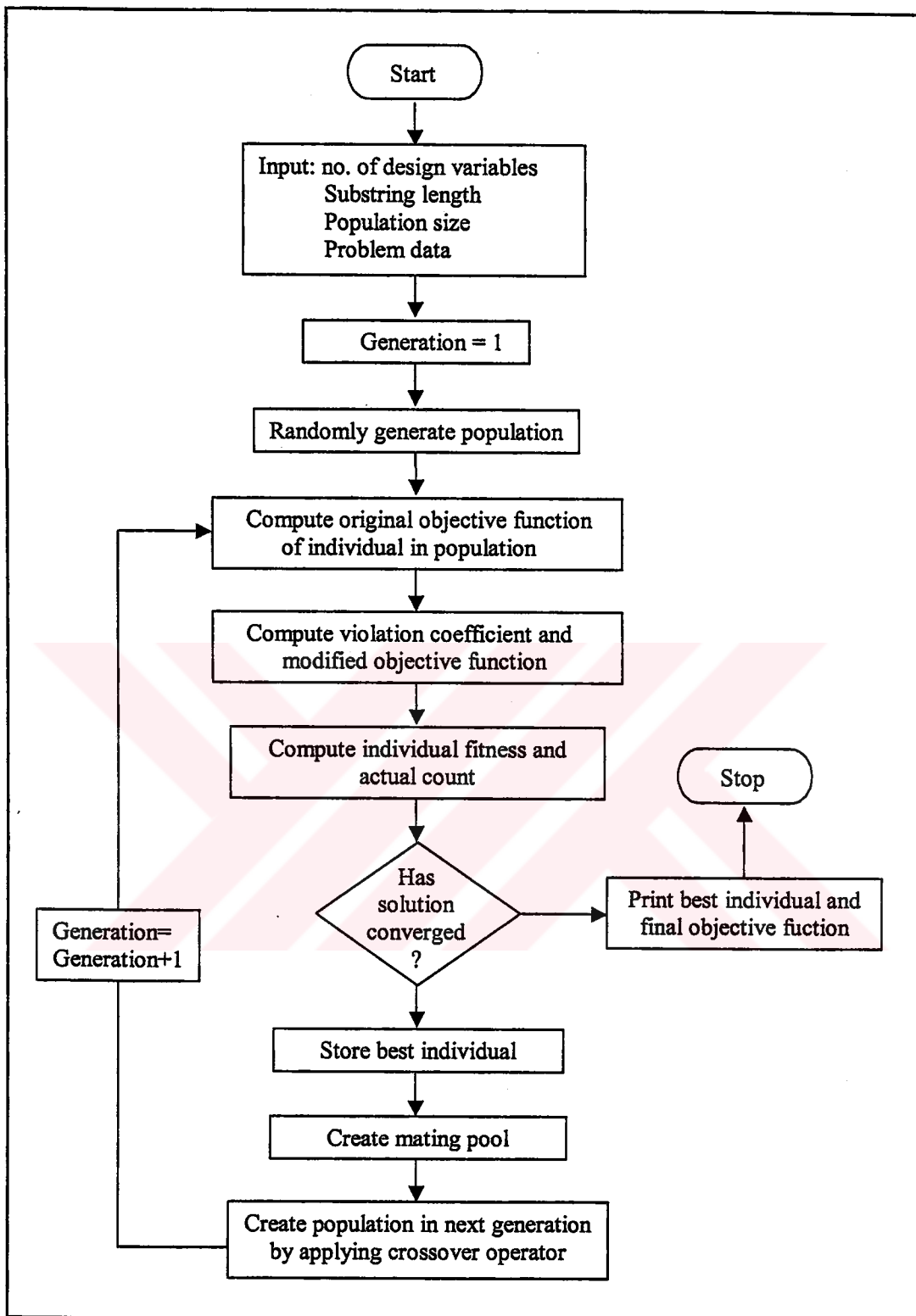
Figure 7.8 Structure chart of genetic algorithm

144

CHAPTER 8

STATIC OPTIMIZATION OF TWO AND THREE DIMENSIONAL STRUCTURES

8.1 Introduction

The relation between structural form, stiffness and strength in discrete structures has been widely recognized by structural engineers and designers. Many discrete structures gain considerable rigidity (stiffness) by a modification of their thickness variation and shape. Such rigid structures have higher resistance against deformation and may therefore be considered structurally more efficient.

Engineers have always been concerned with the task of finding efficient structural forms for truss, frames and arches. Traditional approaches towards the task of finding such forms for structures have been by the use of experimental models or by intuition and experience. However, in many cases the optimum shapes for structures are not evident from experiments and experience. There is there fore a need for better approaches which offer a more general and reliable way for determining optimum shapes under load cases other than self weight.

With the remarkable breakthroughs achieved in computer technology and the increasing trend towards the use of computer based modeling procedures, computer aided SSO tools seem to offer the obvious answer to the problem of finding optimal structural forms. Optimization is a valuable tool to generate efficient innovative layouts for structures, which go beyond the experience of the designer. The objective of optimization is often to produce minimum weight structures with maximum

145

strength and stiffness by changing the layout within a specified design domain and subject to a set of support and load conditions.

After some clean up and testing, the analysis code was converted to an F90 format with the embedding of a suitable F90 data structure to directly transfer the required information to and from the GA. For each individual of a population, this interface updated the member thickness and widths within the analysis with the appropriate GA design variables. Following analysis, each of the member stresses and nodal displacements are extracted to the GA.

8.2 Problem Definition

The optimization based on GA has been defined earlier in Chapter 7. Before any optimization process can be started the objective function, the constraint functions and bounds on the design variables must be specified.

8.2.1 Selection of objective (fitness) function

The objective function is a mathematical function expressed in terms of the design vector s, which quantifies (in a mathematical sense) the worth of any design. It is a criterion, which has to be chosen for comparing the different alternative acceptable designs and for selecting the best one. The choice of the objective function is governed by the nature of the problem.

Problem of structural optimization are characterized by various objective function and constraints, which are nonlinear function of the design variables. The functions can be implicit, discontinuous and non-convex. Detailed formulations of practical optimization problems (i.e objective and restrictions) vary with every application. Typical objective functions and constraints used in SO are listed in Table 8.1.

Weight minimization: Summing for the number of elements n_e, the individual masses (the unmodified objective functions) for individual i and population n_z are calculated from:

$$f(s)_i = \sum_{j=1}^{n_e} \rho \cdot A \cdot l \qquad \text{for:} \quad j = 1,...n_e \quad \text{and} \quad i = 1,...n_z \qquad (8.1)$$

Table 8.1 Design variables, objective functions and constraints used for structural shape optimization of discrete structures

---

Design variables **s**

- Coordinates of key points
- Thickness and/or width at key points
- Cross-sectional area of member

Objective functions $F(\mathbf{s})$

- Weight
- Volume
- Strain energy

Constraint functions g(**s**)

- Stress constraint
- Displacement constraint
- Volume constraint

Strain energy minimization: In the case of the SE minimization, objective function $f(\mathbf{s})_i$ for the structure is computed as the sum of the membrane, bending and shear strain energies

$$f(s)_i = \left\| \hat{W} \right\|_b^2 + \left\| \hat{W} \right\|_m^2 + \left\| \hat{W} \right\|_s^2 \qquad (8.2)$$

where

$$\left\| \hat{W} \right\|_b^2 \approx \int_\Omega [\hat{\sigma}_b]^T D_b^{-1} \hat{\sigma}_b d\Omega$$

$$\left\| \hat{W} \right\|_m^2 \approx \int_\Omega [\hat{\sigma}_m]^T D_m^{-1} \hat{\sigma}_m d\Omega$$

$$\left\| \hat{W} \right\|_s^2 \approx \int_\Omega [\hat{\sigma}_s]^T D_s^{-1} \hat{\sigma}_s d\Omega \tag{8.3}$$

The detail treatment of the volume and SE computation is presented for truss, arch and frame structures in Chapter 4 and 5 respectively.

In order to complete the formulation of the problem, some restrictions must be imposed on the values of the design variables for the mathematical model to be meaningful. Such restrictions are termed the constraints of the problem.

Stress constraint: For the n_e members of each individual design i, the stress constraints are calculated depending on the nature of the stress as:

$$c_i^e = \frac{\sigma_c^e}{\sigma_{c\max}} \quad \text{or} \quad c_i^e = \frac{\sigma_t^e}{\sigma_{t\max}} \tag{8.4}$$

where, c_i^e is the normalized element stress constraint of element e, $\sigma_{c\max}$ and $\sigma_{t\max}$ are the maximum allowable member stresses within the structure, for compression and tension cases respectively . Element compressive and tensile stresses are similarly defined by σ_c^e and σ_t^e.

From the normalized constraint value c_i^e, the member constraint violation $viol_i^e$ is derived from:

$$viol_i^e = c_i^e - 1.0 \qquad \text{for} \quad c_i^e > 1.0$$

$$viol_i^e = 0.0 \qquad \text{for} \quad c_i^e \leq 1.0 \tag{8.5}$$

Displacement constraint: The constraints from the nodal displacement limits for each individual are calculated by:

$$c_i^n = \left| \frac{u_i^n}{u_{\max}} \right| \tag{8.6}$$

where, u_i^n is the maximum nodal displacement component to be compared against the maximum allowable displacement u_{max}.

The nodal constraint violation $viol_i^n$ is obtained from the nodal displacement constraints c_i^n

$$viol_i^n = c_i^n - 1.0 \qquad (8.7)$$

where, n is the node number, and nodal displacements u_i^n must lie within the maximum displacement values of u_{max}, without incurring constraint violation $viol_i^n$.

Weight constraint: Structural weight is kept constant by using the target weight W_T.

$$viol_i = \frac{W_i}{W_T} \qquad \text{for} \quad W_i > W_T$$

$$viol_i = \frac{W_T}{W_i} \qquad \text{for} \quad W_i \le W_T \qquad (8.8)$$

where, W_i is the weight of the structure for individual design i. Note that, this constraint is only used together with SE minimization.

Fitness function: After computing objective function $f(s)$ from Eq (8.1) or Eq (8.2) and constraint violations $viol_i^n$ from Eq (8.5)-(8.7) and/or Eq (8.8), the individual modified objective function $\bar{f}(s)_i$ can be derived:

$$\bar{f}(s)_i = f(s)_i + p_c \sum (viol_i^n)^2 \qquad (8.9)$$

Note that the influence of *viol* on the above modified objective function is controlled by an input penalty multiple p_c. The maximum and minimum modified objective function $(\bar{f}(s)_i)_{max}$ and $(\bar{f}(s)_i)_{min}$ in the population of individuals can then be used to calculate the fitness value of each individuals designs:

$$fit_i = \frac{f_i}{\left(\dfrac{\displaystyle\sum_{dv=1}^{n_{dv}} f_i}{n_z}\right)} \qquad (8.10)$$

where:

$$f_i = (\bar{f}(s)_i)_{max} + (\bar{f}(s)_i)_{min} - \bar{f}(s)_i \qquad (8.11)$$

In GA optimization of structures, the interface method and parsing of information to and from the GA follows the same formats as for the 2D and 3D analysis above, the only differences being the inclusion of a third dimension.

8.2.2 Design variables

The choice of the design variable is a key factor in obtaining the optimum shape since it changes the character of the problem by changing the degree of nonlinearity of the objective or constraint functions.

In SSO, the optimum solutions obtained are based on certain bounds imposed on the design variables. Hence, to avoid ambiguity, there is a need to provide complete information on the upper and lower bounds values considered for the design variables. This information is often lacking in examples presented in the literature. The inclusion of this information eliminates any confusion in the definition of the problem and will enable other researchers to use these examples as benchmark tests.

8.3 Genetic Algorithm Based Solution Items

Apart from the usual definition of the SO problems which includes the structural geometry and members connectivities, loadings, boundary conditions, material properties, design variables, objective function and constraints, in a GA-based solution we must define the following items which may vary from problem to problem:

a) The bitstring length, i.e. the number of binary digits used in the coding of each design variable- this value is usually between 5 and 10.

b) If the design variables are continuous, we must specify the lower and upper bounds for each design variable assuming that all intermediate values are equally spaced between those two bounds, so that

$$r = \frac{s^u - s^l}{2^m - 1.0} \qquad (8.12)$$

where, s^u and s^l are the upper and lower bounds respectively, and m is the string length.

c) If the design variables are discrete then we must supply the catalogue of values, for equally spaced discrete values we use the above expression. Note that the number of catalogue is

$$\ln cat = 2^m \qquad (8.13)$$

d) The population size (usually between 100 and 1000).

We also need to define a set of convergence criteria. The mathematical representation of one of theses convergence criteria may be given in the following formulation:

$$\frac{|f_{av} - f_{best}|}{f_{av}} \times 100 < convg \qquad (8.14)$$

where, f_{av} is the average fitness value in each generation, f_{best} is the best fitness value in each generation, and $convg$ is the convergence value specified by the user.

The other convergence criterion is the maximum allowable number of generations allowed before the optimization is terminated.

8.4 Two Dimensional Truss Examples

In this part two dimensional truss examples which are analyzed in cahpter 4 are optimized under static loads. The objective function is weight minimization under stress and displacement constraints.

8.4.1 Three-bar truss

Problem definition: The three bar truss of Figure 8.1 is to be optimized for minimum weight. A load of 20 kip acts at $45°$ to the horizontal from node 4. Nodes 1, 2, and 3 are the locations of pin-jointed static supports. Two design variables are considered by the GA where design variable $s_1 = A^{(1)} = A^{(3)}$ and $s_2 = A^{(2)}$. Material properties for the truss are: Young's modulus $E = 2.07 \times 10^8 \text{kip/in}^2$, material density $\rho = 1.0$ lb/in^3, maximum tensile stress $\sigma_t = 20.0$ ksi, maximum compressive stress $\sigma_c = -15.0$ ksi, and maximum u_x and u_y displacement at node 4 being 100.0 in.

GA solution parameters: Two different sets of design variables are considered.

   i.   *Pseudo-continuous variables*: a population size of 50 and a maximum generation number of 100 are considered. The design variable binary string length $m = 10$. The range of design variables is 0.1 to 10.0 in^2.

   ii. *Discrete variables*: a population size of 30 and a maximum generation number of 100 are considered. The design variable binary string length $m = 5$. The range of design variables is 0.1 to 10.0 in^2. The number of catalogue values is 32.
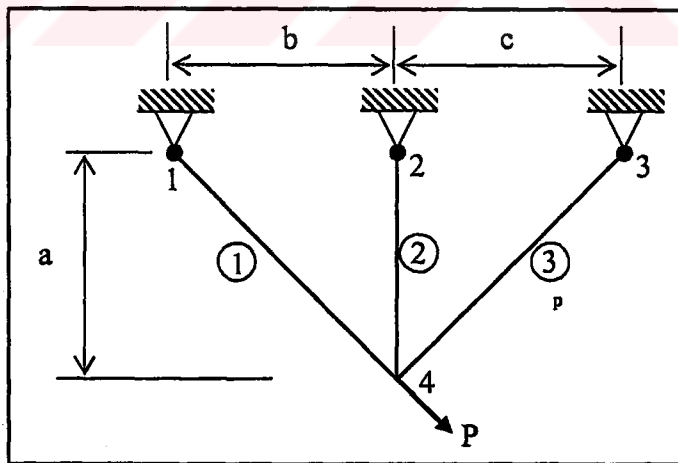
Figure 8.1 Nodal and element numbering for three bar truss (a = b = c = 100 in , P = 20 kip)

Discussion of the results: Table 8.2 gives the results obtained using the GA for pseudo-continuous and discrete design variables. Convergence to the optimal minimum weight design was achieved after 100 and 56 iterations for discrete and continuous design variables respectively. The resulting truss design of the GA for discrete and pseudo-continuous design variables was compared with various references in Table 8.2. The weight of the truss is reduced from 1448.52 to 262.673 lb (81.86 % reduction) and 261.389 lb (81.95 % reduction) for discrete and pseudo-continous design variables respectively. While some design variables vary from the reference values, the total truss weight was found to be very close to that of the reference solutions. Since elements 1 and 3 share the same design variable, the final optimal structure is symmetric. If however the optimization problem had used one design variable per element, the truss would have reduced to only one significant bar with element 2 and 3 at their minimum limits to prevent the structure from turning to a mechanism. The iteration history of the optimization process is illustrated in Figures 8.2 and 8.3 for discrete and pseudo-continuous design variables respectively.

Table 8.2 Comparison of optimum design variables of three bar 2D truss against other solutions

DV	Element number	Optimum design variables (in^2)		Ref. [111]	Ref. [112]	Ref. [112]
		Present GA		GA	GA	DOT
		Discrete	Continuous			
s_1	1,3	0.7800	0.7838	0.7864	0.8140	0.7890
s_2	2	0.4200	0.3967	0.4190	0.3430	0.4080
Optimum weight (lb)		262.6173	261.3896	264.3391	264.6000	263.9000
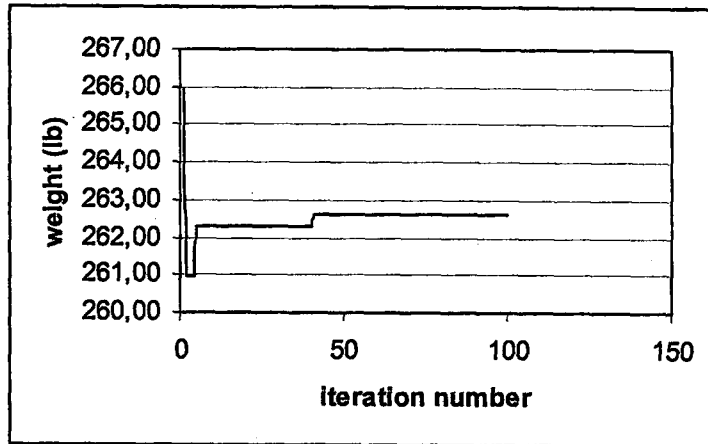
Figure8.2 Convergence curve for three bar 2D truss with discrete design variables
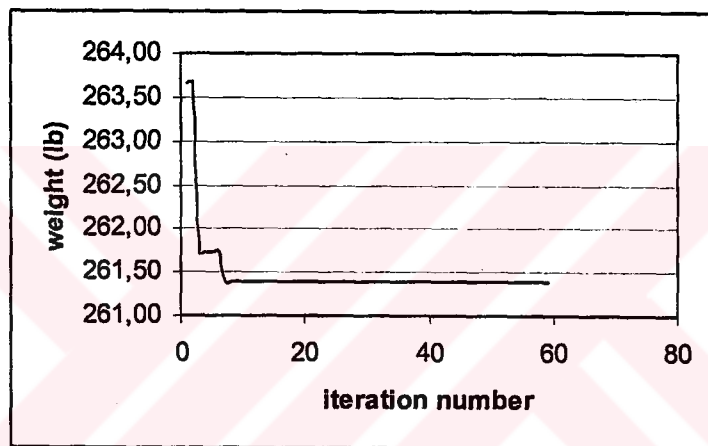
Figure8.3 Convergence curve for three bar 2D truss with pseudo-continuous design variables

8.4.2 Four-bar truss

Problem definition: The second example to be optimized is the four bar truss shown in Figure 8.4. Two cross-sectional area design variables are considered by the GA where design variable $s_1 = A^{(1)} = A^{(2)} = A^{(3)}$ and $s_2 = A^{(4)}$. Vertical download point loads of 10 and 20 kip act on nodes 2 and 3 respectively. The material properties for the problem are as follows: Young's modulus $E = 1.0 \times 10^4 \text{kip/in}^2$, material density $\rho = 1.0$ lb/in^3, maximum tensile stress $\sigma_t = 8.7$ ksi, maximum compressive stress $\sigma_c = -4.83$ ksi, and maximum u_x and u_y displacement at node 3 being 0.0006 in.

154

The GA pseudo- continuous design variables considered are in the range 0.1 to 10.0 in^2, population size 100, number of iterations 100, design variable binary string length $m = 10$.

Figure 8.4 Nodal and element numbering for four bar truss

Discussion of the results: Table 8.3 illustrates the results obtained using the GA for pseudo-continuous design variables. Convergence to the optimal minimum weight design of 89.5478 was achieved after 71 iterations for the four bar truss. The resulting truss design of the GA for pseudo-continuous design variables was compared with various references in Table 8.3. Figure 8.5 illustrates the convergence to the optimum solution for pseudo-continuous design variables.

Table 8.3 Comparison of optimum static four bar 2D truss against other solutions

DV	Element number	Optimum design variables (in^2)			
		Present GA	Ref. [111] GA	Ref. [112] GA	Ref. [112] DOT
s_1	1,2,3	9.4604	9.4683	9.5290	9.4640
s_2	4	9.4643	9.4586	9.3710	9.4640
Optimum weight (lb)		89.5478	89.5751	89.6400	89.5600
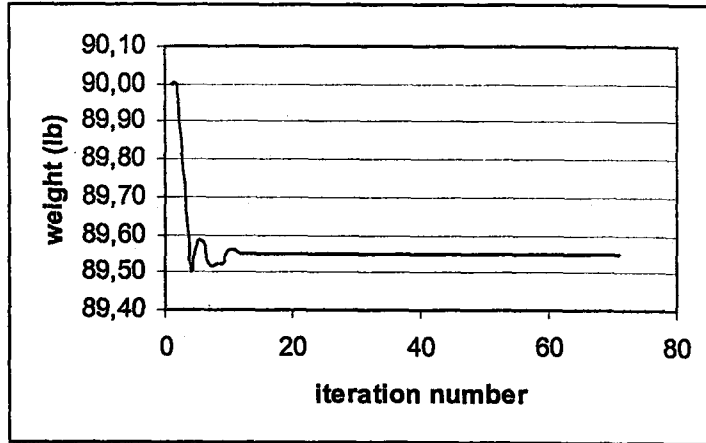
Figure8.5 Convergence curve for four bar 2D truss example with pseudo-continuous design variables

8.4 3 Ten-bar truss

Problem definition: This example is taken from the work of Langley [111] to verify the results obtained using present approach. The geometry and loading of the truss is shown in Figure 8.6. Ten design variables are considered by the GA where a design variable is allocated for each truss member. The following material properties are assumed: Young's modulus $E = 1.0 \times 10^7 \, \text{kip/in}^2$ and material density $\rho = 0.1 \, \text{lb/in}^3$. The objective is to minimize the weight of the truss, subject to the maximum tensile stress $\sigma_t = 0.25 \times 10^5 \, \text{ksi}$, maximum compressive stress $\sigma_c = -0.25 \times 10^5 \, \text{ksi}$ and maximum displacement is 2 in.
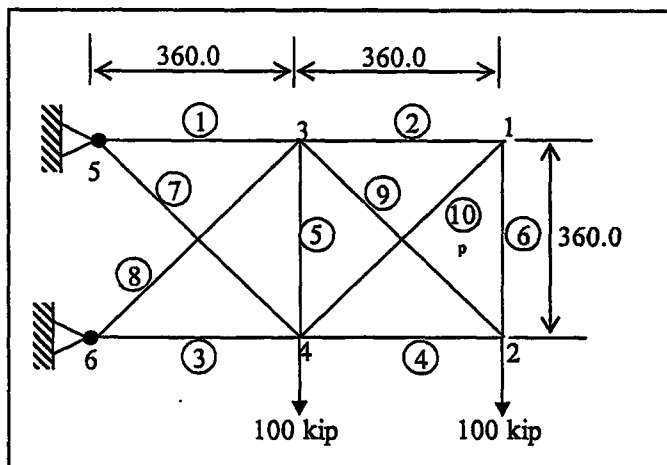
Figure 8.6 Nodal and element numbering for ten bar truss

The GA pseudo-continuous design variables considered are in the range 0.00005 to $10.0\,in^2$, population size 100, number of iterations 100, design variable binary string length $m = 10$.

Discussion of the results: Table 8.4 presents the optimal values of the design variables and the corresponding minimum weight. The weight of the truss reduced from 2098.2 lb to 1692.566 lb. The resulting truss design of the GA for pseudo-continuous design variables was compared with various references in Table 8.4. Convergence to the optimal minimum weight design was achieved after 349 iterations for the ten bar truss.

Table 8.4 Comparison of optimum static three bar 2D truss against other solutions

DV	Element number	Optimum design variables (in^2)			
		Present GA	Ref. [111] GA	Ref. [112] GA	Ref. [112] DOT
s_1	1	7.370	7.44	7.73	7.52
s_2	2	1.251	0.50	0.21	0.46
s_3	3	9.384	8.28	8.12	8.43
s_4	4	3.411	3.62	3.76	3.54
s_5	5	6.256	0.19	0.02	0.10
s_6	6	5.865	0.50	0.23	0.46
s_7	7	6.422	6.24	5.91	6.29
s_8	8	5.004	5.07	5.32	4.99
s_9	9	4.799	3.37	3.76	3.35
s_{10}	10	1.016	0.62	0.31	0.65
Optimum weight (lb)		1692.566	1508.21	1503.20	1516.00

Initial objective function value is 2098.2

8.5 Three Dimensional Truss Examples

8.5.1 Four-bar truss

Problem definition: The four bar truss of Figure 8.7 is to be optimized for minimum weight. Two design variables are considered by the GA where the design variable $s_1 = A^{(1)} = A^{(2)} = A^{(3)}$ and $s_2 = A^{(4)}$. The constraints are maximum tensile stress $\sigma_t = 4500.0\ \text{kN/m}^2$, maximum compressive stress $\sigma_c = -2500.0\ \text{kN/m}^2$ and maximum displacement $0.1\ \text{m}$. Material properties for the truss are: Young's modulus $E = 0.2 \times 10^9\ \text{kN/m}^2$ and material density $\rho = 1.0\ \text{kg/m}^3$. Two horizontal loads of 2.0 and $-4.0\ \text{kN}$ are imposed in the x and y-directions at node 5, along with a 3.0 kN downward vertical load.

The GA pseudo-continuous design variables considered are in the range 0.00001 to $0.0012\ \text{m}^2$, population size 300, number of iterations 100, design variable binary string length $m = 10$.
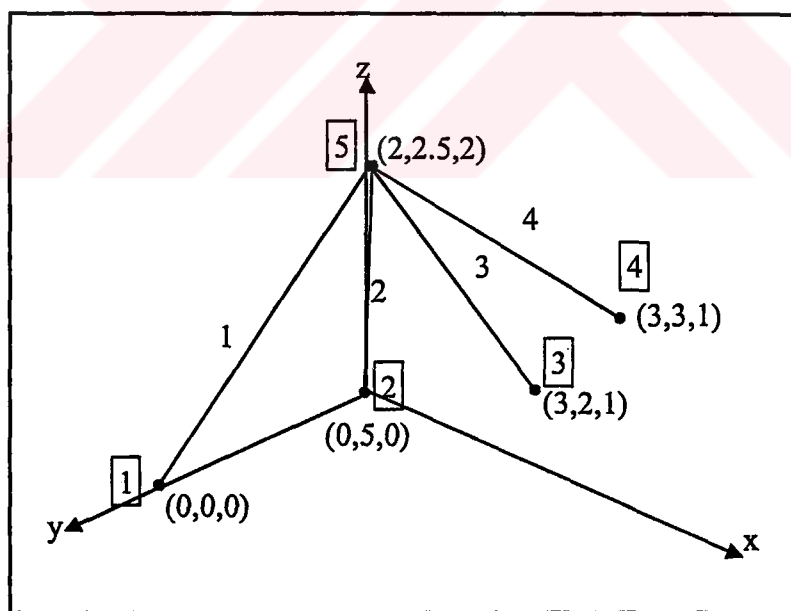
Figure 8.7 Nodal and element numbering for four-bar 3D truss

Discussion of Results: The optimum results are summarized and compared with other solutions, which are available in literature in Table 8.5. Size optimization resulted in

a 12.9 % reduction in the total weight from the initial value of 10.5 kg. The convergence to optimal design for four-bar truss was achieved after 24 iterations. Convergence to the global optimum in this case was rapid, due to the relative simplicity of this optimization problem along with the less restrictive design constraints.

Table 8.5 Comparison of optimum static four bar 3D truss against other solutions

DV	Element number	Optimum design variables (mm^2)			
		Present GA	Ref. [111] GA	Ref. [112] GA	Ref. [112] DOT
s_1	1,2,3	0.001055	0.001102	0.001100	0.001100
s_2	4	0.00057	0.000279	0.000290	0.000250
Optimum weight (kg)		9.677	9.158	9.150	9.200

8.5.2 Twenty five bar truss

Problem definition: The twenty five bar 3D truss of Figure 8.8 is to be optimized for minimum weight. The following material properties are used: elastic modulus $E = 1.0 \times 10^4$ ksi and material density, $\rho = 0.1$ lb/in^3. Nodes 7, 8, 9 and 10 are fully constrained, and nodes 1, 2, 3 and 6 are loaded with different loads values see Table 8.6. The design constraints are maximum tensile stress $\sigma_t = 40.0$ ksi, maximum compressive stress $\sigma_c = -40.0$ ksi and maximum displacement 0.35 in which is imposed for all nodes and in all directions. Eight design variables are considered by the GA. The member groupings for design variables assignment are shown in Table 8.7.

The GA pseudo-continuous design variables considered are in the range 0.1 to 5.0, population size 200, number of iterations 100, design variable binary string length $m = 8$.

159
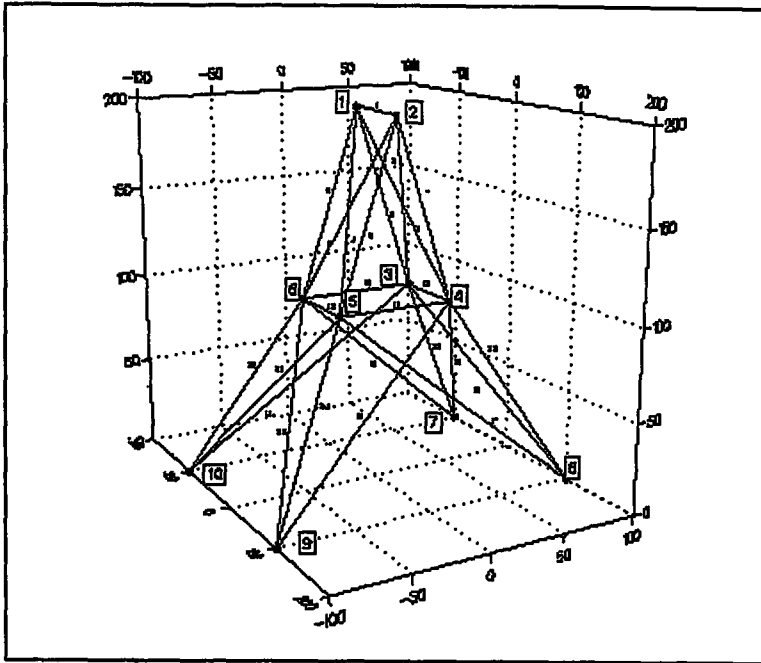
Figure 8.8 Nodal and element numbering for twenty five bar 3D truss

Table 8.6 Loading details for twenty five bar 3D truss

Joint	P_x (lb)	P_y (lb)	P_z (lb)
1	1000	-10000	-10000
2	0	-10000	-10000
3	500	0	0
6	600	0	0

Discussion of Results: The resulting truss design of the GA for pseudo-continuous design variables is presented and compared with various references in Table 8.7. The optimum structure is obtained in less than 50 optimization iteration. Size optimization results in 52 % reduction in total weight from the initial value of 991.84 lb. Initial cross sectional areas for this weight were 3.0 in².

Table 8.7 Comparison of optimum static twenty five bar 3D truss against other solutions

DV	Element number	Optimum design variables (in^2)		
		Present GA	Ref. [111] GA	Ref. [112] DOT
s_1	1	0.1000	0.1000	0.1000
s_2	2,3,4,5	0.1000	0.2537	0.1000
s_3	6,7,8,9	3.2600	3.2322	3.5800
s_4	10,11	0.1000	0.1000	0.1000
s_5	12,13	2.6300	1.9831	2.0500
s_6	14,15,16,17	0.8900	0.8686	0.8000
s_7	18,19,20,21	0.4200	0.2345	0.2200
s_8	22,23,24,25	3.8900	3.9816	3.8700
Optimum weight (lb)		488.74	488.7400	472.4300

The initial objective function value is 991.84

8.6 Two Dimensional Arch Examples

8.6.1 Strain energy minimization of a beam

Problem definition: The beam which has 10 m span length and 0.3×0.3 m cross-section is considered as shown in Figure 8.9. The following material properties are assumed: elastic modulus $E = 200$ GPa and Poisson's ratio $v = 0.3$. The shape of the beam is defined using two segments and eleven key points. A total of five shape design variables is considered. To take the advantage of symmetry, shape variable linking is also used. All the shape design variables are constrained to move in vertical direction only. The initial geometry of the beam and the location of the design variables are shown in Figure 8.9. SE of the beam is minimized subject to Von Misses stress constraint. The value of the stress constraint is equal to maximum value of the Von Misses stress at the initial design (5 MPa). Structure is optimized under the two different load conditions, which are shown in Figure 8.10

    i.)   Point load at the crown

ii.)   Uniformly distributed normal loading

The GA pseudo-continuous design variables considered are in the range 0.001 m to 1.5 m, population size 100 number of iterations 100, design variable binary string length $m = 10$.
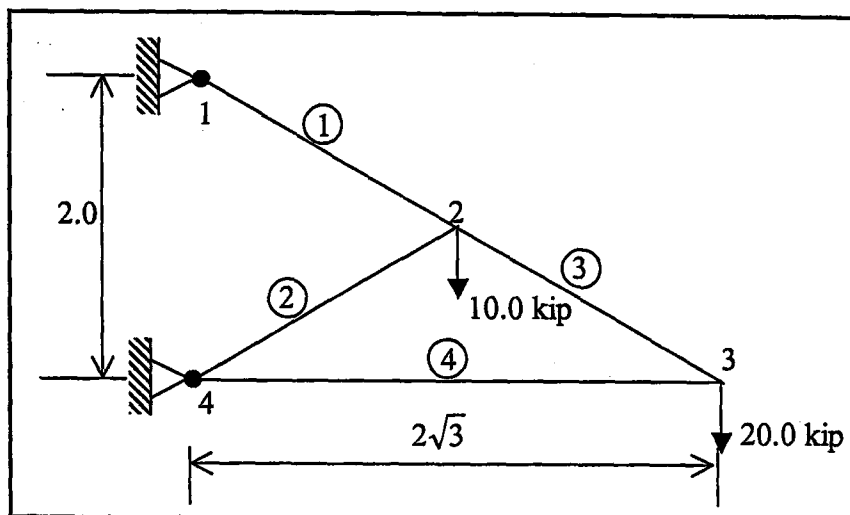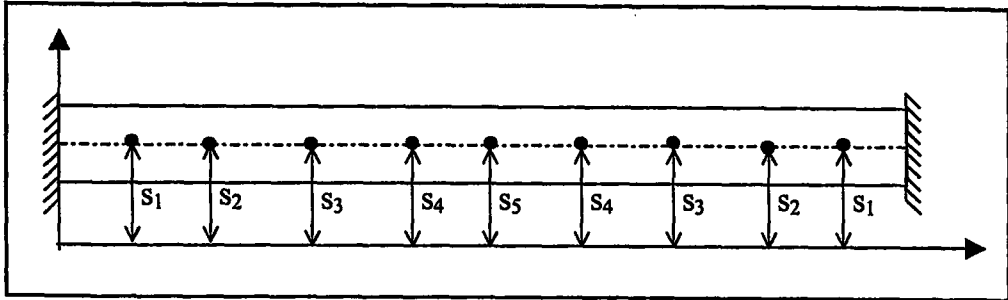

Figure 8.9 Location of design variables
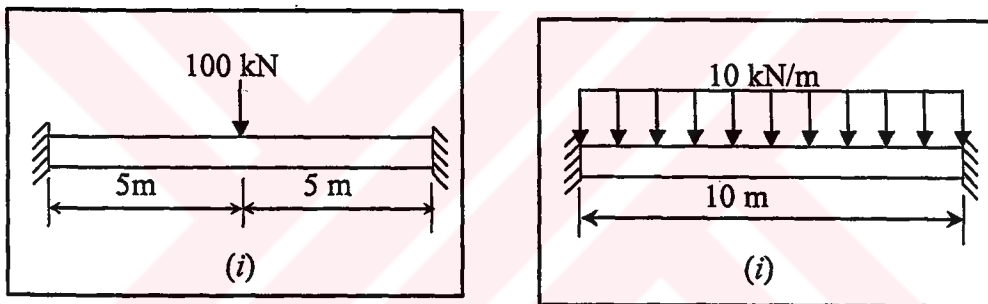
Figure 8.10 Dimensions and loadings of beams (*i*) point load, (*ii*) distributed load

Discussion of results: Table 8.8 presents initial and optimal values and percent improvements of total SE. Note the remarkable reduction in SE that has been obtained. The SE of the structure is reduced from 3901.358 to 241.099 and 52.239 for point and distributed load cases respectively. Also, it is very interesting to note that the changes in the SE contributions associated with membrane and bending behaviors as the shape changes. In the initial shape the contributions to total SE from membrane and shear behavior are both negligible. Subsequently, as the shape changes, the membrane energy becomes dominant (up to 89.6 %) and bending and shear energy becomes negligible. Table 8.9 displays optimal design variables. The optimum shapes of structures are shown in Figures 8.11 and 8.12 for point load and

distributed load cases respectively. As you can see from Figure 8.11 and 8.12, optimum shapes of the beams are becoming an arch structure, because of structural advantages of arches. Figure 8.13 illustrates the convergence to the optimum solution for pseudo-continuous design variables.

Table 8.8 For SE minimization of beam, initial and optimum SE and percent distributions

Loading cases		Total SE ($\times 10^{-4}$)	% SE distribution		
			Membrane	Bending	Shear
Case *i* (point load)	Initial	3901.358	0.00	98.89	1.11
	Ref. [132] MMA	157.341	89.57	9.06	1.37
	Present GA	241.099	73.65	24.44	1.91
Case *ii* (distributed load)	Initial	1043.251	0.00	98.61	1.39
	Ref. [132] MMA	44.033	92.19	6.86	0.95
	Present GA	52.239	89.76	9.47	0.77

Table 8.9 Optimum design variables of minimized beam

DV	Case *i* (point load)		Case *ii* (distributed load)	
	Ref. [132] (MMA)	Optimum (present)	Ref. [132] (MMA)	Optimum (present)
s_1	0.2266	0.25514	0.5107	0.45455
s_2	0.5910	0.41789	1.0010	0.85777
s_3	0.9088	0.83871	1.3010	1.1510
s_4	1.2733	1.0733	1.5000	1.3284
s_5	1.5000	1.3827	1.5000	1.4310
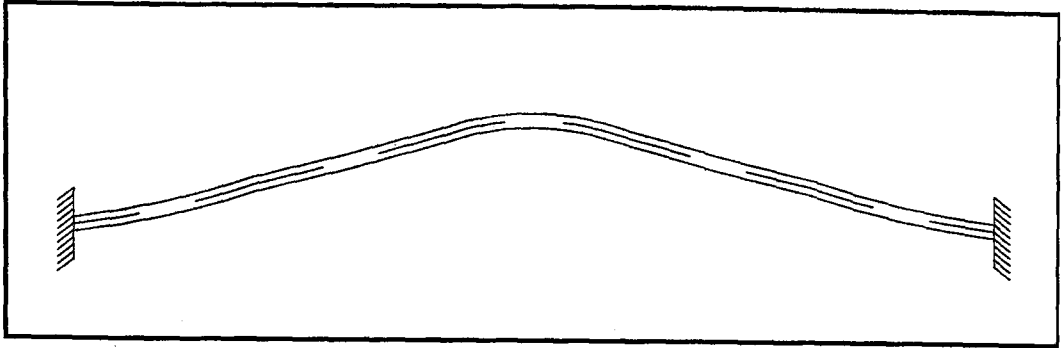
Figure 8.11 Optimum shape of beam under point load, case (a)
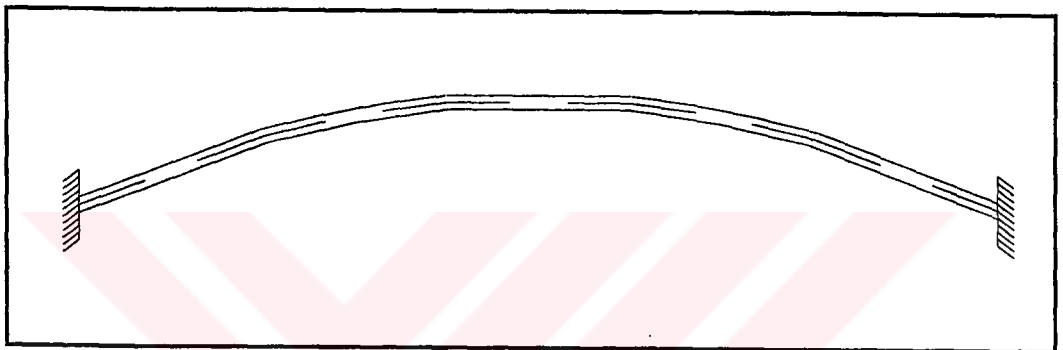
Figure 8.12 Optimum shape of beam under distributed load, case (b)
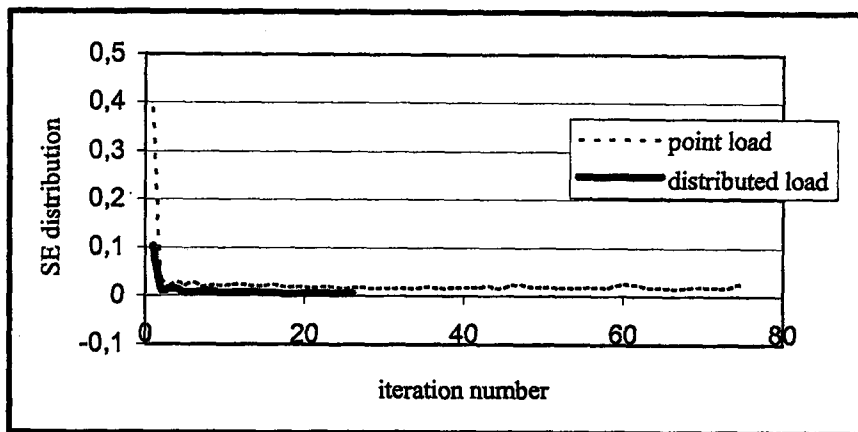
Figure8.13 Convergence curve for beam example with pseudo-continuous design variables

8.6.2 Arches with uniform cross-section

Problem definition: This example involves optimization of a series of arches with rectangle cross-sections, which have been analyzed by Litewka and Rakowski [8] and analyzed in chapter 4. The geometry and loadings of arch which has uniform cross-section with opening angle 120° is considered shown in Figure 8.14. The arch, have a radius of curvature $R = 4\,\mathrm{m}$, the angle $\omega = 2\pi/3$ (span length $l = 8\pi/3$), the rectangular cross-section with depth $h = 0.6\,\mathrm{m}$ and width $b = 0.4\,\mathrm{m}$. The following material properties are used: elastic modulus $E = 30\,\mathrm{GPa}$ and Poisson's ratio $v = 0.17$.

The arches are optimized for the following objective and constraint functions,

- *SE minimization* with constraints that the total material volume of the structure should remain constant and the maximum von-Misses stress should not exceed 300 kPa.

- *Weight (or volume) minimization* subject to the constraint that the maximum von-Misses stress and displacement should not exceed 300 kPa and 0.0005 m respectively

The arch geometry is defined using five key points and two segments. The locations of the shape and thickness design variables are shown in Figure 8.15. Note that the width of the arch is kept constant. Use is made of design variable linking to maintain symmetry of structures. In the case of weight minimization, three thickness design variables are only defined. On the other hand, in the case of the SE minimization three thickness and two shape design variables are used. The shape design variables are allowed to move in radial direction.

165
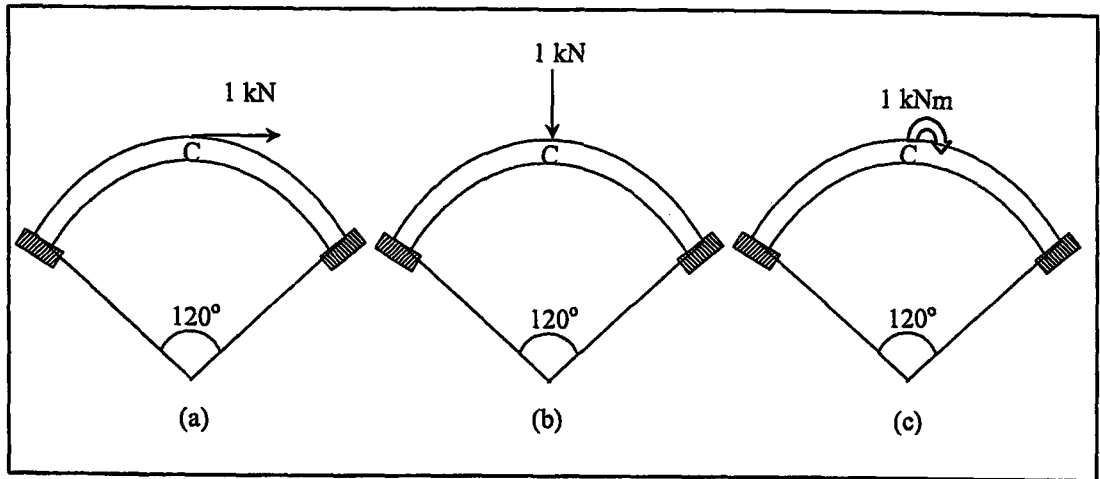
Figure 8.14 Loading conditions of arch

Optimization is repeated for three different loading cases;

    a) Vertical point load at the crown,

    b) Horizontal point load at the crown,

    c) Moment at the crown.

The GA pseudo- continuous design variables considered for 3 height and two radius of the arc as shown in Figure 8.15, population size 100 number of iterations 100, binary string length 10.
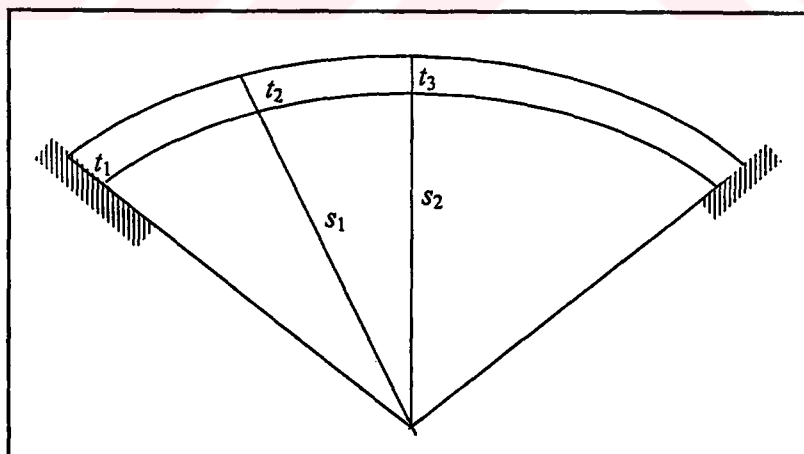
Figure 8.15 Design variables of arch structure

Discussion of results: Table 8.10 shows the initial and optimal values of design variables and weight for the different loadings considered. In all loading cases there is considerable reduction in the magnitude of the weight. The percentage reductions obtained in the weight are 64.56, 62.09 and 72.68 % for loading cases a, b and c respectively.

Table 8.10 For weight minimization of arch, initial and optimum values of design variables

Design variables				Optimum		
Type	Minimum	Initial	Maximum	Case (a)	Case (b)	Case (c)
t_1	0.1	0.6	1.0	0.1992	0.1501	0.2319
t_2	0.1	0.6	1.0	0.1743	0.1932	0.1704
t_3	0.1	0.6	1.0	0.4391	0.4853	0.1836
Weight		5.009		1.7752	1.8991	1.3682

Table 8.11 presents the initial and optimal energies and contributions to the SE from membrane, bending and shear behavior. In loading case (a) and (b) the membrane and bending energies are almost equally distributed. However, for loading case (c), the bending energy is significant in the initial and optimum shapes. Table 8.12 gives the optimum values of the design variables for different loading cases considered.

Table 8.11 For SE minimization of arc, initial and optimum SEs and percent distributions

Loading cases		Total SE $(\times 10^{-6})$	% SE distribution		
			Membrane	Bending	Shear
Point load in x direction	Initial	1.0141	30.374	60.954	8.671
	Optimum	0.5641	40.692	49.234	10.074
Point load in y direction	Initial	2.111	39.729	50.207	10.064
	Optimum	1.4403	61.012	32.289	6.699
Moment	Initial	2.2532	0.606	95.212	4.183
	Optimum	2.1361	1.268	95.332	3.400

Table 8.12 For SE minimization of arc, initial, optimum and constrain values of design variables

Design variables				Optimum		
Type	Minimum	Initial	Maximum	Case (a)	Case (b)	Case (c)
t_1	0.1	0.6	1.0	0.8522	0.9305	0.6973
t_2	0.1	0.6	1.0	0.6780	0.4132	0.8373
t_3	0.1	0.6	1.0	0.2469	0.8364	0.8076
s_1	1.0	4.0	8.0	2.1642	3.9765	2.4027
s_2	1.0	4.0	8.0	2.3402	4.2874	5.1001

8.6.3 Frame structure with curved members

The cylindrical shell roof analyzed in Chapter 4 of this thesis is considered for optimization. The geometry of structure and cross sections of members are shown in Figure 8.16. The structure has the following material properties: elastic modulus $E =$ 200 GPa and Poisson's ratio $v = 0.3$. The curved part of frame, which is shown in Figure 8.16, has uniform cross-section with opening angle 60° and radius of curvature is $R = 6\,\text{m}$.

The symmetric half of the structure is modeled using two segment and four key points and by taking advantage of the symmetry only half of the structure is analyzed. The structure is optimized for SE minimization with constraints that the total material volume of the structure should remain constant and the maximum von-Misses stress should not exceed of its initial value prior to optimization. Both shape and thickness design variables are used. The location of the design variables are shown in Figure 8.17. The cross-sectional area of column and curved member is defined as square. Use is made of design variable linking to maintain square cross-sectional area. Two loading cases are considered:

a) The structure subject to a concentrated vertical 5 kN load at point C, and

b) Distributed load with an intensity of 3 kN/m is applied to curved member.
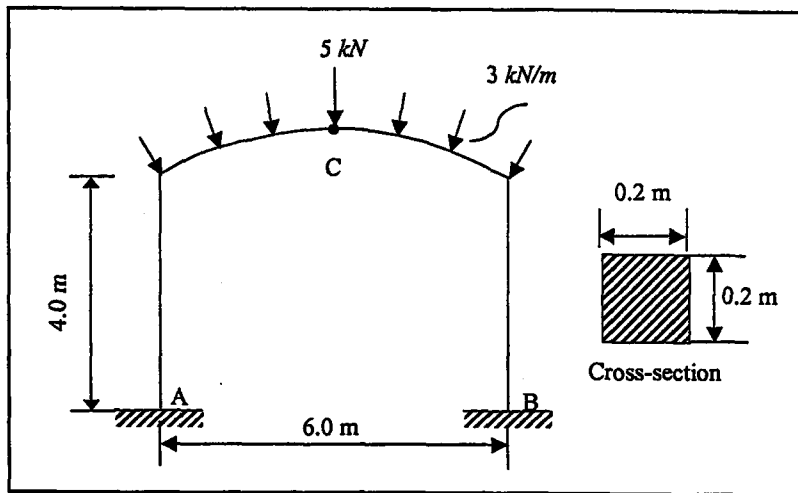
Figure 8.16 Geometry and cross section of frame structure
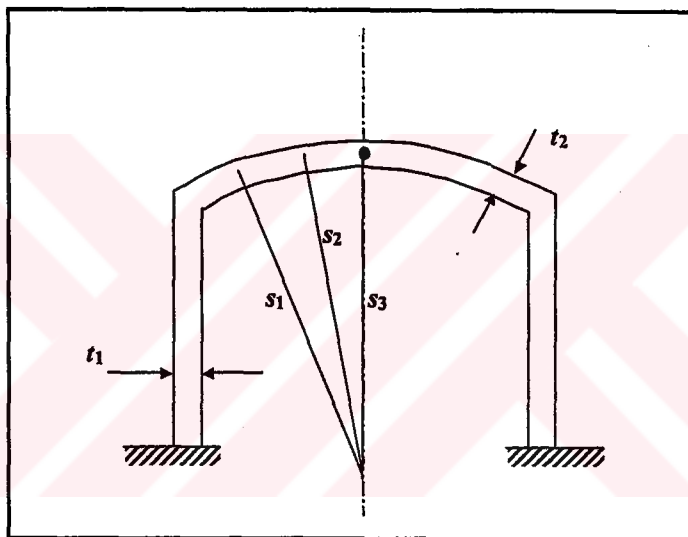
Figure 8.17 The location of the design variables

Discussion of results: This example demonstrates the principal capabilities of the present approach. In Table 8.13 initial and optimal energies and % distributions of membrane, bending and shear energies for three different loading conditions are given. Note that remarkable reduction in SE that has been obtained. In the initial shapes, contribution to SE from the bending behavior is significant. As the optimization process is proceed, in the optimum shape the membrane energy becomes dominant (up to 60%). Table 8.14 displays the optimum values of the design variables for the different loading cases.

169

Table 8.13 Total strain energy and % distribution of frame structure

Load		Total SE($\times 10^{-3}$)	% SE distributions		
			Membrane	Bending	Shear
(a)	Initial	1.47	0.57	98.43	1.00
	Optimum	0.003252	18.53	61.48	19.99
(b)	Initial	5.48	1.89	97.11	1.00
	Optimum	0.02273	60.32	26.24	13.43

Table 8.14 For SE minimization of frame with curved member, initial, optimum and constrain values of design variables

Design variables				Optimum	
Type	Minimum	Initial	Maximum	Loading (a)	Loading (b)
t_1	0.05	0.20	1.00	0.8366	0.8319
t_2	0.05	0.20	1.00	0.9972	0.7130
s_1	3.00	6.00	9.00	5.4340	6.6481
s_2	3.00	6.00	9.00	7.9384	7.0469
s_3	3.00	6.00	9.00	7.4809	7.4927

8.7 Two Dimensional Frame Examples

8.7.1 T-shape frame

Problem definition: This example involves the optimization of frame, which is shown in Figure 8.18. System with uniform rectangular cross sections 0.2×0.1, density $\rho = 800$, Poisson's ratio $\nu = 0.3$ and modulus of elasticity is 2×10^8 is analyzed under three-point load and gravitational force due to self-weight. (All units are consistent).

170
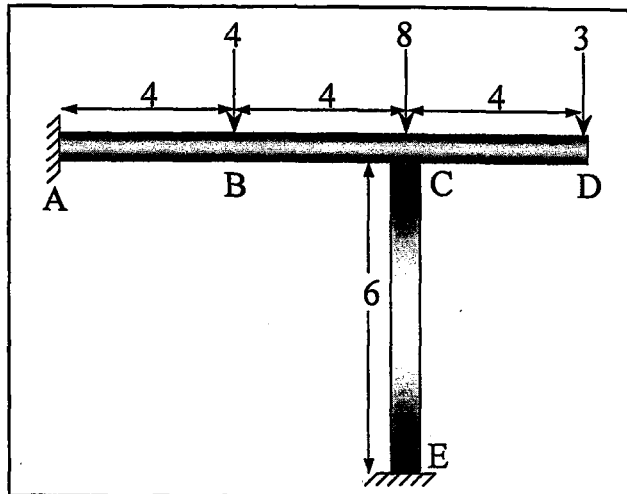
Figure 8.18 Loads and dimensions of frame example

The objective is to minimize the weight of the frame subject to limits on tensile and compressive stresses and displacement. Maximum tensile stress $\sigma_t = 1.0 \times 10^7$, maximum compressive stress $\sigma_c = -1.0 \times 10^7$, and maximum displacement 1.5 are used. In this example, also design variables are linked to achieve desired thickness variation. The thicknesses at all the key points (used to define the structure) are taken as design variables as shown in Figure 8.19. The following two cases are considered.

a) *Piecewise constant*: three design variables are used. These are thickness of the column, cantilever segment and upper beam.

b) *Piecewise linear*: six design variables are defined. These are the thicknesses of key points.

The GA pseudo-continuous design variables considered are in the range 0.01 to 0.5, population size 100, number of iterations 200, design variable binary string length 10.
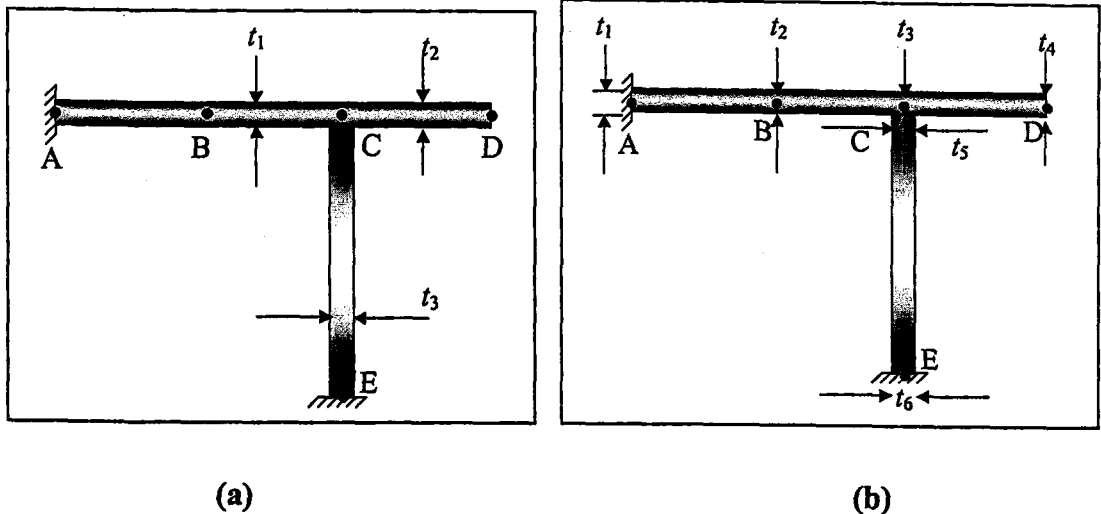
Figure 8.19 Design variables of frame example (a) piecewise constant, (b) piecewise linear

Discussion of results: The convergence to optimal design for two-dimensional frame was achieved after 127 iterations. The initial weight of the frame is equal to 288.0 kg. Tables 15 and 16 give the initial and optimum values of the design variables and objective function. The percentage weight reductions are 30.2 % and 61.3% for piecewise constant and piecewise linear thickness variations respectively. Significant differences in the percentage weight reductions are found for two cases, with the piecewise linear variation of thickness giving the maximum percentage of weight reduction. In general, it can be observed that the volume reduction is greater when more thickness variables are used.

Table 8.15 Initial, optimum and constraints of 2D frame structure piecewise constant design variables

DV	Design variables (mm)			
	Minimum	Initial	Maximum	Optimum
t_1	0.01	0.2	0.5	0.165
t_2	0.01	0.2	0.5	0.221
t_3	0.01	0.2	0.5	0.050
Weight (kg)		288.0		201.02

Table 8.16 Initial, optimum and constraints of 2D frame structure piecewise linear design variables

DV	Design variables (mm)			
	Minimum	Initial	Maximum	Optimum
t_1	0.01	0.2	0.5	0.0407
t_2	0.01	0.2	0.5	0.0638
t_3	0.01	0.2	0.5	0.1695
t_4	0.01	0.2	0.5	0.0869
t_5	0.01	0.2	0.5	0.0100
t_6	0.01	0.2	0.5	0.0580
Weight (kg)		288.0		111.40

8.7.2 Size optimization of a rectangular frame

Problem definition: Next, 2D frame shown in Figure 8.20 is considered for size optimization. The frame subject to horizontal distributed force of intensity 4 kip/ft as shown in Figure 8.20 The frame is made of steel with the following properties: modulus of elasticity, E=29(10^3) ksi and Poisson's ratio $v = 0.3$.

The frame is modeled using two segments and three key points. The thickness and width of the two segments are defined as design variables. The allowable tensile and compressive stresses are constrained to be less than or equal to 2000 psi and the objective is to minimize the weight.

The GA pseudo-continuous design variables considered are in the range 5.0 to 40.0, population size 100, number of iterations 200, design variable binary string length 10.
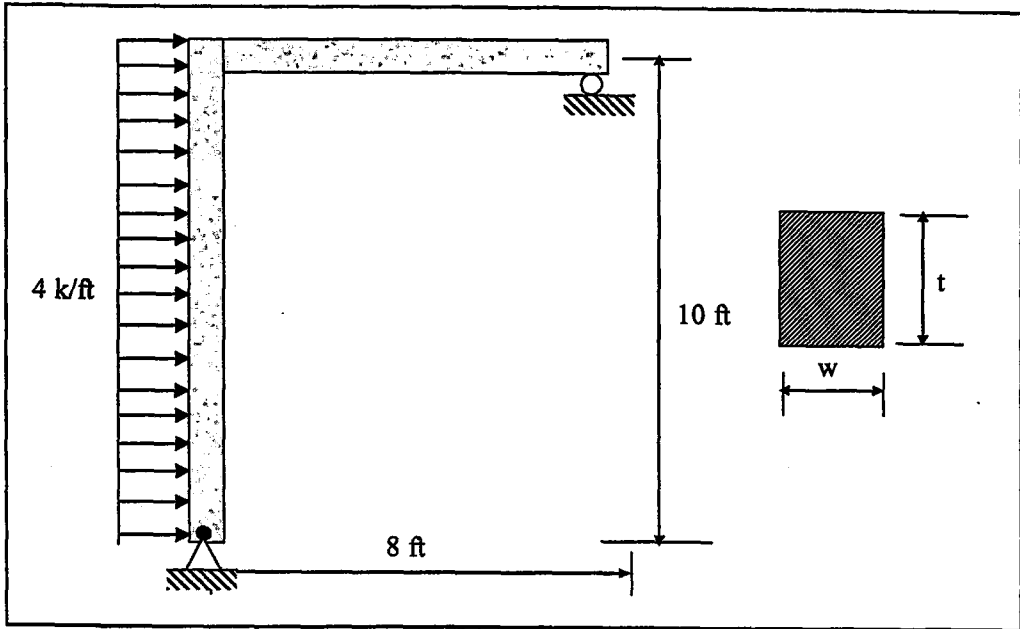
Figure 8.20 Frame structure with rectangular solid cross-section

Discussion of results: Table 8.17 displays the initial and optimal design variables and weight. Note the remarkable reduction in the weight that has been obtained. 47.38 % improvement in objective function is achieved. The result of the present study is compared with GS-USA program result in Table 8.17 and it is found that present approach gives better improvement in the objective function.

Table 8.17 Optimum design variables and volume

DV	Minimum	Initial	Minimum	Optimum (in)	
				GS-USA program	Present
t	5.0		40.0	33.47	34.35
w	5.0		40.0	7.19	6.13
Volume (in³)		864.28		517.71	454.81

8.8 Three Dimensional Frame Examples

8.8.1 Grid under distributed load

Problem definition: A frame example analyzed with matrix stiffness method in [4] is now considered for optimization. The geometry and loading of frame is shown in Figure 8.21. The frame is analyzed for distributed load with an intensity of $2\,k/ft$, which as shown in Figure.8.21. The frame has the following material property: elastic modulus $E = 29000$ ksi, Poisson's ratio $v = 0.26$ and material density $\rho = 0.1\,lb/in^3$.

The design problem is to find the lowest volume subject to allowable tensile and compressive stress of $\sigma = 50.0\,ksi$ and maximum displacement of $3.0\,in$ in all directions. The geometry of the frame is modeled using four key points and three segments. The cross-sectional area of the each segment is defined as design variables. Initial cross-section of members are $A = 256\,in^2$.

The GA pseudo-continuous design variables considered are in the range 50.0 to 500.0, population size 100, number of iterations 300, design variable binary string length 10.
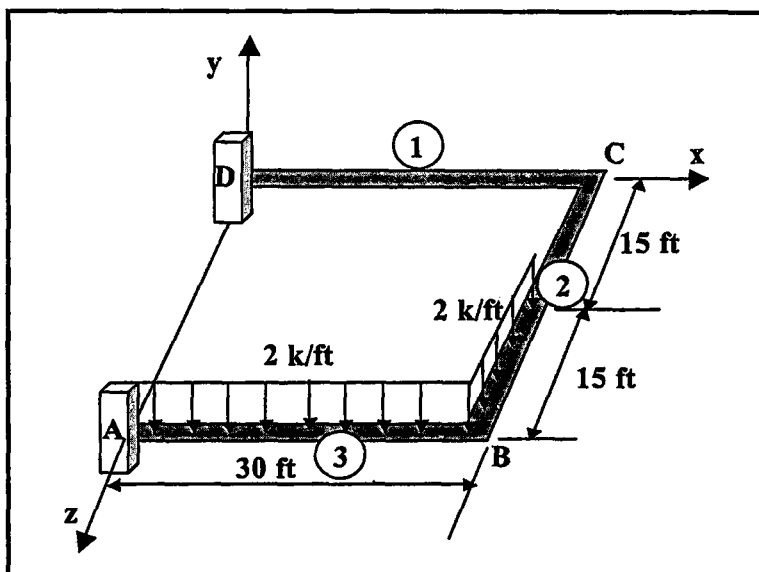
Figure 8.21 Cross section of distributed loaded frame

Discussion of results: The convergence to optimal design for three-dimensional frame was achieved after 230 iterations. The resulting frame design of the GA is listed in Table 8.18. The reduction in the weight of the frame structure is 29.3 %.

Table 8.18 Initial, optimum and constrain values of design variables of grid under distributed load

DV	Element number	Minimum	Initial	Maximum	Optimum
s_1	1	50.0	256.0	500.0	82.56
s_2	2	50.0	256.0	500.0	72.00
s_3	3	50.0	256.0	500.0	388.71
Weight (lb)			276480.0		195579.5

8.8.2 Eight bar frames

Problem definition: The frame to be optimized is shown in Figure 8.22 and has initial uniform rectangular cross sections 0.6×0.6. The frame is subjected to a concentrated point load of 100 unit applied at point B. The following material properties are assumed: Poisson's ratio $v = 0.3$, modulus of elasticity $E = 300 \times 10^6$ and material density $\rho = 100.0$.

The objective is to minimize the weight of the frame with constraints on allowable tensile and compressive stress $\sigma = 800.0$ and maximum displacement for all nodes and direction 0.1 units. All units are consistent. The design variables are the thicknesses and widths at the key points. Two cases of thickness and width variations are considered. Wherever, necessary design variable linking is used to achieve the desired thickness variation. The following cases of the thickness variation are optimized:

- *Piecewise constant:* in which eight segments and eight key points are used, with the thickness and width of the columns and beams taken as design variables. Total number of design variables is four.

- *Piecewise linear:* in which eight segments and eight key points are used, with the thickness and width at all the key points (joints) of columns and the thickness and width of all beam taken as design variables. Total number of design variables is six.

The GA pseudo-continuous design variables considered are in the range 0.2 to 1.0, population size 100, number of iterations 300, design variable binary string length 10.

Figure 8.22 Loads and dimensions of eight bar frame example

Discussion of results: The convergence to optimal design for three-dimensional frame was achieved after 168 and 236 iterations for piecewise constant and piecewise linear design variable cases respectively. The final thickness and width distributions obtained for various cases considered are presented in Table 8.19 and 8.20. The initial weight of the frame is 1152.0. The percentage reductions in weight obtained for piecewise constant and piecewise linear are 31.42 % and 27.68 % respectively.

Table 8.19 Initial, optimum and constrain values of design variables

DV	Minimum	Initial	Maximum	Optimum
Thickness of bottom of 1,2,4,5 columns	0.2	0.6	1.0	0.741935
Width of bottom of 1,2,4,5 columns	0.2	0.6	1.0	0.741935
Thickness of top of 1,2,4,5 columns	0.2	0.6	1.0	0.922581
Width of top of 1,2,4,5 columns	0.2	0.6	1.0	0.354839
Thickness of 5,6,7,8 beams	0.2	0.6	1.0	0.483871
Width of 5,6,7,8 beams	0.2	0.6	1.0	0.225806
Weight		1152.00		790.010

Table 8.20 Initial, optimum and constrain values of design variables

DV	Minimum	Initial	Maximum	Optimum
Thickness of 1,2,4,5 columns	0.2	0.6	1.0	0.870968
Width of 1,2,4,5 columns	0.2	0.6	1.0	0.948387
Thickness of 5,6,7,8 beams	0.2	0.6	1.0	0.200000
Width of 5,6,7,8 beams	0.2	0.6	1.0	0.329032
Weight		1152.00		833.1321

8.8.3 Thirty two bar frame

Problem definition: Last, the multistory building frame is considered for weight minimization. The geometry and loading of multistory building frame is shown in Figure 8.23. The frame is made of steel material with 0.5×0.5 m², Poisson's ratio $v = 0.3$, modulus of elasticity $E = 200 \times 10^9$ Pa and magnitude of applied loads are equal to 250 N.

The objective is to minimize the weight of the frame with constraints on allowable tensile $\sigma_t = 25.0 \times 10^3$ Pa, allowable compressive stress $\sigma_c = -35.0 \times 10^3$ Pa and maximum displacement for all nodes and direction 0.009 m. The design variables are the thicknesses and widths of beams and columns. Wherever, necessary design variable linking is used to achieve the piecewise constant thickness variation. In

which 32 segments and 22 key points are used, with the thickness and width of the columns and beams of each floor taken as design variables. Total number of design variables is eight.
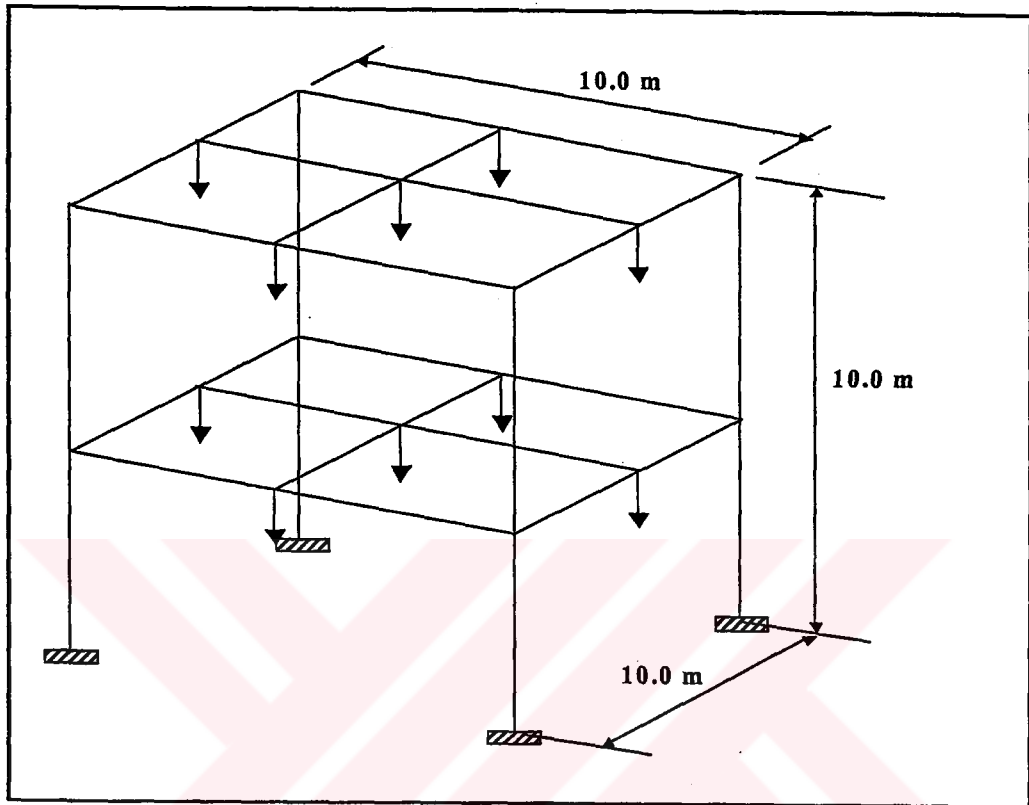
Figure 8.23 Loads and dimensions of 32-bar frame example

Discussion of results: The resulting frame design of the GA is listed in Table 8.21. 21.4 % improvement is achieved in the objective function. After weight minimization a more uniform stress distribution is usually obtained throughout the frame and this can be important in situations where the stress initially varies considerably in the members

Table 8.21 Initial, optimum and constrain values of design variables

DV	Minimum	Initial	Maximum	Optimum
Thickness of bottom floor columns	0.1	0.5	1.0	0.700
Thickness of top floor columns	0.1	0.5	1.0	0.8714
Thickness of bottom floor beams	0.1	0.5	1.0	0.5714
Thickness of top floor beams	0.1	0.5	1.0	0.7571
Width of bottom floor columns	0.1	0.5	1.0	0.2571
Width of top floor columns	0.1	0.5	1.0	0.1857
Width of bottom floor beams	0.1	0.5	1.0	0.4142
Width of top floor beams	0.1	0.5	1.0	0.2285
Weight		314400.00		246996.489

CHAPTER 9

FREE VIBRATION OPTIMIZATION OF
TWO AND THREE DIMENSIONAL STRUCTURES

9.1 Introduction

In the design of major structures, such as bridges, building and machine components etc., it is necessary to study the oscillatory behavior to guard against failure due to resonance. Indeed, the dynamic performance of many truss and frame structure can be improved by modification of their structural shape or form.

The problem of finding such optimal forms can be solved using GA procedures in which the shape and/or thicknesses of the components of the structure are varied to achieve a specific objective satisfying certain design and manufacturing or construction constraints. In this chapter, the aim of these optimizations are; (a) to maximize the structural fundamental frequency while maintaining a constant total structure weight or (b) to minimize the structure weight while keeping the structural fundamental frequency over a limited value.

This chapter was included to illustrate the application of the GA in free vibration optimization of truss and frame structures. All analysis used were updated to a Fortran 90 format, some solvers replaced, and F90 data structures added to enable rapid passing of information between the GA and respective simulation code. Before any optimization was carried out, each analysis program was tested against known benchmark solutions, to confirm integrity of the analyses.

For each individual of the population, the F90 interface directly inputs the relevant GA design variables information (such as member thickness, widths, cross-sectional areas

181

or coordinates of key points) into the analysis, and afterwards extracts the member weights and structure's fundamental frequency.

9.2 Problem Definition

The optimization based on GA has been defined earlier in Chapter 7. Before any optimization process can be started the objective function, the constraint functions and bounds on the design variables must be specified.

9.2.1 Selection of objective (fitness) function

The objective function is a mathematical function expressed in terms of the design vector s, which quantifies (in a mathematical sense) the worth of any design. It is a criteria which has to be chosen for comparing the different alternative acceptable designs and for selecting the best one. The choice of the objective function is governed by the nature of the problem.

Problem of structural optimization are characterized by various objective function and constraints which are nonlinear function of the design variables. The functions can be implicit, discontinuous and non-convex. Detailed formulations of practical optimization problems (i.e objective and restrictions) vary with every application. Typical objective functions and constraints used in SSO are listed in Table 9.1.

Weight minimization: Summing for the number of elements n_e, the individual masses (the unmodified objective functions) for individual i and population n_z are calculated from:

$$f(s)_i = \sum_{j=1}^{n_e} \rho \cdot A \cdot l \qquad \text{for:} \quad j = 1,...n_e \quad \text{and} \quad i = 1,...n_z \qquad (9.1)$$

Table 9.1 Design variables, objective functions and constraints used for structural shape optimization of discrete structures

Design variables **s**

- Coordinates of key points
- Thickness and/or width at key points
- Cross-sectional area of member

Objective functions $f(\mathbf{s})$

- Weight
- Volume
- Fundamental frequency

Constraint functions g(s)

- Frequency constraint
- Weight constraint

Fundamental frequency maximization: In the case of the frequency maximization, objective function $F(\mathbf{s})$ for the structure is computed as the

$$f(\mathbf{x})_i = \omega_p \qquad (9.2)$$

ω is the associated frequency, and well known eigenvalue equation for free vibration is,

$$(\mathbf{K} - \omega_p^2 \mathbf{M})\hat{\mathbf{d}}_p = 0 \qquad (9.3)$$

where **M** and **K** are the assembled mass and stiffness matrices. $\hat{\mathbf{d}}_p$ is the mode shape (eigen-) vector. The detail treatment of the volume and fundamental frequency computation is presented for truss, arch and frame structures in Chapter 4 and 6 respectively.

In order to complete the formulation of the problem, some restrictions must be imposed on the values of the design variables for the mathematical model to be meaningful. The constraints in an optimization problem can be geometric constraints setting a fixed

volume for the structure throughout the entire optimization process. Alternatively, there are behavior constraints imposing limiting values on the frequency.

Fundamental frequency constraint: the constraint from the fundamental frequency for each individual are calculated by:

$$c_i = \frac{\omega_i}{\omega_{initial}} \qquad (9.4)$$

where, ω_i is the individual fundamental frequency to be compared against the initial fundamental frequency $\omega_{initial}$.

The constraint violation $viol_i$ is obtained from the fundamental frequency constraints c_i:

$$viol_i = c_i - 1.0 \qquad (9.5)$$

where, and individual fundamental frequency ω_i must be larger than the initial fundamental frequency values of $\omega_{initial}$, without incurring constraint violation $viol_i$.

Weight constraint: Structural weight is kept constant by using the target weight W_T, which is initial weight of structure.

$$c_i = \frac{W_i}{W_T} \qquad \text{for: } W_i > W_T \qquad (9.6)$$

$$c_i = \frac{W_T}{W_i} \qquad \text{for: } W_i \leq W_T \qquad (9.7)$$

The constraint violation $viol_i$ is obtained from the weight constraints c_i:

$$viol_i = c_i - 1.0 \qquad (9.8)$$

where, and individual weight W_i must lie within the initial weight values of W_T, without incurring constraint violation $viol_i$. This constraint is used together with fundamental frequency maximization.

Fitness function: After computing objective function $F(s)$ from (9.1) or (9.2) and constraint violations $viol_i$ from (9.5)-(9.8), the individual modified objective function $\bar{F}(s)_i$ can be derived:

$$\bar{f}(s)_i = f(s)_i + p_c \sum (viol_i)^2 \qquad (9.9)$$

Note that the influence of *viol* on the above modified objective function is controlled by an input penalty multiple p_c. The maximum and minimum modified objective function $(\bar{f}(s)_i)_{max}$ and $(\bar{f}(s)_i)_{min}$ in the population of individuals can then be used to calculate the fitness value of each individuals designs:

$$fit_i = \cfrac{f_i}{\left(\cfrac{\sum\limits_{dv=1}^{n_{dv}} f_i}{n_z} \right)} \qquad (9.10)$$

where:

$$f_i = (\bar{f}(s)_i)_{max} + ((\bar{f}(s)_i)_{min}) - \bar{f}(s)_i \qquad (9.11)$$

In GA optimization of structures, the interface method and parsing of information to and from the GA follows the same formats as for the 2D and 3D analysis above, the only differences being the inclusion of a third dimension.

9.2.2 Design variables

The selection of design variables is very important in the optimization process. One has to decide a priori where to allow for design changes and evaluate how these changes should take place by defining the location of the design variables and move directions. Design variables which used in this chapter are also listed in Table 9.1.

For various reasons, it is usually necessary to provide upper and lower bounds on the design variables and also we may wish to enforce certain relationships between the variables to impose symmetry etc. and this is done via linking.

185

9.3 Genetic Algorithm Based Solution Items

Apart from the usual definition of the structural optimization problems which includes the structural geometry and members connectivities, loadings, boundary conditions, material properties, design variables, objective function and constraints, in a GA-based solution we must define the following items which may vary from problem to problem:

a) The bitstring length, i.e. the number of binary digits used in the coding of each design variable- this value is usually between 5 and 10.

b) If the design variables are continuous, we must specify the lower and upper bounds for each design variable assuming that all intermediate values are equally spaced between those two bounds, so that

$$r = \frac{s^u - s^l}{2^m - 1.0} \qquad (9.12)$$

where, s^u is the upper bound, s^l is the lower bound, and m is the string length.

c) If the design variables are discrete then we must supply the catalogue of values, for equally spaced discrete values we use the above expression. Note that the number of catalogue is

$$\ln cat = 2^m \qquad (9.13)$$

d) The population size (usually between 100 and 1000).

We also need to define a set of convergence criteria. The mathematical representation of one of theses convergence criteria may be given in the following formulation:

$$\frac{|f_{av} - f_{best}|}{f_{av}} \times 100 < convg \qquad (9.14)$$

where, f_{av} is the average fitness value in each generation, f_{best} is the best fitness value in each generation, and $convg$ is the convergence value specified by the user.

The other convergence criterion is the maximum allowable number of generations allowed before the optimization is terminated.

9.4 Truss Examples

9.4.1 Three bar 2D truss

Problem definition: The three bar truss of Figure 9.1 is to be optimized for maximum fundamental frequency while maintaining a constant total structural weight. Two design variables are considered by the GA. These are cross sectional area of members in which $s_1 = A^{(1)} = A^{(2)}$ and $s_2 = A^{(3)}$. Material properties for the truss are: Young's modulus $E = 2.0 \times 10^{11} \, \text{N/m}^2$ and material density $\rho = 7860.0 \, \text{kg/m}^3$. Nodes 1, 3 and 4 are the locations of the pin-jointed static supports. The initial weight of the truss is 36.551 kg which is kept constant through out optimization

The GA pseudo-continuous design variables considered are in the range 0.00005 to 0.002 m, with initial cross-sections of each bar is equal to 0.001 m², population size 100, design variable binary string length 10 and number of iterations 100.

Figure 9.1 Nodal and element numbering for three bar truss

Discussion of the results: The convergence to optimal design for three bar truss is achieved after 70 iterations. For an initial weight of 36.551 kg, the frequency before optimization is 528.529 Hz. The resulting truss design of the GA for pseudo-continuous design variables is compared with various references in Table 9.2. The increase in fundamental frequency from sizing optimization is 3.1 %.

187

Table 9.2 Comparison of optimum frequencies of three bar 2D truss

DV	Element number	Size opt converged solutions (m²)			
		Present GA	Ref. [111] GA	Ref. [112] GA	Ref. [112] DOT
s_1	1,2	0.000753	0.0007	0.00032	0.00064
s_2	3	0.001266	0.0014	0.00068	0.00139
Initial freq (Hz)		528.53	528.53	542.61	542.61
Optimum freq (Hz)		545.4783	547.6714	547.8530	547.7700

9.4.2 Nine bar 2D truss

Problem definition: In the second truss example, we consider the sizing optimization of nine bar truss. The geometry of the truss is shown in Figure 9.2. Material properties for the truss are: modulus of elasticity $E = 2.0 \times 10^{11} \text{N/m}^2$ and material density $\rho = 7860.0 \text{kg/m}^3$. Node 1 acts as a pin-jointed static support, while node 6 is free to move in the *x*-direction.

In this optimization problem, the objective is to maximize the fundamental frequency with a constraint that the total weight of the structure should remain constant. The objective weight is 55215.89 kg. Nine design variables are considered by the GA where design variables are cross-sectional area of each member.

The GA pseudo-continuous design variables considered are in the range 0.0005 to 0.5 m, with initial cross-sections of each bar is equal to 0.2 m², population size 400, design variable binary string length 10 and number of iterations 100.

Discussion of the results: The convergence to optimal design for nine bar truss is achieved after 61 iterations. The fundamental frequency increases from 30.79 Hz to 36.79 Hz. The increase in fundamental frequency from sizing optimization was 16%. The resulting truss design of the GA for pseudo-continuous design variables, is compared with various references in Table 9.3. The present optimum solution is very close to reference solutions.
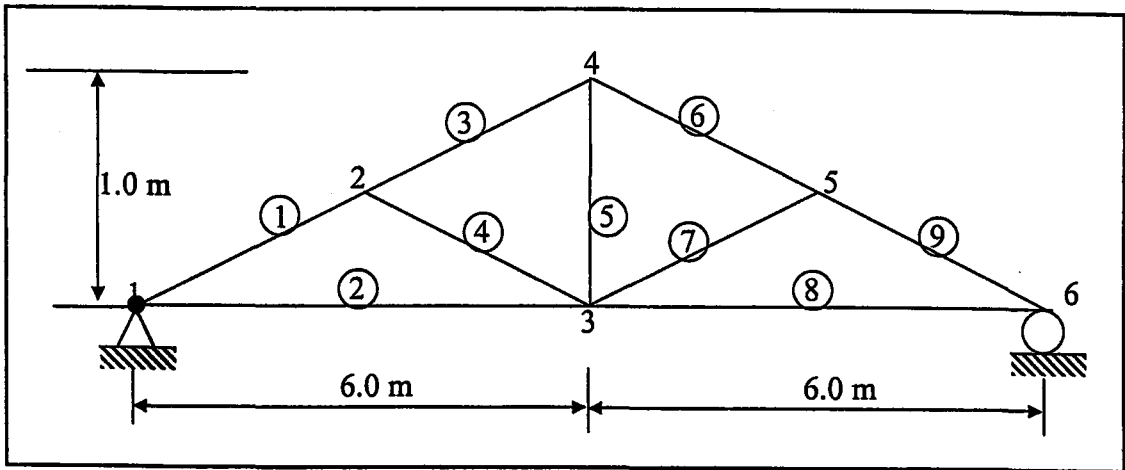
Figure 9.2 Nodal and element numbering for nine bar truss

Table 9.3 Comparison of optimum frequencies three bar 2D truss

DV	Element number	Optimum design variables (m^2)		
		Present	Ref. [111] GA	Ref. [112] DAT
s_1	1	0.3170	0.3501	0.2720
s_2	2	0.3080	0.3975	0.3250
s_3	3	0.1810	0.2139	0.1430
s_4	4	0.0440	0.0474	0.0340
s_5	5	0.0970	0.1279	0.1010
s_6	6	0.1590	0.2539	0.1520
s_7	7	0.0260	0.0503	0.0310
s_8	8	0.2660	0.3809	0.2710
s_9	9	0.2660	0.4263	0.3060
Optimum Freq (Hz)		36.69	37.15	37.38

9.4.3 Three bar 3D truss

Problem definition: This example, involves the optimization of the 3D three bar truss shown in Figure 9.3 was presented by other researchers [111,112]. The following material properties are assumed: Young's modulus $E = 6.7 \times 10^{10}\,\text{N/m}^2$ and material

density $\rho = 2700.0 \text{ kg/m}^3$. Nodes 1,2,3 are the locations of ball and socket static supports. The objective is to maximize the fundamental frequency subject to the constraint that the weight of the truss remains constant. Two design variables are considered by the GA where design variable $s_1 = A^{(1)} = A^{(3)}$ and $s_2 = A^{(2)}$. and The constrained weight is 9.9803 kg.

The GA pseudo-continuous design variables considered are in the range 0.0001 to 0.005 m, with initial cross-sections of each bar is equal to 0.001 m^2, population size 200, design variables binary string length 10, number of iterations 100.
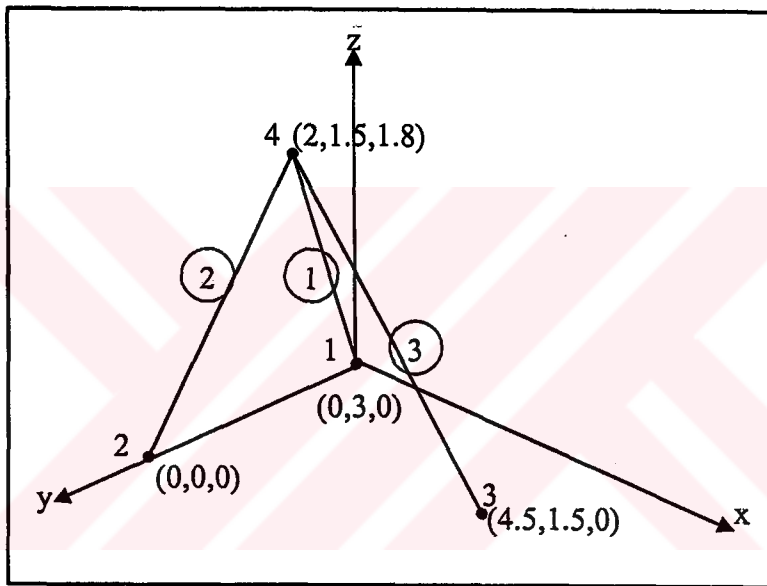
Figure 9.3 Nodal and element numbering for three bar 3D truss
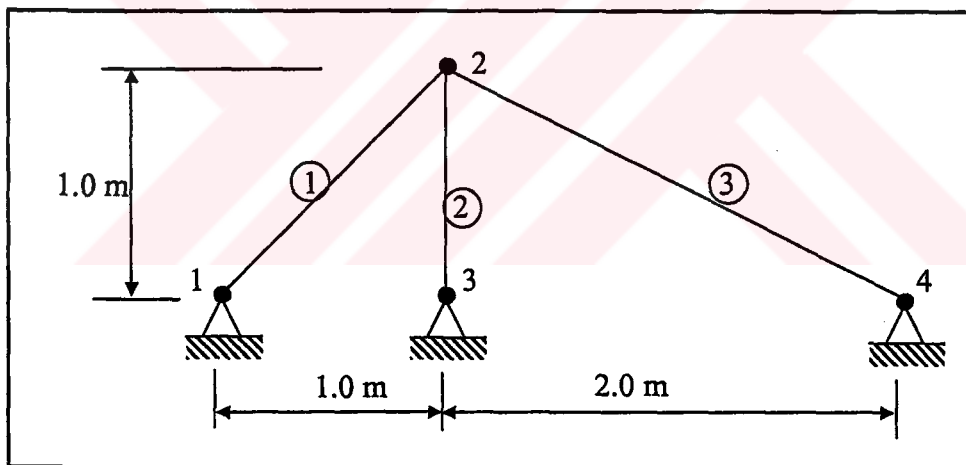
Discussion of the results: The convergence to optimal design for three bar truss was achieved after 70 iterations. For an initial weight of 9.98 kg, the frequency before optimization was 177.08 Hz. Table 9.4 illustrates the results obtained using the GA for continuous design variables. The increase in fundamental frequency from sizing optimization was 13.6 %.

Table 9.4 Comparison of optimum frequencies of three bar 3D truss

DV	Element number	Optimum design variables (m²)			
		Present GA	Ref. [111] GA	Ref. [112] GA	Ref. [112] DOT
s_1	1,3	0.000541	0.000532	0.000542	0.000526
s_2	2	0.000129	0.000332	0.000127	0.000148
Optimum Freq (Hz)		205.022	205.164	205.164	203.056

9.5 Arch Examples

9.5.1 Arches with discontinuously varying cross-section

Problem definition: This example, which involves the optimization of the discontinuously varying cross-section arch shown in Figure 9.4 was originally presented by Gutierrez et al [125] and analyzed in Chapter 6. The arches are optimized for following cases

(a) maximization of the fundamental frequency with a constraint that the total material volume of the structure should remain constant, and

(b) volume (or weight) minimization subject to the constraint that the fundamental frequency should remain constant.

Piecewise constant: The geometry of the arch is modeled using seven key point and three segments. Four design variables are considered these are thickness and width of segment 1 and 2. Design variables of segments 1 and segment 3 are linked. Use is made of design variable linking to achieve desired thickness variation and to maintain symmetry of structures. The piecewise constant (and discontinuous) cross-sectional variation and boundary condition of arch is shown in Figure 9.4 where $h_o / h_1 = 1.25$ and $\beta = 40°$.

The GA pseudo-continuous design variables considered and the minmum and maximum values of design variables are given in Table 9.5 and Table 9.6 for discontinously and continously varying arches respectively. Population size 500, design variables binary string length 10, number of iterations 100.
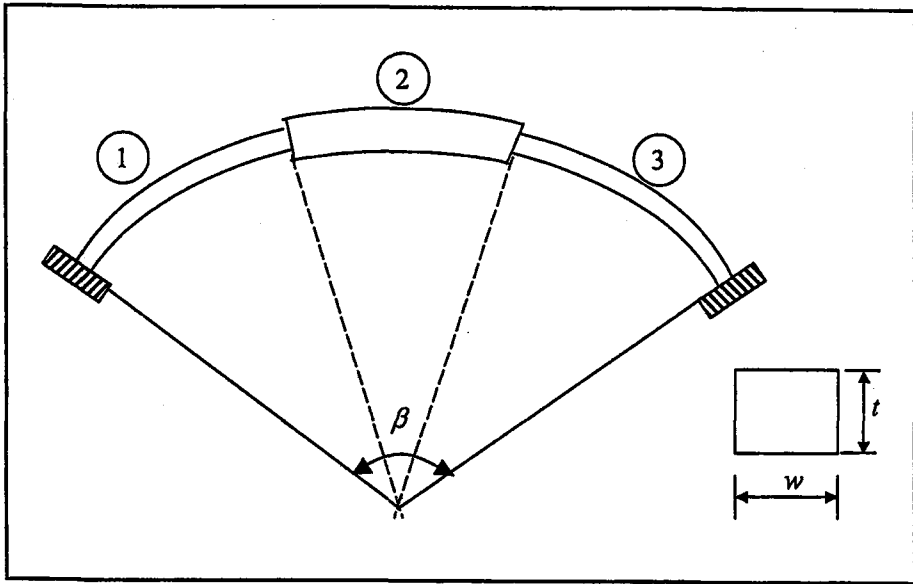
Figure 9.4 Clamped arches of discontinuously varying cross-section

Discussion of results: Table 9.5 presents the initial and optimal values of the design variables and objective functions together with bounds on the design variables for piecewise constant thickness variation. In case (a), the fundamental frequency increases from 7.90 to 9.42. --- an 18% improvement. However, in case (b) the weight reduces from 60.49 and 19.262 % improvement is obtained; initial volume of the arch is 60.49 to 29.49 --- an improvement of more than 51%. The optimum solution is obtained in 56 iterations.

Table 9.5 Initial and optimum design values of discontinuously varying arch

DV	Minimum	Initial	Maximum	Optimum design variables	
				Frequency maximization	Weight minimization
t_1	0.4	1.0	1.5	1.3903	1.07849
t_2	0.4	1.0	1.5	1.1881	0.81183
w_1	0.4	0.8	1.5	0.55483	0.41936
w_2	0.4	1.0	1.5	0.89677	0.44731
Optimum frequency				9.4217	-
Optimum weight				-	29.4936

9.5.2 Arches with continuously varying cross-section

Problem definition: The following example deals with a continuously varying cross-section arch supported by pin joints at both ends as shown in Figure 9.5. The arch was originally analyzed (but not optimized) by Gutierrez et al [125] and analysis is repeated in Chapter 6. The arches are optimized for following cases

(c) maximization of the fundamental frequency with a constraint that the total material volume of the structure should remain constant, and

(d) volume (or weight) minimization subject to the constraint that the fundamental frequency should remain constant.

The location of the design variables and boundary condition for the arch is shown in Figure 9.5 where $h_o / h_1 = 0.43$ and $\beta = 60°$. The geometry of the arch is modeled using five key points and one segment. Six design variables are considered. These are thicknesses of five key points and width of arch. The width of the arch at the key points is same.
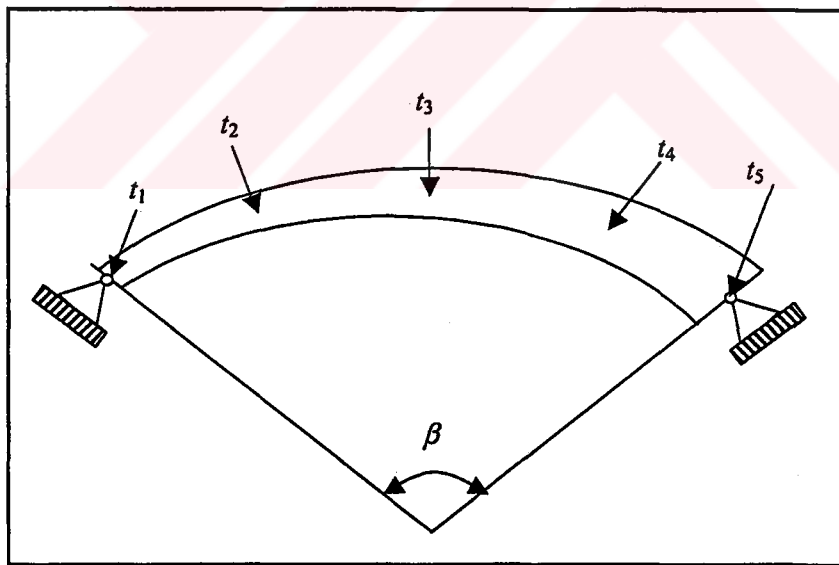
Figure 9.5 Pinned-pinned arches of continuously varying cross-section

Discussion of results: Table 9.6 shows initial and optimum values of design variables and objective functions together with bounds on the design variables for cubic thickness variation. For case (a), the problem of fundamental frequency maximization --- a 77%

increase in the fundamental frequency from 5.58 to 9.69 is obtained. In case (b) involving volume minimization, a reduction of 53% from 104.61 to 49.09 is obtained. Large numbers of thickness design variables, apart from leading to impractical geometries, can sometimes lead to negative thicknesses between key points. Therefore, care is exercised when checking the convergence to optimal structures by studying the effect of increasing the number of thickness design variables. Constraints on the bounds of the design variables are used to guard against negative or zero element thickness. As seen in Table 9.6 the optimum thicknesses of arch shows that, the symmetry varying of thickness gives better results and upper part of arch thickness is smaller than lower parts.

Table 9.6 Initial and optimum design values of continuously varying arch

DV	Minimum	Initial	Maximum	Optimum design variables	
				Frequency maximization	Weight minimization
t_1	0.1	0.6	2.0	1.2302	1.6118
t_2	0.1	0.8	2.0	1.9472	0.97106
t_3	0.1	1.0	2.0	1.4721	0.8596
t_4	0.1	1.2	2.0	1.9853	0.9209
t_5	0.1	1.4	2.0	1.5835	1.6508
w_1	0.1	1.0	2.0	0.5586	0.4436
Optimum frequency				9.6905	-
Optimum weight				-	49.0884

9.6 Three Dimensional Portal Frames

9.6.1 Single story portal frame

Problem definition: The following example deals with a single story portal frame as shown in Figure 9.6. The following material properties are assumed: the modulus of elasticity 1×10^7 psi, Poisson's ratio 0.25 and the material density 0.1/386.4 lb/in^3. The single story frame is optimized for following objective functions and constraints: case

(a) maximization of fundamental frequency with a constraint that the total material volume of the structure should remain constant, case (b) minimization of the volume of material subject to the constraint that the fundamental frequency should be greater than initial values $\omega_i = 3.61\,\text{Hz}$ and case (c) minimization of the weight of material subject to the constraint that the fundamental frequency should be greater than the predefined values of $\omega_p = 50\,\text{rad/s}$ $\omega_p = 7.9577\,\text{Hz}$.

The frame is modeled using three segments and four key points. The geometry of the frame and location of the key points and segments are shown in Figure 9.6. In cases a) and b) it is assumed that each member has a rectangle cross-sectional and the thickness and widths of columns and beam are defined as design variables. Totally, four design variables are defined in these optimization problems. In case c) as in referance solution, it is assumed that each member has a cicular cross-sectional area and the diameter of each segment is defined as design variable. Totally, three design variables are defined in this case.

The GA pseudo-continuous design variables considered and the minimum and maximum values of design variables are 0.5 to 6.0 respectively. Population size 100, design variables binary string length 10, number of iterations 400.
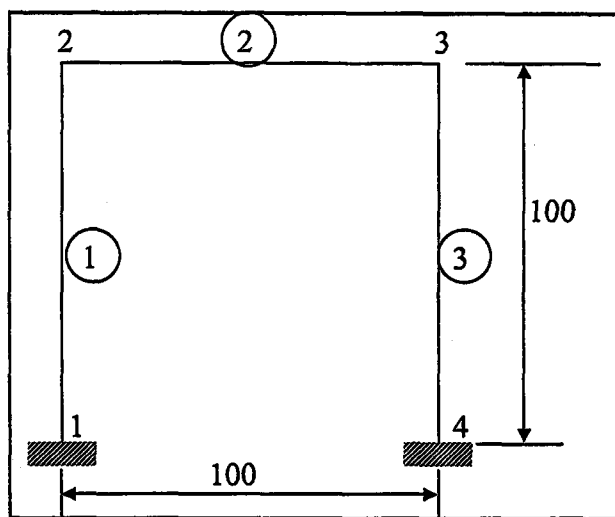
Figure 9.6 Two dimensional portal frame

Discussion of results: Table 9.7 presents the initial and optimum design variables and objective functions together with limits of the design variables. In case (a), the fundamental frequency increases from 3.61 Hz to 6.6408 Hz. A 83.95 % improvement in the fundamental frequency is obtained. In the case (b) involving weight minimization, a reduction of 67.55 % from 0.31 lb to 0.1006 lb is found for a constraint that the fundamental frequency is equal to 3.61Hz. The result indicates that the use of thickness and widths design variables seperately gives better results. It means that rectangular cross ssections are more efficient than square or circular cross sections.

In case (c) we consider an alternative design case for the frame, for which we attempt to minimize the weight of the frame for a given frequency value of 50 rad/s or 7.9577 Hz. If the initial weight is taken as 0.31 lb then the final weight achieved is 0.4666 lb. The optimum solution presented in Table 9.7 gives around 50.32 % weight increase. It is noted that, the initial design is infeasible where the initial frequency is 3.61 Hz and target frequency is 7.9577 Hz. The frequency and final weight values obtained for the portal frame is in good agreement with the optimum solution obtained by Yu and Wang [126].

Table 9.7 Optimum cross-sectional areas for 3D portal frame

DV	Case (a)	Case (b)	Case (c)	Ref.[126]
s_1	1.8655	1.0885	3.5864	3.149
s_2	2.9086	1.5435	1.0683	1.0
s_3	2.1666	1.0269	2.9942	3.1489
s_4	0.68279	0.5137	-	-
Constrain	W = 0.3104 lb	Fre = 3.6473 Hz	Fre = 7.9577 Hz	Fre = 7.9577 Hz
Opt objective function	Fre = 6.6408 Hz	W=0.1006 lb	W=0.4666 lb	W=0.4234 lb

Initial fundamental frequency is 3.61 and initial weight is 0.3104

9.6.2 Two story portal frame

Problem definition: This example, which involves the optimization of the two story portal frame is shown in Figure 9.7, was also originally presented by Yu and Wang [126]. The following material properties are assumed: the modulus of elasticity 1×10^7 psi, Poisson's ratio 0.25 and the material density $0.1/386.4$ lb/in^3. The frame structure is completely fixed at nodes 1 and 4. Three different types of objective functions and constraints are considered in the GA optimization: case (a) maximization of fundamental frequency with a constraint that the total material weight of the structure should remain constant, case (b) minimization of the weight of material subject to the constraint that the fundamental frequency should be greater than initial values $\omega_i = 1.0885\,\text{Hz}$ and case (c) minimization of the weight of material subject to the constraint that the fundamental frequency should be greater than the predefined values of $\omega_p = 20\,\text{rad/s}$ $\omega_p = 3.183\,\text{Hz}$.
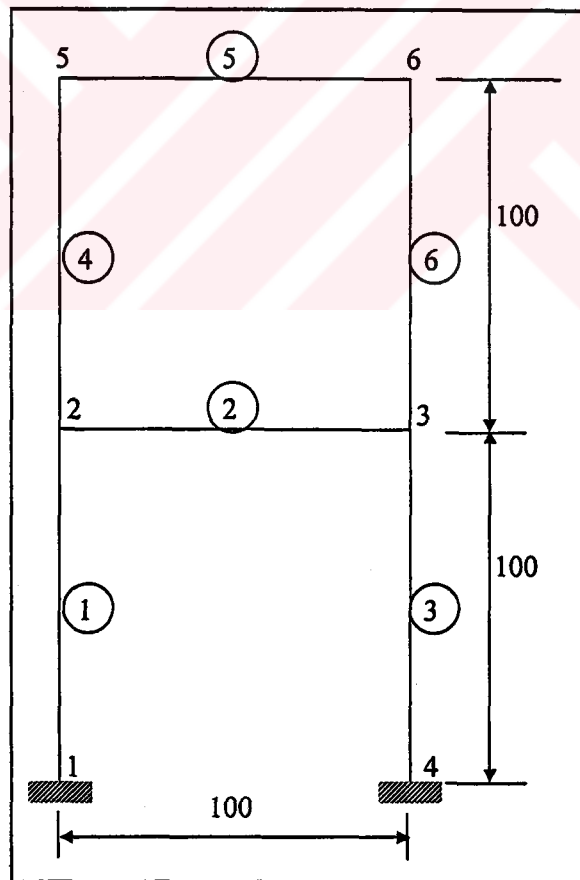
Figure 9.7 Two story portal frame

The frame is modeled using six segments and six key points. The geometry of the frame and location of the key points and segments are shown in Figure 9.7. In cases a) and b), it is assumed that each member has a rectangular cross-sectional area. The thickness and width of columns and beams are defined as design variables. Totally, four design variables are defined in this optimization problems. In case c), It is assumed that each member has a circular cross-sectional area as in reference [126] and the diameter of each segment is defined as design variable. Totally, six design variables are defined in this case.

The GA pseudo-continuous design variables considered and the minimum and maximum values of design variables are 0.5 to 6.0 respectively. Population size 100, design variables binary string length 10, number of iterations 400.

Discussion of results: The results for cases (a), (b) and (c) are listed in Table 9.8. The initial, bounds and optimum values of the design variables are also shown in Table 9.8. Analyses are done by using 3-noded 2 elements in each segment. Analysis result are tested against reference solution and given in Chapter 6

In case (a), the fundamental frequency of the two story portal frame for the initial shape is 1.0885 Hz. For optimum shape, the fundamental frequency increases to 2.2709 Hz which corresponding to 108.63 % improvement in the objective function.

In the case (b) involving weight minimization subject to a constraint that the fundamental frequency is equal to initial value of 1.0885 Hz, a reduction of 72.26 % from 0.6209 lb to 0.1722 lb is found. The result indicates that the use of thickness and widths design variables seperately gives better results. It means that rectangular cross ssections are more efficient than square or circular cross sections.

In case (c) we consider an alternative design case for the frame, for which we attempt to minimize the weight of the frame for a given frequency value of 20 rad/s or 3.183 Hz. If the initial weight is taken as 0.6209 lb then the final weight achieved is 0.8436 lb. The optimum solution presented in Table 9.8 gives around 35 % weight increase. It is noted

that, the initial design is infeasible where the initial frequency is 1.0885 Hz and target frequency is 3.183 Hz. The frequency and final weight values obtained for the portal frame is in good agreement with the optimum solution obtained by Yu and Wang [126].

Table 9.8 Optimum cross-sectional areas for two-level portal frame

DV	Case (a)	Case (b)	Case (c)	Ref. [126]
s_1	1.4731	0.7151	3.8592	3.7062
s_2	3.5268	1.7854	1.1808	1.0
s_3	2.1505	1.5435	3.8592	3.7062
s_4	0.8656	0.5049	2.1144	1.9528
s_5	-	-	1.1808	1.0
s_6	-	-	2.1144	1.9528
Constrains	W = 0.6209 lb	Fre=1.0896 Hz	Fre = 3.183 Hz	Fre = 3.183 Hz
Opt objective function	Fre = 2.2709Hz	W=0.1722 lb	W= 0.8436 lb	W=0.75406 lb

Initial fundamental frequency is 1.0885 and initial weight is 0.6209

9.6.3 Three story space frame

Problem definition: This example, which involves the optimization of the Three-story space frame structure is shown in Figure 9.8, was also originally presented by Yu and Wang [126]. and analyzed in Chapter 6. The frame structure is completely fixed at nodes 1, 2, 3 and 4. The following material properties are assumed: the modulus of elasticity 1×10^7 psi, Poisson's ratio 0.25 and the material density 0.1/386.4 lb/in^3. Three different types of objective functions and constraints are considered in the GA optimization: case (a) maximization of fundamental frequency with a constraint that the total material weight of the structure should remain constant, case (b) minimization of the weight of material subject to the constraint that the fundamental frequency should be greater than initial values (ω_i = 1.8860 Hz) and case (c) minimization of the weight of material subject to the constraint that the fundamental frequency should be greater than the predefined values of ω_p = 20 rad/s ω_p = 3.183 Hz.

The space frame is modeled using 24 segments and 16 key points. The geometry of the frame and location of the key points and segments are shown in Figure 9.8. In cases a) and b), it is assumed that each member has a rectangular cross-sectional area. The thickness and width of columns and beams are defined as design variables. Totally, four design variables are defined in these optimization problems. In case c), it is assumed that each member has a circular cross-sectional area as in reference [126] and the diameter of segments are defined as design variable. The design variables s_1, s_2, s_3, s_4, s_5 and s_6 are the cross sectional areas of members 1-4, 5-8, 9-12, 13-16, 17-20 and 21-24 respectively. Totally, six design variables are defined in this case.
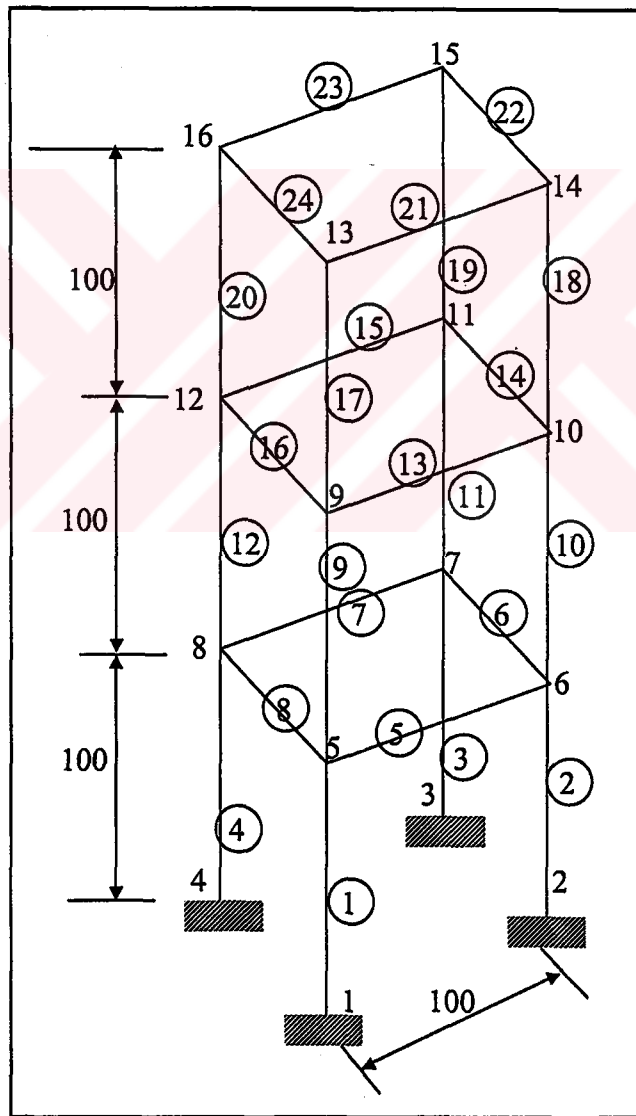
Figure 9.8 Three-story space structure

The GA pseudo-continuous design variables considered and the minimum and maximum values of design variables are 0.5 to 6.0 respectively. Population size 100, design variables binary string length 10, number of iterations 400.

Discussion of results: The results obtained using the proposed method are given in Table 9.9 for cases (a), (b) and (c). Analyses are done by using 3-noded 2 elements in each segment. Analysis result are tested against reference solution and given in Chapter 6.

Table 9.9 Optimum cross-sectional areas for three story space structure

DV	Case (a)	Case (b)	Case (c)	Ref. [126]
s_1	0.58627	4.5764	1.9411	4.2622
s_2	5.3960	0.95294	0.62745	4.0789
s_3	3.2823	0.65098	2.1078	3.1194
s_4	1.4921	1.2549	1.5000	2.8519
s_5	-	-	0.72549	1.9738
s_6	-	-	0.51960	1.0
Constrains	W = 2.4819	Fre = 1.8860	Fre = 3.183	Fre = 3.183
Optimum objective functions	Fre = 3.2190 Hz	W = 1.6075 lb	W= 3.7877lb	W = 4.683 lb

Initial fundamental frequency is 1.8860 and initial weight is 2.4819

In case (a), the fundamental frequency is maximized under weight constraint, which maintaining the first weight of structure is constant with its initial value and equal to 2.4819. The fundamental frequency of the space frame increases from 1.8860 Hz to 3.2190 Hz. A 70.68 % improvement in fundamental frequency is obtained.

In the case (b) involving weight minimization subject to a constraint that the fundamental frequency is equal to initial value of 1.8860 Hz, a reduction of 57.26 % from 2.4819 lb to 1.6075 lb is found in the material weight of the space frame.

In case (c) we consider an alternative design case for the frame, for which we attempt to minimize the weight of the frame for a given frequency value of 20 rad/s or 3.183 Hz. If the initial weight is taken as 2.4865 lb then the final weight achieved is 3.4806 lb. The optimum solution presented in Table 9.9 gives around 39.0 % weight increase. It is noted that, the initial design is infeasible where the initial frequency is 1.8860 Hz and target frequency is 3.183 Hz. The frequency and final weight values obtained for the portal frame is in good agreement with the optimum solution obtained by Yu and Wang [126].

CHAPTER 10

TRANSIENT DYNAMIC ANALYSIS

10.1 Introduction

Many sources of external load that must be considered in the design of structures, the most important by far in term of its potential for disastrous consequences is the dynamic load. It is evident that the design of economic and attractive structures, which can successfully withstand the forces induced by a severe dynamic load, is a challenge demanding the best in structural engineering, art and science. During analysis and design process, it is convenient to distinguish between the static and dynamic components of the applied loading to evaluate the response to each type of loading separately and then to superpose the two response components to obtain their total effect.

Aim of the dynamic analysis to determine the dynamic behavior of a structure, where the inertia or/and damping effects play an important role. Types of dynamic analysis classified into [51,133];
  a) Transient Dynamic Analysis
  b) Modal Analysis
  c) Harmonic Analysis
  d) Spectrum Analysis

Transient Dynamic Analysis is a technique to determine the response of a structure to arbitrary time-varying loads such as an explosion. This is the most general form of dynamic analysis. Loading may be any arbitrary function of time. Equation of

motion is directly integrated step by step over time. At each time point, a set of simultaneous "static" equilibrium equations is solved.

The equation of the dynamic system represent expressions Newton's second law of motion, which, states that the rate of change of momentum of any mass particle m is equal to the force acting on it. The relationship can be expressed mathematically by the differential equation

$$f(t) = \frac{d}{dt}\left(m\frac{du}{dt}\right) \tag{10.1}$$

where $f(t)$ is the applied force vector and $u(t)$ is the position vector of particle mass m. For most problems in structural dynamics it may be assumed that mass does not vary with time, in which case (10.1) may be written

$$f(t) = m\frac{d^2u}{dt^2} \equiv m\ddot{d}(t) \tag{10.2}$$

where the dots represent differentiation with respect to time. Eq (10.2), indicating that force is equal to the product of mass and acceleration, may also be written in the form

$$f(t) - m\ddot{d}(t) = 0 \tag{10.3}$$

in which case, the second term $m\ddot{d}(t)$ is called the inertial force resisting the acceleration of the mass. The concept that a mass develops an inertial force proportional to its acceleration and opposing it is known as D'Alembert's principle. It is a very convenient device in problems of structural dynamics because it permits the equations of motion to be expressed as equations of dynamic equilibrium [57].

In dynamic analysis, force equilibrium of a multi degrees of freedom lumped mass system as a function of time can be expressed by following relationship;

$$\mathbf{F}(t)_I + \mathbf{F}(t)_D + \mathbf{F}(t)_S = \mathbf{F}(t) \tag{10.4}$$

in which the force vectors at time t are; $\mathbf{F}(t)_I$ is a vector of inertia force acting on the node masses, $\mathbf{F}(t)_D$ is a vector of viscous damping, or energy forces, $\mathbf{F}(t)_S$ is a vector of internal forces carried by the structure and $\mathbf{F}(t)$ is a vector of externally applied loads.

Eq (10.4) is based on physical laws and is valid for both linear and nonlinear systems if equilibrium is formulated with respect to the deformed geometry of the structure.

For many structural systems, the approximation of linear structural behavior is made in order to convert the physical equilibrium statement, Eq (10.4), to the following set of second-order, linear, differential equations:

$$\mathbf{M}\ddot{u}(t)_a + \mathbf{C}\dot{u}(t)_a + \mathbf{K}u(t)_a = \mathbf{F}(t) \qquad (10.5)$$

in which $\mathbf{M}$ is the mass matrix (lumped or consistent), and $\mathbf{K}$ is the static stiffness matrix and the derivation of these matrices are same with in static and dynamic analysis and given in previous chapters. $\mathbf{C}$ is viscous damping matrix for the system of structural elements. The time-dependent vectors $u(t)_a$, $\dot{u}(t)_a$ and $\ddot{u}(t)_a$ are the absolute node displacements, velocities and accelerations respectively.

10.2 Types of Loads

The response of a structure to dynamic loads may be categorized as either deterministic or nondeterministic [57,133]. If the magnitude, point of application and time variation of the loading are completely known, the load is said to be prescribed, and the analysis of the structural response to this prescribed loading is defined as deterministic analysis. However, if the time variation and other characteristics of the loading are not completely known, but can be defined only in a statistical sense, the loading is referred to as random, and the corresponding analysis of the structural response is termed nondeterministic.

It is convenient to classify prescribed dynamic loads as either periodic or nonperiodic. Periodic loadings repeat themselves at equal time intervals. A single time interval is called the period T_0. The simplest form of periodic loading can be represented by a sine function as shown in Figure 10.1. This type of periodic loading is referred to as simple harmonic. Another form of periodic load is termed periodic, nonharmonic. Summing a sufficient number of harmonic terms in a Fourier series may accurately represent most periodic loads. Any loading that cannot be characterized as periodic is nonperiodic. Nonperiodic loads range from short duration

impulsive types, such as a wind gust or a blast pressure, to fairly long duration loads, such as an earthquake ground motion [57].
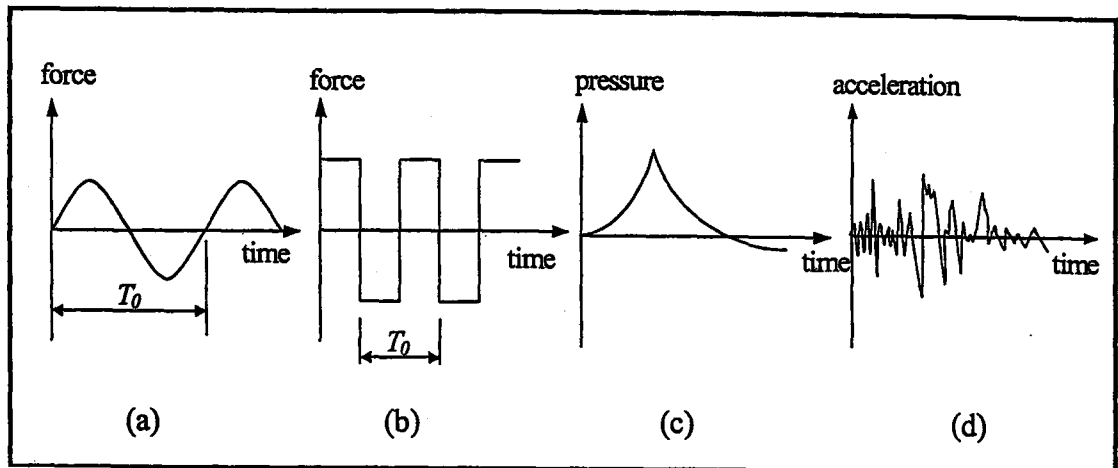
Figure 10.1 Types of dynamic loadings (a) simple harmonic; (b) periodic, nonharmonic; (c) nonperiodic, short duration; (d) nonperiodic, long duration [57]

10.3 Damping

In structural engineering viscous, velocity-dependent damping is very difficult to visualize for most real structural systems. Only a small number of structures have a finite number of damping elements where real viscous dynamic properties can be measured. In most cases modal damping ratios are used in the computer model to approximate unknown nonlinear energy dissipation within the structure. Damping can be classified as;

a) *Viscous damping* occurs when a body moves through a fluid.

b) *Hysteresis (or solid) damping* inherently present in a material. Not well understood and therefore difficult to quantify.

c) *Coulomb (or dry-friction) damping* occurs when a body slides on a dry surface. Damping force is proportional to the force normal to the surface. The proportionality constant μ is called the coefficient of friction.

10.3.1 Construction of damping matrix

It is impractical to determine the coefficients of the damping matrix directly from the structural dimensions, structural member sizes, and the damping properties of the structural materials used. Even if these properties were known, the resulting damping matrix would not account for a significant part of energy dissipated in friction at steel connections, opening and closing of micro cracks in concrete, stressing nonstructural elements — partition walls, mechanical equipment, etc.— friction between the structure it self and nonstructural elements and other similar mechanisms, some of which are even hard to identify.

Thus the damping matrix for a structure should be determined from its modal damping ratios, which account for all energy dissipating mechanisms. The modal damping ratios should be estimated from available data on similar structures shaken strongly during past earthquakes but not deformed into the inelastic range; lacking such data the values of Table 10.1 are recommended [41].

Another form of damping, which is often used in the mathematical model for the simulation of the dynamic response of a structure, is proportional to the stiffness and mass of the structure. This is referred to as Rayleigh damping. Both modal and Rayleigh damping are used in order to avoid the need to form a damping matrix based on the physical properties of the real structure.

Clearly the simplest way to formulate a proportional damping matrix is to make it proportional to either the mass or the stiffness matrix because undamped mode shapes are orthogonal with respect to each of these. Thus the damping matrix might be given by

$$\mathbf{C} = a_0\mathbf{M} \qquad or \qquad \mathbf{C} = a_1\mathbf{K} \tag{10.6}$$

in which the proportionality constants a_0 and a_1 have units of $1/\sec$ and $\sec$, respectively. These are called mass proportional and stiffness proportional damping. The stiffness proportional damping appeals to intuition because it can be interpreted to the energy dissipation arising from story deformation. In contrast, the mass

proportional damping is difficult to justify physically because the air damping it can be interpreted to model is negligibly small for most structures. Neither of the two damping models is appropriate for practical application [41,57].

Table 10.1 Recommended damping values [41]

Stress level	Type and condition of structure	Damping ratio (%)
Working stress, no more than about ½ yield point	• Welded steel, prestressed concrete, well-reinforced concrete (only slight cracking)	2-3
	• Reinforced concrete with considerable cracking	3-5
	• Bolted and/or riveted steel, wood structures with nailed or bolted joints	5-7
At or just below yield point	• Welded steel, prestressed concrete (without complete loss in prestress)	5-7
	• Prestressed concrete with no prestress left	7-10
	• Reinforced concrete	7-10
	• Bolted and/or riveted steel, wood structures bolted joints	10-15
	• Wood structures with nailed	15-20

Mass proportional damping: We now relate the modal damping ratios for a system with mass proportional damping to the coefficient a_0. The generalized damping for nth mode is,

$$\mathbf{C_n} = a_0 \mathbf{M_n} \tag{10.7}$$

and the modal damping ratio is,

$$\xi_n = \frac{a_0}{2} \frac{1}{\omega_n} \tag{10.8}$$

the damping ratio is inversely proportional to the natural frequency (See Figure 10.2). The coefficient a_0 can be selected to obtain a specified value of damping ratio in any one node, say ξ_i for the ith mode, (10.8) the gives,

$$a_0 = 2\xi_i \omega_i \tag{10.9}$$

208

with a_0 determined, the damping matrix C_n is known from (10.6), and the damping ratio in any other mode, say the nth mode, is given by (10.8).

Stiffness proportional damping: Similarly, the modal damping ratios for a system with stiffness proportional damping can be related to the coefficient a_1. In this case

$$\mathbf{C_n} = a_1 \mathbf{K_n} \quad \text{and} \quad \xi_n = \frac{a_1}{2} \omega_n \qquad (10.10)$$

The damping ratio increases linearly with the natural frequency (See Figure 10.2). The coefficient a_1 can be selected to obtain a specified value damping ratio in any mode one mode, say ξ_i for the jth mode, (10.10) the gives,

$$a_1 = \frac{2\xi_i}{\omega_j} \qquad (10.11)$$

with a_1 determined, the damping matrix C is known from (10.6), and the damping ratio in any other mode, say the nth mode, is given by (10.10). Neither of the damping matrices defined by (10.6) is appropriate for practical analysis of multi degrees of freedom systems. The variations of modal damping ratios with natural frequencies they represent Figure 10.2 are not consistent with experimental data that indicate roughly the same damping ratios for several vibration modes of a structure.
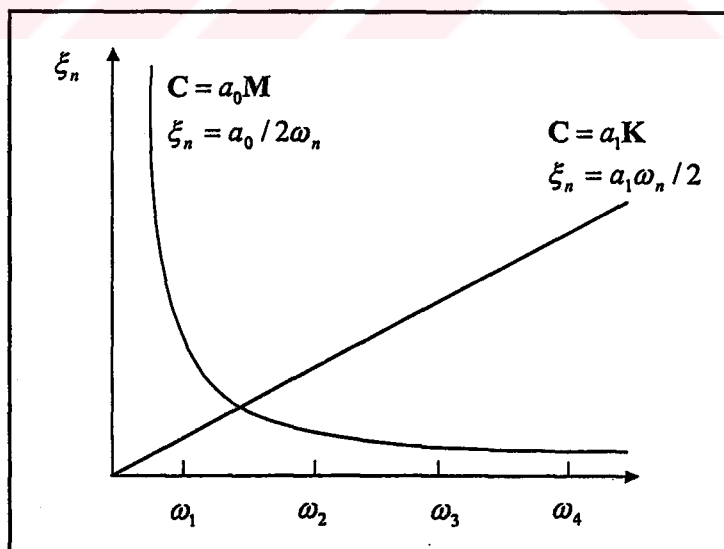
Figure 10.2 Variation of modal damping ratios with natural frequency mass proportional and stiffness proportional damping

Rayleigh damping: As a first step toward constructing a classical damping matrix consistent with experimental data, we consider Rayleigh damping:

$$\mathbf{C} = a_0\mathbf{M} + a_1\mathbf{K} \qquad (10.12)$$

the damping ratio for nth mode of such a system is

$$\xi_n = \frac{a_0}{2}\frac{1}{\omega_n} + \frac{a_1}{2}\omega_n \qquad (10.13)$$

these two algebraic equations can be solved to determine the coefficients a_0 and a_1 can be determined from specified damping ratios ξ_i and ξ_j for the ith and jth modes, respectively. Expressing (10.13) for these two modes in matrix form leads to

$$\frac{1}{2}\begin{bmatrix} 1/\omega_i & \omega_i \\ 1/\omega_j & \omega_j \end{bmatrix}\begin{Bmatrix} a_0 \\ a_1 \end{Bmatrix} = \begin{Bmatrix} \xi_i \\ \xi_j \end{Bmatrix} \qquad (10.14)$$

these two algebraic equations can be solve to determine the coefficients a_0 and a_1. If both modes are assumed to have same damping ratio ξ, which is reasonable based on experimental data, then

$$a_0 = \xi\frac{2\omega_i\omega_j}{\omega_i + \omega_j} \qquad a_1 = \xi\frac{2}{\omega_i + \omega_j} \qquad (10.15)$$

the damping matrix is then known from (10.12) and the damping ratio for any other mode, given by (10.13), varies with natural frequency as shown in Figure 10.3 [41].
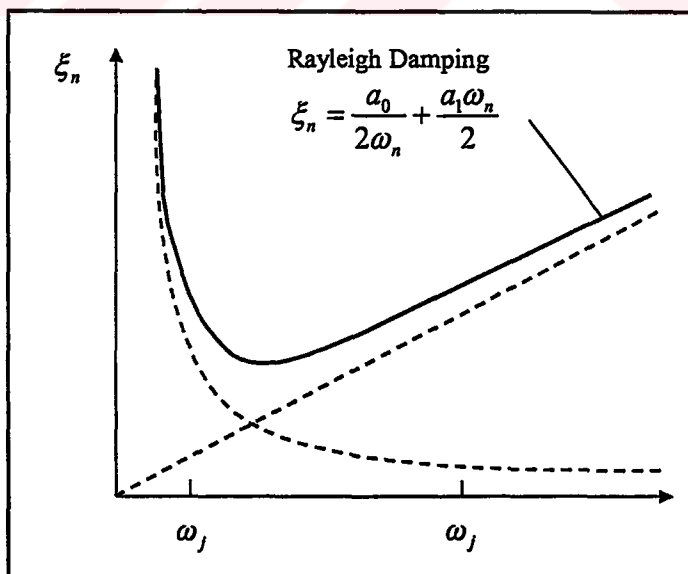
Figure 10.3 Variation of modal damping ratios with natural frequency

10.4 Method of Linear Analysis

Detail treatment about evaluation of stiffness and mass matrices mentioned before in Chapter 4 and Chapter 5, respectively. Types of loads and construction of damping matrix is mentioned above. Already, equation of motion is presented at (10.5) is constructed. Classically; there are many different mathematical models to solve dynamic equilibrium equations. These methods are;

- Mode superposition
- Direct Integration

10.4.1 Mode superposition method

The mode superposition method was employed to obtain the dynamic response of the linear multi degrees of freedom systems by transforming equations of motion to principal (normal) coordinates and solving the resulting set of uncoupled equations of motion. For simple excitation functions, the uncoupled model equations could be solved in closed form [14]. However, for more complex or arbitrary excitations it was necessary to implement one of the numerical methods to evaluate the response. The mode superposition method is not valid for multi degrees of freedom systems with nonlinearities or with non-classical damping (i.e., damping that is not orthogonal or that is coupled). Such systems require direct integration of set of coupled differential equations to evaluate the dynamic response. If the system under consideration exhibits any nonlinearities or is characterized by non-classical damping, then a mode superposition analysis is precluded. Mode superposition analysis is most effective for large systems when the dynamic response can be accurately evaluated by consideration vibration. This is because the majority of the computational effort expended for a mode superposition analysis is associated with the eigenproblem solution. The mode superposition analysis is ideally suited for situations where the dynamic disturbance is confined to the lowest modes of vibration system, and the duration of the disturbance is relatively long [40].

The mode superposition approach [3,133] is commonly used for the dynamic response analysis of structural systems and especially for the response spectrum

analysis of linearly behaving structures subjected to earthquake induced ground motions. To obtain dynamic characteristics such as mode shapes, natural frequencies and participation factors required in the mode superposition approach, the eigenvalue analysis of the structure is performed. In a modal analysis, it is a common practice to use only a first few modes in the calculation of the structural response because the contribution of the high modes to the response is usually small. Quite often, therefore, one needs to calculate only a first few modes by eigenvalue analysis. To obtain a first few modes, it is not necessary to solve the full eigenvalue problem. Therefore several techniques have been proposed to reduce the size of the eigenvalue problem. Some types of schemes used to reduce the size of the problem are calling condensation techniques [41].

10.4.2 Direct integration methods

A direct integration analysis should be conducted in situations when a large number of vibration modes must be included in response calculations. This is generally the scenario for structures subjected to high-intensity, short duration impulse type loading, such as shock or blast load. For non-classically damped systems or systems exhibiting any nonlinear characteristics a direct integration analysis is required [3,57,41].

Direct numerical integration of the dynamic equilibrium equations involves after the solution is defined at time zero, the attempt to satisfy dynamic equilibrium at discrete points in time. Most methods use equal time intervals Δt, $2\Delta t$, $3\Delta t$,..........$n\Delta t$. Numerical techniques can fundamentally be classified as either explicit or implicit integration methods;

a.) Explicit Methods
   - Central Difference Method

b.) Implicit Methods
   - Newmark Family Methods
   - Houbolt Method
   - Wilson θ Method

- Hilber, Hughes and Taylor α Method

In explicit (or open, or predictor) methods, such as the central difference method, dynamic equilibrium is considered at time t to evaluate the solution at time $t+\Delta t$. Therefore, all explicit methods conditionally stable with respect to the size of the time step. In implicit (or closed, or corrector) methods, such as the Wilson-θ and Newmark methods, the solution $u_{t+\Delta t}$ is found expressions that consider equilibrium at time $t+\Delta t$. These methods require the solution of a set of linear equations at each time step; however, larger time steps may be used. Implicit methods may be conditionally or unconditionally stable [133].

Newmark family of methods: In 1959, Newmark [43] presented a family of single-step integration methods of solution of structural dynamic problems for both blast and seismic loading. During the past 40 years Newmark's method applied to the dynamic analysis of many practical engineering structures. In addition, has been modified and improved by many other researchers. In order to illustrate the use of this family of numerical integration methods consider the solution of the linear dynamic equilibrium equations as in (10.5) is mentioned. The direct use of Taylor's series provides a rigorous approach to obtain the two additional equations. First to obtain the u_t by $u_{t-\Delta t}$ and it's following order derivatives terms. The ladder is $\dot{u}_t$ by $\dot{u}_{t-\Delta t}$ and it's following order derivatives terms. Newmark truncated these equations and rearrange them. He produces Newmark's equations in standard form

$$\dot{u}_{t+\Delta t} = \dot{u}_t + \left[(1-\gamma)\ddot{u}_t + \gamma\,\ddot{u}_{t+\Delta t}\right]\Delta t \tag{10.16}$$

$$u_{t+\Delta t} = u_t + \dot{u}_t \Delta t + \left[(1/2 - \beta)\ddot{u}_t + \beta\,\ddot{u}_{t+\Delta t}\right]\Delta t^2 \tag{10.17}$$

Two special cases of Newmark's method are the well-known average acceleration and linear acceleration methods. The assumption in average acceleration is made that within small increment of time Δt, the acceleration is the average value of the acceleration at the beginning of the interval $\ddot{u}_t$ and the acceleration at the end of the time interval $\ddot{u}_{t+\Delta t}$, as illustrated in Figure 10.4. The assumption in linear

acceleration is made that a linear variation of acceleration from time t to time $t+\Delta t$ as illustrated in Figure 10.5.
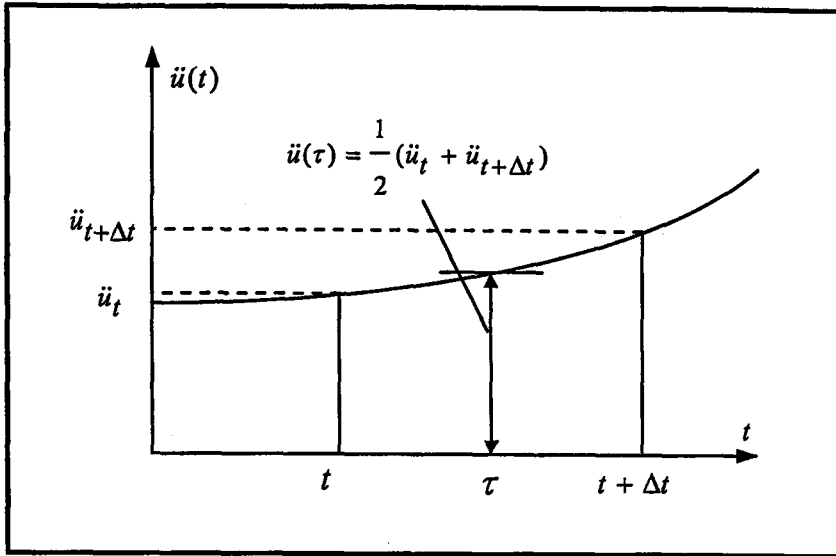
Figure 10.4 Numerical integration using; the average acceleration method

The parameters β and γ define the variation of acceleration over time step and determine the stability and accuracy characteristics of the method. τ is the arbitrary time between time t and time $t+\Delta t$. Typical selection of $\gamma = 1/2$ and $1/6 \leq \beta \leq 1/2$ is satisfactory from all points of view, including that of accuracy. Newmark's equations with $\gamma = 1/2$ and $\beta = 1/2$ are the same as those derived assuming constant average acceleration, and those with $\gamma = 1/2$ and $\beta = 1/6$ correspond to assumption of linear variation of acceleration [40,41,57133].

Stability of Newmark's method: For zero damping Newmark's method is conditionally stable if;

$$\gamma \geq 1/2, \ \beta \leq 1/2 \ \text{and} \ \Delta t \leq \frac{1}{\omega_{max}\sqrt{\frac{\gamma}{2} - \beta}} \tag{10.18}$$

where ω_{max} is the maximum frequency in the structural system [43]. Newmark's method is unconditionally stable if;

$$2\beta \geq \gamma \geq 1/2 \tag{10.19}$$
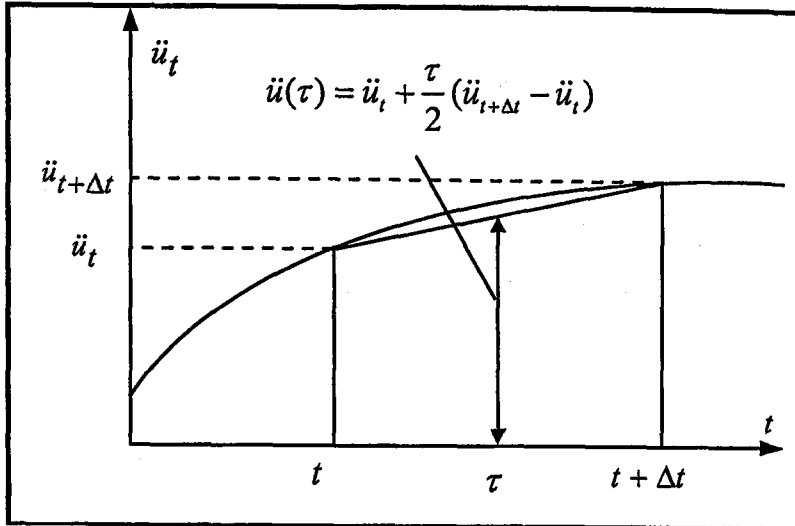
Figure 10.5 Numerical integration using; linear acceleration method

Géradin and Rixen [134] proposes another constraint of β and γ is can summarized;

$$\gamma = 1/2 + \alpha \quad \text{and} \quad \beta = 1/4(\gamma + 1/2)^2 \quad \text{with} \quad \alpha > 0 \qquad (10.20)$$

However, if γ is greater than 1/2, errors are introduced. These errors are associated with "numerical damping" and "period elongation".

For large multi degrees of freedom structural systems the time step limit, given by Eq (10.18), can be written in a more useable form as

$$\frac{\Delta t}{T_{min}} \leq \frac{1}{2\pi\sqrt{\dfrac{\gamma}{2} - \beta}} \qquad (10.21)$$

Computer models of large real structures normally contain a large number of periods which are smaller than the integration time step; therefore, it is essential that one select a numerical integration method that is unconditional for all time steps [40]. The stability region of the Newmark method is shown in Figure 10.6.

215
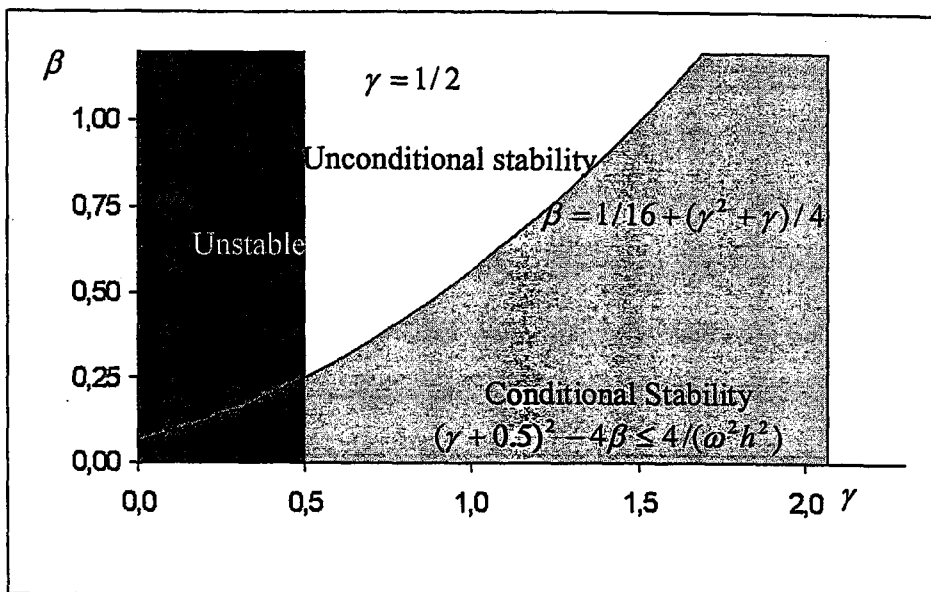
Figure 10.6 Stability region for the Newmark's method [134]

Selection of a direct integration method: It is apparent that large number different direct numerical integration methods are possible by specifying different integration parameters. A few of the most commonly used methods are summarized in Table 10.2.

Table 10.2 Summary of Newmark methods modified by the δ factor [40]

Method	γ	β	δ	$\dfrac{\Delta t}{T_{min}}$	Accuracy
Central difference	$\dfrac{1}{2}$	0	0	0.3183	Excellent for small Δt Unstable for large Δt
Linear acceleration	$\dfrac{1}{2}$	$\dfrac{1}{6}$	0	0.5513	Very good for small Δt Unstable for large Δt
Average acceleration	$\dfrac{1}{2}$	$\dfrac{1}{4}$	0	∞	Good for small Δt No energy dissipation
Modified average acceleration (using stiffness proportional damping)	$\dfrac{1}{2}$	$\dfrac{1}{4}$	$\dfrac{\Delta t}{\pi}$	∞	Good for small Δt No energy dissipation

216

For single degree of freedom systems the central difference method is most accurate; and the linear acceleration method is more accurate than the average acceleration method. However, if only single degree of freedom systems are to be integrated the piece-wise exact method, previously presented, and should be used since there is no need to use an approximate method.

It appears that the modified average acceleration method, with a minimum addition of stiffness proportional damping, is a general procedure that can be used for the dynamic analysis of all structural systems. Using $\delta = \Delta T / \pi$ will damp out periods shorter than the time step and introduces a minimum error in the long period response [40].

10.5 Examples of Transient Dynamic Analysis

To verify that the formulation of the FE model can be successfully used for the transient dynamic analysis of the beam and frame structures, several examples for which solutions are available have been considered.

10.5.1 Cantilever beam with sinusoidal tip load example

The cantilever beam shown in Figure 10.7 is a benchmark example to test dynamic analysis schemes. The cantilever beam of unit length is subjected to a tip loading $p(t)$ given by a half-sine pulse shown in Figure 10.8. The tip loading has the following characteristics, an amplitude EI and duration equal to fundamental period. T. The material properties of the beam are given by an EI of 3.1941 and a mass per unit length ρA of 1.0.
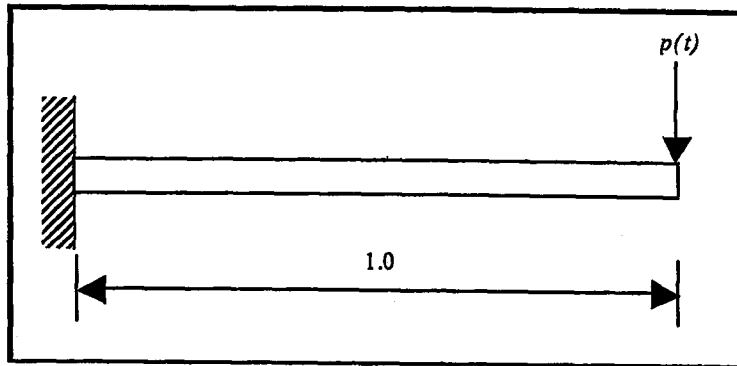
Figure 10.7 Geometry of cantilever beam
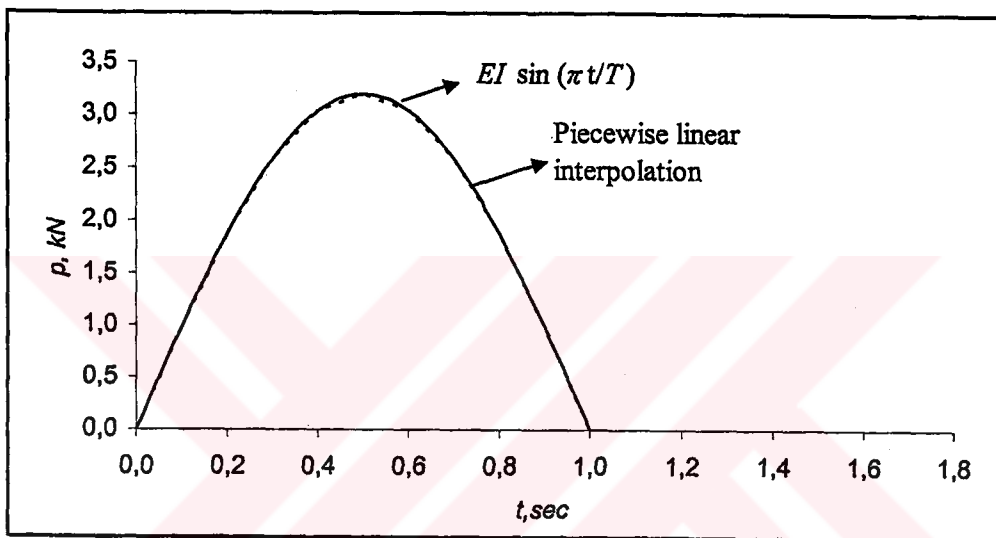
Figure 10.8 Loading history of cantilever beam

Discussion of results: First, the free vibration analysis is carried out. The fundamental frequency of the beam is computed and equal to 6.239 rad/sec. A very good agreement is obtained between the present solution and the analytical (exact) solution presented by Smith and Griffiths [135] which indicates a fundamental frequency value of $\omega = 6.284$ rad/sec (or $\omega = 3.5160\sqrt{EI/\overline{m}L^4}$). So the exact fundamental period is found to be $T = 2\pi/\omega = 1.0$ sec.

This problem is solved by average acceleration method. The interval value of $\Delta t = 0.05$ sec is taken. The damping ratio is equal to zero. The result of presented study and values given by Smith and Griffiths [135] is tabulated in Table 10.3. The

numerical results obtained for tip displacement of beam is compared with Smith and Griffiths [135] and analytical solution in Figure 10.9. Remarkably good agreement between results is observed.

Table 10.3 Tip displacement results of cantilever beam

Time	Analytical	Ref. [135]	Present study	Time	Analytical	Ref. [135]	Present study
0.00	0.0000	0.0000	0.0000	0.90	0.2632	0.2659	0.2755
0.05	0.0022	0.0019	0.0020	0.95	0.1357	0.1393	0.1546
0.10	0.0093	0.0095	0.0101	1.00	0.0000	0.0043	0.0203
0.15	0.0255	0.0253	0.0269	1.05	-0.1335	-0.1284	-0.1153
0.20	0.0538	0.0529	0.0542	1.10	-0.2540	-0.2487	-0.2380
0.25	0.0958	0.0949	0.0945	1.15	-0.3495	-0.3455	-0.3368
0.30	0.1513	0.1497	0.1489	1.20	-0.4109	-0.4081	-0.4051
0.35	0.2182	0.2153	0.2153	1.25	-0.4320	-0.4308	-0.4365
0.40	0.2925	0.2892	0.2875	1.30	-0.4108	-0.4123	-0.4249
0.45	0.3688	0.3650	0.3618	1.35	-0.3494	-0.3534	-0.3711
0.50	0.4410	0.4361	0.4337	1.40	-0.2538	-0.2597	-0.2833
0.55	0.5023	0.4976	0.4957	1.45	-0.1333	-0.1415	-0.1704
0.60	0.5464	0.5420	0.5403	1.50	0.0002	-0.0093	-0.0403
0.65	0.5677	0.5633	0.5626	1.55	0.1337	0.1244	0.1026
0.70	0.5622	0.5589	0.5602	1.60	0.2541	0.2452	0.2265
0.75	0.5278	0.5261	0.5302	1.65	0.3496	0.3423	0.3246
0.80	0.4646	0.4638	0.4704	1.70	0.4109	0.4067	0.3986
0.85	0.3750	0.3757	0.3836	1.75	0.4320	0.4310	0.4335
0.90	0.2632	0.2659	0.2755	1.80	0.4108	0.4132	0.4251
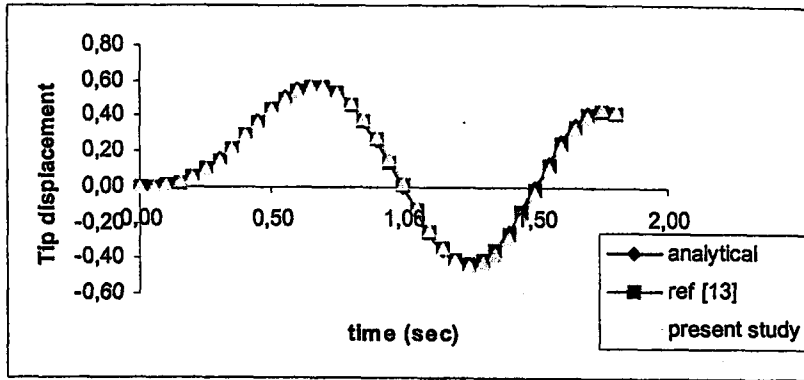
Figure 10.9 Tip displacements of cantilever beam respect to time

10.5.2 Two bay-two story reinforced concrete frame

Problem definition: Figure 10.10 shows the next example considered which consists of a two bay-two story reinforced concrete frame subject to ramp loads. The frame is assumed to be clamped at the base and the mass and flexural rigidity is computed from the gross area of concrete (neglecting the reinforcing steel). The unit weight of concrete is 24kN/m^3 and its elastic modulus $E_c = 28.5 \times 10^6$ kN/m^2. All column cross-sections are identical and are 0.40m$\times$0.40m in dimensions. All beam cross-sections are also identical and are 0.25m$\times$0.50m in dimensions. Frame is subjected to ramp loads shown in Figure 10.11, which are at story levels and are half of the previous value.

Figure 10.10 Geometry of two bay-two story reinforced concrete frame
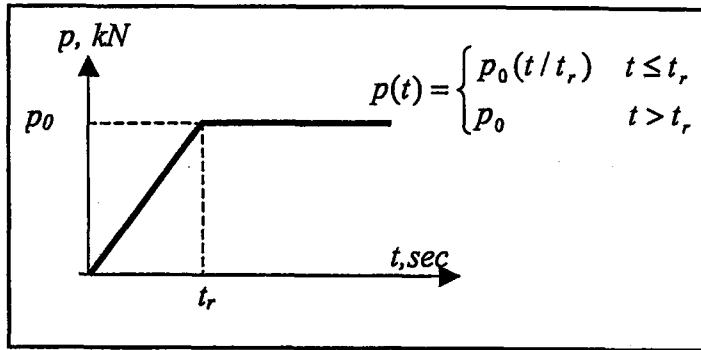
Figure 10.11 Loading history of ramp loads

Discussion of results: The first two fundamental periods are computed using free vibration program and results are presented and compared with SAP 2000 in Table 10.4. By making the assumption $t_r / T_n \cong 0.2$, rise time of ramp load t_r is found to be $t_r = 0.08\,\text{sec}$. As a result of this assumption the dynamic response of the structure is clearly observed. Loading history of ramp load can be summarized as shown in Figure 10.11. The response of structure computed for a time period of $1.0\,\text{sec}$ with $\Delta t = 0.01\,\text{sec}$. This problem is solved by average acceleration method. The analysis results are tabulated and compared with SAP 2000 for undamped situation in Table 10.5. The numerical results obtained for displacements of point A and rotations of point B are compared with the results obtained by SAP2000 in Figure 10.12 and 10.13. Remarkably good agreement between results is observed. This problem is solved for $t_r / T_n \cong 0.2$. The other t_r / T_n ratios computed and presented in Figure 10.14. If t_r / T_n ratio is increased the dynamic disturbances are getting decreased.

For damped case, by making the assumption $\xi = 0.10$ is more convenient to observe effects of damping forces, clearly. The response of structure computed for a time period of $1.0\,\text{sec}$ with $\Delta t = 0.01\,\text{sec}$ for damped situation. The numerical results obtained for displacements of point A and rotations of point B for damped case are compared with the results obtained by SAP2000 in Figure 10.15 and 10.16. Again, remarkably good agreement between results is observed.

Table 10.4 Periods for two bay-two story reinforced concrete frame

Mode	Periods (sec)	
	Present study	SAP2000
1	0.3622	0.3622
2	0.1120	0.1120

Table 10.5 Displacement results of point A and rotation results of point B for undamped situation $\xi = 0.0$

Time	Point A ($m \times 10^{-3}$)		Point B($rad \times 10^{-3}$)	
	SAP2000	Present study	SAP2000	Present study
0.00	0.0000	0.0000	0.0000	0.0000
0.01	0.0016	0.0016	0.0000	0.0000
0.02	0.0067	0.0068	0.0000	0.0002
0.03	0.0168	0.0169	0.0000	0.0009
0.04	0.0344	0.0345	0.0026	0.0026
0.05	0.0620	0.0621	0.0054	0.0054
0.06	0.1008	0.1010	0.0091	0.0091
0.07	0.1519	0.1521	0.0141	0.0141
0.08	0.2164	0.2166	0.0206	0.0206
0.09	0.2927	0.2929	0.0286	0.0286
0.10	0.3792	0.3794	0.0377	0.0377
0.20	1.2700	1.2677	0.1301	0.1302
0.30	0.8213	0.8208	0.0837	0.0836
0.40	0.0709	0.0710	0.0054	0.0054
0.50	0.7516	0.7524	0.0762	0.0763
0.60	1.2800	1.2839	0.1317	0.1317
0.70	0.4363	0.4352	0.0434	0.0433
0.80	0.1771	0.1779	0.0166	0.0167
0.90	1.1100	1.1124	0.1139	0.1140
1.00	1.0800	1.0735	0.1101	0.1100

222
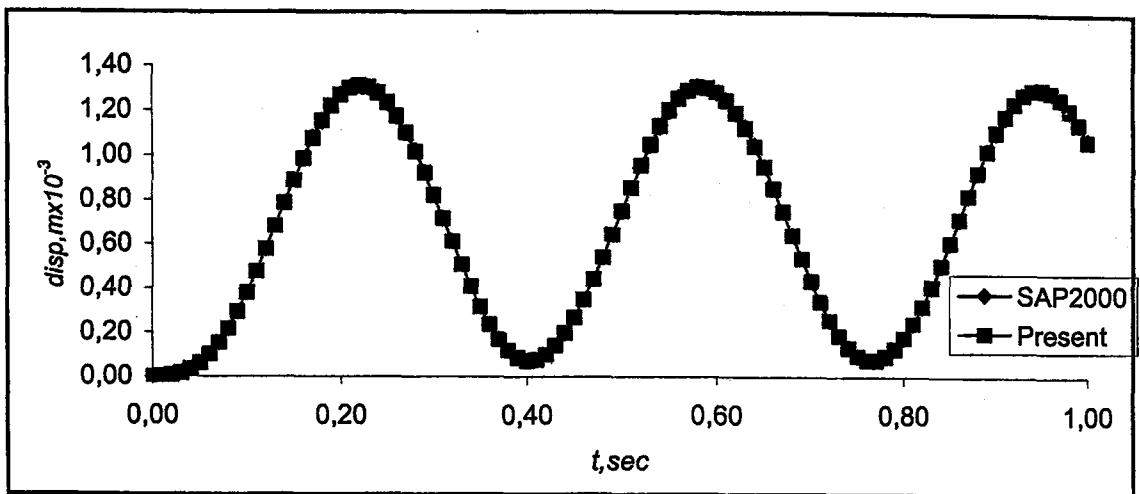
Figure 10.12 Displacements of point A with respect to time for undamped situation
$\xi = 0.0$
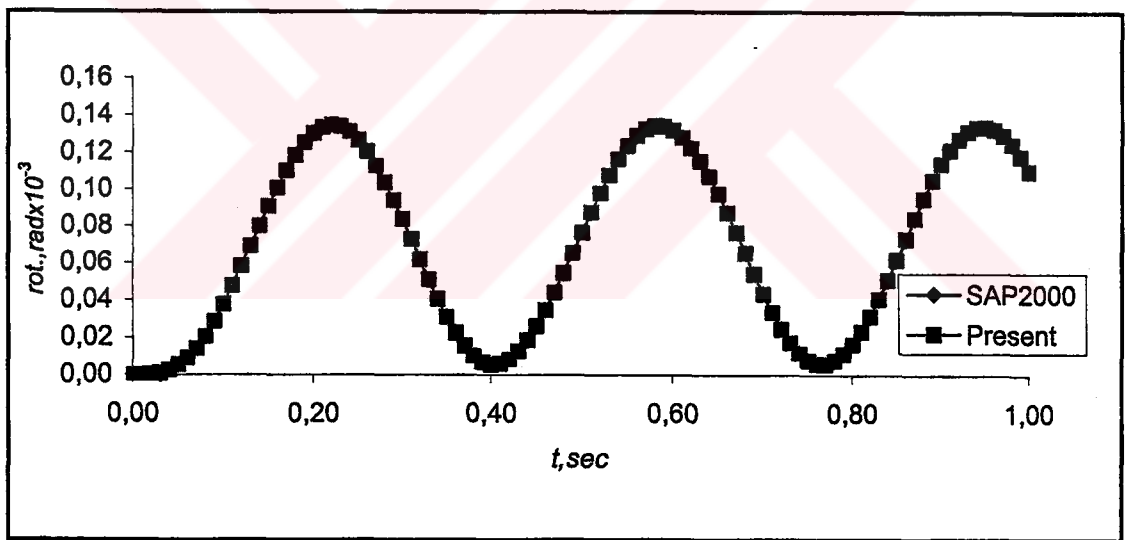
Figure 10.13 Rotations of point B with respect to time for undamped situation
$\xi = 0.0$
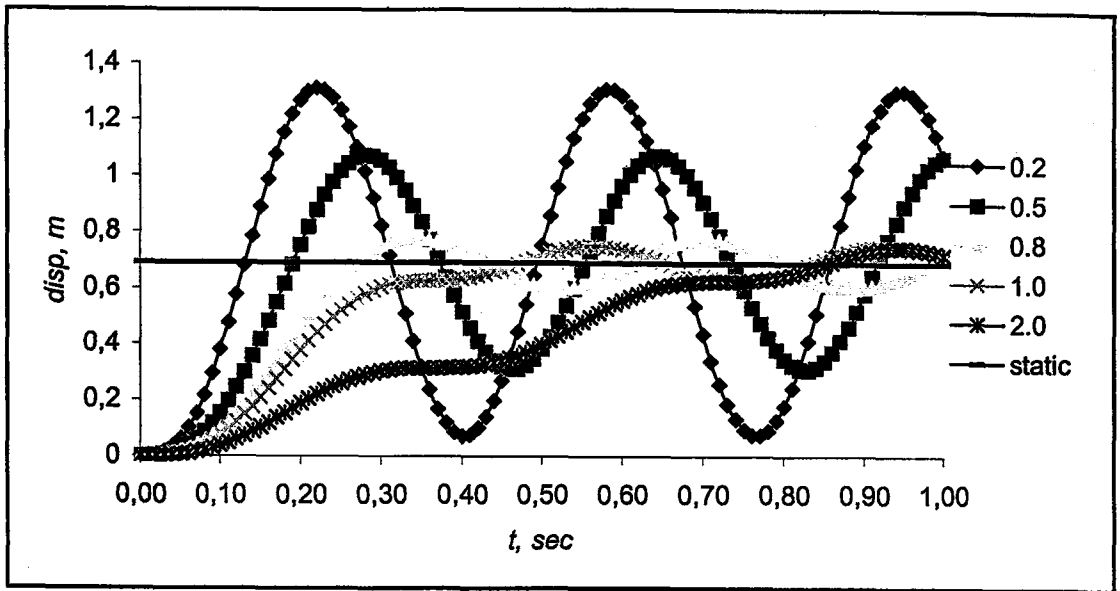
Figure 10.14 Comparisons of displacements results of point A for static and different t_r / T_n ratios -- undamped situation $\xi = 0.0$
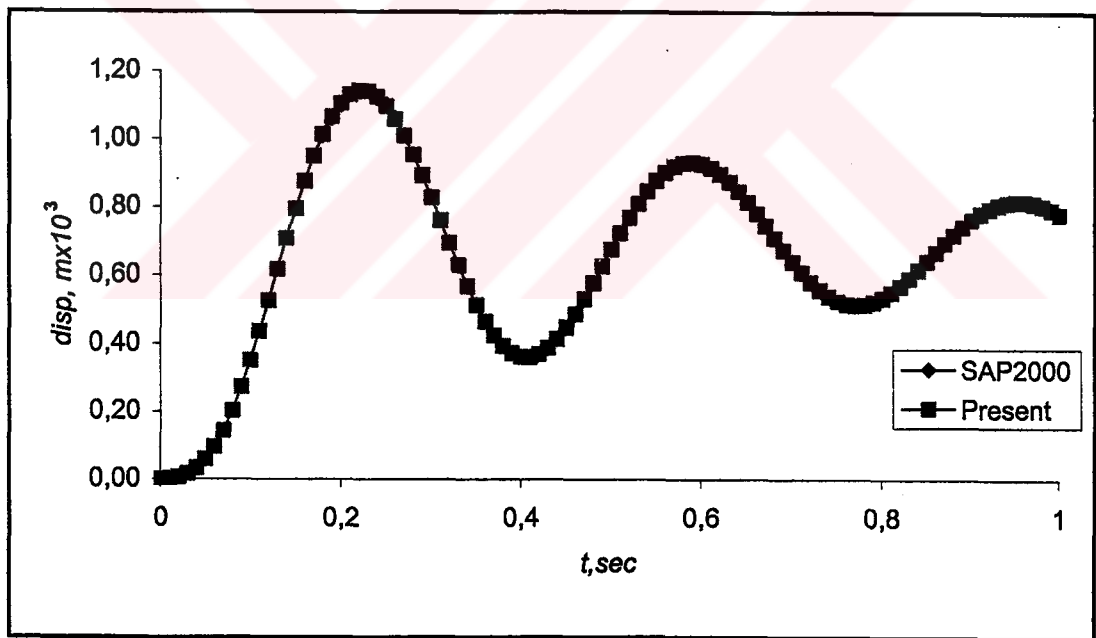
Figure 10.15 Displacements of point A with respect to time for damped situation $\xi = 0.10$
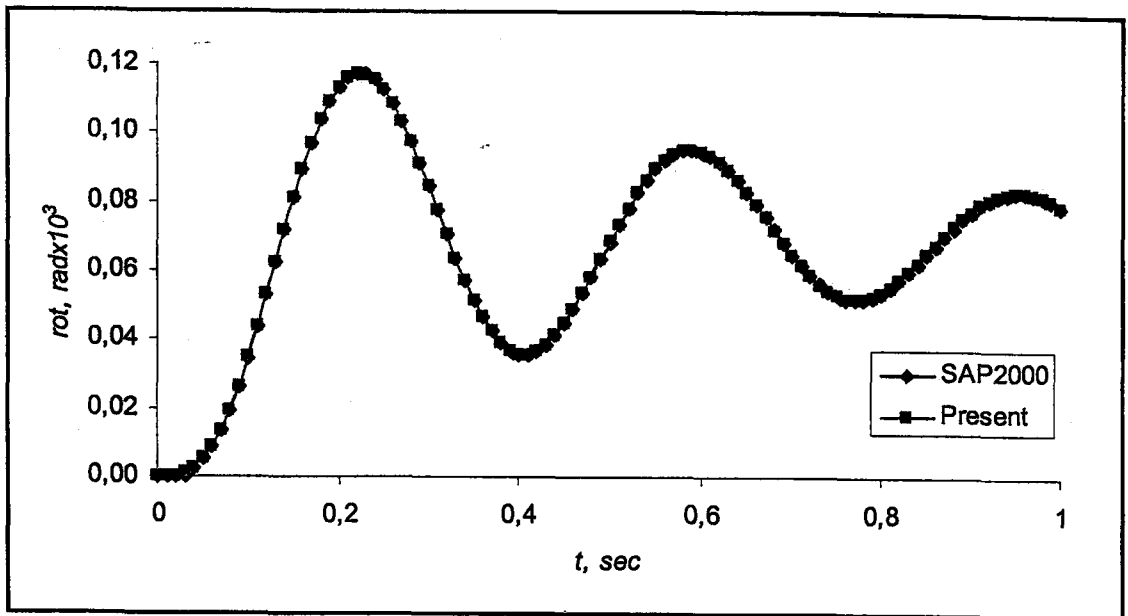
Figure 10.16 Rotations of point B with respect to time for damped situation
$$\xi = 0.10$$

10.5.3 Three-dimensional portal frame

The three-dimensional portal frame considered in the next transient dynamic study is subject to ramp loading as shown in Figure 10.17. The frame is assumed to be clamped at the base and the mass and flexural rigidity is computed from the gross area of concrete (neglecting the reinforcing steel). The unit weight of concrete is 24 kN/m³ and its elastic modulus $E_c = 28.5 \times 10^6 \, \text{kN/m}^2$. All column cross-sections are identical and are 0.40 m × 0.40 m in dimensions. All beam cross-sections are also identical and are 0.25 m × 0.50 m in dimensions. Frame is subjected to ramp loads shown in Figure 10.11, which are at story levels and are half of the previous value.

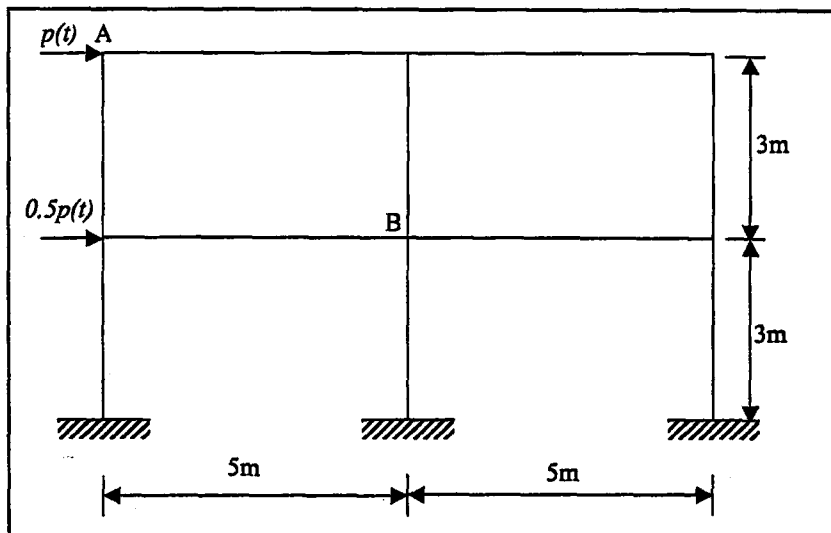*Discussion of results:* The first two fundamental periods are computed using free vibration program and results are presented and compared with SAP 2000 in Table 10.6. By making the assumption $t_r / T_n \cong 0.2$, rise time of ramp load t_r is found to be $t_r = 0.08 \, \text{sec}$. As a result of this assumption the dynamic response of the structure is clearly observed. Loading history of ramp load can be summarized as shown in Figure 10.11. The response of structure computed for undamped situation $\xi = 0.0$

and a time period of $1.0\sec$ with $\Delta t = 0.01\sec$. This problem is solved by average acceleration method. The analysis results are tabulated in Table 10.7. The numerical results obtained for displacements of point A and rotations of point B are compared with the results obtained by SAP2000 in Figure 10.18 and 10.19. Remarkably good agreement between results is observed.
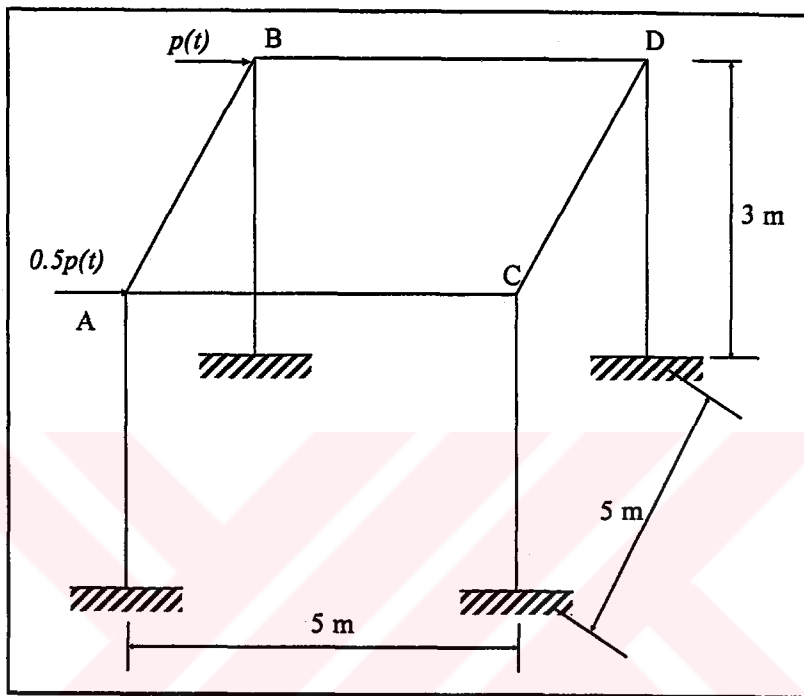
Figure 10.17 Geometry of three-dimensional portal frame

Table 10.6 Periods of three-dimensional portal frame.

Mode	Periods (sec)	
	Present study	SAP2000
1&2	0.22071	0.22078
3	0.17221	0.17559

Table 10.7 Displacement results of point A and rotation results of point B

Time	Point A (m×10⁻³)		Point B(rad×10⁻³)	
	SAP2000	Present study	SAP2000	Present study
0.00	0.0000	0.0000	0.0000	0.0000
0.01	0.0078	0.0081	0.0000	0.0000
0.02	0.0380	0.0388	0.0000	0.0002
0.03	0.1034	0.1055	0.0000	0.0009
0.04	0.2144	0.2179	0.0026	0.0026
0.05	0.3710	0.3754	0.0054	0.0054
0.06	0.5664	0.5707	0.0091	0.0091
0.07	0.7943	0.7971	0.0141	0.0141
0.08	1.0502	1.0506	0.0206	0.0206
0.09	1.3202	1.3262	0.0286	0.0286
0.10	1.6101	1.6151	0.0377	0.0377
0.20	2.3213	2.3218	0.1301	0.1302
0.30	0.4681	0.4816	0.0837	0.0836
0.40	3.1603	3.0924	0.0054	0.0054
0.50	-0.0343	0.0381	0.0762	0.0763
0.60	3.2614	3.1118	0.1317	0.1317
0.70	0.1869	0.2821	0.0434	0.0433
0.80	2.7407	2.6141	0.0166	0.0167
0.90	0.8661	0.8713	0.1139	0.1140
1.00	1.9405	1.9001	0.1101	0.1100
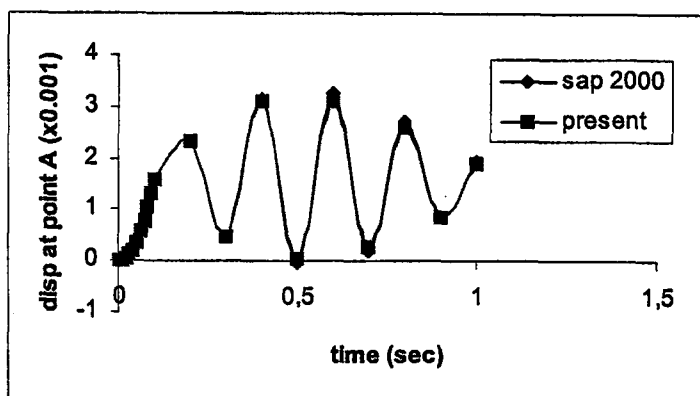
Figure 10.18 Displacements of point A with respect to time
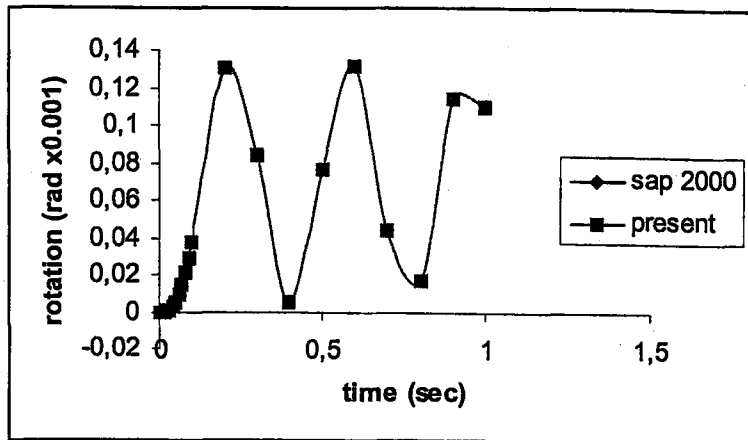
Figure 10.19 Rotations of point B with respect to time

10.6 Transient Dynamic Behavior of Optimized Structures

10.6.1 Cantilever beam with sinusoidal tip load example (SE minimization)

The cantilever beam analyzed in Section 10.4.1 of this chapter is now optimized in order to compare the dynamic behavior of structure before and after the optimization. The geometry and loading of the structure is shown in Figure 10.7. The material properties and loading are same as Section 10.4.1. The problem is solved in two stages. First of all, the beam is optimized and then the transient dynamic analysis is carried out for initial and optimum shape.

The beam is optimized for the SE minimization with a constraint that the total material volume of the structure should remain constant and the maximum von Misses stress should not exceed of its initial value prior to optimization. The beam is modeled using one segment and two key points. The thickness and width of the beam are defined as design variables.

Discussion of optimization results: The initial and optimum values of SE and design variables are given in Table 10.8. The SE of the beam is reduced from 0.1051 to 0.007775. Note that, a remarkable reduction in the SE is obtained. SE minimization leads to an increase in the stiffness of the structure thereby reducing the deformations.

228

Table 10.8 Initial and optimum design variables of cantilever beam

Design variables				Optimum
Type	Minimum	Initial	Maximum	
Thickness	0.001	0.1	1.0	0.3916
Width	0.1	10.0	15.0	2.5469
SE		0.1051		0.007775

Discussion of dynamic analysis results: The free vibration analyses are carried out for initial and optimum shapes. The results of the analysis are given in Table 10.9. After the SE minimization, the fundamental frequency increases from 6.2390 rad/sec to 22.251 rad/sec which corresponding to 256% increase.

Table 10.9 Initial and optimum frequencies of cantilever beam

Mode	Frequency (rad/sec)	
	Initial shape	Optimum shape
1	6.2390	22.251
2	37.985	96.502

This problem is solved by average acceleration method. The interval value of $\Delta t = 0.05$ sec is taken. The damping ratio is equal to zero. The results of presented study are tabulated in Table 10.10 for initial and optimum shape. Figure 10.20 shows that the displacements for initial and optimum shapes. Note the remarkable reduction in the amplitude of the vibration that has been obtained.

Table 10.10 Tip displacement results of cantilever beam for initial and optimum shape

Time	Initial Shape	Optimum Shape	Time	Initial Shape.	Optimum Shape
0.00	0.0000	0.00000	0.90	0.2755	0.00940
0.05	0.0020	0.00099	0.95	0.1546	0.00239
0.10	0.0101	0.00462	1.00	0.0203	-0.00329
0.15	0.0269	0.01079	1.05	-0.1153	-0.00488
0.20	0.0542	0.01705	1.10	-0.2380	-0.00184
0.25	0.0945	0.02045	1.15	-0.3368	0.00292
0.30	0.1489	0.02044	1.20	-0.4051	0.00494
0.35	0.2153	0.01942	1.25	-0.4365	0.00227
0.40	0.2875	0.02011	1.30	-0.4249	-0.00253
0.45	0.3618	0.02326	1.35	-0.3711	-0.00495
0.50	0.4337	0.02676	1.40	-0.2833	-0.00269
0.55	0.4957	0.02747	1.45	-0.1704	0.00211
0.60	0.5403	0.02455	1.50	-0.0403	0.00491
0.65	0.5626	0.01990	1.55	0.1026	0.00307
0.70	0.5602	0.01649	1.60	0.2265	-0.00168
0.75	0.5302	0.01583	1.65	0.3246	-0.00484
0.80	0.4704	0.01611	1.70	0.3986	-0.00343
0.85	0.3836	0.01443	1.75	0.4335	0.00122
0.90	0.2755	0.00940	1.80	0.4251	0.00940
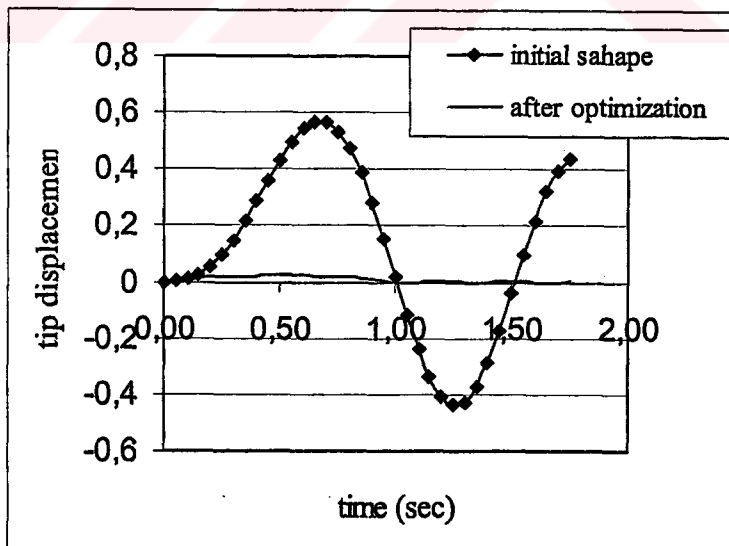
Figure 10.20 Comparison of tip displacements of initial and optimum cantilever beam

230

10.6.2 Cantilever beam with sinusoidal tip load example (weight minimization)

The cantilever beam analyzed in Section 10.5.1 of this chapter is now optimized in order to compare the dynamic behavior of structure before and after the optimization. The geometry and loading of the structure is shown in Figure 10.7. The material properties and loading are same as Section 10.5.1. The problem is solved in two stages. First of all, the beam is optimized and then the transient dynamic analysis is carried out for initial and optimum shape.

The beam is optimized for the weight minimization subject to a constraint that the maximum von Misses stress and displacement should not exceed of its initial value prior to optimization. The beam is modeled using one segment and two key points. The thickness and width of the beam are defined as design variables.

Discussion of optimization results: The initial and optimum values of weight and design variables are given in Table 10.11. The weight of the beam is reduced from 1.0 to 0.2938. Weight minimization leads to a decrease in the mass of the structure thereby improve the dynamic behavior.

Table 10.11 Initial and optimum design variables of cantilever beam

Design variables				
Type	Minimum	Initial	Maximum	Optimum
Thickness	0.001	0.10	5.0	1.2715
Width	0.100	10.0	15.0	0.2311
Weight		1.0		0.2938

Discussion of dynamic analysis results: The free vibration analyses are carried out for initial and optimum shapes. The results of the analysis are given in Table 10.12. After the weight minimization, the fundamental frequency increases from 6.2390 rad/sec to 45.1307 rad/sec which corresponding to 623% increase.

This problem is solved by average acceleration method. The interval value of $\Delta t = 0.05\,\text{sec}$ is taken. The damping ratio is equal to zero. Figure 10.21 shows that the displacements for initial and optimum shapes. Note the remarkable reduction in the amplitude of the vibration that has been obtained.

Table 10.12 Initial and optimum frequencies of cantilever beam

Mode	Frequency (rad/sec)	
	Initial shape	Optimum shape
1	6.2390	45.1307
2	37.985	97.2589
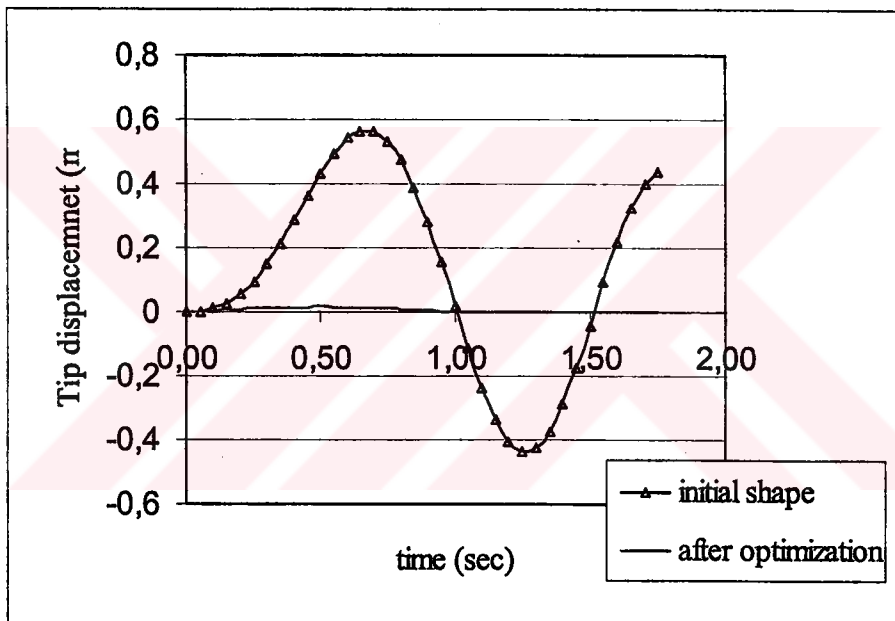
Figure 10.21 Comparison of tip displacements of initial and optimum cantilever beam

10.6.3 Two bay-two story reinforced concrete frame (SE minimization)

The Two bay-two story reinforced concrete frame analyzed in Section 10.5.2 of this chapter is now optimized in order to compare the dynamic behavior of structure before and after the optimization. The geometry and loading of the structure is shown in Figure 10.10. The material properties and loading are same as Section 10.5.2. The

problem is solved in two stages. First of all, the frame is optimized and then the transient dynamic analysis is carried out for initial and optimum shape.

The frame is optimized for the SE minimization with a constraint that the total material volume of the structure should remain constant and the maximum von Misses stress should not exceed of its initial value prior to optimization. The frame is modeled using ten segment and nine key points. The thickness and width of the column and beam are defined as design variables.

Discussion of optimization results: The initial and optimum values of SE and design variables are given in Table 10.13. The SE of the beam is reduced from 0.858×10^{-4} to 0.0448×10^{-4}. Note that, a remarkable reduction in the SE is obtained. SE minimization leads to an increase in the stiffness of the structure thereby reducing the deformations.

Table 10.13 Initial and optimum design variables of two bay-two story frame

Design variables				Optimum
Type	Minimum	Initial	Maximum	
Thickness and width of columns	0.1	0.4	1.0	0.8645
Thickness of beams	0.1	0.5	1.0	0.9049
Widths of beams	0.1	0.25	1.0	0.9569
SE		0.858×10^{-4}		0.448×10^{-5}

Discussion of dynamic analysis results: The free vibration analyses are carried out for initial and optimum shapes. The results of the analysis are given in Table 10.14. After the SE minimization, the fundamental frequency increases from 2.76 rad/sec to 4.961 rad/sec which corresponding to 79.74 % increase.

This problem is solved by average acceleration method. The interval value of $\Delta t = 0.01$ sec is taken. The damping ratio is equal to zero. The results of presented study are tabulated in Table 10.15 for initial and optimum shape. Figure 10.22 shows

233

that the displacements for initial and optimum shapes. Note the remarkable reduction in the amplitude of the vibration that has been obtained.

Table 10.14 Initial and optimum frequencies of two bay-two story frame

Mode	Frequency (rad/sec)	
	Initial	After optimization
1	2.76	4.961
2	8.927	15.658

Table 10.15 Tip displacement results of two bay two story frame for initial and optimum shape

Time	Initial Shape	Optimum Shape	Time	Initial Shape.	Optimum Shape
0.00	0.0	0.0	0.50	7.5243×10^{-5}	3.8198×10^{-6}
0.05	6.2139×10^{-6}	8.7550×10^{-7}	0.55	12.0320×10^{-5}	6.1933×10^{-6}
0.10	3.7940×10^{-5}	4.3304×10^{-6}	0.60	12.8388×10^{-5}	3.5107×10^{-6}
0.15	8.8881×10^{-5}	6.1118×10^{-6}	0.65	9.5384×10^{-5}	9.9411×10^{-7}
0.20	12.6767×10^{-5}	2.9913×10^{-6}	0.70	4.3525×10^{-5}	3.5653×10^{-6}
0.25	12.3306×10^{-5}	1.0575×10^{-6}	0.75	9.4723×10^{-6}	6.1958×10^{-6}
0.30	8.2076×10^{-5}	4.0757×10^{-6}	0.80	1.7792×10^{-5}	3.7687×10^{-6}
0.35	3.1646×10^{-5}	6.1694×10^{-6}	0.85	6.1302×10^{-5}	1.0057×10^{-6}
0.40	0.7100×10^{-5}	3.2437×10^{-6}	0.90	11.1242×10^{-5}	3.3019×10^{-6}
0.45	2.6795×10^{-5}	1.0183×10^{-6}	0.95	13.0428×10^{-5}	6.1783×10^{-6}
0.50	7.5243×10^{-5}	3.8198×10^{-6}	1.00	11.5024×10^{-5}	4.7878×10^{-6}
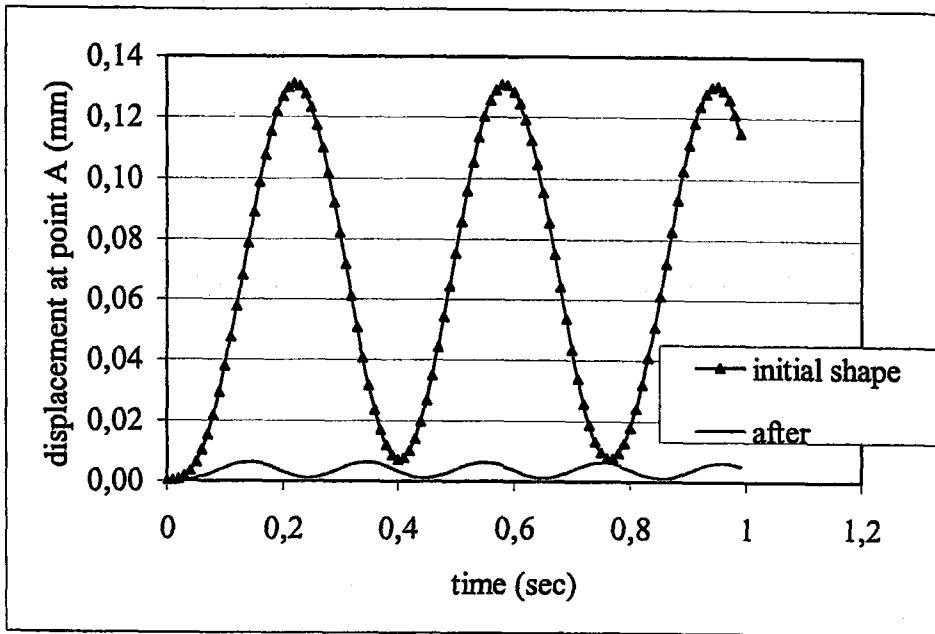
Figure 10.22 Comparison of tip displacements of initial and optimum two bay two story frame

CHAPTER 11

CONCLUSION

11.1 Summary of Achievements

In this work, computational tools have been developed for geometric modeling, automatic mesh generation, static and free vibration analysis, sizing and SSO using GAs and transient dynamic analysis. During this research work, five computer programs have been developed and verified using several benchmark examples. FREET deals with the free vibration analysis and shape optimization of 2D and 3D trusses. STATT deals with the static analysis and shape optimization of 2D and 3D trusses. DYNABAF deals with the transient dynamic analysis of 2D and 3D beam, arch and frame structures. BAFF-GA deals with free vibration analysis and GA optimization of 2D and 3D beam, arch and frame structures and BAFS-GA deals with static analysis and GA optimization of 2D and 3D beam, arch and frame structures. Each of these programs has four main ingredients:

- a geometrical modeling tool,
- an automatic mesh generation scheme,
- a structural analysis tool,
- a GA optimization tool.

11.1.1 Geometric modeling and automatic mesh generator

A geometric modeling tool, based on parametric cubic spline, has been implemented for the shape and thickness definition of 2D and 3D structures. The geometry and thickness of arbitrary and complex beam, arches, frames and combination of them can be defined with the aid of only few representative key points using this geometric modeling tool.

236

Moreover, procedures have been incorporated allowing for either smooth $C(2)$ continuity or alternatively, kinks with $C(0)$ continuity at the junctions of segments.

In this present study, the automatic 2D mesh generator presented by Sienz [137] was extended to handle 3D structural geometries. Along the parametric cubic splines, mesh generation is performed according to a specified mesh density. The mesh generator can generate meshes of two- three- and four noded elements. The thickness and width of structures and pressure loading along the segments are interpolated from key points to the nodal points using cubic splines. A bandwidth minimization is implemented and is carried out before the boundary and loading conditions are transferred to the FE model. As the structural shape changes during the optimization, the mesh generator has a facility to produce new geometry and mesh automatically.

11.1.2 Structural analysis

Truss structures: An existing FE code for the linear elastic analysis of 2D and 3D structures was upgraded by adding new subroutines for free vibration analysis. The existing Gauss elimination solver was replaced by skyline (profile) solver.

Beam, arch and frame structures: A family of new, curved, variable thickness, $C(0)$, MR, curved beam FEs has been developed for the linear elastic, static and free vibration analysis of beam, arch and frame structures in 2D and 3D. The implementations of these FEs have been verified using several benchmark examples in which the results have been compared with available analytical and numerical data.

11.1.3 Structural shape optimization

A general methodology for SSO of beam, arch and frame structures has been presented by integrating the tools developed for shape definition, automatic mesh generation and FE analysis with GA. The optimization capabilities of these programs have been verified using known benchmark examples wherever available.

Various optimization examples were presented, minimizing SE, maximizing fundamental frequency and minimizing the weight of the structures. Thickness, widths and shape design variables were used. The influence of the number of design variable employed was also investigated. The changes in the relative contributions of bending, membrane and shear energies were monitored for static optimization of frames, arches and beams during optimization process.

11.1.4 Transient dynamic analysis

Procedures for the transient dynamic analysis of 2D and 3D discrete structures using Newmark's method have been presented together with some details of their computer implementations. Some problems and limitations in the usage of Newmark's method were pointed out. Newmark's method provided good approximations for the evaluation of transient dynamic behavior provided that the FE results were calculated with sufficient accuracy. Various examples were presented. The transient dynamic characteristics of initial and optimum structures were investigated so that their safety was assured.

11.2 General Conclusions

Throughout this thesis, brief conclusions were given after each example; therefore the main conclusions are drawn from various aspects and summarized in the following sections.

11.2.1 Geometric modeling and mesh generation

Cubic splines offer a flexible and versatile tool for modeling 2D and 3D shapes. End tangent conditions have a strong influence on the shape of the structure modeled using cubic splines. A coupling between the modeling system and the analysis/optimization system is desirable and reduces the time spent in the design-analysis cycle.

The mesh generation algorithm presented was efficient and fully automatic. It incorporated a convenient geometric representation of boundaries and was able to

represent complex shapes easily. It possessed a convenient means of prescribing the element size variation over the domain. This feature is important for adaptivity study. In the present study adaptivity was not considered. The input data to mesh generator was kept to a minimum. It was flexible, so that its potential could be exploited in other applications (e.g. SSO or adaptivity analysis)

11.2.2 Structural analysis

Truss structures: The fourth chapter of this thesis dealt with 2D and 3D trusses under static and free vibration conditions. Matrix displacement methods were used and gave exact results proving that their implementation was correct.

Beam, arch and frame structures: The curved, variable thickness, isoparametric MR FE method was employed. The FEs performed well for both straight and curved elements, as well as for thick, thin uniform and variable thickness cases. The method has proved to be most appropriate for the analysis of such structures as it is inexpensive, accurate and reliable.

Most of the results obtained using FEs was compared well with the results of other researchers based on different formulations. The superior performance of the higher order curved elements for beam, arch and frame has been demonstrated. Quadratic and cubic FEs exhibit a higher rate of convergence than 2-noded linear elements as anticipated.

When transverse shear deformation is taken into account in the free vibration analysis of thin beams and arches, the lower values of fundamental frequency are usually obtained with values predicted using formulations ignoring transverse shear deformation. For much thicker beams and arches or higher modes, the frequencies can be significantly lower when transverse shear deformation is included.

The results illustrate that the FE method presented here can be used with confidence for static or the free vibration analysis of beam, arc and frame structures.

11.2.3 Structural optimization

The GA method proved to be powerful, reliable and accurate. It is a costly method in terms of CPU time, but the use of parallel computations may overcome this problem. Two classes of design variables were used: continuous and discrete.

The GA method allowed the option of choosing a set of design variables from a certain specified catalogue. The advantages of using this method are:

- discrete optimum design variables may be used,
- very simple calculations are involved, complex problems can be solved reasonably reliably
- problems that have many local optima can be solved, and
- it is easy to interface the GA method to existing simulations and models.

One of the major disadvantages of using this method is that CPU time is high; however the use of parallel computations may help to circumvent this problem. The GA was applied to optimization under static and free vibration conditions.

The optimization method used is useful creative design aids for structural engineers and could be used for teaching purposes. It allows a reduction in weight or SE or an increase in the fundamental frequency of the optimal structures obtained by introducing thickness and widths as well as shape variation. The introduction of thickness as well as shape variation leads to a significant improvement in the objective function as demonstrated by several examples. Some of the optimal shapes obtained are not practical and are included to illustrate the optimization method. However, introducing certain constraints can lead to practical solutions.

Difficulties in GAS: In the GAs method, many difficulties that were faced in selecting the different solution parameters. The most important ones are listed below:

- *String length:* Different string lengths have been chosen for discrete and continuous design variables. In most examples used in this thesis, the string length of 5 has been adopted for the discrete design variables, and for the continuous design variables a string length of 5-10 has been chosen. These values can, of course, vary for different problem types.

- *Population size:* For different sized problems, population sizes must be adjusted for the best results. In general, for small problems with a small number of design variables, a small population size between 100-200 will be adequate, while for large problems with large number of design variables, a large population size between 300-1000 will be adequate.

- *Mutation factor:* In most of the examples considered in this work, a mutation factor value of 0.0015 has been chosen for the small problems where a small number of design variables were used. However, a value of 0.5 has been chosen for the large problems where a large number of design variables were used.

- *Penalty coefficient factors:* Penalty coefficient factor values of 200, 300 and 1000 were adopted for the small problems with a small number of design variables, while for the large problems where a large number of design variables, values of 2000, 3000 and 10000 were chosen. Once again these values can be varied for different types of structure.

11.2.4 Transient dynamic analysis

The dynamic behavior of the optimized structures was investigated so that their safety was assured. SSO with volume/weight and SE minimization as the objective seems to be a mathematically better behaved problem and better dynamic behavior than those obtained other objective function. It was observed that the dynamic behavior of the optimum structure was much better than the initial geometry. In other words, optimization of structure in static situation improved the dynamic behavior of the structures.

It was observed that the selection of an appropriate time step size Δt was one of the most critical aspects of the dynamic analysis. The time step affects not only the stability and accuracy of the solution, but also the computational effort expended as well. The results are very sensitive to round off truncation errors. Due to that FE code written in FORTRAN 90 using double precision and higher order elements were used in analyses.

11.3 Suggestion for Further Work

Some suggestions for further work are listed as follows:

- By integrating a standard CAD system to the programs developed, a wider range of optimization problems could be solved.

- Although currently computer processing power is growing exponentially, the option of parallel progressing during GA optimization should be used when considering large three dimensional flow problems.

- Modified rebirthing or other similar techniques could be further investigated to improve the consistency and reliability of GA optimum solutions without the need for fine tuning GA control parameters. A more sophisticated set of convergence criteria is also necessary.

- The GA method could be applied to the optimization of composite structures.

- The use of multi-objective functions should be investigated.

- Inclusion of the topology optimization should be added to the GA for truss structures.

- The FE method presented in this work could be extended to the analysis of buckling behavior for homogeneous as well as composite structures.

- The use of different discrete optimization methods such as the evolution method would be useful to check the optimum results obtained with the GAs.

REFERENCES

[1] Zienkiewicz, O.C. and Taylor, R.L. (1991). *The Finite Element Method: Vol. 1 Basicconcepts and linear applications* (4th ed.). Maidenhead: Mc Graw-Hill.

[2] Reddy, J.N. (1991). *An introduction to the Finite element method* (2nd ed.). New York: Mc Graw-Hill.

[3] Bathe, K.J. (1996). *Finite element procedures*. New Jersey: Prentice Hall.

[4] Kassimali, A. (1999). *Matrix Analysis of Structures*. Pacific Grove: Brooks/Cole Publishing Company.

[5] Chandrupatla, T.R and Belegundu, A.D. (2002) *Introduction to finite elements in engineering*, (3th ed.). New Jersey: Prentice Hall, Inc.

[6] Arslan, M.A, (2003). A computational tool for determining optimum shapes of linearly elastic arches. MSc Thesis, University of Gaziantep.

[7] Ashwell, D.G. and Sabir, A.B. (1971). Further studies in the application of curved finite elements to circular arches. *Int. J. Num. Mech. Sci.*, 13, 507-517.

[8] Litewka, P. and Rakowski, J. (1998). The exact thick arch finite element. *Computers and Structures*, 68, 369-379.

[9] Uzman, Ü., Daloğlu, A. and Saka, M.P. (1999). Optimum design of parabolic and circular arches with varying cross section. *Structural Engineering and Mechanics*, 8, 465-476.

[10] Yamada, Y. and Ezawa, Y. (1977). On curved finite elements for the analysis of curved beams. *Int. J. Num. Meth. Eng*, 11, 1635-1651.

[11] Zienkiewicz, O.C. and Taylor, R.L. (1992). *The finite element method: Vol: 2 solid and fluid mechanics and non-linearity*. Maidenhead: McGraw-Hill.

[12] Hinton, E. and Huang, H.C. (1986). A family of quadrilateral Mindlin plate elements with substitute shear strain field. *Computers and Structures*, 23, 409-431.

[13] Huang, H.C. (1989). *Static and dynamic analysis of plates and shells*. London: Springer-Verlag.

[14] Hinton, E. Sienz, J. and Özakça, M. (2003). Analysis and optimization of prismatic and axisymmetric shell structures: Theory, Practice and Software. London: Springer.

[15] Lee, P.G., and Sin, H.C. (1994). Locking free curved beam element based on curvature. *Int. J. Num. Meth. Eng.*, **37**, 989-1007.

[16] Friedman, Z. and Kosmatka, J.B. (1998). An accurate two-node finite element for shear deformable curved beam. *Int. J. Num. Meth. Eng.*, **41**, 473-498.

[17] Cheng, X., Han, W., and Huang, H. (1997). Finite element methods for Timoshenko beam, circular arch and Reissner-Mindlin plate problems. *J. Comp. and Appl. Math.*, **79**, 215-234.

[18] Zhang, C. and Di, S. (2003). New accurate two-noded shear-flexible curved beam elements. *Computational Mechanics*, **30**, 81-87.

[19] Chapelle, D. (1997). A locking free approximation of curved rods by straight beam elements. *Numerische Mathematic*, **77**, 299-322.

[20] Raveendranath, P., Singh, G. and Rao, G.V. (2001). A three-nodded shear flexible curved beam element based on coupled displacement field interpolations. *Int. J. Numer. Meth. Engng.*, **51**, 85-101.

[21] Kim, J.G. and Kim Y.Y. (1998). A new higher order hybrid mixed curved beam element. *Int. J. Numerical Methods in Engineering*, **43**, 925-940.

[22] Krishnan, A. and Suresh Y.J. (1998). A simple cubic linear element for static and free vibration analyses of curved beams. *Computer and Structures*, **68**, 473-489.

[23] Day, R.A. and Potts, D.M. (1990). Curved Mindlin beam and axi-symmetric shell elements: a new approach. *Int. J. Numerical Methods in Engineering*, **30**, 1263-1274.

[24] Mou, Y.H., Han, R.P.S. and Shah, A.H. (1997). Exact dynamic stiffness matrix for beams of arbitrarily varying cross-sections. *Int. J. Numerical Methods in Engineering*, **40**, 233-250.

[25] Rossi, R.E., Reyes, J.A. and Laura, P.A.A. (1995). Dynamic stiffening of orthogonal beam grillages. *J. Sound and Vibration*, **187**, 281-286.

[26] Corn, S., Bouhaddi, N. and Piranda, J. (1997). Transverse vibrations of short beams: finite element models obtained by a condensation method. *J. Sound and Vibration*, **201**, 353-363.

[27] Howson, W.P. and Jemah, A.K. (1999). Exact out-of-plane natural frequencies of curved Timoshenko beams. *J. of Engineering Mechanics*, **125**, 19-25.

[28] Lee, F.J.H.H. and Lee, K.H. (1994). On the free vibration of stepped beams. *Int. J. Solids and Structures*, **22**, 3125-3137.

[29] Gupta, A. (1985). Vibration of tapered beams. *J. Structural Engineering*, **111**, 19-36.

[30] Stanley, A.J. and Ganesan, N. (1995). Dynamic response of cantilever beams with discontinuity in thickness subjected to a point load. *Computers and Structures*, **54**, 167-176.

[31] Laura, P.A.A., Gutierrez, R.H. and Rossi, R.E. (1996). Free vibrations of beams of bilinearly varying thickness. *Ocean Engineering*, **23**, 1-6.

[32] Houmat, A. (1995). Vibration of Timoshenko beams by variable order finite elements. *J. Sound and Vibration*, **187**, 841-849.

[33] Krishnan, A. and Suresh, Y.J. (1998). A simple cubic linear element for static and free vibration analyses of curved beams. *Computers and Structures*, **68**, 473-489.

[34] Auciello, N.M. and De Rosa, M.A. (1994). Free vibrations of circular arches: a review. *J. Sound and Vibration*, **176**, 433-458.

[35] Morales, C.A. (2000). Dynamic analysis of frames by a Rayleigh-Ritz based substructure synthesis method. *Engineering Structures*, **22**, 1632-1640.

[36] Lee, I.W., Kim, O. and Jung, G.H. (1999). Natural frequencies and mode shape sensitivities of damped systems: Part I, distinct natural. *J. Sound and Vibration*, **223**, 399-412.

[37] Lee, I.W., Kim, O. and Jung, G.H. (1999). Natural frequencies and mode shape sensitivities of damped systems: Part II, multiple natural. *J. Sound and Vibration*, **223**, 413-424.

[38] Baychev, I. (1996). Finite element method for frames with variable characteristics. *Mechanics Research Communications*, **23**, 213-220.

[39] Irvine, H.M. (1986). *Structural dynamics for the Practicing engineer*, Boston: Allyn and Unwin.

[40] Wilson, E.L. (2000). Three dimensional static and dynamic analysis of structures. *Computers and Structures*, Inc. University Avenue Berkley, California, USA.

[41] Chopra, A.K. (2000). Dynamics of structures: theory and applications to earthquake engineering, New Jersey: Prentice Hall.

[42] Houbolt, J.C. (1950). A recurrence matrix solution for the dynamic response of elastic aircraft. *J. Aero. Science*, **17**, 540.

[43] Newmark, N.M. (1959). A method of computation for structural dynamics. *Journal American Society of Civil Engineers*, **1**, 67.

[44] Belytschko, T. and Hughes, T.J.R. (1983). *Computational methods in transient analysis*, North Holland: Prentice-Hall.

[45] Wilson, E.L. (1968). *A computer program for dynamic stress analysis of underground structures*, SESM, Berkeley: Univ. California.

[46] Park, K.C. (1975). An improved stiffly stable method for direct integration of nonlinear structural dynamic equations. *Transactions of the American Society of Mechanical Engineers*, 1, 464.

[47] Zienkiewicz, O.C. (1977). A new look at Newmark, Houbolt and other time stepping formulas: A weighted residual approach. *Earthquake Engineering and Structural Dynamics*, 5, 283.

[48] Zienkiewicz, O.C., Wood, W.L., Hine, N.W. and Taylor, R.L. (1984). A unified set of single-step algorithms, Part 1: General formulations and applications. *Int. J. Numerical Methods in Engineering*, 20, 1529.

[49] Hilber, H.M. and Hughes, T. J.R. (1978). Collocation, dissipation and 'overshoot' for time integration schemes in structural dynamics. *Earthquake Engineering and Structural Dynamics*, 6, 99.

[50] Veletsos, A.S. and Ventura, C.E. (1986). Modal analysis of nonclasically damped linear systems. *Earthquake Engineering Structural Dynamics*, 14, 217-243.

[51] Clough, R.W., and Penzien, J. (1993). *Dynamics of structures*, New York: McGraw-Hill.

[52] Wilson, E.L. and Itoh, T. (1983). An eigen solution strategies for large systems. *Computers and Structures*, 16, 259-265.

[53] Wilson, E:L., Yuan, M.W., and Dickens, J.M. (1982). Dynamic analysis by direct superposition of Ritz vectors. *Earthquake Engineering Structural Dynamics*, 10, 813-824.

[54] Caughey, T.K. (1960). Classical normal modes in damped linear dynamic systems. ASME, *Journal of Applied Mechanics*, 27, 269-271.

[55] İbrahimbegovic, A. and Wilson, E.L. (1989). Simple numerical algorithms for the mod superposition analysis of linear structural systems with non-proportional damping. *Computers and Structures*, 33, 523-531.

[56] Choi, W.S. and Park, G.J. (1999). Transformation of dynamic loads into equivalent static loads based on modal analysis. *Int. J. Numerical Methods in Engineering*, 46(1), 281-298.

[57] Clough, R.W. and Mojtahedi, S. (1976). Earthquake response analysis considering non-proportional damping. *Earthquake Engineering Structural Dynamics*, 4, 489-496.

[58] Bayo, E.P. and Wilson, E.L. (1984). Finite element and Ritz vector technique for the solution of three-dimensional soil structure interaction problem in the time domain. *Engineering Computations*, **1**, 311-324.

[59] Subbaraj, K. and Dokainish, M.A. (1989). A survey of direct time-integration methods in computational structural dynamics - II. Implicit method. *Computers and Structures*, **32(6)**, 1387–1401.

[60] Kassimali, A. (1983). Large deformation analysis of elastic-plastic frames. *Journal of structural engineering*, ASCE, **109**, 1869-86.

[61] Saka, M.P. and Hayalioğlu, M.S. (1991). Optimum design of geometrically non-linear elastic-plastic steel frames. *Computers and Structures*, **38**, 329-44.

[62] Ding, Y. (1986). Shape optimization of structures a literature survey. *Computers and Structures*, **24**, 985-1004.

[63] Mackerle, J. (2002). Topology and shape optimization of structures using FEM and BEM: a bibliography (1999–2001). *Finite Elements in Analysis and Design*, **39**, 234-253.

[64] Tadjbakhsh, I.G. (1981). Stability and optimum design of arch-type structures. *Int. J. of Solids and Structures*, **17**, 565-574.

[65] Zienkiewicz, O.C. and Campbell, J.S. (1973). *Shape Optimization and Sequential Linear Programming*. New York: John Wiley.

[66] Templeman, A.B., and Yates, D.F. (1983). A linear programming approach to discrete optimum design of trusses. *Optimization methods in structural design*.

[67] Zhu, D.M. (1986). An improved Templeman's algorithm for optimum design of trusses with discrete member sizes. *Engineering Optimization*, **9**, 303-12.

[68] Reklaitis, G.V., Ravindran, A. and Ragsdell, K.M. (1983). *Engineering optimization methods and applications*, New York: John Wiley & Sons.

[69] Vanderplaats, G.N. (1984). *Numerical optimization techniques for engineering design*, London: McGraw-Hill, Inc.

[70] Arora, J. S. (1989). *Introduction to optimum design*, Singapore: McGraw-Hill.

[71] Brandt, A.M. (1989). *Foundations of optimum design in civil engineering*, London: Martinus Nijhoff Publishers.

[72] Haftka, R. T. and Gurdal, Z. (1993). *Elements of structural optimization*, London: Kluwer Academic Publishers.

[73] Adeli, H. (1994). *Advances in design optimization*, London: Chapman & Hall.

[74] Vanderplaats, G. N. and Thanedar, P.B. (1991). A survey of discrete variable optimization for structural design. *Proceeding of the 10th ASCE Congress Conference on Electronic Computation*, Indianapolis, Indiana 173-180.

[75] Schittkowski, K., Zillober, C. and Zotemantel, R. (1994). Numerical comparison of nonlinear programming algorithms for structural optimization. *Structural Optimization*, 7, 1-19.

[76] Arora, J.S., Huang, M.W. and Hsieh, C.C. (1994). Methods for optimization of nonlinear problems with discrete variables: A review. *Structural Optimization*, 8, 69-85.

[77] Huang, M. W. and Arora J. S. (1995). Engineering optimization with discrete variables. *Proceeding of the 36th Conference AIAA/ASME/ASCE/AHS/ASC Structures, Structural Dynamics and Materials*, New Orleans, AIAA, Reston, 1475-1485.

[78] Svanberg, K. (1987). The method of moving asymptotes-a new method for structural optimization. *Int. J. Num. Meth. Engng.*, 23, 359-373.

[79] Moses, F. (1964).Optimum structural design using linear programming. *Journal of structural division*, ASCE, 90(6), 89-104.

[80] Rashedi, R. and Moses, F. (1986). Application of linear programming to structural system reliability. *Computers and Structures*, 24(3), 375-384.

[81] Erbatur, F. and Al-Huseyin, M.M. (1992). Optimum design of frames. *Computers and Structures*, 45(5/6), 887-891.

[82] Kuhn, H.W. and Tucker, A.W. (1951). Nonlinear programming, *Proc. 2nd Berkley Symp. On Mathematics, Statistics and Probability*, Berkeley: University of California Press, 481-492.

[83] Lin, C.C. and Liu, I.W. (1989). Optimal design based on optimality criterion for frame structures including buckling constraint. *Computers and Structures*, 31, 535-44.

[84] Khan, M.R., Willmerrt, K.D. and Thornton, W.A. (1979). An optimality criterion method for large scale structures. *AIAA J.*, 17(7), 753-761.

[85] Zhou, M. and Rozvany, G. I. N. (1991). The COC algorithm, Part II: Topological, geometry and generalized shape optimization. *Comput. Methods Appl. Mech. Engrg.*, 89, 197-224.

[86] Saka, M.P. and Ülker, M. (1992). Optimum design of geometrically nonlinear space trusses. *Comput. Struct.*, 42, 289-299.

[87] Barsan, G.M. (1994). Optimal design of planar frames based on structural performance criteria. *Computers and Structures*, 53, 1395-400.

[88] Pezeshk, S. and Hjelmstad, K.D. (1991). Optimal design of planar frames based on stability criterion. *Journal of Structural Engineering*, 117, 896-913.

[89] Karihaloo, B.L. and Kanagasundaram, S. (1993). Optimum design of plane structural frames by non-linear programming. *Kluwer Academic Publishers*, 897-926.

[90] Holland, J.H. (1975). *Adaptation in natural and artificial systems*. The University of Michigan Press.

[91] Goldberg, D.E. (1989). Genetic algorithms in search, optimization and machine learning. Addisson-Wesley.

[92] Forrest, S. (1993). Genetic Algorithms: Principles of natural selection applied to computation. *Science*, 261, 872-878.

[93] Hayalioğlu, M.S. (1999). Optimum design of geometrically non-linear elastic-plastic steel frames via genetic algorithm. *Computers and Structures*, 77, 527-538.

[94] Rajeev, S. and Krishnamoorthy, C.S. (1992). Discrete optimization of structures using genetic algorithms. *Journal of Structural Engineering*, 118, 1233-50.

[95] Adeli, H. and Cheng, N.T. (1994). Augmented Lagrangian genetic algorithm for structural optimization. *Journal of Aerospace Engineering*, ASCE, 7, 104-18.

[96] Camp, C., Pezeshk, S. and Cao, G. (1998). Optimized design of two dimensional structures using a genetic algorithm. *Journal of Structural Engineering*, 124(5), 551-559.

[97] Goldberg, D.E. and Samtani, M.P. (1986). Engineering optimization via genetic algorithm. *Proc. 9th Conf. Electronic computation*, ASCE, 471-482.

[98] Lin, C.Y. and Hajela, P. (1992). Genetic algorithms in optimization problems with discrete and integer design variables. *Engineering Optimization*, 19, 309-327.

[99] Xie, Y.M. and Steven, G.P. (1996). Evolutionary structural optimization for dynamic problems. *Computers and Structures*, 58, 1067-73.

[100]Fogel, L.J., Owens, A.J. and Walsh, M.J. (1966). *Artificial intelligence through simulated evolution*, New York: Wiley.

[101]Schwefel, H.P. (1981). *Numerical optimization for computer models*, Chichester: Wiley & Sons.

[102]Papadrakakis, M., Tsompanakis, Y., Hinton, E., and Sienz, J. (1996). .Advanced solution methods in topology optimization and shape sensitivity analysis , *Journal of Engineering Computations*, 13(5), 57-90.

[103]Papadrakakis, M., Tsompanakis, Y. and Lagaros, N.D. (1999). Structural shape optimization using Evolution Strategies. *Engineering Optimization*, 31, 515-540.

[104] Chu, D.N., Xie, Y.M., Hira, A. and Steven, G.P. (1996). Evolutionary structural optimization for problems with stiffness constraints. *Finite elements Anal. Des.*, 21, 239-51.

[105] Li, G., Zhou, R.G., Duan, L. and Chen, W.F. (1999). Multiobjective and multilevel optimization for steel frames. *Engineering Structures*, 21, 519-529.

[106] Salajegheh, E. (1996). Approximate discrete variable optimization of frame structures with dual methods. *Int. J. Numerical Methods in Engineering*, 39, 1607-1617.

[107] Saka, M.P. and Kameshki, E.S. (1998). Optimum design of unbraced rigid frames. *Computers and Structures*, 69(4-5), 433-442.

[108] Sarma, K.C. and Adeli, H. (2000). Fuzzy genetic algorithm for optimization of steel structures. *Journal of Structural Engineering*, 126(5), 596-604.

[109] Keane, A. J. (1995). Passive vibration control via unusual geometries: the application of genetic algorithm optimization to structural design. *Journal of Sound and Vibration*, 185(3), 441-453.

[110] Nair, P. B., Keane, A. J. and Langley, R. S. (1998). On the approximation of frequency constraints structural optimization. *ISSMO/NASA/AIAA First Internet conference on approximation and fast reanalysis in engineering optimization*, 14-27.

[111] Langley, S. (2003). Genetic algorithm focused comparative optimization study for a broad scope of engineering applications. PhD Thesis, University of Wales Swansea.

[112] Al-Khamis, M.T.A. (1996). Structural optimization for static and free vibration conditions using genetic and gradient-based algorithms. PhD Thesis, University of Wales Swansea.

[113] Quing, S. and Yuan, L.D. (1989). *Computational geometry curve and surface modeling*. London: Academic Press Inc.

[114] Faux, I.D. and Pratt, M.J. (1979). *Computational geometry for design and manufacture*. Chichester: Ellis Horwood.

[115] Peraire, J., Vahadati, M., Morgan, K. and Zienkiewicz, O.C. (1987.). Adaptivity remeshing for compressible flow computations. *Journal of Computational Physics*, 72, 449-446.

[116] Peiro, J. (1989). Afinite Element procedure for the solution of euler equations on unstructures meshes. PhD Thesis, University Collage of Swansea.

[117] Bhavikatti, S.S. and Ramakrishnan, C.V. (1980). Optimum shape design of ratating disks. *Computers and Structures*, 11, 397-401.

[118] Braibant, V. and Fleury, C. (1984). Shape optimal design using B-spline. *Comp. Meth. App. Mech. Engng.*, **44**, 247-267.

[119] Kimmich, S. and Ramm, E. (1989). *Structural optimization and analysis with program CARAT.* Discritization methods in structural optimization- procedures and applications, Springer-Verlag.

[120] MotaSoares, C.M., MotaSoares, J.I. and Pinto, P. (1987). Optimal shape design of axisymmetric shells. *FEMCAD.*

[121] Héteny, M. (1971). Beams on elastic foundation: Theory with applications in the fields of civil and mechanical engineering (9th ed.). Michigan: The University of Michigan Press.

[122] Bowles, J.E. (1988). *Foundation analysis and design* (4th ed.). Singapore: Mc Graw-Hill.

[123] Abbassian. F., Dawswell. D.J. and Knowle. N.C. (1987). Free vibration benchmarks. *NAFEMS Benchmark.* **1**. 106-117.

[124] Hinton, E., Özakça, M. and Jantan, M.H. (1992). A computational tool for determining optimum shapes of vibrating arches. *Struct. Eng. Review.*, **4**, 162-174.

[125] Gutierrez, R.H. and Laura, P.A.A. (1989). In-plane vibration of non-circular arcs of non-uniform cross section. *Journal of Sound and vibration*, **129(2)**, 181-200.

[126] Yu, J.F. and Wang, B.P. (2004). An optimization of frame structures with exact dynamic constraints based on Timoshenko beam theory. *Journal of Sound and vibration*, **269**, 589-607.

[127] Rao, S.S. (1996.). *Engineering optimization.* (3th ed.). Canada: Wiley-Interscience Publication.

[128] Rajan, S.D. (2000). *Introduction to structural analysis and design.* John Wiley & Sons.

[129] Courrant, R. (1943. Variational methods for the solution of problems of equilibrium and vibrations. *Bulletin of the American mathematical society*, **49**, 1-23

[130] Rajan S.D. (1995). Sizing, shape and topology design optimization of trusses using genetic algorithm. *Structural engineering*, 1480-1487.

[131] Ghasemi, M.R. (1996). Structural optimization of trusses and axysmmetric shells using gradient-based methods and genetic algorithms. Phd thesis, Swansea: University of Wales Swansea.

[132] Tayşi, N., Göğüş, M.T. and Özakça, M. (2004). Static analysis and shape optimization of arch structures - Part II. Shape optimization. *Submitted to Journal of Computational and Applied Mathematics.*

[133] Tedesco, J.W., McDougal, W.G. and Ross, C.A. (1999). *Structural dynamics: Theory and applications*. California: Addison Wesley Longman, Inc.

[134] Géradin, M. and Rixen, D. (1994). Mechanical vibrations: Theory and applications to structural dynamics. Paris: Mason.

[135] Simith, I.M. and Griffiths, D.V. (1998). *Programming the finite element method*. (3th ed.). Chichester: John Wiley & Sons.

[136] Chen, C.N. (1999). The Timoshenko beam element of the differential quadrature element method. *Computational Mechanics*, **24**, 65-69.

[137] Sienz, J. (1994). *Integrated structural modeling, adaptive analysis and shape optimization*. Phd thesis, Swansea: University of Wales Swansea.

APPENDIX A

TRANSFORMATION MATRICES

A.1 Introduction

In many truss and frame structures, the bar and beam structural elements are found in many different orientations. Analysis of such structures for displacement and stress requires the setting up of a global coordinate system and referencing of all quantities of individual elements to the common (global) coordinate system in order to assemble the elements and impose boundary conditions on the whole structure. When a truss element is oriented at an angle from the global axis, its axial displacements at the nodes have components along the global axes. Thus, every node of a truss will have two displacements in the global coordinates: one along the global x axis and another transverse to the x axis. Therefore, the element will have two dof per node in the global coordinate system.

In the previous section, in which we focused on orthogonal structures derivation of the structures element stiffness matrices $[K^e]$. The determination of the element stiffness matrix in global coordinates, from the element stiffness matrix in local coordinates requires the introduction of a transformation.

This section will examine the 2D and 3D transformations required to obtain an element stiffness matrix in global coordinate system prior to assembly. Recalling that [6]

$$\{p\} = [K^{(e)}] \{\delta\} \tag{A.1}$$

$$\{P\} = [K^{(e)}] \{\Delta\} \tag{A.2}$$

Let us define a transformation matrix $[T]$ such that:

$$\{\delta\} = [T]\{\Delta\} \tag{A.3}$$

253

$${p} = [T]{P} \tag{A.4}$$

Note that we use the same matrix **T** since both ${\delta}$ and ${p}$ are vector quantities (or tensors of order one). Substituting Eq (A.3) and Eq (A.4) into Eq (A.1) we obtain

$$[T]{P} = [k^{(e)}][T]{\Delta} \tag{A.5}$$

pre-multiplying by $[T]^{-1}$

$${P} = [T]^{-1}[k^{(e)}][T]{\Delta} \tag{A.6}$$

But since the rotation matrix is orthogonal, we have

$$[T]^{-1} = [T]^{T} \tag{A.7}$$

and

$$\underbrace{{P} = [T]^{T}[k^{(e)}][T]{\Delta}}_{[K^{(e)}]} \tag{A.8}$$

$$[K^{(e)}] = [T]^{T}[k^{(e)}][T] \tag{A.9}$$

which is the general relationship between element stiffness matrix in local and global coordinates.

A.2 Transformation Matrices for 2D Framework Elements

The vector rotation matrix $[\gamma]$ is identical for 2D frame. For the 2D case, we will note that four angles are interrelated (l_{xX}, l_{xY}, l_{yX}, l_{yY}) and can all be expressed in terms of a single one α, were α is the direction of the local x axis (along the member from the first to the second node) with respect to the global X axis. The remaining 5 terms are related to the angle between Z axis and x-y plane. This angle is zero because we select an orthogonal right handed coordinate system. Thus the rotation matrix can be written as:

$$[\gamma] = \begin{bmatrix} l_{xX} & l_{xY} & l_{xZ} \\ l_{yX} & l_{yY} & l_{yY} \\ l_{zX} & l_{zY} & l_{zZ} \end{bmatrix} = \begin{bmatrix} \cos\alpha & \cos\left(\dfrac{\pi}{2}-\alpha\right) & 0 \\ \cos\left(\dfrac{\pi}{2}+\alpha\right) & \cos\alpha & 0 \\ 0 & 0 & 1 \end{bmatrix} = \begin{bmatrix} \cos\alpha & \sin\alpha & 0 \\ -\sin\alpha & \cos\alpha & 0 \\ 0 & 0 & 1 \end{bmatrix} \tag{A.10}$$

and we observe that the angles are defined from the second subscript to the first, and that counterclockwise angles are positive.

254

The element rotation matrix [T]will then be given by

$$\begin{bmatrix} \cos\alpha & \sin\alpha & 0 & 0 & 0 & 0 \\ -\sin\alpha & \cos\alpha & 0 & 0 & 0 & 0 \\ 0 & 0 & 1 & 0 & 0 & 0 \\ 0 & 0 & 0 & \cos\alpha & \sin\alpha & 0 \\ 0 & 0 & 0 & -\sin\alpha & \cos\alpha & 0 \\ 0 & 0 & 0 & 0 & 0 & 1 \end{bmatrix} \qquad (A.11)$$
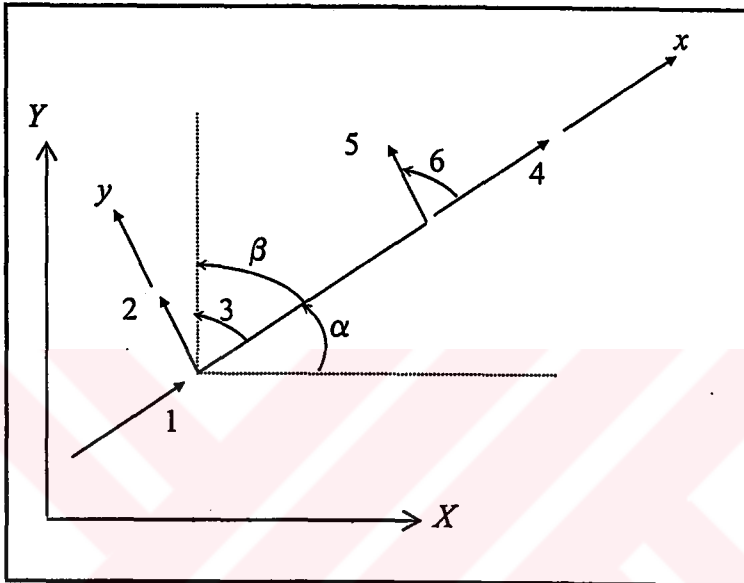
Figure A.1 Two dimensional frame element rotation

A.3 Transformation Matrices for 3D Framework Elements

Given that rod elements, are defined in such a way to have their local x axis aligned with their major axis, and that the element is defined by the two end nodes (of known coordinates), then recalling the definition of the direction cosines it should be apparent that the evaluation of the first row, only is quite simple. However evaluation of the other two is more complex.

The rotation matrix $[T]$ will obviously vary with the element type. In the most general case (3D element 6 dof per node) we would have to define:

$$\begin{Bmatrix} F_{x1} \\ F_{y1} \\ F_{z1} \\ M_{x1} \\ M_{y1} \\ M_{z1} \\ F_{x2} \\ F_{y2} \\ F_{z2} \\ M_{x2} \\ M_{y2} \\ M_{z2} \end{Bmatrix} = \underbrace{\begin{bmatrix} [\gamma] & & & \\ & [\gamma] & & \\ & & [\gamma] & \\ & & & [\gamma] \end{bmatrix}}_{[\mathbf{T}]} \begin{Bmatrix} F_{X1} \\ F_{Y1} \\ F_{Z1} \\ M_{X1} \\ M_{Y1} \\ M_{Z1} \\ F_{X2} \\ F_{Y2} \\ F_{Z2} \\ M_{X2} \\ M_{Y2} \\ M_{Z2} \end{Bmatrix} \qquad (A.12)$$

and should distinguish between the vector transformation $[\gamma]$ and the element transformation matrix $[\mathbf{T}]$.

Figure A.2 Three dimensional vector transformation

This generalized transformation from X, Y, Z to x, y, z was accomplished in one step in the two dimensional case, but intermediary ones will have to be defined in the 3D case.

Starting with reference (X_1, Y_1, Z_1) coordinate system which corresponds to the global co-ordinate system, we can define another one X_2, Y_2, Z_2 such that X_2 is aligned along the element.

In the 2D case this was accomplished through one single rotation α and all other angles where defined in terms of it. In the 3D case, it will take a minimum of two rotations β and γ, and possibly a third one α (different than the one in 2D) to achieve this transformation.

We can start with the first row of the transformation matrix which corresponds to the direction cosines of the reference axis (X_1, Y_1, Z_1) with respect to X_2. This will define the first row of the vector rotation matrix $[\gamma]$.

$$[\gamma] = \begin{bmatrix} C_X & C_Y & C_Z \\ l_{21} & l_{22} & l_{23} \\ l_{31} & l_{32} & l_{33} \end{bmatrix} \qquad (A.13)$$

where

$$C_X = \frac{x_j - x_i}{L}, C_Y = \frac{y_j - y_i}{L}, C_Z = \frac{z_j - z_i}{L} \text{ and } L = \sqrt{(x_j - x_i)^2 + (y_j - y_i)^2 + (z_j - z_i)^2}.$$

Note that this does not uniquely define the new coordinate system. This will be achieved in two ways: a reduced and a generalized one.

A.3.1 Simple 3D case

We start by looking at a simplified case one in which Z_2 is assumed to be horizontal in the X_1-Z_1 plane this will also define Y_2. We note that there will be no ambiguity unless the member is vertical. This transformation can be used if:

1. The principal axes of the cross section lie in the horizontal and vertical plane (i.e the web of an I Beam in the vertical plane).
2. If the member has 2 axis of symmetry in the cross section and same moment of inertia about each one of them (i.e circular or square cross section).

The last two rows of Eq (A.13) can be determined through two successive rotations (assuming that X_1, Y_1, Z_1 and X_2, Y_2, Z_2 are originally coincident):

1. Rotation by β about the Y_1 axis this will place the X_1 axis along X_β. This rotation $[\mathbf{R}_\beta]$ is made of the direction cosines of the β axis $(X_\beta, Y_\beta, Z_\beta)$ with respect to (X_1, Y_1, Z_1):

$$[\mathbf{R}_\beta] = \begin{bmatrix} \cos\beta & 0 & \sin\beta \\ 0 & 1 & 0 \\ -\sin\beta & 0 & \cos\beta \end{bmatrix} \tag{A.14}$$

we note that: $\cos\beta = \dfrac{C_X}{C_{XZ}}$ $\sin\beta = \dfrac{C_Z}{C_{XZ}}$ and $C_{XZ} = \sqrt{C_X^2 + C_Z^2}$.

2. Rotation by γ about the Z_2 axis

$$[\mathbf{R}_\gamma] = \begin{bmatrix} \cos\gamma & \sin\gamma & 0 \\ -\sin\gamma & \cos\gamma & 0 \\ 0 & 0 & 1 \end{bmatrix} \tag{A.15}$$

where $\cos\gamma = C_{XZ}$ and $\sin\gamma = C_Y$.

Combining Eq (A.14) and (A.15) yields

$$[\gamma] = [\mathbf{R}_\gamma][\mathbf{R}_\beta] \begin{bmatrix} C_X & C_Y & C_Z \\ \dfrac{-C_X C_Y}{C_{XZ}} & C_{XZ} & \dfrac{-C_Y C_Z}{C_{XZ}} \\ \dfrac{-C_Z}{C_{XZ}} & 0 & \dfrac{C_X}{C_{XZ}} \end{bmatrix} \tag{A.16}$$

For vertical member the preceding matrix is no longer valid as C_{XZ} is undefined. However we can obtain the matrix by simple inspection as we note that:

1. X_2 axis aligned with Y_1
2. Y_2 axis aligned with X_1
3. Z_2 axis aligned with Z_1

Hence the rotation matrix with respect to the y axis is similar to the one previously derived for rotation with respect to the z axis except for the reordering of terms:

$$[\gamma] = \begin{bmatrix} 0 & C_Y & 0 \\ -C_Y & 0 & 0 \\ 0 & 0 & 1 \end{bmatrix} \qquad (A.17)$$

which is valid for both cases (C_Y=1 for $\gamma = 90\deg$ and C_Y=-1 for $\gamma = 270\deg$).

A.3.2 General case

In the most general case, we need to define an additional rotation to the preceding transformation of an angle α about the $X\gamma$ axis, Figure 6. This rotation is defined such that:

1. $X\alpha$ is aligned with X_2 and normal to both Y_2 and Z_2

2. $Y\alpha$ makes an angle 0, α and $\beta = \dfrac{\pi}{2} - \alpha$ with respect to X_2, Y_2 and Z_2 respectively

3. $Z\alpha$ makes an angle 0, $\dfrac{\pi}{2} + \alpha$ and α with respect to X_2, Y_2 and Z_2 respectively

Noting that $\cos(\dfrac{\pi}{2} + \alpha) = -\sin\alpha$ and $\cos\beta = \sin\alpha$, the direction cosines of this transformation are given by:

$$[\mathbf{R}_\alpha] = \begin{bmatrix} 1 & 0 & 0 \\ 0 & \cos\alpha & \sin\alpha \\ 0 & -\sin\alpha & \cos\alpha \end{bmatrix} \qquad (A.18)$$

causing the Y_2-Z_2 axis to coincide with the principal axes of the cross section. This will yield:

$$[\gamma] = [\mathbf{R}_\alpha][\mathbf{R}_\gamma][\mathbf{R}_\beta] \qquad (A.19)$$

$$[\gamma] = \begin{bmatrix} C_X & C_Y & C_Z \\ \dfrac{-C_X C_Y \cos\alpha - C_Z \sin\alpha}{C_{XZ}} & C_{XZ}\cos\alpha & \dfrac{-C_Y C_Z \cos\alpha + C_X \sin\alpha}{C_{XZ}} \\ \dfrac{C_X C_Y \sin\alpha - C_Z \cos\alpha}{C_{XZ}} & -C_{XZ}\sin\alpha & \dfrac{C_Y C_Z \sin\alpha + C_X \cos\alpha}{C_{XZ}} \end{bmatrix} \qquad (A.20)$$

As for the simpler case, the preceding equation is undefined for vertical members, and a counterpart to Eq (A.17) must be derived. This will be achieved in two steps:

1. Rotate the member so that:

    (a)X_2 axis aligned with Y_1

    (b)Y_2 axis aligned with $-X_1$

    (c)Z_2 axis aligned with Z_1

this was previously done and resulted in Eq (A.17)

$$[\mathbf{R}_\gamma] = \begin{bmatrix} 0 & C_Y & 0 \\ -C_Y & 0 & 0 \\ 0 & 0 & -1 \end{bmatrix} \tag{A.21}$$

2. The second step consists in performing a rotation of angle α with respect to the new X_2 as defined in Eq (A.18).

3. Finally, we multiply the two transformation matrices [Rγ] [Rα]given by Eq (A.21) and (A.18) to obtain:

$$[\mathbf{T}] = [\mathbf{R}_\gamma]\ [\mathbf{R}_\alpha]\begin{bmatrix} 0 & C_Y & 0 \\ -C_Y \cos\alpha & 0 & \sin\alpha \\ C_Y \sin\alpha & 0 & \cos\alpha \end{bmatrix} \tag{A.22}$$

Note with $\alpha = 0$, we recover Eq (A.17).

CURRICULUM VITAE

Nildem Tayşi was born in Gaziantep on October 21, 1972. She received his B.S. degree in Civil Engineering from the University of Gaziantep in February 1995. Since then she has been a research assistant in the Department of Civil Engineering. She received her M. Sc. degree in Civil Engineering from the University of Gaziantep in August 1998. Her main areas of interest are static and free vibration finite element analysis of structures and structural shape optimization.